

# DIFFRACTION BY TWO CONDUCTING WEDGES

A Dissertation  
Presented to the Faculty of Graduate Studies  
University of Manitoba

In Partial Fulfillment  
of the Requirements for the Degree  
Doctor of Philosophy  
in  
Electrical Engineering

by

*ATEF ZAKARIA MOSTAFA ELSHERBENI*

B.Sc. E.E., Cairo University, 1976  
B.Sc. Appl. Phys., Cairo University, 1979  
M.Eng., Cairo University, 1982

September 1986 ©

Permission has been granted to the National Library of Canada to microfilm this thesis and to lend or sell copies of the film.

The author (copyright owner) has reserved other publication rights, and neither the thesis nor extensive extracts from it may be printed or otherwise reproduced without his/her written permission.

L'autorisation a été accordée à la Bibliothèque nationale du Canada de microfilmer cette thèse et de prêter ou de vendre des exemplaires du film.

L'auteur (titulaire du droit d'auteur) se réserve les autres droits de publication; ni la thèse ni de longs extraits de celle-ci ne doivent être imprimés ou autrement reproduits sans son autorisation écrite.

ISBN 0-315-37326-1

DIFFRACTION BY TWO CONDUCTING WEDGES

BY

ATEF ZAKARIA MOSTAFA ELSHERBENI

A thesis submitted to the Faculty of Graduate Studies of  
the University of Manitoba in partial fulfillment of the requirements  
of the degree of

DOCTOR OF PHILOSOPHY

© 1987

Permission has been granted to the LIBRARY OF THE UNIVERSITY OF MANITOBA to lend or sell copies of this thesis, to the NATIONAL LIBRARY OF CANADA to microfilm this thesis and to lend or sell copies of the film, and UNIVERSITY MICROFILMS to publish an abstract of this thesis.

The author reserves other publication rights, and neither the thesis nor extensive extracts from it may be printed or otherwise reproduced without the author's written permission.

## ABSTRACT

The problem of multiple diffraction of an incident plane wave by a perfectly conducting double wedge is investigated. A new technique based on the spectrum of cylindrical waves (CWS) is developed to calculate the multiply scattered fields between two cylindrical objects in general. In this technique the current induced on the surface of each scatterer due to the original source of excitation is viewed as an array of line sources. Each order of interaction between the two scatterers is then expressed as an integral over these sources with the integrand corresponding to the solution for a single line source excitation. The method is applied to solve for the diffraction by a double wedge and to the scattering by two parallel cylinders. The results for the scattering by two cylinders agree numerically with those based on the available exact boundary value solution, whereas the transmission coefficient compares favorably with the exact values for the special case of a slit geometry and with asymptotic results for a wide double wedge configuration.

In order to focus on the nature of the edge-to-edge interaction, a two term asymptotic solution with modified formulation is also derived. The first term is the non-interaction field due to the incident plane wave, whereas the second term is the interaction diffracted field due to two fictitious line sources located at the edges of the two wedges. In particular, the dependence of the transmission coefficient on the sharpness of the edges is specifically investigated by considering rounded, capped and dielectric loaded edges. The analogous modification of the aperture through loading with a third scatterer, such as a conducting or a dielectric cylinder, is also investigated. Although the radius of rounding or capping is considered small relative to the wavelength, significant changes in the diffraction pattern and transmission coefficient are observed. It is also noticed that the aperture loading by a dielectric cylinder produces a higher transmission coefficient while loading by a conducting cylinder yields a lower transmission coefficient relative to the unloaded aperture.



In order to establish the accuracy of the CWS technique for narrow wedge to wedge separations, the method of moments is modified and initially verified by application to the scattering by two large parallel cylinders as well as the diffraction by a double semi-infinite wedges (with sharp and blunt edges) where favourable agreement with published data is shown.

## **ACKNOWLEDGEMENT**

I would like to express my sincere gratitude to Professor M. Hamid for his advice, continuous encouragement and helpful discussion throughout the course of this research.

The author also wishes to thank Professor R. G. Kouyoumjian of the Electrical Engineering Department, Ohio State University, for suggesting the use of the uniform theory of diffraction instead of the geometrical theory of diffraction in order to get reliable results near the wedge surface.

The financial assistance of the Natural Sciences and Engineering Research Council of Canada and the University of Manitoba Faculty of Graduate Studies in the form of a University Fellowship is highly appreciated.

The use of the computing facilities at the University of Manitoba as well as the plotting and printing facilities at the Electrical Engineering Department are also appreciated.

Finally, my sincere thanks to my parents and my wife for their great support during the time of this work.

# TABLE OF CONTENTS

	Page
<i>ABSTRACT</i>	ii
<i>ACKNOWLEDGEMENTS</i>	iv
<i>TABLE OF CONTENTS</i>	v
<i>LIST OF TABLES</i>	vii
<i>LIST OF FIGURES</i>	ix
<i>LIST OF PRINCIPAL SYMBOLS</i>	xii
<i>CHAPTER 1- INTRODUCTION</i>	1
<i>CHAPTER 2- RIGOROUS SOLUTION BY THE CYLINDRICAL WAVE SPECTRUM TECHNIQUE</i>	7
2.1 Computation of the induced surface current	10
2.2 Far field pattern	21
2.3 Numerical examples	26
<i>CHAPTER 3- MODIFIED ASYMPTOTIC SOLUTION FOR A LOADED APERTURE</i>	48
3.1 Diffraction by a wide double wedge with sharp edges	51
3.2 Diffraction by a wide double wedge with capped edges	56
3.3 Diffraction by a wide double wedge with rounded edges	60
3.4 Scattering by a wide double wedge and a parallel cylinder	65
3.5 Numerical examples	74
<i>CHAPTER 4- SOLUTION BY MODIFIED METHOD OF MOMENTS</i>	100
4.1 Scattering by two parallel conducting circular cylinders	103
4.2 Diffraction by two wedges with blunt edges	105
4.3 Numerical examples	108

<i>CHAPTER 5- DISCUSSION AND CONCLUSIONS</i>	135
5.1 Suggestions for future research	137
<i>APPENDIX A - DERIVATION OF EQUATION (2-21)</i>	140
<i>APPENDIX B - FAR SCATTERED FIELD PATTERN OF A LINE SOURCE EXCITING A SHARP WEDGE</i>	142
<i>APPENDIX C - SCATTERING BY A CYLINDRICAL SHELL WITH RADIAL AND AZIMUTHAL PERMITTIVITY PROFILES</i>	144
<i>REFERENCES</i>	154

## LIST OF TABLES

Table	Page
2-1 Scattering cross-section of two parallel circular conducting cylinders with $\phi_0 = 90^\circ$ .	31
2-2 Scattering cross-section of two parallel circular conducting cylinders with $\phi_0 = 180^\circ$ .	32
2-3 Slit transmission coefficient for $\phi_0 = 90^\circ$ .	37
3-1 Diffraction pattern characteristics of a double rounded-wedge for $\theta_0 = 0^\circ$ , $ks = 10$ and $\gamma = 10^\circ$ .	85
3-2 Slit transmission coefficient for $\phi_0 = 90^\circ$ .	87
3-3 Diffraction pattern characteristics of a slit loaded by a cylindrical shell in the aperture plane for $\phi_0 = 90^\circ$ , $ks = 8$ , $\epsilon_r = 5$ , $k\rho_b = 1.0$ , $k\rho_a = 0.2$ and $\eta = 2.5$ .	98
3-4 Diffraction pattern characteristics of a slit loaded by a cylindrical shell in the aperture plane for $\phi_0 = 90^\circ$ , $ks = 8$ , $\epsilon_r = 5$ , $k\rho_b = 1.0$ , $k\rho_a = 0.2$ and $\delta = 1.0$ .	99
4-1 Slit transmission coefficient for $\phi_0 = 90^\circ$ .	116
4-2 Diffraction pattern characteristics of a double truncated wedge for $\phi_0 = 90^\circ$ , $ks = 7$ and $\gamma = 20^\circ$ .	126
4-3 Diffraction pattern characteristics of a double truncated wedge for $\phi_0 = 90^\circ$ , $ks = 7$ and $kd = 0.5$ .	127
4-4 Diffraction pattern characteristics of a double truncated wedge for $\phi_0 = 90^\circ$ , $\gamma = 10^\circ$ and $kd = 0.5$ .	128
4-5 Diffraction pattern characteristics of a double capped wedge for $\phi_0 = 90^\circ$ , $ks = 7$ and $\gamma = 20^\circ$ .	132
4-6 Diffraction pattern characteristics of a double capped wedge for $\phi_0 = 90^\circ$ , $ks = 7$ and $kr = 0.5$ .	133

Table	Page
4-7 Diffraction pattern characteristics of a double capped wedge for $\phi_0 = 90^\circ$ , $\gamma = 15^\circ$ and $kr = 0.5$ .	134

## LIST OF FIGURES

Figure	Page
2-1 Double wedge geometry.	16
2-2 Capped wedge geometry.	18
2-3 Two parallel conducting cylinders geometry.	22
2-4 The total scattered field pattern for two parallel circular conducting cylinders.	27
2-5 The interaction scattered field pattern for two parallel circular conducting cylinders.	29
2-6 Amplitude of the tangential electric field vs. $\psi$ .	30
2-7 $E_{PO}^S$ and amplitude of $C_0$ vs. $ks$ .	34
2-8 Diffraction pattern of a slit.	36
2-9 $T$ vs. wedge angle $\gamma$ .	39
2-10 Surface current vs. $kl$ of a double conducting capped-wedge for $ks = 7$ , $\gamma = 10^\circ$ and $kr = 0.05$ .	40
2-11 Surface current vs. $kl$ of a double conducting capped-wedge for $ks = 7$ , $\gamma = 10^\circ$ and $kr = 0.1$ .	41
2-12 Surface current vs. $kl$ of a double conducting capped-wedge for $ks = 7$ , $\gamma = 10^\circ$ and $kr = 1.0$ .	42
2-13 Surface current vs. $kl$ of a double conducting capped-wedge for $ks = 7$ , $\gamma = 10^\circ$ and $kr = 0.5$ .	43
2-14 Diffracted field vs. $\theta$ of a double conducting capped slit for $ks = 4$ and $kr = 1.0$ .	45
2-15 Diffracted field vs. $\theta$ of a double conducting capped slit for $ks = 6$ and $kr = 1.0$ .	46
2-16 Diffracted field vs. $\theta$ of a double conducting capped slit for $ks = 8$ and $kr = 1.0$ .	47
3-1 Schematic diagram of different types of loading the aperture of a double wedge.	49
3-2 Double sharp-wedge geometry.	53

Figure	Page
3-3 Double capped-wedge geometry.	57
3-4 Double rounded-wedge geometry.	63
3-5 Double sharp-wedge and a parallel cylindrical scatterer.	66
3-6 Scattered field components due to a plane wave incident on two sharp wedges and a parallel cylindrical scatterer.	71
3-7 Alternative representation of the scattered field components due to a plane wave incident on two sharp wedges and a parallel cylindrical scatterer.	72
3-8 Normalized diffracted field vs. $\theta$ for $\theta_0 = 0^\circ$ , $\gamma = 15^\circ$ and $ks = 5$ .	75
3-9 $T$ , $c_1$ (or $c_2$ ) and $E''$ vs. $ks$ for $\theta_0 = 0^\circ$ and $\gamma = 15^\circ$ .	76
3-10 Normalized diffracted field vs. $\theta$ of a double conducting capped-wedge for $ks = 8$ and $\gamma = 5^\circ$ .	77
3-11 Normalized diffracted field vs. $\theta$ of a double dielectric capped-wedge for $ks = 7$ , $\gamma = 10^\circ$ and $kr = 0.5$ .	78
3-12 $T$ vs. $ks$ of a conducting capped slit.	80
3-13 $T$ vs. $ks$ of a dielectric capped slit for $kr = 0.5$ .	81
3-14 $T$ vs. $ks$ of a double dielectric capped-wedge for $kr = 0.5$ and $\epsilon_r = 4$ .	82
3-15 Normalized diffracted field vs. $\theta$ of a double rounded-wedge for $\theta_0 = 0^\circ$ , $\gamma = 10^\circ$ and $ks = 10$ .	83
3-16 Normalized diffracted field vs. $\theta$ of a double rounded-wedge for $\theta_0 = 0^\circ$ , $\gamma = 10^\circ$ and $ks = 10$ .	84
3-17 $T$ vs. $ks$ of a loaded slit for $\theta_0 = 0^\circ$ and $ka = 0.5$ .	88
3-18 $T$ vs. $ks$ of a loaded slit for $\theta_0 = 0^\circ$ , $ka = 0.5$ and $kd = 5$ .	89
3-19 $T$ vs. $ks$ of a loaded slit for $\theta_0 = 40^\circ$ .	91
3-20 $T$ vs. $ks$ of a loaded slit for $\theta_0 = 40^\circ$ and $kd = 1.5$ .	92
3-21 $T$ vs. $ks$ of a loaded slit for $\theta_0 = 0^\circ$ .	93
3-22 $T$ vs. $ks$ of a loaded slit for $\theta_0 = 0^\circ$ and $kd = 5$ .	94



Figure	Page
3-23 $T$ vs. $ks$ of a loaded double wedge for $\theta_0 = 0^\circ$ , $ka = 0.5$ and $\gamma = 20^\circ$ .	95
3-24 Diffracted field vs. $\theta$ of a slit loaded by an inhomogeneous dielectric shell for $ks = 8$ , $\epsilon_a = 3$ , $k\rho_a = 0.2$ , $\eta = 2$ and $\delta = 1.0$ .	96
4-1 Schematic diagram of different types of a double wedge geometry with non-sharp edges.	102
4-2 Scattered field pattern for two circular cylinders.	109
4-3 Scattered field pattern for two circular cylinders.	110
4-4 Amplitude of the interaction current vs. $\psi$ .	112
4-5 Amplitude of the interaction field vs. $ka$ .	113
4-6 Amplitude of the interaction field vs. $ks$ .	114
4-7 $T$ vs. wedge angle $\gamma$ .	117
4-8a Amplitude of the slit aperture field for $\phi_0 = 90^\circ$ .	118
4-8b Amplitude of the slit aperture field for $\phi_0 = 90^\circ$ .	119
4-9 Phase of the slit aperture field for $\phi_0 = 90^\circ$ .	120
4-10 Current density vs. $kl$ for $ks = 8.06$ .	121
4-11 Normalized diffracted field vs. $\theta$ of a thick slit for $ks = 8.06$ .	123
4-12 Current density vs. $kl$ for $ks = 8.06$ and $\gamma = 15^\circ$ .	124
4-13 Normalized diffracted field vs. $\theta$ of a double truncated-wedge for $\gamma = 15^\circ$ and $ks = 8.06$ .	125
4-14 Normalized diffracted field vs. $\theta$ of a conducting capped-slit for $ks = 8.0$ .	129
4-15 Amplitude of the aperture field of a double capped wedge for $\phi_0 = 90^\circ$ .	131
C-1 Plane wave incident on a cylindrical dielectric shell in circular cylindrical co-ordinates.	145
C-2 $W$ vs. $\phi$ .	153

## LIST OF PRINCIPAL SYMBOLS

$j$	$\sqrt{-1}$
$e$	base of the natural logarithm (2.718281828...)
$e^{j\omega t}$	time dependence
$(\rho, \phi, z)$	circular cylindrical co-ordinates
$\phi_0$	plane wave incident angle
$E_p^i$	incident plane wave
$E^S$	scattered field
$\eta$	intrinsic impedance of free space
$k$	wave number
$\pi$	3.141592653...
$\lambda$	wavelength
$H_0(x)$	Hankel function of the second kind of order zero and argument $x$
$E_p^S$	scattered field due to a plane wave incident
$E_l^S$	scattered field due to a line source field
$\epsilon_n$	Neumann's number ( 1 for $n = 0$ and 2 for $n \geq 1$ )
$J_n(x)$	Bessel function of the first kind of order $n$ and argument $x$
$H_n(x)$	Hankel function of the second kind of order $n$ and argument $x$
$(\rho_0, \phi_0)$	position of the line source
$\hat{n}$	outward unit vector normal to a conducting surface
$\hat{\rho}$	unit vector in the $\rho$ direction

$\hat{\phi}$	unit vector in the $\phi$ direction
$\vec{H}^t$	total magnetic field vector
$H_\rho$	$\rho$ component of the magnetic field vector
$H_\phi$	$\phi$ component of the magnetic field vector
$J_p$	$z$ directed linear current density due to a plane wave incident
$a$	radius of a circular cylinder; radius of rounding of a rounded wedge
$J_l$	$z$ directed linear current density due to a line source field
$\gamma$	interior wedge angle
$E_p^{tW}$	total field of a plane wave incident in the presence of a sharp wedge
$E_l^{tW}$	total field of a line source field in the presence of a sharp wedge
$J^{UW}$	$z$ directed linear current density on the upper surface of a sharp wedge
$J^{LW}$	$z$ directed linear current density on the lower surface of a sharp wedge
$J_p^{UW}$	$z$ directed linear current density on the upper surface of a sharp wedge due to a plane wave incident
$J_p^{LW}$	$z$ directed linear current density on the lower surface of a sharp wedge due to a plane wave incident
$J_l^{UW}$	$z$ directed linear current density on the upper surface of a sharp wedge due to a line source field
$J_l^{LW}$	$z$ directed linear current density on the lower surface of a sharp wedge due to a line source field
$E_{PO}^S$	scattered field component due to the physical optic current on the top surface of a wedge

$r$	radius of a conducting or dielectric cap whose axis coincides with the wedge axis
$E_p^{IC}$	component of the total field of a plane wave incident on a capped wedge due to the conducting cap.
$E_l^{IC}$	component of the total field of a line source field exciting a capped wedge due to the conducting cap.
$J_p^{UC}$	$z$ directed linear current density on the upper surface of a capped wedge due to a plane wave incident
$J_l^{UC}$	$z$ directed linear current density on the upper surface of a capped wedge due to a line source field
$J_p^{LC}$	$z$ directed linear current density on the lower surface of a capped wedge due to a plane wave incident
$J_l^{LC}$	$z$ directed linear current density on the lower surface of a capped wedge due to a line source field
$J_p^C$	$z$ directed linear current density on the cap surface of a capped wedge due to a plane wave incident
$J_l^C$	$z$ directed linear current density on the cap surface of a capped wedge due to a line source field
$J'$	total $z$ directed linear current density due to all infinite interactions between two cylindrical scatterers
$E'$	non-interaction field
$E''$	interaction field
$E^g$	geometrical optics field

$F(\phi)$	scattered or diffracted field pattern
$\sigma(\phi)$	scattering cross-section
$g^W$	Keller's wedge diffraction pattern of a sharp wedge due to a plane wave incident
$g^C$	component of the capped wedge diffraction pattern due to the conducting cap with a plane wave incident
$f^W$	Keller's wedge diffraction pattern of a sharp wedge due to a line source field
$f^C$	component of the capped wedge diffraction pattern due to the conducting cap with a line source excitation
$E^d$	total diffracted field
$T$	transmission coefficient of a double wedge
$E_p^{dW}$	diffracted field due to a plane wave incident on a sharp wedge
$E_l^{dW}$	diffracted field due to a line source field incident on a sharp wedge
$e_A$	edge of wedge $A$
$e_B$	edge of wedge $B$
$c_1$	intensity of an inhomogeneous line source at $e_B$
$c_2$	intensity of an inhomogeneous line source at $e_A$
$s_{12}$	physical distance between $e_A$ and $e_B$
$E^d$	total diffracted field
$g^D$	component of the capped wedge diffraction pattern due to the dielectric cap with a plane wave incident

- $f^D$  component of the capped wedge diffraction pattern due to the dielectric cap with a line source excitation
- $\epsilon_r$  relative permittivity of a dielectric cap or a dielectric cylinder
- $f_R$  scattered field pattern due to a rounded wedge due to a plane wave incident
- $E_S$  singly diffracted field
- $E_m$  multiply diffracted field
- $E_p^{SW}$  scattered field from a sharp wedge due to a plane wave incident
- $E_l^{SW}$  scattered field from a sharp wedge due to a line source field
- $E_p^{SC}$  scattered field from a cylindrical scatterer due to a plane wave incident
- $E_l^{SW}$  scattered field from a cylindrical scatterer due to a line source field
- $g_c$  scattered field pattern of a conducting circular cylinder due to a plane wave incident
- $f_c$  scattered field pattern from a conducting circular cylinder due to a line source field
- $g_d$  scattered field pattern of a dielectric circular cylinder due to an incident plane wave
- $f_d$  scattered field pattern of a dielectric circular cylinder due to a line source field
- $g_s$  scattered field pattern of a dielectric shell with inhomogeneous permittivity profiles due to an incident plane wave
- $f_s$  scattered field pattern of a dielectric shell with inhomogeneous permittivity profiles due to a line source field

$J'$	$z$ directed non-interaction linear current density
$J''$	$z$ directed interaction linear current density
$J^{PO}$	physical optics current due to a plane wave incident on an infinite conducting plane
$J^d$	$z$ directed diffraction linear current density
$E_p^r$	reflected wave from an infinite conducting plane due to a plane wave incident
$\rho_a$	outer radius of a dielectric shell
$\rho_b$	inner radius of a dielectric shell
$\alpha_m$	characteristic number of the Mathieu function
$ce_m$	cosine elliptic function of period $\pi$
$ce_{2m+1}$	cosine elliptic function of period $2\pi$
$W$	echo width of a cylindrical dielectric shell

## CHAPTER 1

### INTRODUCTION

The diffraction of a plane wave incident on a slit in an infinite conducting screen has received considerable attention due to its importance in optics and microwave applications. However, a comprehensive study of the diffraction characteristics by the aperture between two conducting semi-infinite planes or wedges is not available for practical applications, especially when a third scatterer is located at or near the aperture plane or when the edges of the half planes are not sharp. Since the slit is one of the special cases of the double wedge geometry, it is useful to consider the double wedge in the present investigation rather than the slit case.

There is a wide variety of geometries which fall under the double semi-infinite wedge problem. Some of these geometries are the parallel plate waveguide with and without flanges, slit and staggered parallel half planes or wedges. The ray optical method has been successfully employed for the analysis of propagating modes in parallel plate waveguides and horn antennas [1]. The radiation from parallel plate waveguide with right flanges was treated extensively using different methods. One of these methods was introduced by Nussenzvieg where the radiation problem is reduced to an infinite system of linear equations [2]. The linear system of equations is then solved using Neumann's iteration method where the initial step was evaluated by the Kirchhoff approximation. Following Nussenzvieg's analysis, the diffraction of the principal mode at the open end of a semi-infinite parallel plate waveguide terminated by an infinite plane flange was studied for narrow waveguide widths by Amaral and Vidal [3]. They computed the evanescent mode correction term to the reflection amplitude using three different asymptotic approximations. The geometrical theory of diffraction (GTD), originally proposed by Keller [4-8] was also used to



evaluate the coupling between  $TEM$  and  $TE_{01}$  modes of two parallel plate waveguide apertures where each waveguide was formed of two wedges [9]. Furthermore, the reflection coefficients of these modes at the aperture were analyzed for different wedge angles by Rudduk and Tsai [10]. On the other hand, the usefulness of high frequency methods in analyzing the radiation characteristics of a parallel flanged waveguide was extended by using the surface integration technique where the surface integral was obtained by Green's second identity [11]. A totally different approach for the diffraction of an H-polarized plane wave obliquely incident on a flanged parallel plate waveguide was presented by Henke et. al. [12]. They used discrete spectra of periodic functions inside the waveguide region and Mathieu functions in the half space. The solution is then obtained by matching the diffracted field components in the aperture plane. Reflection coefficient at the waveguide-horn junction (open end of a waveguide with infinite flanges) was studied by Hamid and Jull using the GTD [13,14]. Schwartz's iterative procedure of overlapping region was also employed by Iskander and Hamid to determine the scattering coefficients at the horn junction [15]. Furthermore, the coefficients of the scattering matrix describing transmission, reflection and conversion of modes at the junction were obtained asymptotically by Borovikov and Kaloshin [16].

With respect to the staggered parallel wedges geometry, an approximation to the attenuation of an incident wave due to single diffraction by the knife edges of double parallel wedges was presented in terms of the single knife edge diffraction coefficient by Wilkerson [17]. However, the multiply diffracted fields by the knife edges was expressed by Vogler as a multiple integral which can be transformed into series form for calculation purposes [18]. More recently a new ray approximation for calculating the diffraction attenuation due to several knife edges was derived by Whittaker using the Fresnel approximation [19]. Asymptotic and experimental results of the radiation pattern of a slotted-waveguide antenna with wedges were also reported by Borovikov and Narbut in terms of a generalized Fresnel integral [20].

Tiberio and Kouyoumjian used a uniform extension to the GTD (namely the uniform theory of diffraction (UTD) [21] along with the modified slope diffraction (MSD) [22]) to determine the contribution from the doubly diffracted ray due to a pair of staggered wedges with parallel edges [23,24]. In this geometry the edge of one wedge is illuminated by the shadow boundary field of the other edge, whereas the original illumination was considered plane, cylindrical or spherical wave. The diffraction by an infinite set of parallel half planes was also investigated by Luneburg and Hurd, where in one case the total field on each plate vanishes on one side and the normal derivative vanishes on the other side [25], while in other case the total field or its normal derivative vanishes on alternative half planes [26]. It should be pointed out that the multiple diffraction by perfectly conducting parallel half planes has been the subject of intensive research due to its usefulness in modeling a waveguide array which can be built by a number of parallel equi-spaced semiplanes orthogonal to the straight line joining their edges [27-32].

It is well known that an exact solution of the slit problem (double wedge of zero angle) can be found in terms of eigenfunction series of Mathieu functions [33-35], but its usefulness is limited to small slit widths because of the difficulty in tabulating the Mathieu functions and because of poor convergence of the series. Power series solutions in terms of the slit electrical width for narrow slit widths was reported by Bouwkamp [36]. For wide slits, Clemmow [37] and Karp and Russek [38] used the concept of edge currents, while Millar presented an asymptotic solution of the resulting integral equations by successive iterations [39]. A Wiener-Hopf treatment of the integral equation approach was given by Levine [40]. Clemmow proposed a plane wave spectrum representation of the first order diffracted field by a modified Wiener-Hopf method and formulated the second order diffraction by a slit in integral form [41,42]. Further, he derived approximate solutions for the narrow and wide slits. Keller and Karp proposed an alternative asymptotic approach based on the GTD for the diffraction by the aperture of a wide slit [5,43]. The method

they proposed provides physical insight into the mechanism of diffraction since the geometrical parameters dictate the paths of the propagating rays. Another advantage of this method lies in its simplicity as it employs elementary (trigonometric) functions for the far field calculations and the resulting asymptotic solution is comparable in accuracy with the infinite series solution resulting from using the boundary value approach for large aperture dimensions. The closely related problem of diffraction by a thick slit is also investigated in great detail in the literature using different approaches. Some of the reported methods are the Wiener-Hopf and the generalized scattering matrix techniques which were used by Kashyap and Hamid [44]. Although numerical methods are not suitable for semi-infinite scatterers, Morita was able to use the method of moments (MM) along with the current on an infinite conducting plane as *a priori* knowledge to study the diffraction of a plane wave by a two-dimensional aperture with arbitrary cross-section [45-47]. Furthermore, experimental investigations of the diffraction characteristics of a thick slit were reported by Hamid et. al. [48,49], but they are limited in number and scope.

The diffraction by a double wedge forming a slit type geometry was only investigated asymptotically by Teague and Zitron [50]. Their analysis is based on the Zitron and Karp approximation for the scattering by multiple cylinders [51]. It is obvious that further investigation is needed, especially when variations in the geometry are considered. One of the main objectives of this thesis is to show the relation between the double wedge geometry (wedge angle, shape of the wedge edge and separation between the two wedges relative to wavelength) and diffraction characteristics (induced surface currents, diffracted pattern, transmission coefficient, aperture field, etc.) for an incident plane wave. More important for engineering applications is the interdependence between the various variables. It is obvious that the absence of an exact solution for this problem corresponds to lack of knowledge of the exact edge-to-edge interaction mechanism and the resulting exact field distribution on the aperture plane. Therefore, a novel technique based on the spectrum of cylindrical waves

(CWS) will be developed in Chapter 2 to solve the problem of scattering by multiple bodies. The CWS technique is first applied to the problem of scattering by two parallel conducting cylinders to verify its validity. Then the diffraction by two semi-infinite wedges is attempted for wedges with sharp as well as cylindrically capped edges.

In view of the advantages of using dielectric inserts to improve the behavior of aperture antennas [52], asymptotic solutions for the loaded aperture of a wide double wedge are presented in Chapter 3. These inserts are introduced in order to control the effect of edge-to-edge interaction on the total diffracted field by placing an additional cylindrical scatterer near or at the aperture plane. This scatterer is chosen to be a circular conducting cylinder, a circular homogeneous dielectric cylinder or a circular dielectric shell with inhomogeneous permittivity profiles. In addition the effects of rounding or cylindrically capping the sharp edges of the two wedges on the diffraction characteristics are also presented. It is worth mentioning that the main asymptotic solution in Chapter 3 is based on an extension of the Karp and Russek [38] technique to the diffraction by a wide slit to handle the problem of scattering by three different cylindrical objects (dielectric and/or conducting). Keller's ray technique for the diffraction by a slit in a perfectly conducting screen [5], is also used in some geometries to derive alternative simple expressions for the diffracted fields and the transmission coefficient.

Since there has been no comprehensive solution to cover the entire scope of geometrical possibilities of a double wedge in a simple analytical form and to further check the CWS results for narrow separations between the two wedges, a numerical method based on modification of the MM for the scattering by two cylindrical scatterers is investigated in Chapter 4. The method is verified by comparing the numerical results for some special cases, namely two parallel cylinders, thin slit and thick slit with previously published data. Furthermore, the diffraction characteristics of a double truncated and capped wedge are presented.

Chapter 5 summarizes the general conclusions of this thesis and points out the areas of future research. In particular, the possibility of partial cancellation of the edge diffraction terms is suggested through an active technique involving a line source located near the edge of each wedge.

## CHAPTER 2

### *RIGOROUS SOLUTION BY THE CYLINDRICAL WAVE SPECTRUM TECHNIQUE*

The two body scattering problem is a special case of the multiple body scattering problem and is encountered in a variety of engineering applications. For example, the solution may be applied to antenna coupling, aperture arrays and grid simulation of reflector antennas and many more. An exact solution for the scattering problem is usually obtained using analytical techniques which involve the boundary value approach. This is only useful if the geometry of the bodies permits separation of variables in the wave equation and frequently when the size and separation between the bodies are of the order of the wavelength. Various analytical and numerical methods have been developed for finding solutions to multiple scattering problems. However, the great majority of these techniques is restricted to different approximations, such as the low frequency (Rayleigh) or high frequency approximations. The non-uniform GTD is useful for large bodies with large separations although it suffers when the bodies become too close to one another or complex in shape (bodies containing sharp points, or curves with small radii of curvature such as edges and corners) or when the contribution of the geometrical shadow regions becomes important [8]. On the other hand the MM is most useful for small bodies and relatively small separations; however the memory size needed to store and invert the generated impedance matrix becomes unmanageable as the size and complexity of the problem increases. Therefore successive scattering in the frequency domain may be considered the most logical approach to determine the total scattered field due to multiple bodies. Previous attempts to solve the multiple scattering problem by successive scattering assume plane or cylindrical waves or combination of plane waves and their

derivatives (with respect to incident and observation angles) in order to account more accurately for the interaction between the bodies. Unfortunately these methods tend to fail when the separation distance approaches zero as the wave front of the interaction becomes more and more complex. This problem can be avoided by adopting a different approach which consists of first evaluating the exact current distribution initially induced on a sheet which coincides with the surface of each body (due to a specified source) prior to taking interaction into account. If the nature of the body and the source are such that there is an exact solution for the initial current distribution on each body due to the given source, then the multiple interaction process can in principle be treated exactly resulting in a series where each term accounts for one interaction. This is achieved by employing the solution for the scattering of either body by a point or a line source field. Thus if the initial current sheet is viewed as an array of infinitesimal point or line sources, then each order of interaction can be expressed as an integral over these sources with the integrand corresponding to a solution for a single point or line source, and the integral designated as a spherical wave spectrum (SWS) or a cylindrical wave spectrum (CWS), respectively. Theoretically the multiple interaction problem reduces to the computation of an infinite number of terms each involving a spectrum type integral. It is obvious that in two-dimensional scattering problems, the point source array reduces to line source array in the same manner as aperture diffraction is computed by Huygens' principle for apertures of infinite extent in one dimension.

In this chapter an iterative scattering is developed where in each iteration a cylindrical wave spectrum (CWS), due to induced Huygens type line sources on the scattering surface and emanating from each object towards the other, is computed. This is employed iteratively in order to determine the additional interaction field due to multiple scattering and consequently the modified surface current distribution on all the scattering surfaces. Once the final induced surface current distributions are



known, the fields can be evaluated using well known relations. This technique does not suffer from any limitation on separation and can handle small as well as large scatterers, provided that the scattering by a single body in isolation is obtained in a rigorous form. The method is applied specifically here to two parallel circular conducting cylinders and two semi-infinite conducting wedges, whereas it can in fact be used for any number of similar or different scatterers.

In the past the problem of scattering by two or multiple circular conducting cylinders has received great attention in the literature. Row considered the scattering from an arbitrary array of parallel cylinders in general and two identical conducting cylinders in particular where an infinite matrix equation is involved [53]. He considered a finite number of equations as an approximation and solved the matrix equation numerically using a diagonal approximation. Twersky employed an iterative procedure to obtain closed form solutions for several cases by retaining only the largest terms involving the separation between the scatterers in each order of scattering [54]. Some of these forms are for two scatterers with radii and spacing small compared to wavelength, for two arbitrary cylinders with each in the far field of the other and for multiple equi-spaced coplanar cylinders (a finite grating) when end effects are neglected. Millar considered the two cases of parallel and perpendicular polarization for a row of perfectly conducting cylinders of arbitrary cross-sectional shape [55]. For two cylinders and parallel polarization, his closed form approximations for the multiple scattering coefficients are identical with those forms given by Twersky for two arbitrary scatterers. Zitron and Karp showed that the diffraction by two parallel cylinders of arbitrary shape can be expressed in terms of the unperturbed scattering amplitudes of the individual cylinders [51]. The formula is valid when the spacing between the scatterers is large compared to their dimensions. It involves derivatives of the scattering amplitudes with respect to the angles of incidence and observation. A formulation based on multipole expansion of the



scattered field due to two or three parallel conducting cylinders is presented by Howarth and Pavlasek [56,57]. They also evaluated the diffracted field and the induced current on the surface of two cylinders and verified their numerical results experimentally. Hongo gave a comparison between two asymptotic approximations for the multiple scattering by two circular conducting cylinders [58]. A boundary value solution was also derived by Young and Bertrand for the scattering by two parallel cylinders [59]. Their solution includes all terms of multiple scattering between the two cylinders. Ragheb and Hamid used Twersky's technique for the scattering by  $N$  parallel cylinders to develop an infinite matrix equation which they solved numerically after truncation [60]. They also extended one of the asymptotic solutions used by Hongo for the scattering by two cylinders to the scattering by multiple cylinders. The scattering by parallel conducting cylinders of arbitrary cross-section was also investigated numerically by Andreasen [45] and Mullin et al. [61] using two different methods, while the problem is usually reduced to a solution of integral equations which result from applying the boundary conditions in terms of the unknown induced surface currents. The numerical evaluation of the integral equations is usually carried out using the method of moments [45,46]. More recently a modification to the method of moments is presented for the case of scattering by two circular cylinders [62,63].

## 2.1 Computation of the induced surface currents

Consider the E-polarization case (TM with respect to  $z$  axis) where the electric field has a  $z$  component only with all vectors independent of  $z$  of the circular cylindrical coordinates  $(\rho, \phi, z)$ , while the time dependence  $e^{j\omega t}$  is considered and suppressed throughout. For a plane wave of unit amplitude incident on two parallel cylindrical scatterers at angle  $\phi_0$  with respect to the negative  $x$  axis, the incident field  $E_p^i$  is given by

$$E_p^i = e^{j k \rho \cos(\phi - \phi_0)} \quad (2-1)$$

where  $k$  is the wave number  $2\pi/\lambda$ ,  $\lambda$  is the wavelength and the subscript  $p$  refers to a plane wave. The boundary condition on a conducting surface is

$$E_p^i + E^S = 0 \quad (2-2)$$

while the scattered field  $E^S$  is given by

$$E^S = - \frac{\eta k}{4} \int_C J(\rho') H_0(k|\bar{\rho} - \bar{\rho}'|) dC \quad (2-3)$$

where  $C$  is the total contour of the cross-section of the scatterer, the superscript  $S$  refers to the scattered field,  $\eta$  is the intrinsic impedance of free space and  $J$  is the  $z$  directed linear surface current.  $H_0(x)$  is the Hankel function of order zero and argument  $x$  while the superscript (2) is implied and suppressed throughout. It is also known that the field of any infinite line source of unit amplitude located at  $(\rho_0, \phi_0)$  and parallel to the  $z$  axis can be expressed in terms of the Hankel function as follows [64]:

$$E_l^i = - \frac{\eta k}{4} H_0(kR) \quad (2-4)$$

where  $R$  is the distance between the line source and the field point and the subscript  $l$  refers to the line source.

For the scattering by two bodies one may consider each of the two bodies as excited by the original incident field and the scattered field which results from the other body due to the original incident field where only first order interaction between the two bodies is assumed. For higher orders of interaction, the resulting scattered field from previous order is considered as a new excitation for the other body. In each interaction the basic formula that describes the scattered field is given by Eq. (2-3), where the Hankel function in the integrand represents a cylindrical wave of normalized intensity  $J$ . In view of Eqs. (2-3) and (2-4) we notice that the

scattered field in each iteration can be represented as an integral or sum over cylindrical waves with different amplitudes and origins. Each of these waves is incident on the second scatterer and produce additional scattered fields. It is clear that the application of this method requires knowledge of the induced currents on the surfaces under consideration due to an incident plane wave and a line source field separately. For geometries which consist of scatterers like half planes, circular or elliptic cylinders, wedges or any combinations, it is always possible to use the exact expressions for the surface currents since there are exact solutions for the scattering by each of these individual bodies in isolation. In fact the proposed technique is still applicable to bodies of arbitrary cross-sectional shape once the surface currents are obtained using any appropriate method [45,46,61,65-67].

As an example, consider a perfectly conducting circular cylinder defined by the surface  $\rho = a$  with its axis coinciding with the  $z$  axis of the circular cylindrical coordinates  $(\rho, \phi, z)$ . The exact expression for the scattered field due to an incident plane wave and a line source field (defined by Eqs. (2-1) and (2-4), respectively) are given by  $E_p^S$  and  $E_l^S$ , respectively [64] and can be rewritten after some mathematical manipulations in the following modified form

$$E_p^S = - \sum_{n=0}^{\infty} \epsilon_n j^n \frac{J_n(ka)}{H_n(ka)} H_n(k\rho) \cos n(\phi - \phi_0) \quad (2-5)$$

$$E_l^S = \frac{\eta k}{4} \sum_{n=0}^{\infty} \epsilon_n \frac{J_n(ka)}{H_n(ka)} H_n(k\rho_0) H_n(k\rho) \cos n(\phi - \phi_0) \quad (2-6)$$

where Neumann's number  $\epsilon_n$  is 1 for  $n = 0$  and 2 for  $n > 0$ ,  $J_n(x)$  is the Bessel function of the first kind of order  $n$  and argument  $x$  and  $H_n(x)$  is the Hankel function of the second kind of order  $n$  and argument  $x$ .

From the boundary conditions the electrical surface current on a conducting surface  $\bar{J}$  can be given in terms of the total magnetic field  $\bar{H}^t$  on the surface as

follows :

$$\vec{J} = \hat{n} \times \vec{H}' \quad (2-7)$$

where  $\hat{n}$  is the outward unit vector normal to the conducting surface and the total magnetic field in this case is

$$\vec{H}' = H_\rho \hat{\rho} + H_\phi \hat{\phi} . \quad (2-8)$$

The electric surface current can then be determined using Eq. (2-7) where  $\hat{n}$  is replaced by the outward unit vector normal to the cylinder surface, i.e.  $\hat{\rho}$ . Since

$$H_\phi = \frac{1}{j\eta k} \frac{\partial E'}{\partial \rho} \quad (2-9)$$

where  $E'$  denotes the total field ( $E^i + E^S$ ) due to the original incident field, the exact expression for the  $z$  directed linear current density due to an incident plane wave  $J_p$  is given by

$$J_p = \frac{2}{\pi \eta k a} \sum_{n=0}^{\infty} \epsilon_n j^n \frac{\cos n(\phi - \phi_0)}{H_n(ka)} . \quad (2-10)$$

For a line source field defined by Eq. (2-4), the corresponding  $z$  directed linear current density  $J_l$  is derived using Eqs. (2-4), (2-6), (2-7), (2-9) and the Wronskians of Bessel functions. The result is

$$J_l = - \frac{1}{2 \pi a} \sum_{n=0}^{\infty} \epsilon_n \frac{H_n(k\rho_0)}{H_n(ka)} \cos n(\phi - \phi_0) . \quad (2-11)$$

Another example is a sharp wedge defined by two half-planes at  $\phi = 0$  and  $\phi = 2\pi - \gamma$  intersecting along the  $z$  axis. In order to find the exact current distribution on the surface of the wedge due to an incident plane wave or line source field, we use the exact expressions for the total field  $E'_\rho$  and  $E'_l$ , respectively, i.e.

$$E_p^{tW} = \frac{4}{\nu} \sum_{n=1}^{\infty} j^{n/\nu} J_{\frac{n}{\nu}}(k\rho) \sin\left(\frac{n}{\nu}\phi\right) \sin\left(\frac{n}{\nu}\phi_0\right) \quad (2-12)$$

$$E_l^{tW} = \begin{cases} \frac{-\eta k}{\nu} \sum_{n=1}^{\infty} J_{\frac{n}{\nu}}(k\rho_0) H_{\frac{n}{\nu}}(k\rho) \sin\left(\frac{n}{\nu}\phi\right) \sin\left(\frac{n}{\nu}\phi_0\right) & , \rho > \rho_0 \\ \frac{-\eta k}{\nu} \sum_{n=1}^{\infty} J_{\frac{n}{\nu}}(k\rho) H_{\frac{n}{\nu}}(k\rho_0) \sin\left(\frac{n}{\nu}\phi\right) \sin\left(\frac{n}{\nu}\phi_0\right) & , \rho < \rho_0 \end{cases} \quad (2-13)$$

where the superscripts  $t$  and  $W$  refer to the total field and a sharp wedge, respectively, and

$$\nu = (2\pi - \gamma) / \pi. \quad (2-14)$$

Since the outward unit vector normal to the wedge surface  $\hat{n}$  is defined by

$$\hat{n} = \begin{cases} \hat{\phi} & , \phi = 0 \\ -\hat{\phi} & , \phi = 2\pi - \gamma \end{cases} \quad (2-15)$$

the electrical surface current can be written using Eqs. (2-7), (2-8) and (2-15) in the following form

$$\left. \begin{aligned} J^{UW} &= -H_\rho & , \phi &= 0 \\ J^{LW} &= H_\rho & , \phi &= 2\pi - \gamma \end{aligned} \right\} \quad (2-16)$$

where the  $J^{UW}$  and  $J^{LW}$  are the  $z$  directed surface currents and the superscripts  $U$  and  $L$  refer to the upper and lower surfaces of the wedge, respectively. Furthermore, we have

$$H_\rho = -\frac{1}{j\eta k\rho} \frac{\partial E^{tW}}{\partial \phi}. \quad (2-17)$$

Thus, using Eqs. (2-12) and (2-13), the exact expressions for the surface currents reduce to

$$\left. \begin{aligned} J_p^{UW} &= \frac{4}{j\eta k \rho v^2} \sum_{n=1}^{\infty} n j^{n/v} J_{\frac{n}{v}}(k\rho) \sin\left(\frac{n}{v}\phi_0\right) \\ J_p^{LW} &= \frac{-4}{j\eta k \rho v^2} \sum_{n=1}^{\infty} n (-1)^n j^{n/v} J_{\frac{n}{v}}(k\rho) \sin\left(\frac{n}{v}\phi_0\right) \end{aligned} \right\} \quad (2-18)$$

$$\left. \begin{aligned} J_l^{UW} &= \frac{j}{\rho v^2} \sum_{n=1}^{\infty} n J_{\frac{n}{v}}(k\rho_0) H_{\frac{n}{v}}(k\rho) \sin\left(\frac{n}{v}\phi_0\right) \\ J_l^{LW} &= -\frac{j}{\rho v^2} \sum_{n=1}^{\infty} n (-1)^n J_{\frac{n}{v}}(k\rho_0) H_{\frac{n}{v}}(k\rho) \sin\left(\frac{n}{v}\phi_0\right) \end{aligned} \right\}, \quad \rho_0 < \rho \quad (2-19)$$

For  $\rho_0 > \rho$ , the arguments of the Bessel and Hankel functions in Eq. (2-19) are interchanged. To avoid the numerical difficulty which would arise if we use the surface currents on the upper surface of each of the two wedges, we let  $J_p^{UW}$  be written as a sum of the physical optical current  $J^{PO}$  plus the edge diffraction current  $J^d$ . Obviously  $J^d$  and  $J_p^{LW}$  decay as the distance from the wedge edge increases until they finally vanish at infinity. Moreover, the scattered field component,  $E_{PO}^S$ , from a single wedge due to  $J^{PO}$  can be written for a normally incident plane wave as

$$E_{PO}^S = -\frac{k}{2} \int_0^{\infty} H_0(k|\bar{\rho} - \bar{x}|) dx. \quad (2-20)$$

In terms of the local coordinates of the wedge, it is obvious that  $E_{PO}^S$  is zero in the far region to the left of the  $x = 0$  plane, while in the far region to the right of the  $x = 0$  plane and for  $y < 0$ ,  $E_{PO}^S$  represents the wave which completely cancels the incident wave, while for  $y > 0$  it corresponds to the wave that would be reflected from an infinite conducting plane. Since we are interested in the near as well as the far fields, the value of  $E_{PO}^S$  is investigated at the position of the edge of the opposite wedge. Since  $E_{PO}^S$  can be expressed in a simple closed form in the near field [68,69], therefore in the presence of a second wedge (see Fig. 2-1)  $E_{PO}^S$  is replaced by a line source located at the wedge edge. The intensity  $C_0$  of that line source is found to be

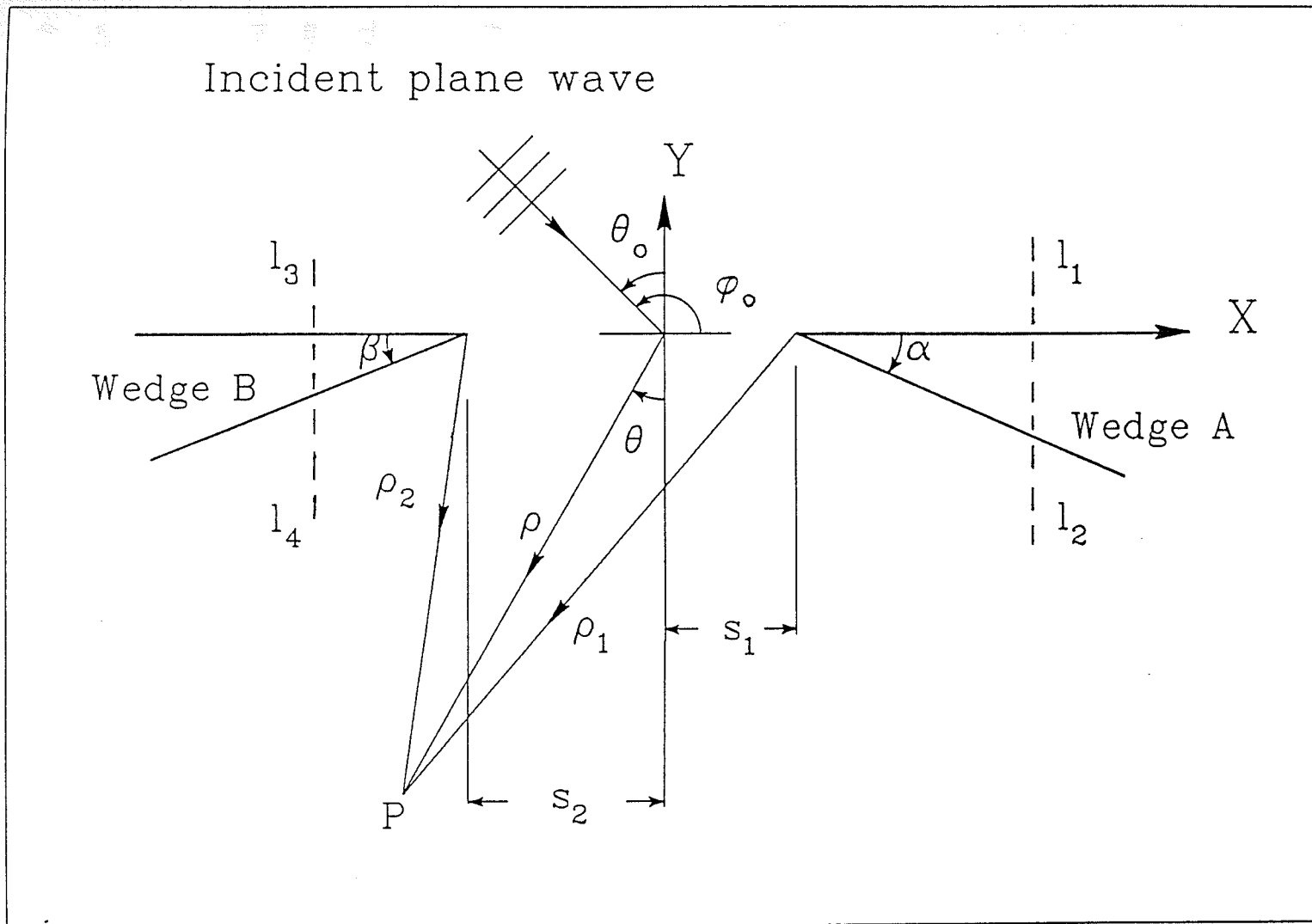


Fig. 2-1 : Double wedge geometry.



(see Appendix A)

$$C_0 = \left[ \frac{2}{\eta k} - \frac{2}{\eta} \int_0^{s_{12}} H_0(kt) dt \right] / H_0(ks_{12}) \quad (2-21)$$

in order to represent  $E_{PO}^S$  at the edge of the opposite wedge.

For a single wedge with cylindrical cap of radius  $r$  and axis coinciding with the wedge edge, the total fields  $E_p'$  or  $E_l'$  due to a plane wave incident or a line source field, respectively, are given exactly by

$$E_p' = E_p'^W + E_p'^C \quad (2-22)$$

$$E_l' = E_l'^W + E_l'^C \quad (2-23)$$

where  $E_p'^W$  and  $E_l'^W$  are given by Eqs. (2-12) and (2-13), respectively, and

$$E_p'^C = \frac{-4}{v} \sum_{n=1}^{\infty} j^{\frac{n}{v}} H_{\frac{n}{v}}(k\rho) \frac{J_{\frac{n}{v}}(kr)}{H_{\frac{n}{v}}(kr)} \sin\left(\frac{n}{v}\phi\right) \sin\left(\frac{n}{v}\phi_0\right) \quad , \rho \geq r \quad (2-24)$$

$$E_l'^C = \frac{\eta k}{v} \sum_{n=1}^{\infty} H_{\frac{n}{v}}(k\rho_0) \frac{J_{\frac{n}{v}}(kr)}{H_{\frac{n}{v}}(kr)} H_{\frac{n}{v}}(k\rho) \sin\left(\frac{n}{v}\phi\right) \sin\left(\frac{n}{v}\phi\right) \quad , \rho \geq r. \quad (2-25)$$

The surface of the capped wedge,  $S_{CW}$ , is composed of two plane surfaces say  $S_U$  and  $S_L$  and the cylinder cap surface  $S_C$  as shown in Fig. 2-2.  $S_{CW}$  may be characterized by the following relations

$$S_{CW} = S_U + S_C + S_L \quad (2-26)$$

where for  $S_U$ ,  $\phi = 0^\circ$ ,  $\rho > r$ , for  $S_C$ ,  $\rho = r$ ,  $0 \leq \phi \leq 2\pi - \gamma$  and for  $S_L$ ,  $\phi = 2\pi - \gamma$ ,  $\rho > r$ . The unit vectors normal to the surfaces  $S_U$ ,  $S_C$  and  $S_L$  are then defined by  $\hat{n}_U$ ,  $\hat{n}_C$  and  $\hat{n}_L$ , respectively, and given by



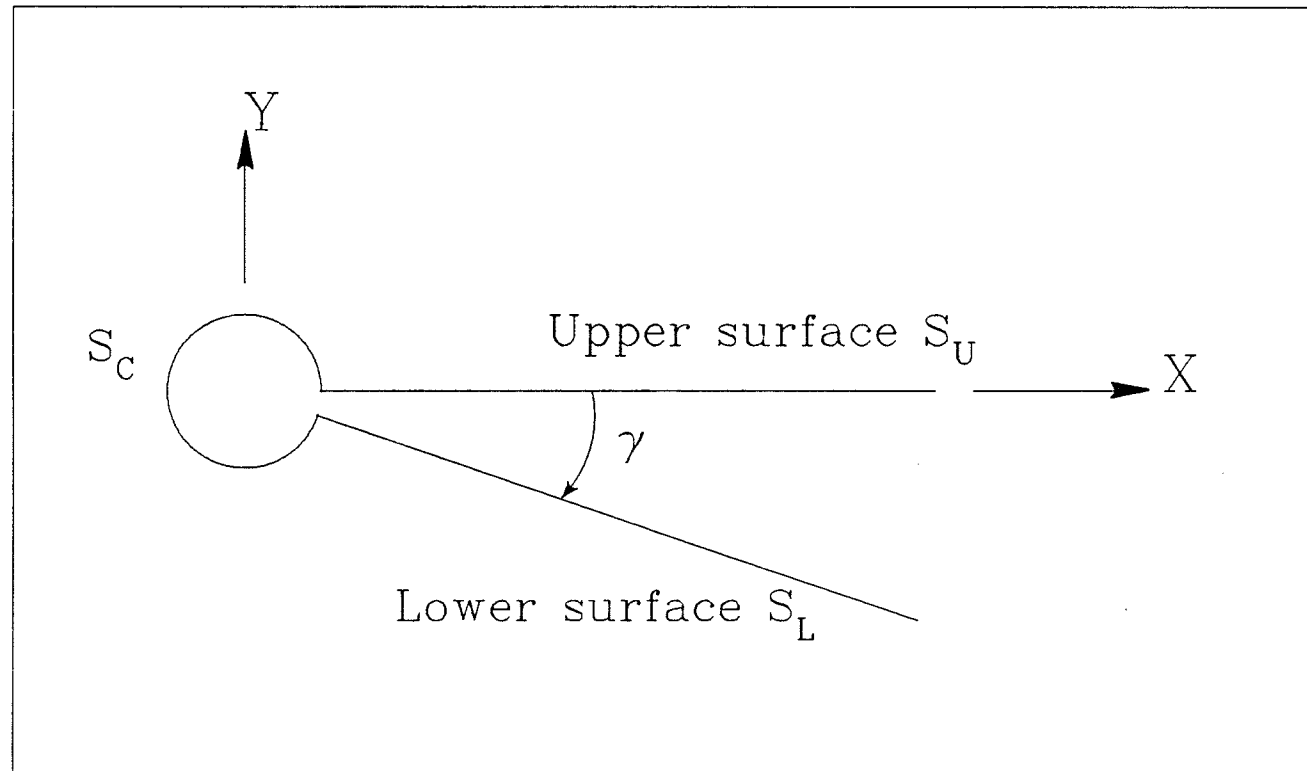


Fig. 2-2 : Capped wedge geometry.

$$\left. \begin{aligned} \hat{n}_U &= \hat{\phi} \\ \hat{n}_C &= \hat{\rho} \\ \hat{n}_L &= -\hat{\phi} \end{aligned} \right\} \quad (2-27)$$

On  $S_U$ , the electric surface current due to a plane wave or a line source field are denoted by  $J_p^U$  and  $J_l^U$ , respectively, and are given by

$$J_p^U = J_p^{UW} + J_p^{UC} \quad (2-28)$$

and

$$J_l^U = J_l^{UW} + J_l^{UC} \quad (2-29)$$

Similarly on  $S_L$ , we have

$$J_p^L = J_p^{LW} + J_p^{LC} \quad (2-30)$$

and

$$J_l^L = J_l^{LW} + J_l^{LC} \quad (2-31)$$

where  $J_p^{UW}$ ,  $J_l^{UW}$ ,  $J_p^{LW}$  and  $J_l^{LW}$  are given by Eqs. (2-18) and (2-19), respectively, while

$$J_p^{UC} = \frac{-4}{j \eta k \rho v^2} \sum_{n=1}^{\infty} n j^{\frac{n}{v}} H_{\frac{n}{v}}(k \rho) \frac{J_{\frac{n}{v}}(kr)}{H_{\frac{n}{v}}(kr)} \sin\left(\frac{n}{v} \phi_0\right) \quad (2-32)$$

$$J_l^{UC} = \frac{1}{j \rho v^2} \sum_{n=1}^{\infty} n H_{\frac{n}{v}}(k \rho_0) H_{\frac{n}{v}}(k \rho) \frac{J_{\frac{n}{v}}(kr)}{H_{\frac{n}{v}}(kr)} \sin\left(\frac{n}{v} \phi_0\right) \quad (2-33)$$

$$J_p^{LC} = \frac{4}{j \eta k \rho v^2} \sum_{n=1}^{\infty} n (-1)^n j^{\frac{n}{v}} H_{\frac{n}{v}}(k \rho) \frac{J_{\frac{n}{v}}(kr)}{H_{\frac{n}{v}}(kr)} \sin\left(\frac{n}{v} \phi_0\right) \quad (2-34)$$

$$J_l^{LC} = \frac{1}{j\rho v^2} \sum_{n=1}^{\infty} n (-1)^n H_{\frac{n}{v}}(k\rho_0) H_{\frac{n}{v}}(k\rho) \frac{J_{\frac{n}{v}}(kr)}{H_{\frac{n}{v}}(kr)} \sin\left(\frac{n}{v}\phi_0\right). \quad (2-35)$$

However, for the current distribution on  $S_C$  due to a plane wave incident, we have

$$J_p^C = \frac{8}{\eta kr \pi v} \sum_{n=1}^{\infty} \frac{j^{\frac{n}{v}}}{H_{\frac{n}{v}}(kr)} \sin\left(\frac{n}{v}\phi\right) \sin\left(\frac{n}{v}\phi_0\right) \quad (2-36)$$

whereas for a line source field, the corresponding expression of the surface current is given by

$$J_l^C = \frac{-2}{\pi r v} \sum_{n=1}^{\infty} \frac{H_{\frac{n}{v}}(k\rho_0)}{H_{\frac{n}{v}}(kr)} \sin\left(\frac{n}{v}\phi\right) \sin\left(\frac{n}{v}\phi_0\right). \quad (2-37)$$

Furthermore, it should be noted that the upper limit of the integral in Eq. (2-21) which is denoted by  $s_{12}$  for a double sharp wedge geometry, should be replaced by  $s_{12} + c$  for the double capped wedge case.

In this representation the final induced surface current  $J'$  is given by

$$J' = J_p + \sum_{N=1}^{\infty} J_l^N \quad (2-38)$$

where  $J_p$  represents the surface current due to the original incident wave,  $J_l^N$  represents the additional surface current due to the previously induced surface current on the other body and the superscript  $N$  denotes the order of interaction. In other words  $J_l^1$  is evaluated from the scattered field due to the initial surface currents  $J_p$  produced by the incident plane wave times an appropriate phase difference according to  $\phi_0$ , whereas  $J_l^2, J_l^3, \dots$  on one body are due to  $J_l^1, J_l^2, \dots$  on the other body.

## 2.2 Far field pattern

A convenient representation of the total field can be written as

$$E' = E' + E'' \quad (2-39)$$

where the non-interaction field  $E'$  represents the geometrical optics field  $E^s$  plus the diffracted fields (or the incident field  $E^i$  plus the scattered fields) when each body is excited by the original incident field separately. The interaction field  $E''$  can be determined once the total surface current  $J'$  is evaluated. Referring to Fig. 2-3,  $E'$  due to two parallel cylinders of radii  $a$  and  $b$  can be given exactly by

$$E' = E^i - \sum_{n=0}^{\infty} \epsilon_n j^n \left[ e^{+jks_1 \cos \phi_0} \frac{J_n(ka)}{H_n(ka)} H_n(k\rho_1) \cos n(\phi_1 - \phi_0) \right. \\ \left. + e^{-jks_2 \cos \phi_0} \frac{J_n(kb)}{H_n(kb)} H_n(k\rho_2) \cos n(\phi_2 - \phi_0) \right] \quad (2-40)$$

while  $E''$  may be written as

$$E'' = \frac{\eta k}{4} \left\{ \sum_{n=0}^{\infty} \epsilon_n \frac{J_n(kb)}{H_n(kb)} H_n(k\rho_2) \int_0^{2\pi} J'(\phi_1) \cos n(\phi_2 - q_2) H_0(k\rho_2) d\phi_1 \right. \\ \left. + \sum_{n=0}^{\infty} \epsilon_n \frac{J_n(ka)}{H_n(ka)} H_n(k\rho_1) \int_0^{2\pi} J'(\phi_2) \cos n(\phi_1 - q_1) H_0(k\rho_1) d\phi_2 \right\} \quad (2-41)$$

where  $J'$  is given by Eq. (2-38) and

$$p_1 = \sqrt{(s_{12} - b \cos \phi_2)^2 + (b \sin \phi_2)^2} \quad (2-42)$$

$$q_1 = \pi - \tan^{-1} \frac{b \sin \phi_2}{s_{12} - b \cos \phi_2} \quad (2-43)$$

$$p_2 = \sqrt{(s_{12} - a \cos \phi_1)^2 + (a \sin \phi_1)^2} \quad (2-44)$$

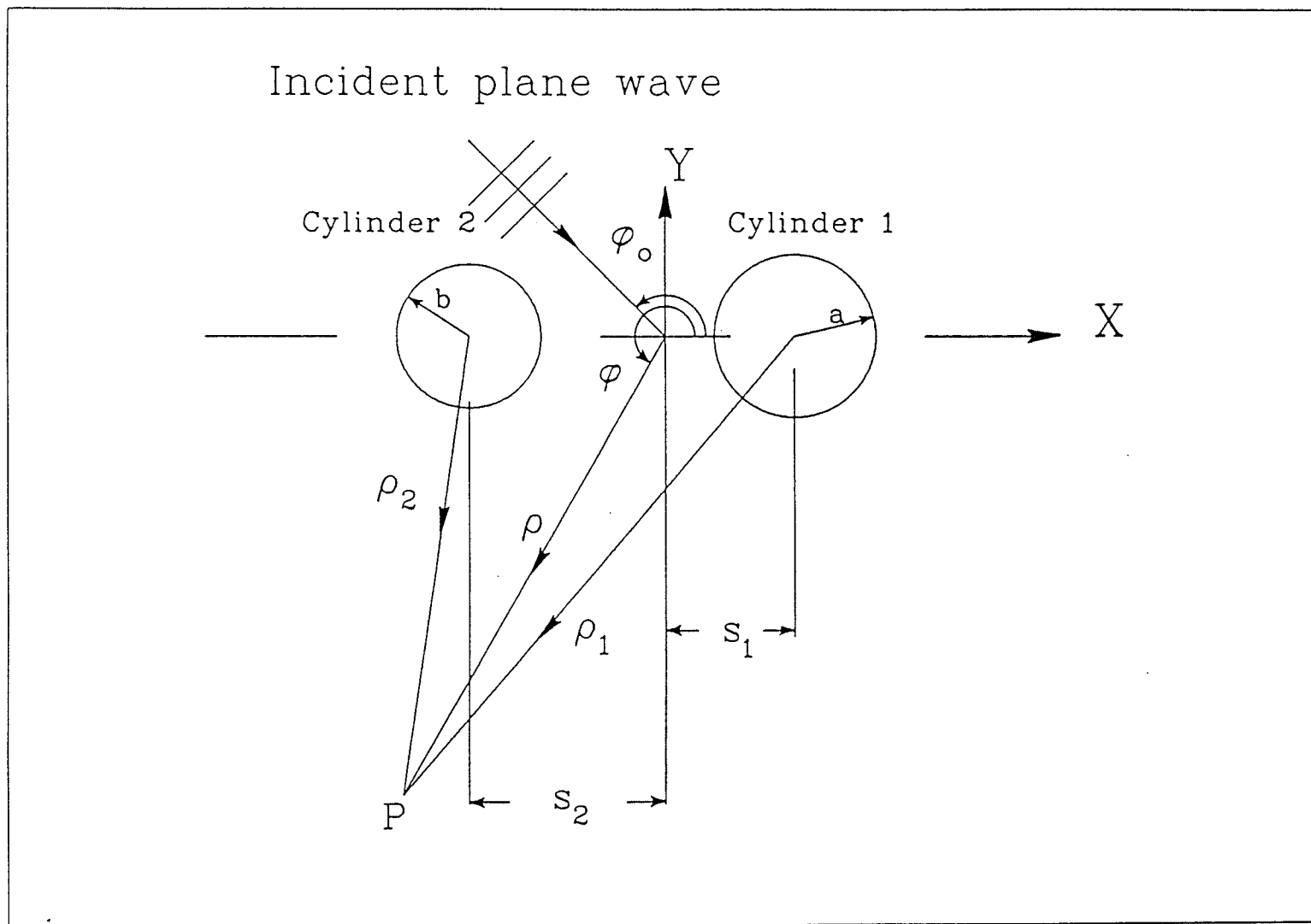


Fig. 2-3 : Two parallel conducting cylinders geometry.

$$q_2 = \pi - \tan^{-1} \frac{a \sin \phi_1}{s_{12} - a \cos \phi_1} \quad (2-45)$$

$$s_{12} = s_1 + s_2. \quad (2-46)$$

Upon using the far field approximations

$$\rho_1 \approx \rho - s_1 \cos \phi \quad (2-47)$$

$$\rho_2 \approx \rho + s_2 \cos \phi \quad (2-48)$$

$$\phi_1 = \phi_2 \approx \phi \quad (2-49)$$

the scattered field pattern  $F(\phi)$  of the two parallel cylinders can be conveniently expressed as

$$E^S(\rho, \phi) = \frac{e^{-jk\rho}}{\sqrt{\pi k \rho}} F(\phi) \quad (2-50)$$

where  $F$  may represent the non-interaction scattered field pattern ( $E' - E^i$ ) or the  $E''$  pattern or the total scattered field pattern  $E^S$  (i.e.  $E' + E'' - E^i$ ).

The properties of plane wave scattering by any conducting cylindrical structure of infinite length along one of the coordinate axes are usually described in terms of the scattering cross-section which is denoted by  $\sigma$  and defined as follows [64]

$$\sigma(\phi) = \lim_{\rho \rightarrow \infty} 2\pi\rho \left| \frac{E^S(\rho, \phi)}{E^i} \right|^2 \quad (2-51)$$

From Eqs. (2-1) and (2-50), the scattering cross-section of the double cylinder geometry is given by

$$\sigma(\phi) = \frac{1}{\pi} |F(\phi)|^2. \quad (2-52)$$

For the double wedge geometry (see Fig. 2-1) the far non-interaction field can be determined using Keller's geometrical theory of diffraction for all observation points away from the shadow and reflection boundaries. Upon using the asymptotic expression of the diffracted field due to an incident plane wave on a conducting sharp wedge,  $E'$  can be written in the following form

$$E' = E^s + \frac{\pi}{2j} [ H_0(k\rho_1) e^{+jks_1 \cos \phi_0} g(\phi_1, \phi_{01}, \nu_1, r_1) + H_0(k\rho_2) e^{-jks_2 \cos \phi_0} g(\phi_2, \phi_{02}, \nu_2, r_2) ] \quad (2-53)$$

while the diffraction pattern function  $g$  is replaced by  $g^W$  or  $g^W + g^C$  for a sharp or capped wedge, respectively, where

$$g^W(\phi, \phi_0, \nu) = \frac{\sin(\pi/\nu)}{\pi\nu} \left\{ \left[ \cos\left(\frac{\pi}{\nu}\right) - \cos\left(\frac{\phi - \phi_0}{\nu}\right) \right]^{-1} - \left[ \cos\left(\frac{\pi}{\nu}\right) - \cos\left(\frac{\phi + \phi_0}{\nu}\right) \right]^{-1} \right\} \quad (2-54)$$

and

$$g^C(\phi, \phi_0, \nu, r) = \frac{-8j}{\pi\nu} \sum_{n=1}^{\infty} j \frac{2n}{\nu} \frac{J_n(kr)}{H_n(kr)} \sin\left(\frac{n}{\nu}\phi\right) \sin\left(\frac{n}{\nu}\phi_0\right). \quad (2-55)$$

Furthermore,  $\nu_1$  and  $\nu_2$  are defined by Eq. (2-14) except that  $\gamma$  equals  $\alpha$  or  $\beta$  for  $\nu_1$  or  $\nu_2$ , respectively and  $r_1$  and  $r_2$  are the radii of the cylindrical caps at the edges of the two wedges A and B, respectively.  $\phi_{01}$ ,  $\phi_{02}$  are the angles of the incident plane wave in terms of the local coordinates of the two wedges A and B, respectively.

For any far field point  $E''$  can be determined using Eqs. (2-3) and (2-13) and can be written as

$$E'' = - \frac{\eta k}{4} \left\{ H_0(k \rho_2) \int_{C_1} J'(\rho_1) f(\phi_2, \rho_2, q_2, \nu_2) d\rho_1 \right. \\ \left. + H_0(k \rho_1) \int_{C_2} J'(\rho_2) f(\phi_1, \rho_1, q_1, \nu_1) d\rho_2 \right\} \quad (2-56)$$

where for a sharp wedge

$$p_1 = \begin{cases} \rho_2 + s_{12} & , \phi_2 = 0 \\ \sqrt{(\rho_2 \cos \beta + s_{12})^2 + (\rho_2 \sin \beta)^2} & , \phi_2 = 2\pi - \beta \end{cases} \quad (2-57)$$

$$p_2 = \begin{cases} \rho_1 + s_{12} & , \phi_1 = 0 \\ \sqrt{(\rho_1 \cos \alpha + s_{12})^2 + (\rho_1 \sin \alpha)^2} & , \phi_1 = 2\pi - \alpha \end{cases} \quad (2-58)$$

$$q_1 = \begin{cases} \pi & , \phi_2 = 0 \\ \pi + \tan^{-1} \frac{\rho_2 \sin \beta}{\rho_2 \cos \beta + s_{12}} & , \phi_2 = 2\pi - \beta \end{cases} \quad (2-59)$$

$$q_2 = \begin{cases} \pi & , \phi_1 = 0 \\ \pi + \tan^{-1} \frac{\rho_1 \sin \alpha}{\rho_1 \cos \alpha + s_{12}} & , \phi_1 = 2\pi - \alpha \end{cases} \quad (2-60)$$

while  $f$  is given by  $f^W$  for a sharp wedge or by  $f^W + f^C$  for a capped wedge, whereas according to Appendix B, we have

$$f^W(\phi, \rho_0, \phi_0, \nu) = - e^{jk \rho_0 \cos(\phi - \phi_0)} \\ + \frac{4}{\nu} \sum_{n=1}^{\infty} j^{\frac{n}{\nu}} J_{\frac{n}{\nu}}(k \rho_0) \sin\left(\frac{n \phi}{\nu}\right) \sin\left(\frac{n \phi_0}{\nu}\right) \quad (2-61)$$

and



$$f^C(\phi, \rho_0, \phi_0, \nu, r) = \frac{-4}{\nu} \sum_{n=1}^{\infty} j^{\frac{n}{\nu}} \frac{J_{\frac{n}{\nu}}(kr)}{H_{\frac{n}{\nu}}(kr)} H_{\frac{n}{\nu}}(k\rho_0) \sin\left(\frac{n}{\nu}\phi\right) \sin\left(\frac{n}{\nu}\phi_0\right). \quad (2-62)$$

$C_1$  and  $C_2$  are finite parts of the semi-infinite cross-sectional contours of the two wedges A and B, respectively, on which  $J^d$  and  $J_p^L$  exist. It is to be noticed that  $J^d$  in Eq. (2-56) is given by Eq. (2-38) except that  $J_p$  is replaced by  $J^d$  and the assumed line source intensity  $C_0$  at the edge of the wedge. Hence, the total far diffracted field  $E^d$  from the two wedges ( $E' + E'' - E^s$ ) is completely determined and the far diffracted field pattern  $F(\phi)$  can be defined when the far diffracted field is expressed as

$$E^d(\rho, \phi) = \frac{e^{-jk\rho}}{\sqrt{\pi k\rho}} F(\phi). \quad (2-63)$$

As a result, the transmission coefficient  $T$  for a normally incident plane wave is given by

$$T = \text{Re}\left[(1-j) F\left(\frac{3\pi}{2}\right)\right]/ks_{12}. \quad (2-64)$$

### 2.3 Numerical examples

Due to the numerical limitations, the maximum number of interactions used in the following results is assumed the value 9, whereas the number of line sources per wavelength is chosen to be approximately 10 to give appropriate accuracy up to the third decimal point in the values of  $\sigma$  and  $T$  for the closest separation between the two wedges or cylinders. In Fig. 2-4, we present the total scattered field pattern due to a plane wave incident at angle  $\phi_0 = 90^\circ$  on two identical conducting parallel cylinders of radii  $ka = kb = 0.5$  and  $ks = 2$ . As shown in the figure the  $E^S$  pattern due to the CWS technique approaches the pattern due to the boundary value solution [59,60] as the number of interactions  $N$  increases. It is found that the maximum

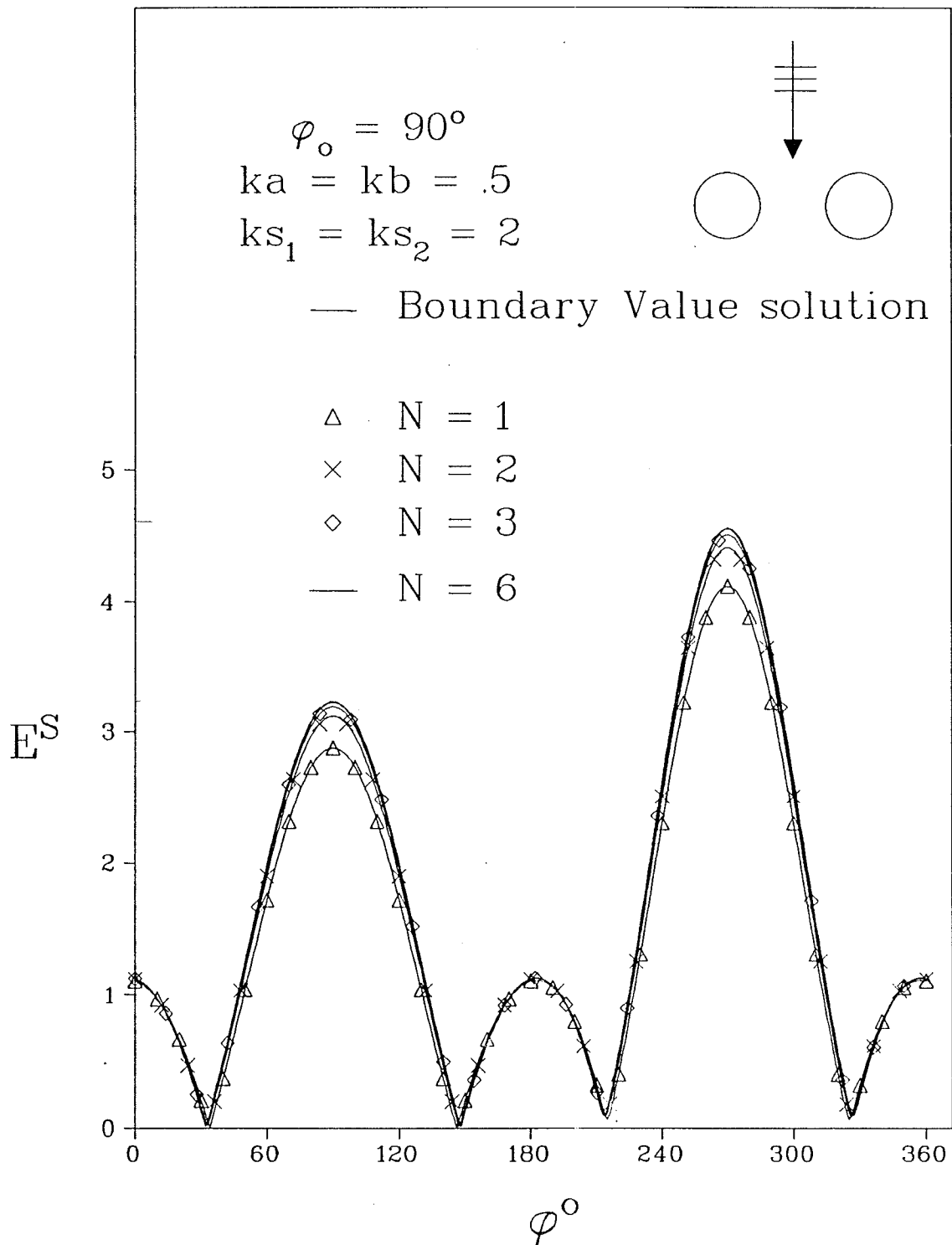


Fig. 2-4 : The total scattered field pattern for two parallel circular conducting cylinders.

deviations from the exact pattern for any small value of  $N$  are always in the forward and backward directions of the incident plane wave. To further indicate this behaviour the interaction scattered field component  $E''$  is computed and presented in Fig. 2-5 for the same parameters in Fig. 2-4.

As a criterion for terminating the interaction process, one may observe the additional increment in  $J'$  after each iteration and set a minimum quantity for that increment after which the interactions can be terminated. In fact a better approach is to check the tangential electric field  $E_t$  on the surface of one of the two cylindrical conductors due to the scattered field from the additional induced surface current on the other conductor. An example of this process is shown in Fig. 2-6 for  $E_t$  on the surface of cylinder 1 which is part of the two cylinders geometry as shown in Fig. 2-3. In the figure  $\phi_0 = 90^\circ$ ,  $ka = kb = 0.5$  and  $ks_1 = ks_2 = 2$ . It is found that the peak value of  $E_t$  is nearly at  $\psi = 180^\circ$  which is the direction of cylinder 2 and where the multiple interactions between the two cylinders reach a maximum. It is also clear that all the points of the  $E_t$  pattern decay as  $N$  increases and approaches zero when  $N$  tends to infinity.

One of the important parameters in the scattering by conducting bodies is the scattering cross-section. In table 2-1 the forward and backward scattering cross-sections of the double cylinder geometry are indicated for different values of  $ks$ , namely 3 and 6, and for  $\phi_0 = 90^\circ$ . The numerical values of  $\sigma$  are shown for two identical cylinders of radii  $ka = kb = 0.5, 1.0$  and  $1.5$ . From the table one notices that  $\sigma$  increases with  $ka$  regardless of the value of  $ks$ . It is clear that the required number of iterations to obtain a value of  $\sigma$  close to the exact value depends on the ratio  $s/a$ . As an example, for  $s/a \geq 10$  four interactions ( $N = 4$ ) are sufficient for at least two digits of accuracy. Higher values of  $N$  are needed when  $s/a < 10$  as shown in the table. Table 2-2 is similar to table 2-1 except for  $\phi_0 = 180^\circ$ . In comparing the numerical results in tables 2-1 and 2-2, we find that the forward as well as

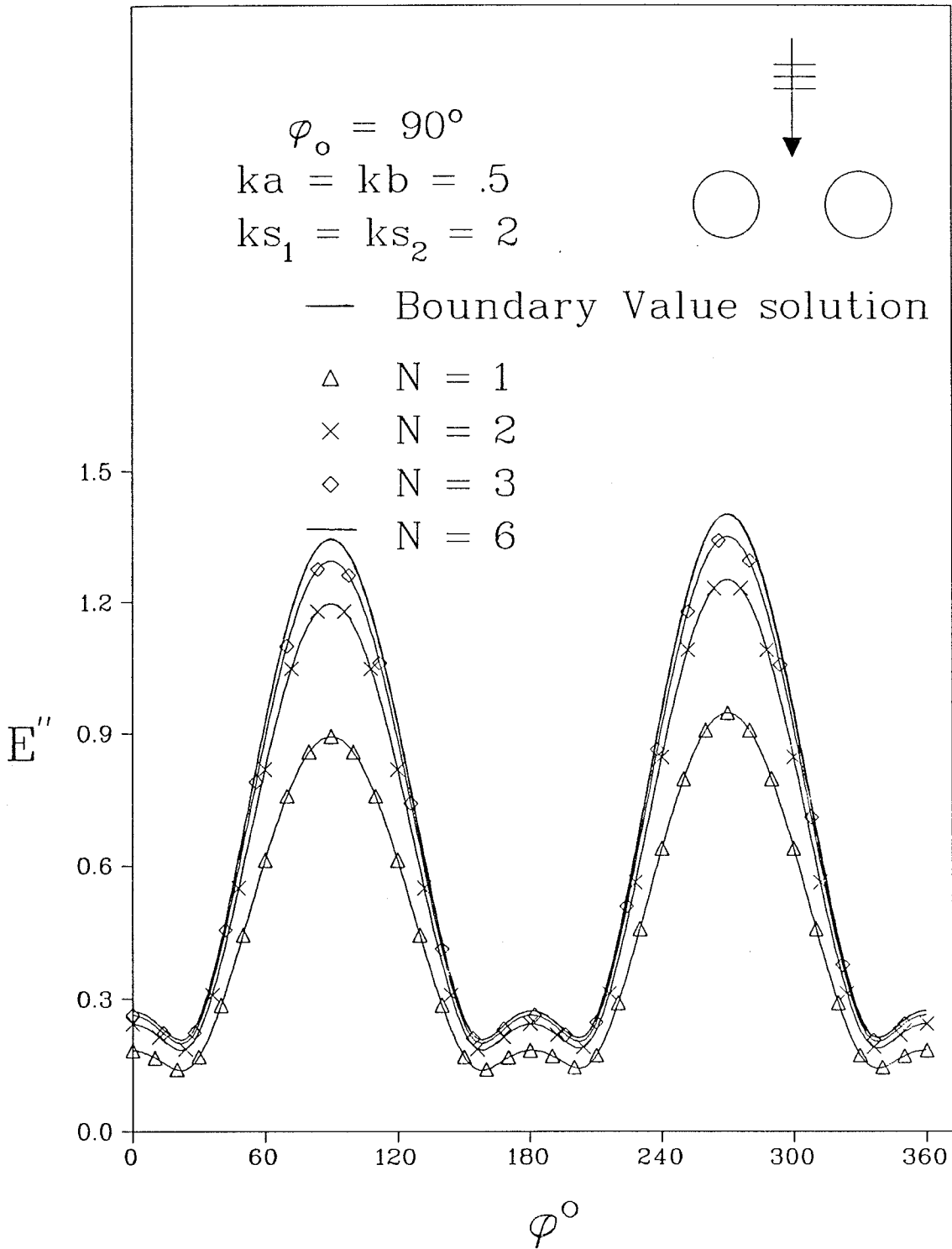


Fig. 2-5 : The interaction scattered field pattern, for two parallel circular conducting cylinders.

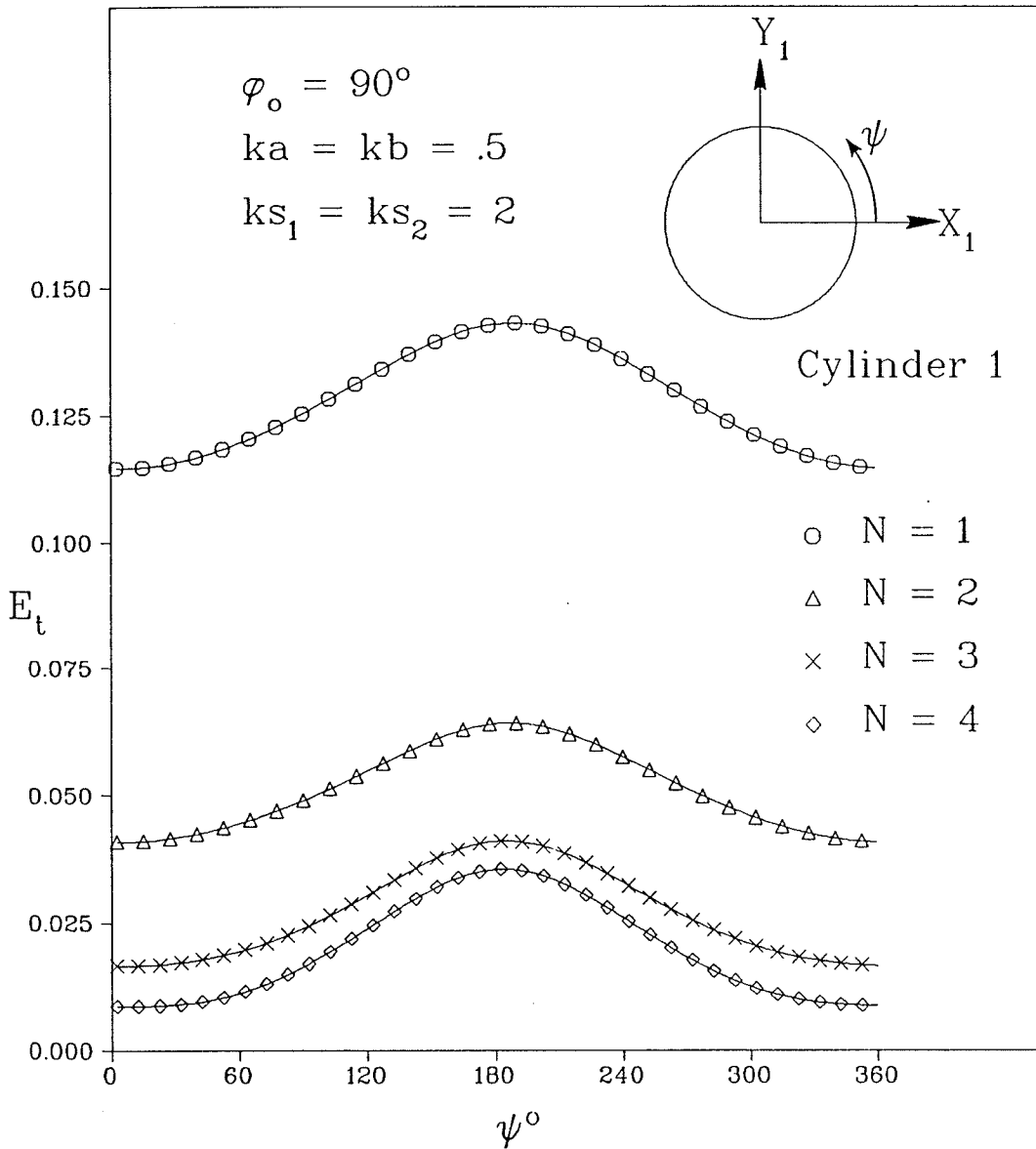


Fig. 2-6 : Amplitude of the tangential electric field vs.  $\psi$ .

N	$\sigma$					
	ks=3			ks=6		
	ka=0.5	ka=1.0	ka=1.5	ka=0.5	ka=1.0	ka=1.5
1	2.4765	9.3566	19.7297	2.9273	9.2810	16.5740
2	2.2977	8.9939	22.7429	2.7688	9.3779	17.2872
3	2.3881	8.5758	24.1345	2.7932	9.3046	17.4196
4	2.3743	8.4624	24.7672	2.7957	9.2733	17.4334
5	2.3718	8.4736	25.0520	2.7946	9.2666	17.4300
6	2.3735	8.4921	25.1796	2.7946	9.2661	17.4269
7	2.3732	8.4974	25.2366	2.7947	9.2663	17.4255
8	2.3732	8.4969	25.2620	2.7947	9.2664	17.4250
9	2.3732	8.4961	25.2734	2.7947	9.2664	17.4249
Boundary value	2.3728	8.4962	25.2913	2.7945	9.2680	17.4272

( a ) Forward scattering cross-section (  $\phi = 270^\circ$  ).

N	$\sigma$					
	ks=3			ks=6		
	ka=0.5	ka=1.0	ka=1.5	ka=0.5	ka=1.0	ka=1.5
1	0.7164	1.4324	3.0372	0.9950	1.8684	3.4599
2	0.7417	0.9923	2.9375	0.9488	1.6338	3.6272
3	0.7795	0.9537	2.9449	0.9680	1.5832	3.7166
4	0.7662	0.9913	2.9627	0.9674	1.5787	3.7513
5	0.7673	1.0092	2.9743	0.9668	1.5800	3.7629
6	0.7679	1.0110	2.9804	0.9669	1.5807	3.7665
7	0.7676	1.0093	2.9835	0.9669	1.5808	3.7675
8	0.7677	1.0084	2.9850	0.9669	1.5809	3.7677
9	0.7677	1.0084	2.9857	0.9669	1.5809	3.7678
Boundary value	0.7674	1.0079	2.9870	0.9667	1.5805	3.7683

( b ) Back scattering cross-section (  $\phi = 90^\circ$  ).

Table 2-1 : Scattering cross-section of two parallel circular conducting cylinders with  $\phi_0 = 90^\circ$ .

N	$\sigma$					
	ks=3			ks=6		
	ka=0.5	ka=1.0	ka=1.5	ka=0.5	ka=1.0	ka=1.5
1	2.3800	5.0808	4.6033	2.7506	5.2042	6.4998
2	2.2076	4.3791	7.4917	2.5904	5.2124	7.7396
3	2.2667	4.5418	5.9731	2.6087	5.2255	7.3913
4	2.2512	4.4522	6.5665	2.6111	5.1873	7.4460
5	2.2514	4.4656	6.2699	2.6106	5.1943	7.4384
6	2.2531	4.4870	6.3892	2.6107	5.1940	7.4374
7	2.2528	4.4826	6.3303	2.6107	5.1940	7.4387
8	2.2528	4.4814	6.3541	2.6107	5.1941	7.4382
9	2.2528	4.4817	6.3424	2.6107	5.1941	7.4383
Boundary value	2.2524	4.4804	6.3432	2.6104	5.1932	7.4365

( a ) Forward scattering cross-section (  $\phi = 0^\circ$  ).

N	$\sigma$					
	ks=3			ks=6		
	ka=0.5	ka=1.0	ka=1.5	ka=0.5	ka=1.0	ka=1.5
1	0.6009	0.6971	0.7848	0.6513	0.9785	1.3613
2	0.6528	0.9298	1.3704	0.6560	1.0920	1.3031
3	0.6958	0.8678	0.9898	0.6727	1.0247	1.3468
4	0.6859	0.8721	1.1371	0.6715	1.0360	1.3148
5	0.6865	0.8980	1.0656	0.6710	1.0373	1.3256
6	0.6868	0.8929	1.0956	0.6711	1.0370	1.3211
7	0.6865	0.8907	1.0817	0.6711	1.0372	1.3223
8	0.6865	0.8912	1.0876	0.6711	1.0372	1.3219
9	0.6865	0.8911	1.0849	0.6711	1.0372	1.3220
Boundary value	0.6863	0.8908	1.0851	0.6709	1.0369	1.3217

( b ) Back scattering cross-section (  $\phi = 180^\circ$  ).

Table 2-2 : Scattering cross-section of two parallel circular conducting cylinders with  $\phi_0 = 180^\circ$ .

the backward values of  $\sigma$  for  $\phi_0 = 180^\circ$  are always smaller than the corresponding values when  $\phi_0 = 90^\circ$  regardless of  $ka$  and  $ks$ . The good agreement between the numerical results in tables 2-1 and 2-2 obtained by the CWS technique and those evaluated using the boundary value solution establishes the validity of the CWS technique.

For all double wedge results, we consider for simplicity the symmetric configuration where  $\phi_0 = 90^\circ$ ,  $ks_1 = ks_2 = ks$ ,  $kr_1 = kr_2 = kr$  and  $\alpha = \beta = \gamma$ . Furthermore, it is worth presenting the behaviour of some of the physical parameters involved in the calculations. As an example, consider Fig. 2-7 in which the field due to the physical optics current on the surface of one wedge at the edge of the opposite wedge is shown as a function of  $ks$ . Obviously it is necessary to include  $E_{PO}^S$  in the double wedge analysis for all narrow separations between the two wedges. However for wide separations it can be ignored since the value of  $E_{PO}^S$  decays in an oscillatory fashion and tends to zero as  $ks$  approaches infinity. On the other hand, the peak to peak value of the intensity of the assumed line source  $C_0$  is found to be increasing as  $ks$  increases. Although the oscillations of  $E_{PO}^S$  and  $C_0$  are similar and have the same period, it is clear that the maxima and minima of these oscillations do not coincide with each other.

Since there is an exact solution for the diffraction by a slit (double wedge geometry with  $\alpha = \beta = 0^\circ$ ), the diffracted field is computed for the slit geometry in order to check the accuracy of the solution. For this special case, each of the series in Eqs. (2-18) and (2-19) can be transformed into two new series. As an example for  $\nu = 2$ , Eq. (2-18) can be written after some mathematical manipulations in the following form,

$$J_p = \frac{1}{j\eta k \rho} \left\{ \sum_{m=0}^{\infty} (2m+1) j^{m+\frac{1}{2}} J_{m+\frac{1}{2}}(k\rho) \sin \left[ \left(m + \frac{1}{2}\right) \phi_0 \right] \right.$$



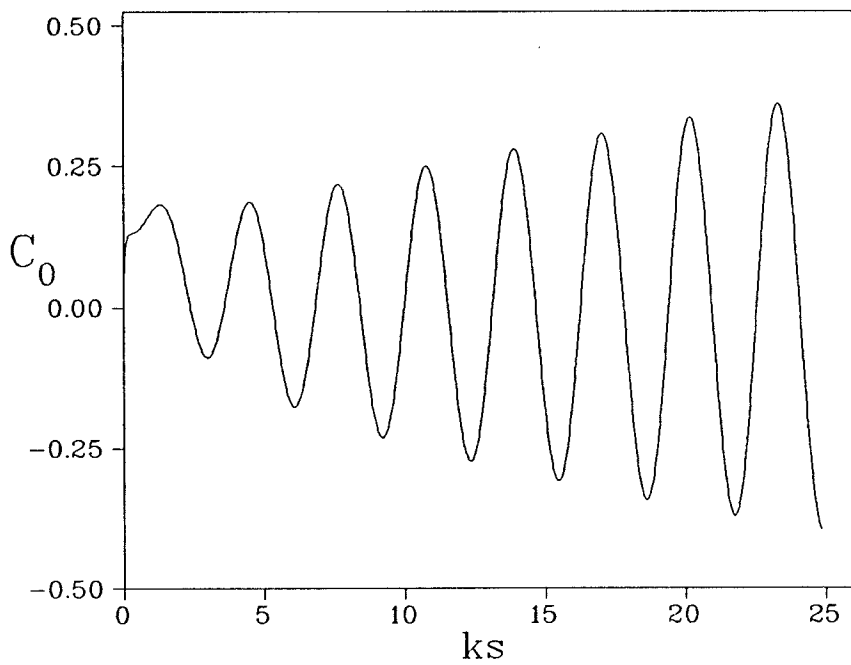
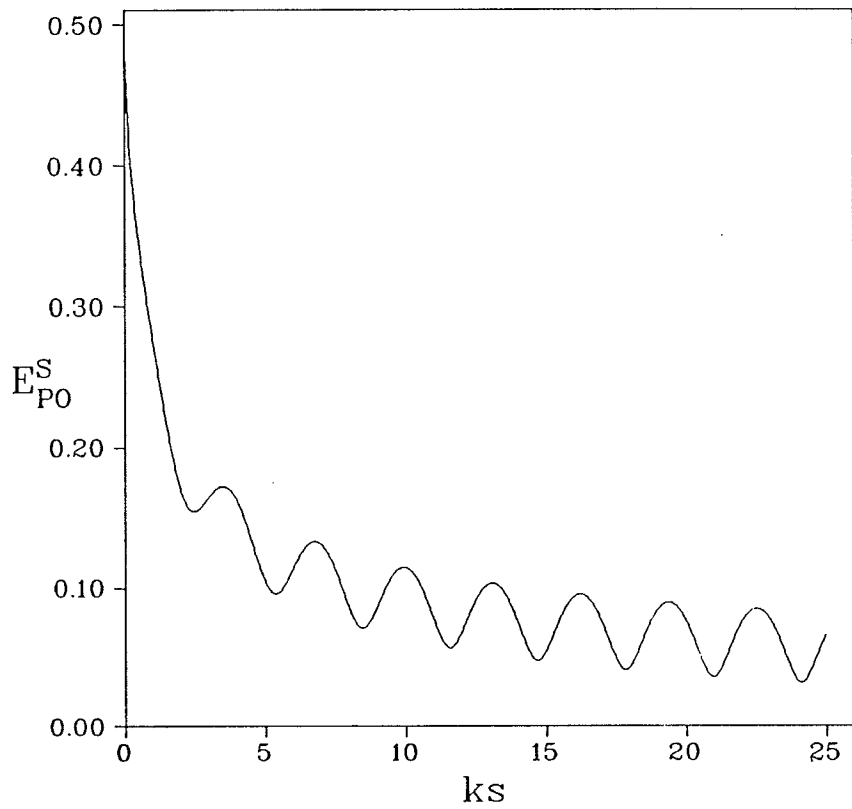


Fig. 2-7 :  $E_{PO}^S$  and amplitude of  $C_0$  vs.  $ks$ .

$$\pm 2 \sum_{l=1}^{\infty} l j^l J_l(k\rho) \sin(l\phi_0) \left. \vphantom{\sum} \right\} \quad (2-65)$$

where the upper sign pertains to  $J_p^{UW}$  and the lower sign to  $J_p^{IW}$ . In comparing Eqs. (2-18) and (2-65), it is found that the expressions given by Eq. (2-65) for the surface currents are much simpler than those given by Eq. (2-18) regarding the numerical calculations. This is simply due to the use of the recurrence relation of the Bessel function ( $J_{\nu+1}(x) = \frac{2\nu}{x} J_{\nu}(x) - J_{\nu-1}(x)$ ) while evaluating the summation in Eq. (2-65), whereas in Eq. (2-18) the orders of the Bessel functions prevent the use of any recurrence relation and one is therefore forced to evaluate  $J_{n/\nu}(k\rho)$  for each different value of  $n$ . Furthermore, since the Bessel functions of an order equal to integer plus half (as those in the first series of Eq. (2-65)) have simple expressions in terms of trigonometric functions, the execution time is greatly reduced when using Eq. (2-65) instead of Eq. (2-18). Similarly Eq. (2-19) can be written in terms of two series. The first series contains Bessel functions of orders equal to integer plus half while the second series contains Bessel functions of integer orders only. Fig. 2-8 shows the diffracted field pattern of the slit due to an incident plane wave and  $ks = 8$ . It is obvious that the dashed curve, which represents the singly and multiply diffracted fields up to the fifth order of interaction, is closer to the exact solution than the solid curve which accounts for the singly diffracted fields. For narrow slits, one expects a significant contribution from the multiply diffracted fields to the total field. This is clearly shown for one case in the same figure, namely  $ks = 4$ .

To further check the accuracy of the numerical calculations, the transmission coefficient  $T$  defined by Eq. (2-64) is computed. The resulting values of  $T$  obtained using the CWS technique are compared in table 2-3 with the available exact as well as asymptotic (GTD) values of  $T$  [34,5]. It is to be noticed that the values based on the CWS technique are computed with relatively small number of interactions and

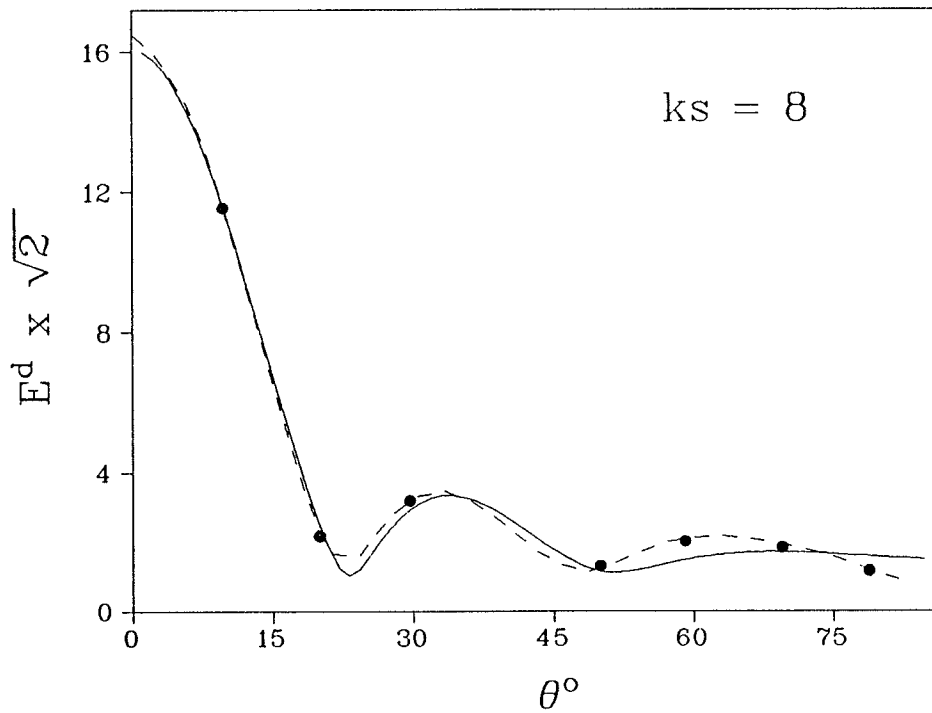
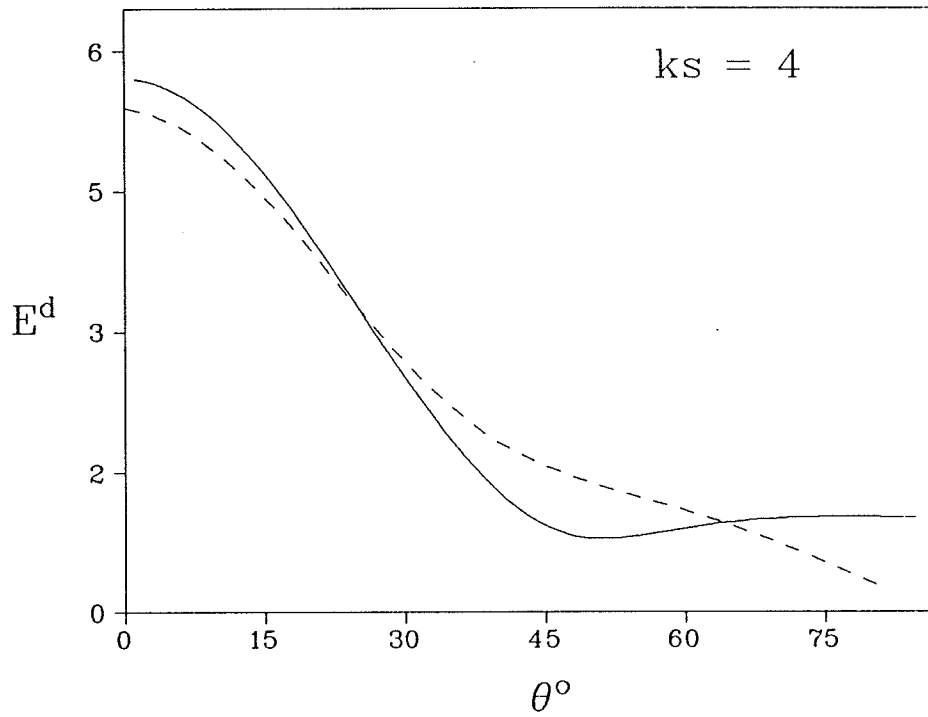


Fig. 2-8 : Diffraction pattern of a slit.

- Single diffraction.
- - - CWS (  $N = 5$  ).
- • • Exact values.

<i>N</i>	<i>T</i>					
	<i>k<sub>s</sub></i> = 0.8	<i>k<sub>s</sub></i> = 1	<i>k<sub>s</sub></i> = 2	<i>k<sub>s</sub></i> = 3	<i>k<sub>s</sub></i> = 5	<i>k<sub>s</sub></i> = 8
1	0.4439	0.7099	1.1912	0.9625	1.0475	1.0217
2	0.2779	0.5930	1.1913	0.9751	1.0504	1.0232
3	0.2525	0.5562	1.1838	0.9724	1.0498	1.0232
4	0.2550	0.5466	1.1838	0.9729	1.0498	1.0232
5	0.2580	0.5446	1.1841	0.9728	1.0498	1.0232
6	0.2590	0.5444	1.1841	0.9728	1.0498	1.0232
7	0.2592	0.5444	1.1841	0.9728	1.0498	1.0232
8	0.2592	0.5444	1.1841	0.9728	1.0498	1.0232
Exact	0.2605	0.5454	1.1842	0.9720	1.0499	1.0233
GTD	0.1555	0.6428	1.1861	0.9601	1.0512	1.0239

Table 2-3 : Slit transmission coefficient for  $\phi_0 = 90^\circ$ .

are in better agreement with the exact values than those based on Keller's asymptotic solution in which all infinite interactions are considered.

Figure 2-9 shows the transmission coefficient of a double wedge geometry as a function of interior wedge angle  $\gamma$  for different values of  $ks$ , namely 1, 2 and 4. In this figure the results based on the CWS technique are shown along with two different asymptotic solutions. The first asymptotic solution [70,71] is an extension of a technique used for the diffraction by a wide slit [38]. In this solution the interaction between the two wedges is in the form of cylindrical waves. In the second asymptotic approach the interaction between the two wedges is expressed in terms of plane waves and derivatives of plane waves with respect to the incidence and observation angles [50]. The numerical results in Fig. 2-9 indicate good agreement between the CWS technique and the other two asymptotic techniques for  $ks = 4$ , whereas for  $ks = 2$  small deviations are observed. It is believed that the results obtained using the CWS technique are closer to the exact solution as in the case of  $\gamma = 0$ . Furthermore, for small separations, namely  $ks = 1$ , it is clearly shown that both asymptotic solutions deviate from the CWS results. In general one observes that the effect of the interior wedge angle on  $T$  is large for small values of  $ks$  whereas for large values of  $ks$  the changes in  $T$  become very small except for very large  $\alpha$  or  $\beta$ .

With respect to the double capped wedge geometry, the total current distribution on the surface of one of the two wedges is shown in Figs. 2-10, 2-11 and 2-12 where  $kr$  is equal to 0.05, 0.1 and 1.0, respectively, and for  $N = 1, 2, 3, \dots, 6$ . One can easily notice that  $J'$  converges after a few interactions between the two wedges for the case when  $\phi_0 = 90^\circ$ ,  $ks = 7$  and  $\gamma = 10^\circ$ . It is also found that the peak value of  $J'$  decreases with increasing  $kr$ . The transmission coefficient is shown for different values of  $\gamma$ , namely  $\gamma = 0^\circ$ ,  $\gamma = 10^\circ$  and  $\gamma = 20^\circ$  with  $\phi_0 = 90^\circ$  and for  $kr = 0.5$  in Fig. 2-13. The Figure also shows an asymptotic solution [72,73] based on

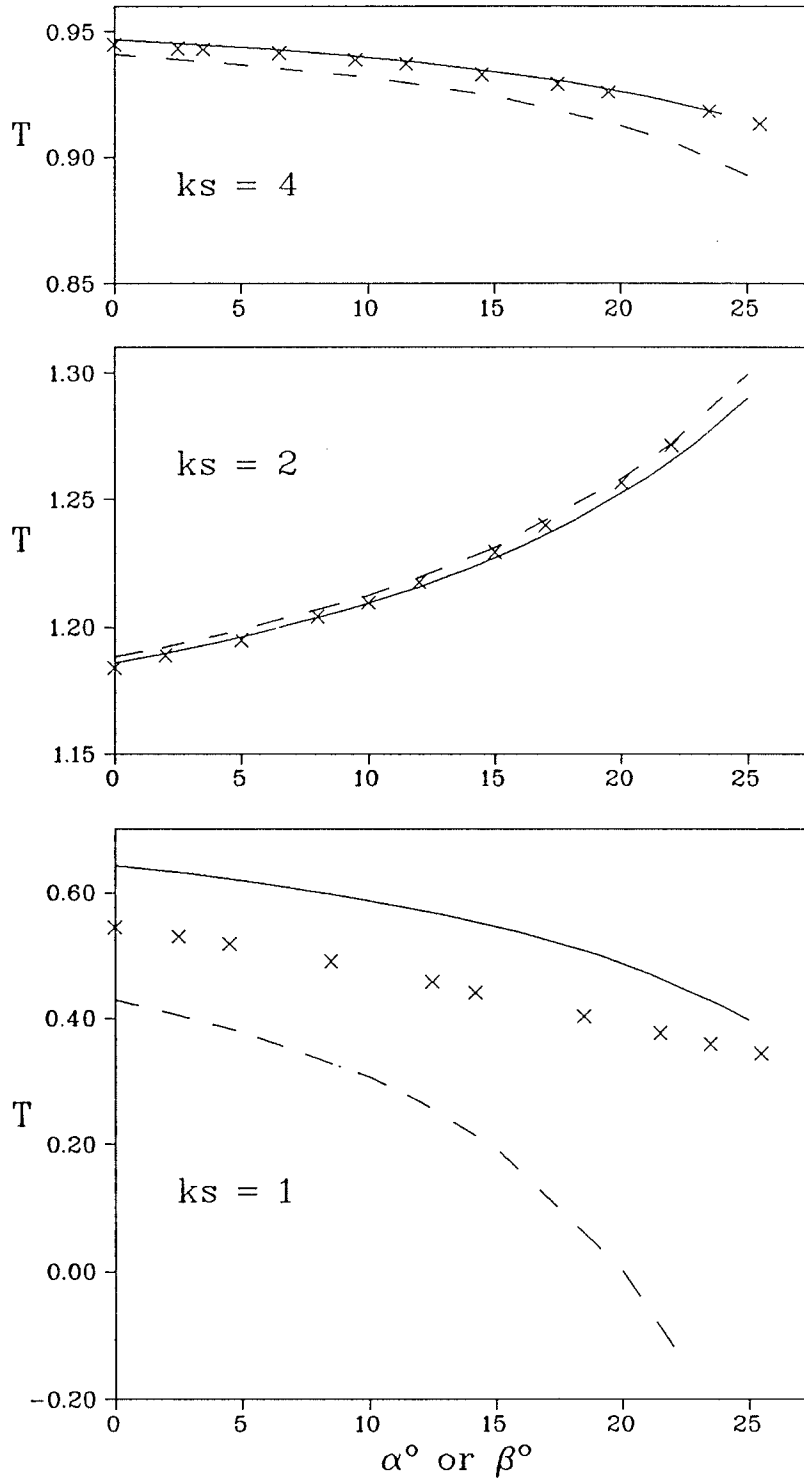


Fig. 2-9 :  $T$  vs. wedge angle  $\gamma$ .

- Asymptotic (Proposed solution)
- - - Asymptotic (Teague & Zitron)
- x x x C W S ( $N = 6$ )

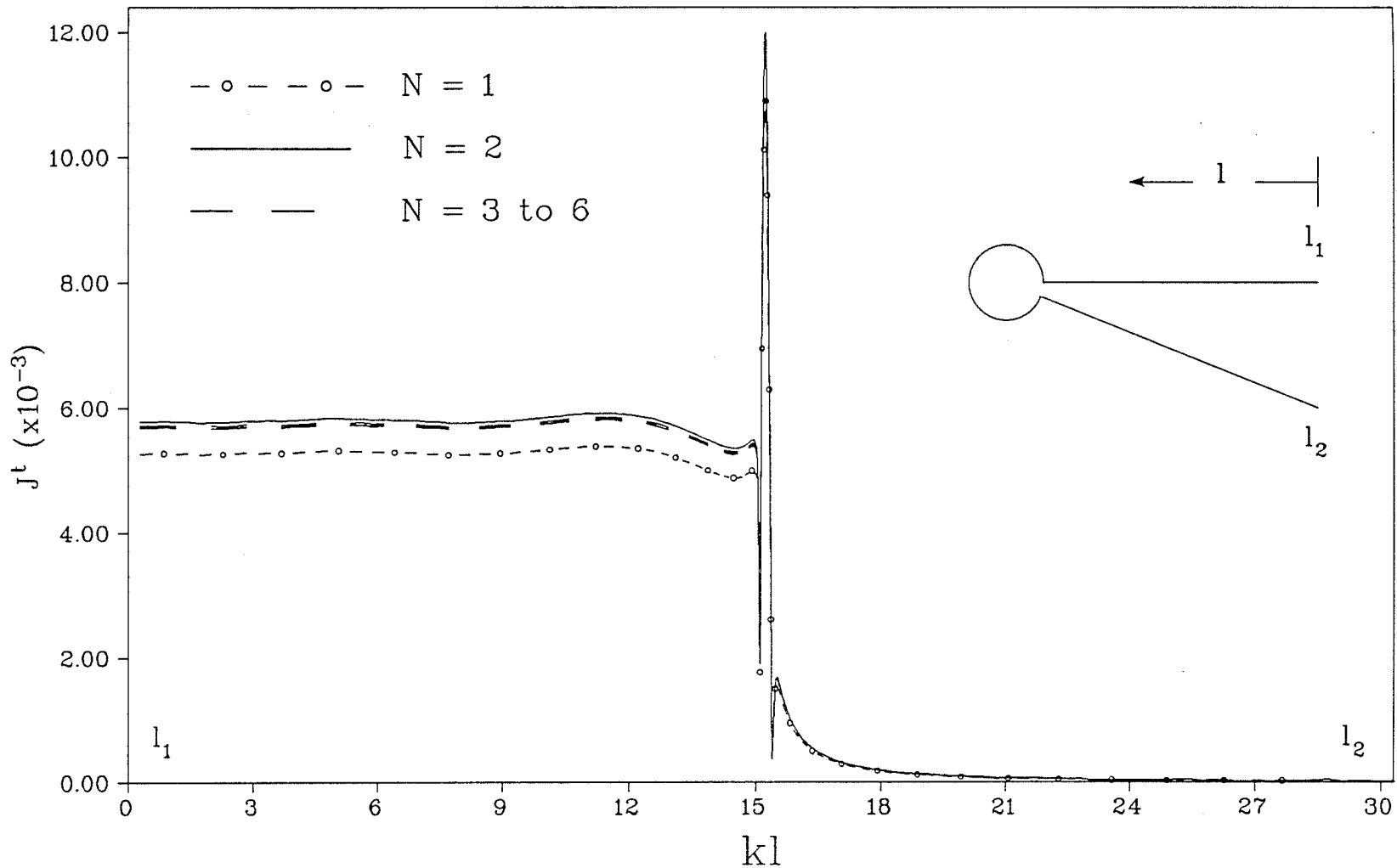


Fig. 2-10 : Surface current vs.  $kl$  of a double conducting capped-wedge for  $k_s = 7$ ,  $\gamma = 10^\circ$  and  $kr = 0.05$ .

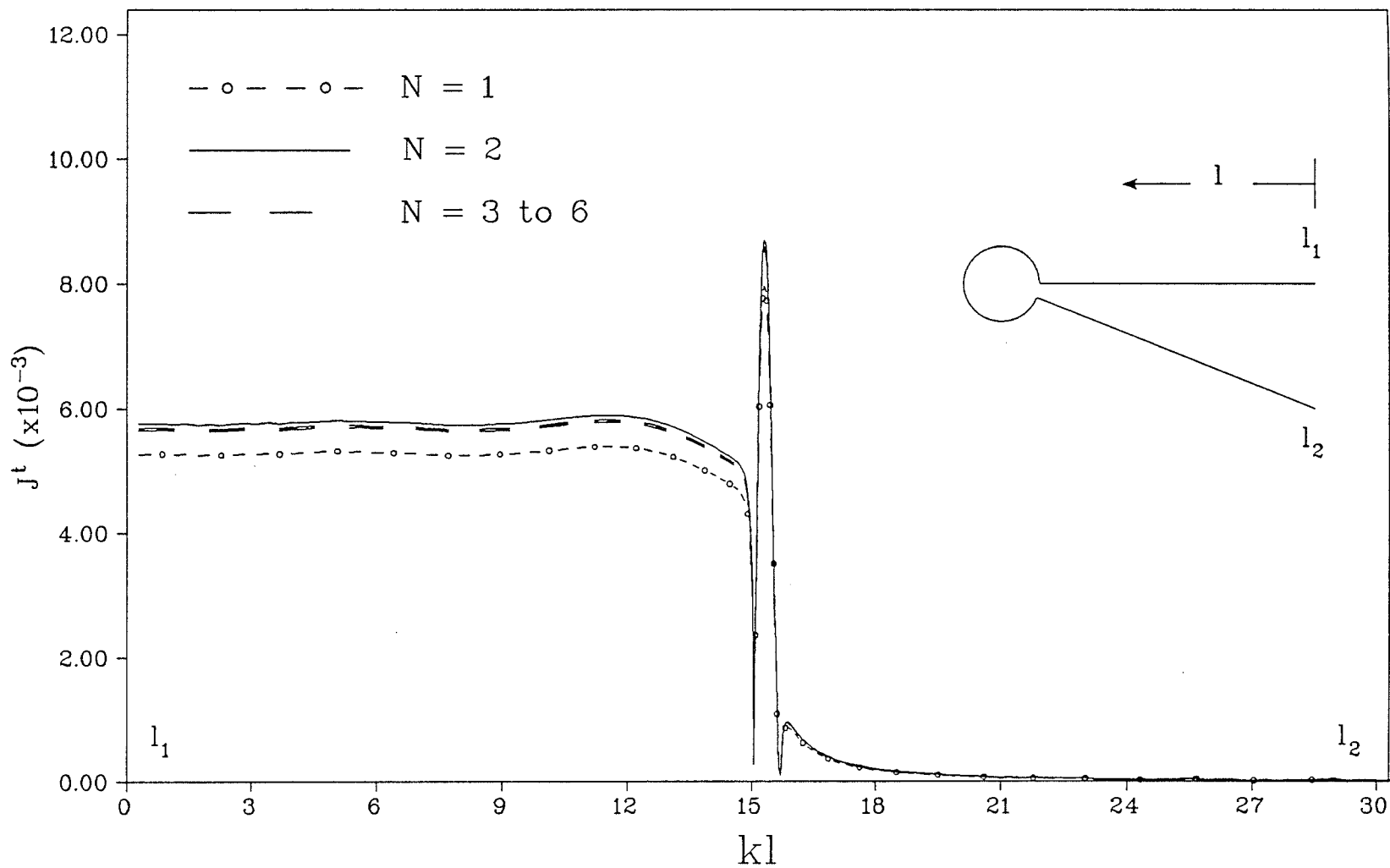


Fig. 2-11 : Surface current vs.  $kl$  of a double conducting capped-wedge  
 for  $k_s = 7$ ,  $\gamma = 10^\circ$  and  $kr = 0.1$ .



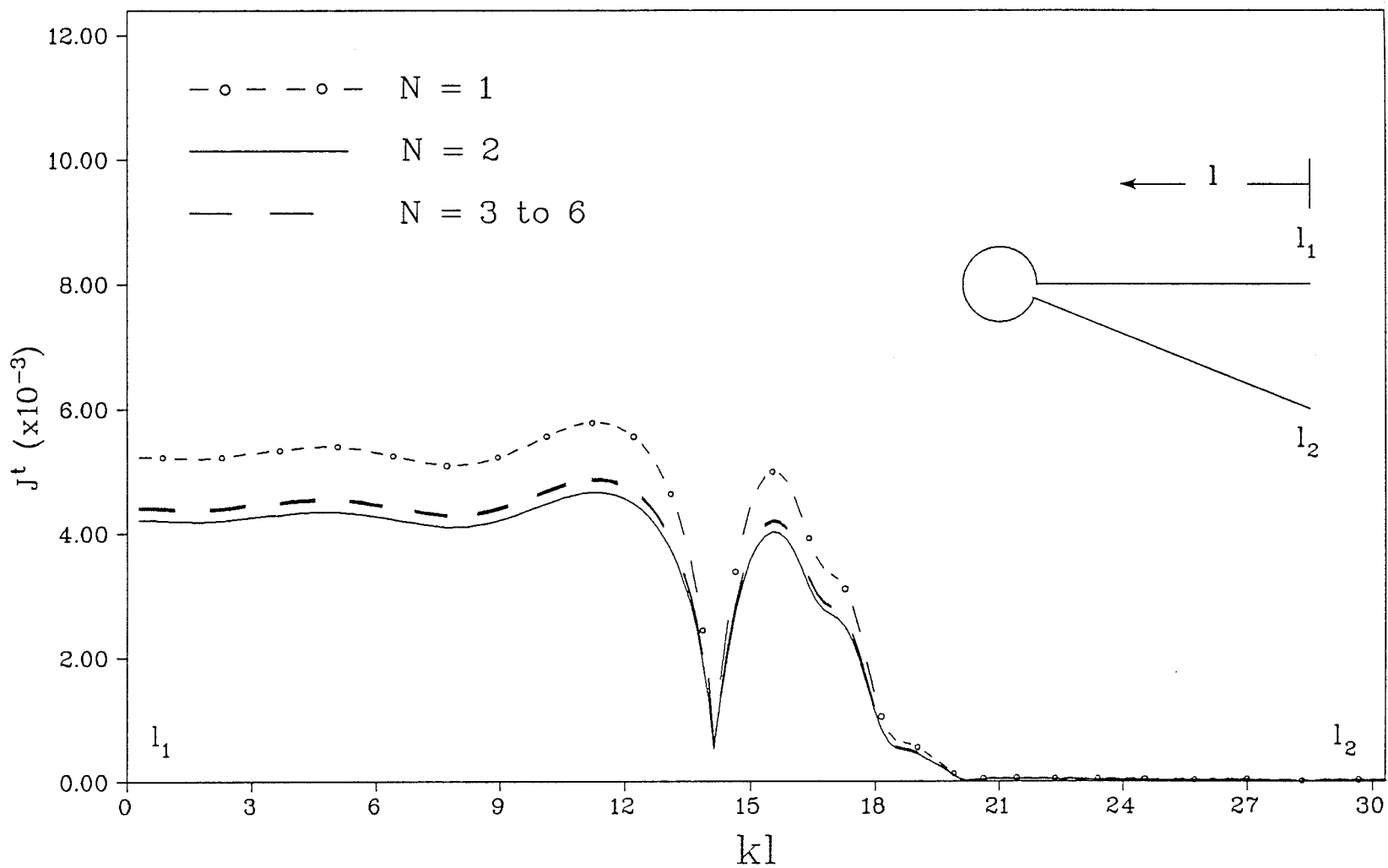


Fig. 2-12 : Surface current vs.  $kl$  of a double conducting capped-wedge for  $k_s = 7$ ,  $\gamma = 10^\circ$  and  $kr = 1.0$ .

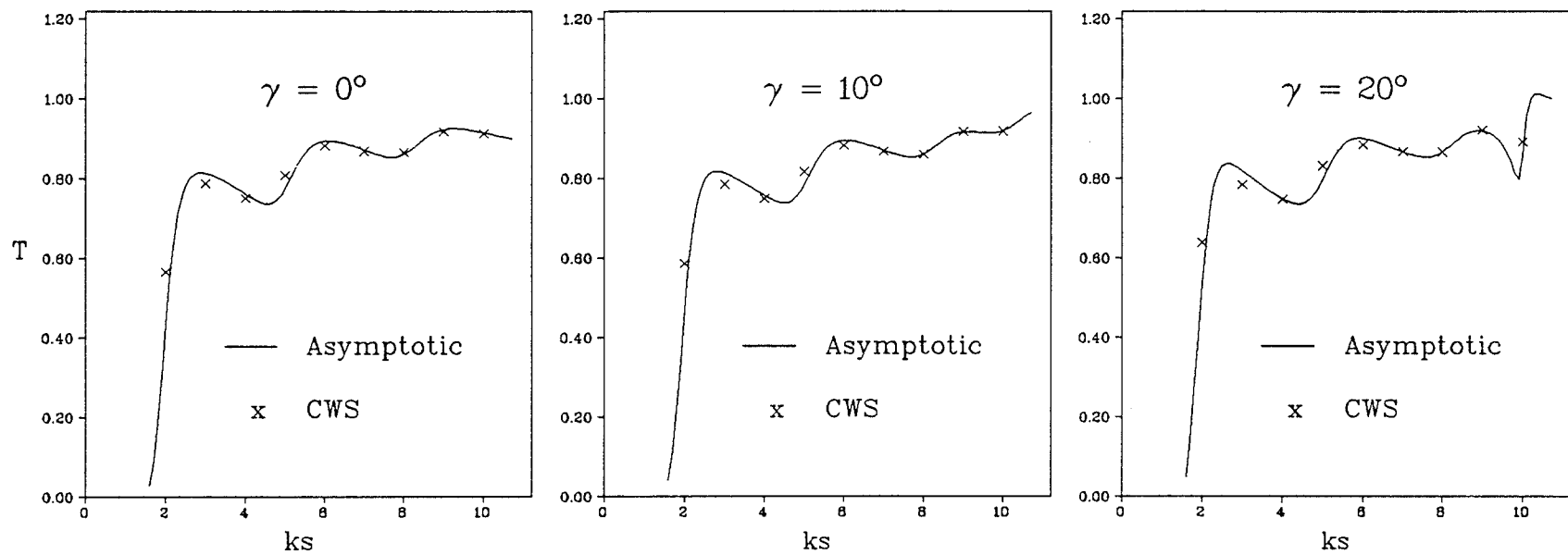


Fig. 2-13 :  $T$  vs.  $ks$  of a double conducting capped-wedge for  $kr = 0.5$ .

the assumption that two fictitious line sources (located at the virtual edges of the two wedges) are used to account for the total interaction between the wedges. It is clearly shown that there is an excellent agreement between the computed values of  $T$  using the CWS technique and the asymptotic method for all large values of  $ks$ . However, for small values of  $ks$  some deviations are observed. Although, these deviations are small (because  $T$  is an integral quantity based on the diffracted field values at all observation points), it is obvious that the deviations in the diffraction pattern are significant especially for small values of  $ks$ . These deviations in the diffraction field pattern are shown in Fig. 2-8 for the uncapped slit and in Figs. 2-14, 2-15 and 2-16 for the capped slit geometry where  $ks = 4, 6,$  and  $8,$  respectively, and  $kr = 1.0$ . It is obvious that as  $ks$  increases the results based on the asymptotic solution are in good agreement with those obtained using the CWS technique, as expected.

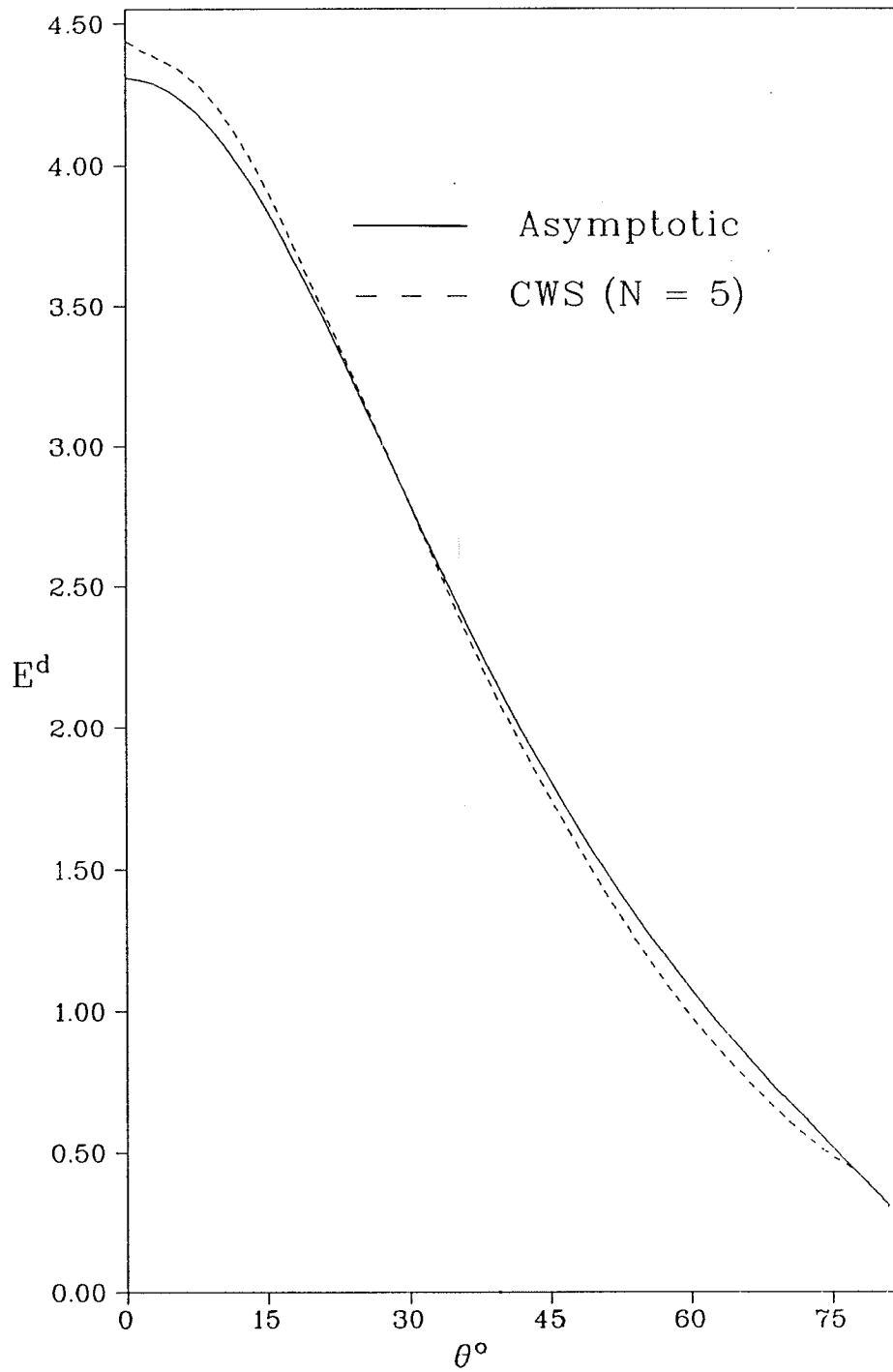


Fig. 2-14 : Diffracted field vs.  $\theta$  of a double conducting capped-slit for  $ks = 4$  and  $kr = 1.0$

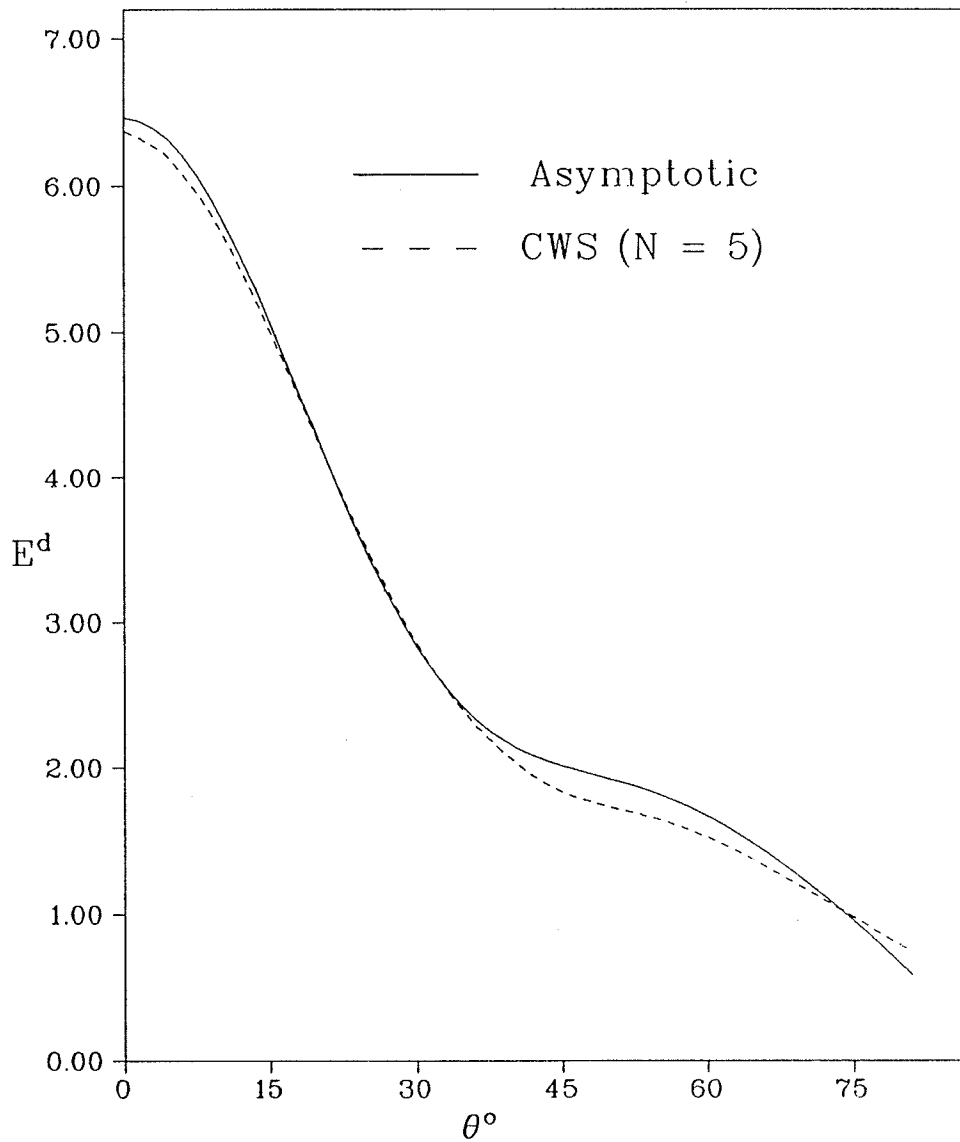


Fig. 2-15 : Diffracted field vs.  $\theta$  of a double conducting capped-slit for  $ks = 6$  and  $kr = 1.0$

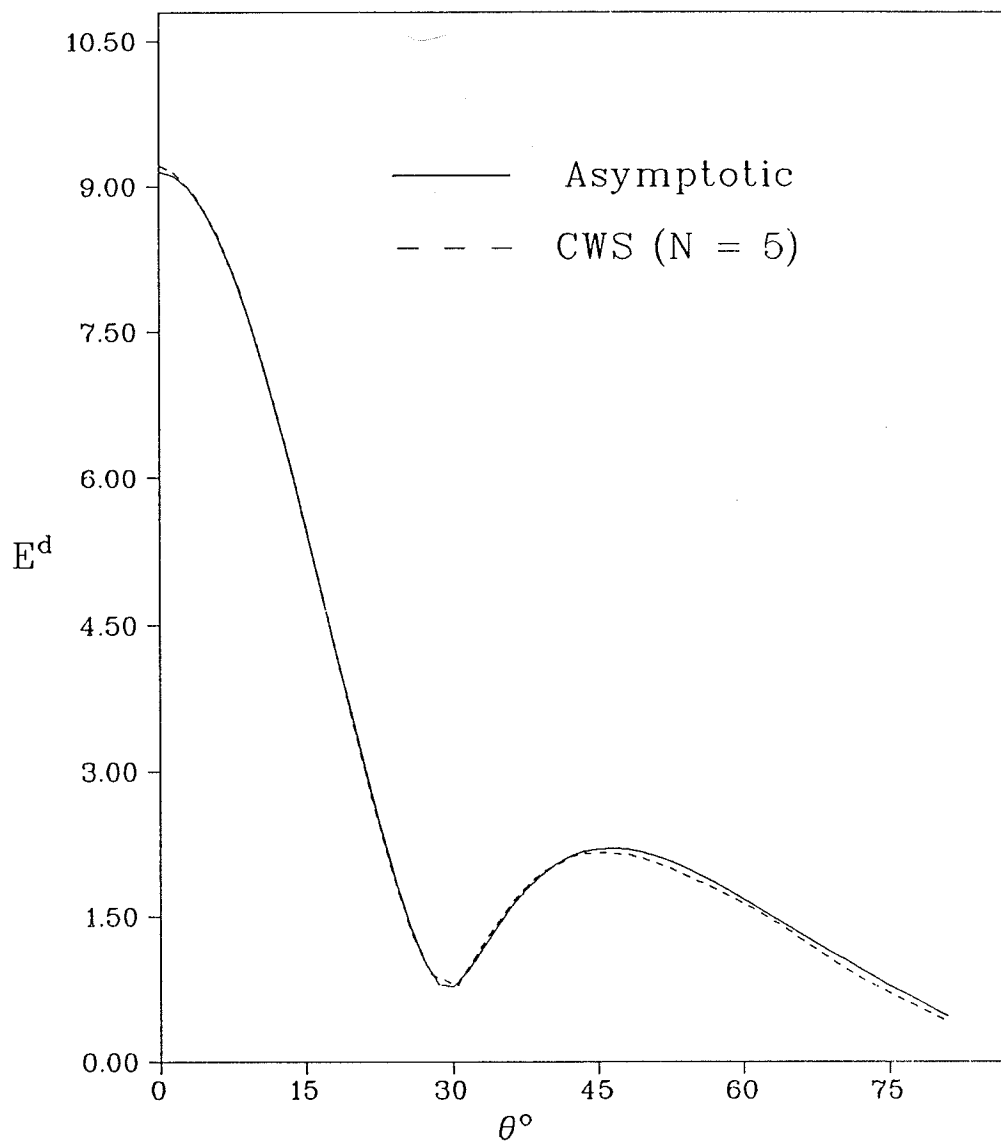
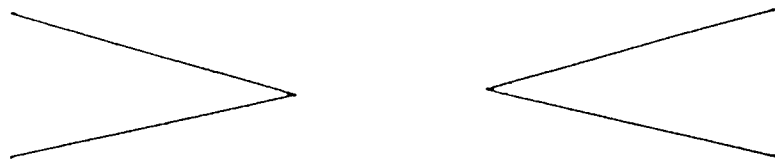


Fig. 2-16 : Diffracted field vs.  $\theta$  of a double conducting capped-slit for  $ks = 8$  and  $kr = 1.0$

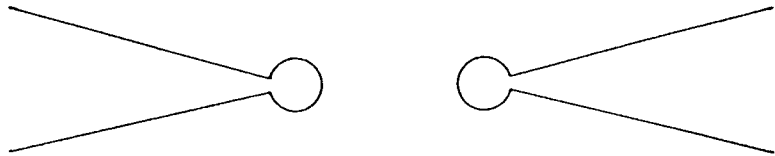
## CHAPTER 3

### *MODIFIED ASYMPTOTIC SOLUTION FOR A LOADED APERTURE*

In the previous chapter, the problem of two-dimensional scattering by two bodies is formulated rigorously using a novel CWS technique. Although the CWS technique is valid for small as well as wide electrical separations between the two bodies, it is found that for wide separation the numerical results based on the asymptotic solution agree very well with those obtained by the CWS technique. Therefore, it is appropriate to use an asymptotic solution where it is valid to show the relation between the diffraction characteristics and the geometrical parameters of the double wedge. Moreover, the effect of adding new scatterers or changing some of the geometrical shapes of the two wedges (see Fig. 3-1) on the diffraction characteristics can be investigated if the asymptotic solution is valid for obtaining the parameters in question. Among the suitable loading objects for the double wedge geometry is the circular cylinder or cylindrical shell, where the cylinder may be located at, above or below the aperture plane. For example, if the cylinder axis coincides with either edge of the wedge, the resulting geometry is nothing more than a capped wedge. Thus, for a metallic cylinder loading the edge of the wedge may be physically blocked and the resulting diffracted field from the capped wedge will depend mainly on the radius of the metallic cap. However, if the cap is a dielectric cylinder the edge diffracted field will be modified according to the cylinder radius and the dielectric permittivity. One should also point out that the edge diffracted field can be partially or totally absorbed if the dielectric is considered lossy. Another loading geometry is when the cylinder is along the center of the aperture plane while the plane wave is normally incident; in such case the forward diffracted field will be



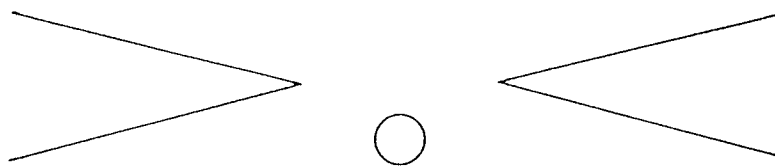
Unloaded double sharp-wedge.



Double capped-wedge.



Double rounded-wedge.



Double sharp-wedge with a cylindrical scatterer  
near or in the aperture plane.

Fig. 3-1 : Schematic diagram of different types of  
loading the aperture of a double wedge.



greatly affected by the cylinder radius as well as the permittivity of the dielectric cylinder. In addition to variations in the diffracted field in the forward direction, new diffraction lobes may appear which are considered as losses. It is predicted that the existence of a third scatterer near the edges of the two wedges may create more oscillations in the forward transmission coefficient through the aperture. Although the location of the additional scatterer is arbitrary, there may be some restrictions on the spacing between the edges of the two wedges and the additional scatterer or scatterers to allow using the asymptotic solutions.

In this chapter, two simple asymptotic solutions are obtained in a physically interpretable form and are convenient for calculation purposes. Furthermore, the proposed solutions offer much physical insight into the complex mechanism of multiple interaction between the scatterers. The double wedge diffraction problem is attempted in Sec. 3.1 using the known solution of the diffracted field from a single wedge. The dependence of the total diffracted field from the two wedges on the interaction between the two edges is clearly represented by simple relations.

In Sec. 3.2, we investigate the effect of loading the sharp edges of the two wedges by cylindrical caps whose axes coincide with the edges. The caps are considered to be conducting or dielectric infinite cylinders with circular cross-sections.

Since the edge of a wedge is assumed perfectly sharp, it is also our objective to investigate the effect of small rounding of the two edges on the diffraction characteristics of the double wedge problem. Therefore, we present in Sec. 3.3 the effect of small edge rounding using an asymptotic solution based on plane wave interaction between the two wedges.

The scattering of an incident plane wave by two sharp wedges and an additional cylindrical scatterer with circular cross-section is derived in Sec. 3.4. Some numerical examples for the diffracted field and the transmission coefficient due to an incident plane wave are presented in Sec. 3.5. The range of validity of the proposed

asymptotic solutions as well as the effects of aperture loading are also investigated.

### 3.1 Diffraction by a wide double wedge with sharp edges.

For a single wedge defined by two half-planes at  $\phi = \gamma$  and  $\phi = 2\pi - \gamma$  intersecting along the z-axis of the circular cylindrical coordinates  $(\rho, \phi, z)$ , the total field is the geometrical optics field  $E^g$  plus the diffracted field. The asymptotic diffracted fields due to a plane wave (Eq. (2-1)) and a line source field (Eq. (2-4)) incident on a conducting sharp wedge are denoted by  $E_p^{dW}$  and  $E_l^{dW}$ , respectively, [74] where

$$E_p^{dW} = \frac{-\eta k}{4} H_0(k\rho) g^W(\phi, \phi_0, \nu) \quad (3-1)$$

$$E_l^{dW} = \frac{-\eta k}{4} H_0(k\rho) f^W(\phi, \rho_0, \phi_0, \nu). \quad (3-2)$$

The diffraction patterns  $g^W$  and  $f^W$  are given, respectively by

$$g^W(\phi, \phi_0, \nu) = \frac{2j}{\eta k \nu} \sin(\pi/\nu) \left\{ \left[ \cos\left(\frac{\pi}{\nu}\right) - \cos\left(\frac{\phi - \phi_0}{\nu}\right) \right]^{-1} - \left[ \cos\left(\frac{\pi}{\nu}\right) - \cos\left(\frac{\phi + \phi_0 - 2\gamma}{\nu}\right) \right]^{-1} \right\} \quad (3-3)$$

$$f^W(\phi, \rho_0, \phi_0, \nu) = \frac{-\eta k}{4} H_0(k\rho_0) g^W(\phi, \phi_0, \nu) \quad (3-4)$$

where

$$\nu = 2(\pi - \gamma) / \pi \quad (3-5)$$

while the superscript  $w$  refers to a sharp wedge and the asymptotic form of the Hankel function is replaced by the Hankel function itself in the  $f^W$  function. From Eqs. (3-1) and (3-2) one notices that the field diffracted by a sharp wedge due to either a plane wave or a line source field, is in the form of a cylindrical wave

emanating from a fictitious line source at the edge of the wedge.

Employing the Karp and Russek technique for the interaction between the two sharp wedges [38], the diffracted field due to an incident plane wave plus a fictitious line source, located at the edge of the second wedge, is derived.

For the case of two wedges separated by  $s_{12}$  (sharp edge to edge distance where  $ks_{12} \gg 1$ ) and illuminated by a plane wave of unit amplitude (see Fig. 3-2), the total field at any point is considered as being composed of the incident field plus a response field from each of the two wedges or, alternatively, as a geometrical optics field plus two diffracted fields (one from each wedge). It is assumed that each of these diffracted fields is of the same nature as the field known to be diffracted by an isolated wedge. These fields can be presented in the region far from the edge of the wedge ( $e_A$  or  $e_B$ ) by Eqs. (3-1) and (3-2). Since  $\phi_1$  has the constant value  $\pi$  at  $e_B$ , the diffracted field due to wedge A at  $e_B$  is of the form  $e^{-jk\rho}/\sqrt{k\rho}$  which represents the asymptotic field of a line source at  $e_A$ . A similar remark holds for the excitation of wedge A. Hence each wedge may be thought of as being excited by the incident field plus a line source located at the edge of the opposite wedge. The strength of this line source depends on the value of  $f^W(\pi, s_{12}, \pi, \nu)$  for the opposite wedge.

The total field can be expressed as a linear combination of the fields due to the diffraction of the incident plane wave (non-interaction term), and line source fields diffracted by the two wedges (interaction term). In this representation the total diffracted field  $E^d$  for  $-\frac{\pi}{2} + 2\alpha \leq \theta \leq \frac{\pi}{2} - 2\beta$  and  $0 \leq \alpha$  or  $\beta < \frac{\pi}{4}$  is given by

$$E^d = E^{d1} + E^{d2} \tag{3-6}$$

where

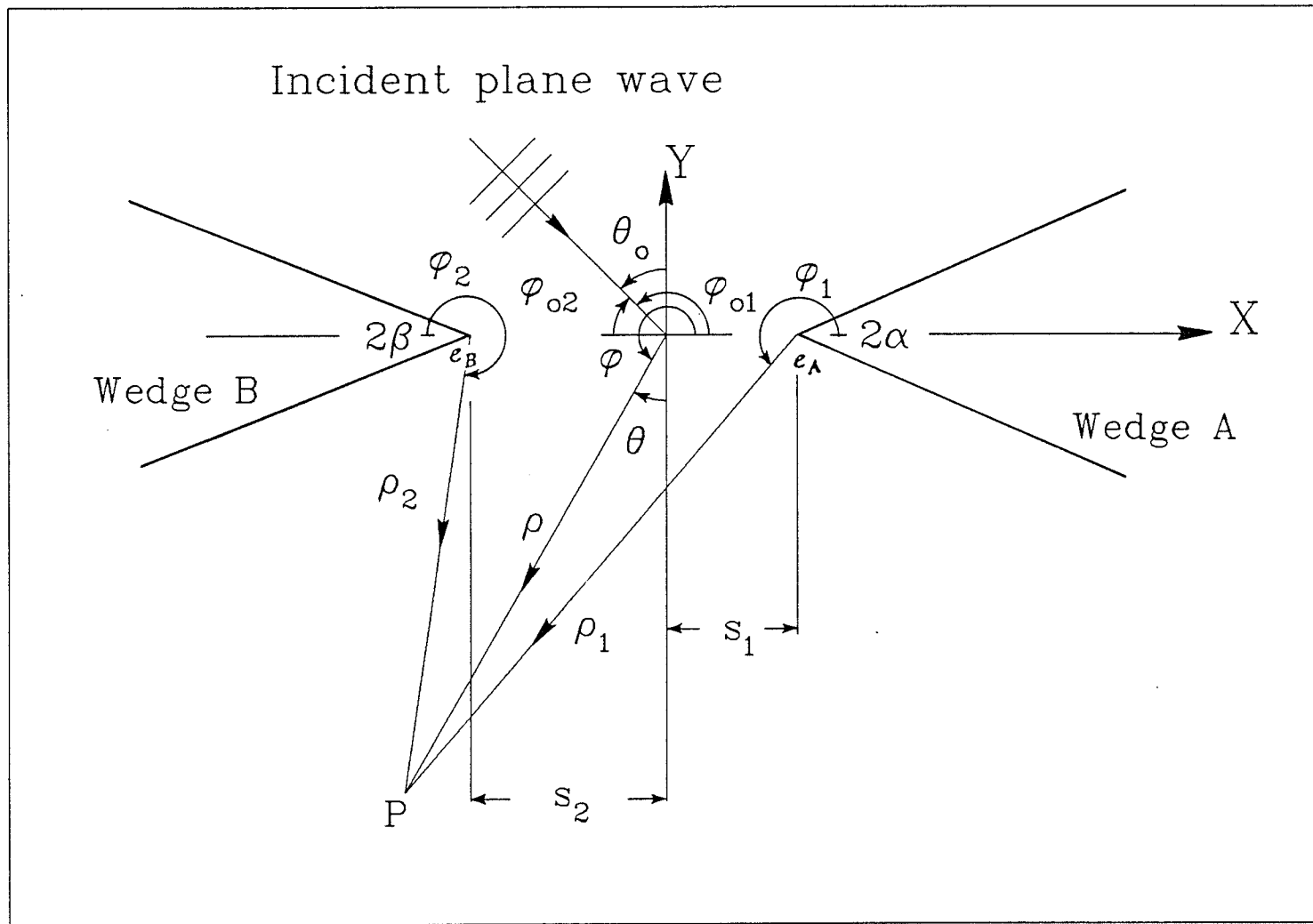


Fig. 3-2 : Double sharp-wedge geometry.

$$E^{d1} = \frac{-\eta k}{4} H_0(k\rho_1) [ e^{-jks_1 \sin \theta_0} g^W(\phi_1, \phi_{01}, \nu_1) + c_1 f^W(\phi_1, s_{12}, \pi, \nu_1) ] \quad (3-7)$$

$$E^{d2} = \frac{-\eta k}{4} H_0(k\rho_2) [ e^{+jks_2 \sin \theta_0} g^W(\phi_2, \phi_{02}, \nu_2) + c_2 f^W(\phi_2, s_{12}, \pi, \nu_2) ] . \quad (3-8)$$

In Eqs. (3-7) and (3-8)  $c_1$  and  $c_2$  are the unknown strengths of the fictitious line sources at  $e_B$  and  $e_A$ , respectively, and  $\nu_1$  and  $\nu_2$  are defined by Eq. (3-5) where  $\gamma$  is replaced by  $\alpha$  and  $\beta$ , respectively.  $s_{12}$  is defined by Eq. (2-46) whereas  $\phi_{01}$  and  $\phi_{02}$  are the polar angles of the incident plane wave measured in terms of the local coordinates of the two wedges A and B, respectively. For any far field point the quantities  $\rho_1$ ,  $\rho_2$ ,  $\phi_1$  and  $\phi_2$  are given in terms of  $\rho$  and  $\phi$  by Eqs. (2-47) to (2-49) where  $\theta = \frac{3\pi}{2} - \phi$ .

To determine the complex values of  $c_1$  and  $c_2$ , one may follow the same analysis given in [38] by imposing the requirement that the diffracted fields of the two wedges be consistent with each other. This leads to the following equations

$$c_1 = [ e^{-jks_1 \sin \theta_0} g^W(\pi, \phi_{01}, \nu_1) f^W(\pi, s_{12}, \pi, \nu_2) + e^{+jks_2 \sin \theta_0} g^W(\pi, \phi_{02}, \nu_2) ] / w \quad (3-9)$$

$$c_2 = [ e^{+jks_2 \sin \theta_0} g^W(\pi, \phi_{02}, \nu_2) f^W(\pi, s_{12}, \pi, \nu_1) + e^{-jks_1 \sin \theta_0} g^W(\pi, \phi_{01}, \nu_1) ] / w \quad (3-10)$$

where

$$w = 1 - f^W(\pi, s_{12}, \pi, \nu_1) f^W(\pi, s_{12}, \pi, \nu_2) . \quad (3-11)$$

Hence, the total diffracted field  $E^d$  is fully determined and can be written after

using the far field approximations in the following form

$$E^d = \frac{e^{-jk\rho}}{\sqrt{\pi k\rho}} F(\theta, s_1, s_2, \nu_1, \nu_2) \quad (3-12)$$

where  $F$  is the diffraction pattern of a double sharp wedge.

Another convenient representation for the total field can be written as

$$E^t = E' + E'' \quad (3-13)$$

where

$$E' = E^s + \frac{-\eta k}{4} [ H_0(k\rho_1) e^{-jks_1 \sin \theta_0} g^W(\phi_1, \phi_{01}, \nu_1) + H_0(k\rho_2) e^{+jks_2 \sin \theta_0} g^W(\phi_2, \phi_{02}, \nu_2) ] \quad (3-14)$$

$$E'' = \frac{-\eta k}{4} [ c_1 H_0(k\rho_1) f^W(\phi_1, s_{12}, \pi, \nu_1) + c_2 H_0(k\rho_2) f^W(\phi_2, s_{12}, \pi, \nu_2) ]. \quad (3-15)$$

The non-interaction term  $E'$  represents the excitation of each sharp wedge separately by the incident plane wave. This may be a good approximation for extremely wide wedges. However, for narrower wedges the interaction term  $E''$  is required.

The transmission coefficient  $T$  for a plane wave incident at angle  $\theta_0$  is given by [38, Eq. (31)],

$$T = \text{Re} [ (1 - j) \tilde{F} ] / ks_{12} \quad (3-16)$$

where  $\tilde{F}$  is given by  $F(\theta, s_1, s_2, \nu_1, \nu_2)$  in the limit as  $\theta$  approaches  $\theta_0$ .

### 3.2 Diffraction by a wide double wedge with capped edges.

The diffraction of an incident E-polarized plane wave by a cylindrical dielectric capped wedge was derived by Adey [75] and generalized by Towaij et al. [76] to many concentric dielectric shells. Hamid presented a diffraction coefficient for the dielectrically capped wedge [77], while Hamid and Towaij showed the effects of the dielectric cap on the radiation characteristics of a capped half plane excited by a line source field [78].

The diffraction by a wedge with a conducting cylindrical cap was solved exactly by Karp in terms of an infinite series of angular eigenfunctions [79]. The half plane with a conducting cap was studied by many authors. Keller investigated the darkness of the shadow of rounded and capped screens using ray theory and GTD [80]. A modification to Keller's approach to this problem was proposed by Kouyoumjian and Burnside by including additional ray systems and using a more accurate diffraction coefficient [81]. Keller and Magiros [82] gave an alternative exact solution for the diffraction by a capped half plane in terms of an infinite series of radial eigenfunctions and showed that their solution agrees with Karp's solution [79]. They also derived an approximate asymptotic expression for the diffracted field in the shadow and illuminated regions. Starting with the exact solution, Chu et al. derived an alternative uniform far field asymptotic solution for the diffraction of an electromagnetic plane wave by a conducting capped half plane [83]. More recently, Hallidy derived uniform asymptotic expressions for electric and magnetic type plane waves diffracted by a perfectly conducting cylinder-tipped wedge [84].

The present analysis of multiple diffraction between two cylindrically capped wedges (see Fig. 3-3) is based upon the exact field expressions for a single capped wedge due to an incident plane wave at any angle and a line source field derived using the boundary value approach [76,79], as well as the technique used in Sec. 3.1 for the diffraction by a wide double wedge. The single capped wedge geometry may be defined by two half-planes at  $\phi = \gamma$  and  $\phi = 2\pi - \gamma$  intersecting along the  $z$

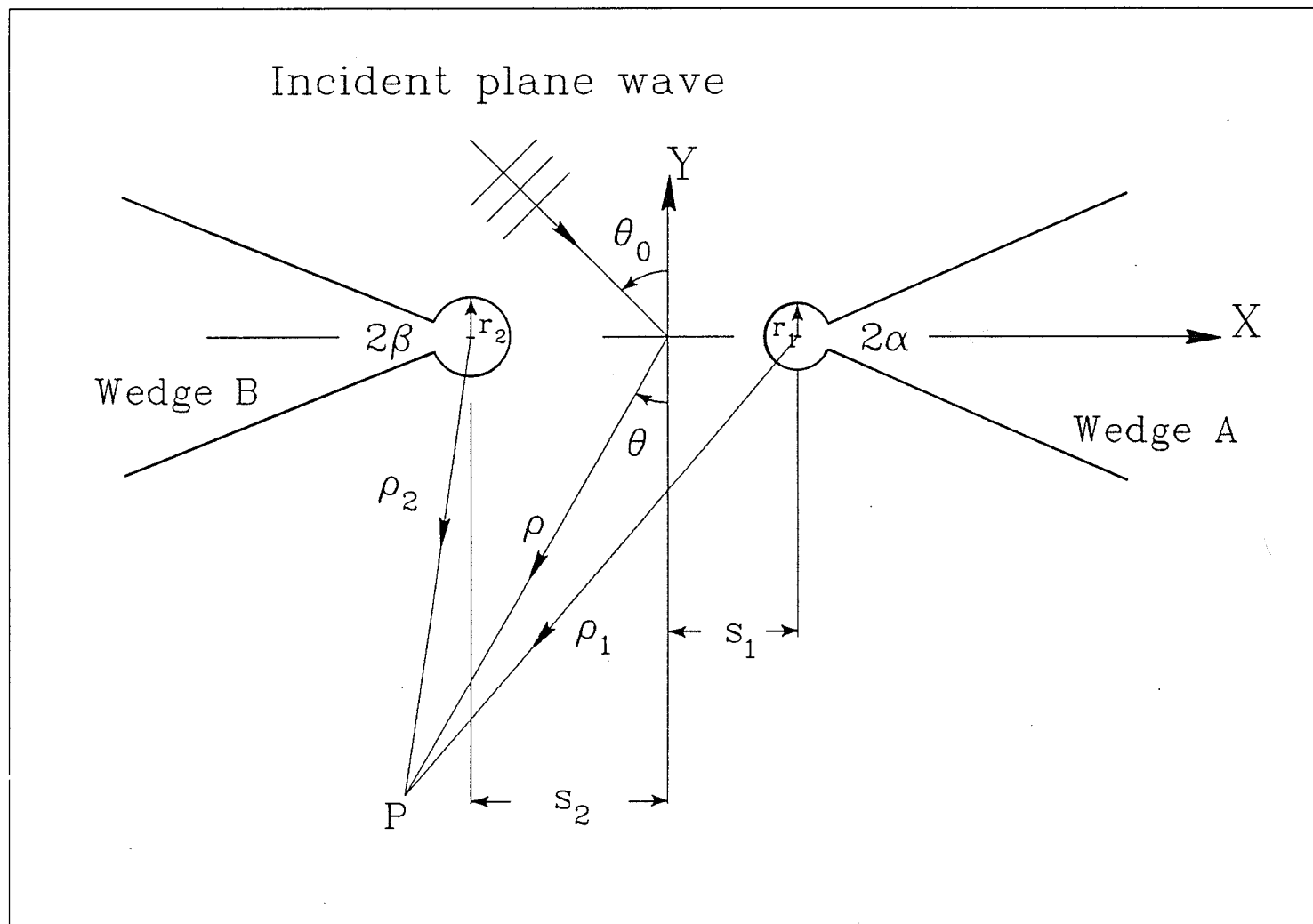


Fig. 3-3 : Double capped-wedge geometry.



axis and an infinite circular cylinder of radius  $r$  whose axis coincides with the  $z$  axis.

For a conducting capped wedge the diffracted field patterns due to a plane wave given by Eq. (2-1) and a line source field defined by Eq. (2-4) are given for small values of  $kr$  by

$$g(\phi, \phi_0, \nu, r) = g^W(\phi, \phi_0, \nu) + g^C \quad (3-17)$$

and

$$f(\phi, \rho_0, \phi_0, \nu, r) = f^W(\phi, \rho_0, \phi_0, \nu) + f^C \quad (3-18)$$

respectively, where

$$g^C = -\frac{16}{\eta k \nu} \sum_{n=1}^{\infty} j^{\frac{2n}{\nu}} \frac{J_{\frac{n}{\nu}}(kr)}{H_{\frac{n}{\nu}}(kr)} \sin \frac{n}{\nu}(\phi - \gamma) \sin \frac{n}{\nu}(\phi_0 - \gamma) \quad (3-19)$$

$$f^C = -\frac{4}{\nu} \sum_{n=1}^{\infty} j^{\frac{n}{\nu}} \frac{J_{\frac{n}{\nu}}(kr)}{H_{\frac{n}{\nu}}(kr)} H_{\frac{n}{\nu}}(k\rho_0) \sin \frac{n}{\nu}(\phi - \gamma) \cdot \sin \frac{n}{\nu}(\phi_0 - \gamma) \quad (3-20)$$

while the superscript  $C$  refers to a conducting cap.

For a dielectric capped wedge the diffracted field patterns due to a plane wave and line source field are given, respectively, by

$$g(\phi, \phi_0, \nu, r, \epsilon_r) = g^W(\phi, \phi_0, \nu) + g^D \quad (3-21)$$

$$f(\phi, \rho_0, \phi_0, \nu, r, \epsilon_r) = f^W(\phi, \rho_0, \phi_0, \nu) + f^D \quad (3-22)$$

where the superscript  $D$  refers to a dielectric cap,  $k_1 = \sqrt{\epsilon_r} k$ ,  $\epsilon_r$  is the relative permittivity of the dielectric cap and provided that  $k_1 r$  is not too large relative to

unity. This leads to the relations

$$g^D = - \frac{16}{\eta k \nu} \sum_{n=1}^{\infty} j^{\frac{2n}{\nu}} T_{\frac{n}{\nu}} \sin \frac{n}{\nu}(\phi - \gamma) \sin \frac{n}{\nu}(\phi_0 - \gamma) \quad (3-23)$$

$$f^D = - \frac{4}{\nu} \sum_{n=1}^{\infty} j^{\frac{n}{\nu}} T_{\frac{n}{\nu}} H_{\frac{n}{\nu}}(k \rho_0) \sin \frac{n}{\nu}(\phi - \gamma) \sin \frac{n}{\nu}(\phi_0 - \gamma) \quad (3-24)$$

$$T_{\frac{n}{\nu}} = \frac{k \frac{J_{\frac{n}{\nu}}(k_1 r)}{\nu} \frac{J'_{\frac{n}{\nu}}(kr)}{\nu} - k_1 \frac{J_{\frac{n}{\nu}}(kr)}{\nu} \frac{J'_{\frac{n}{\nu}}(k_1 r)}{\nu}}{k \frac{J_{\frac{n}{\nu}}(k_1 r)}{\nu} \frac{H'_{\frac{n}{\nu}}(kr)}{\nu} - k_1 \frac{H_{\frac{n}{\nu}}(kr)}{\nu} \frac{J'_{\frac{n}{\nu}}(k_1 r)}{\nu}} \quad (3-25)$$

where the prime denotes differentiation with respect to the full argument.

For small values of  $kr$  and  $k_1 r$  relative to unity, the geometrical optics component due to the cylindrical cap (in the presence of the wedge) is much less than the diffracted field component [77]. Therefore, the terms denoted by  $g^C$ ,  $f^C$ ,  $g^D$ , and  $f^D$  (which account for the reflected and diffracted fields due to a cylindrical cap in each of Eqs. (3-17), (3-18), (3-21) and (3-22)) may be considered as a perturbation to the diffracted field due to a sharp wedge.

From Eqs. (3-1), (3-2), (3-17), (3-18), (3-21) and (3-22) one notices that the field diffracted by a conducting or dielectric capped wedge, due to either a plane wave or line source excitation, is in the form of a cylindrical wave emanating from a fictitious line source at the virtual edge of the sharp wedge. Therefore, the same technique used in Sec. 3.1 can be applied here to obtain the total diffracted field and the transmission coefficient through the aperture of a double capped wedge. However, it should be noted that the diffraction pattern functions  $g^W$  and  $f^W$  defined by Eqs. (3-3) and (3-4) must be replaced by the corresponding  $g$  and  $f$  functions of the conducting capped wedge or those of the dielectric capped wedge.

### 3.3 Diffraction by a wide double wedge with rounded edges.

The multiple diffraction between the two wedges with rounded edges is based upon the scattered field expression from a single rounded wedge due to an incident plane wave at any angle which was derived by Ross and Hamid [85], and the technique proposed by Karp and Keller for the diffraction by a slit in an infinite conducting screen [43].

The far scattered field  $E^S$ , due to an incident plane wave on a perfectly conducting wedge of half angle  $\gamma$  with a rounded edge of radius  $a$  with the virtual apex located along the  $z$  axis, is given by

$$E^S = E_0 f_R (\nu, \phi_0, \phi, a) \quad (3-26)$$

where

$$f_R (\nu, \phi_0, \phi, a) = E_1 + E_2 + E_3 \quad (3-27)$$

$$E_0(\rho) = \frac{-\eta k}{4} H_0(k\rho) \quad (3-28)$$

$$E_1 = g^W \quad (3-29)$$

$$E_2 = g^C \quad (3-30)$$

$$E_3 = \frac{-8}{\pi \eta k \nu} e^{jkd \cos \phi_0} \sum_{n=1}^{\infty} e^{jn\pi/2\nu} \frac{\sin \left[ \frac{n}{\nu}(\phi - \gamma) \right]}{H_{n/\nu}(kr)} \sum_{p=0}^{\infty} \sum_{q=-\infty}^{\infty} J_p(kr) \cdot \left[ J_{p+q}(kd) - \frac{J_p(ka)}{H_p(ka)} H_{p+q}(kd) \right] [d_p I_1 + h_p I_2] \quad (3-31)$$

$$d = a \csc \gamma \quad (3-32)$$

$$r = d \cos \gamma = a \cot \gamma \quad (3-33)$$

$$I_1 = \int_{\gamma}^{2\pi-\gamma} \sin \left[ \frac{m}{\nu}(\phi - \gamma) \right] \cos(q\phi) d\phi$$

$$\begin{aligned}
 &= \frac{m/v}{\left(\frac{m}{v}\right)^2 - q^2} [1 - (-1)^m] \cos(q\gamma) , & \frac{m}{v} \neq |q| \\
 &= \pm \left[ \frac{\pi v}{2} - \frac{\sin(2q\gamma)}{2q} \right] \sin(q\gamma) , & \frac{m}{v} = \mp q
 \end{aligned} \tag{3-34}$$

$$\begin{aligned}
 I_2 &= \int_{\gamma}^{2\pi-\gamma} \sin \left[ \frac{m}{v}(\phi - \gamma) \right] \sin(q\phi) d\phi \\
 &= \frac{m/v}{\left(\frac{m}{v}\right)^2 - q^2} [1 + (-1)^m] \sin(q\gamma) , & \frac{m}{v} \neq |q| \\
 &= \pm \left[ \frac{\pi v}{2} + \frac{\sin(2q\gamma)}{2q} \right] \cos(q\gamma) , & \frac{m}{v} = \pm q .
 \end{aligned} \tag{3-35}$$

Further, we have

$$\begin{aligned}
 &\sum_{p=0}^{\infty} \sum_{q=-\infty}^{\infty} \left[ J_q(kr) H_{\frac{m}{v}}'(kr) - J_q'(kr) H_{\frac{m}{v}}(kr) \right] \\
 &\cdot \left[ J_{p+q}(kd) - \frac{J_p(ka)}{H_p(ka)} H_{p+q}(kd) \right] [d_p I_1 + h_p I_2] \\
 &= - \frac{4j}{kr} \sin \left[ \frac{m}{v}(\phi_0 - \gamma) \right] \exp \left[ -j(kd \cos \phi_0 - \frac{m\pi}{2v}) \right] .
 \end{aligned} \tag{3-36}$$

In Eq. (3-26) the first term  $E_0 E_1$  is the field diffracted by a sharp wedge. The first and the second terms,  $E_0 (E_1 + E_2)$ , denote the solution of a plane wave incident on a wedge with a metallic cylindrical cap of radius  $r$ . All these terms  $E_0 (E_1 + E_2 + E_3)$  represent the scattered field expression for the rounded wedge. Furthermore, for small rounding (i.e.  $ka$  not too large relative to unity) we may consider  $f_R$  as the diffracted field pattern where  $E_0 (E_2 + E_3)$  is considered to be a perturbation term due to the edge rounding of the sharp wedge diffraction term  $E_0 E_1$ . Equation (3-36) represents a solution for the coefficients  $d_p$  (when  $m$

is odd), and  $h_p$  (when  $m$  is even) and leads to two independent sets of simultaneous equations.

Figure 3-4 shows the case of two identical conducting rounded wedges separated by  $2s$  (apex to apex distance between the virtual sharp edges) where  $2ks \gg 1$  and illuminated by a plane wave represented by Eq. (2-1). The field at any point is considered to be composed of the geometric optics field, a single diffracted field from each wedge, and a diffracted field due to multiple interaction between the two wedges. The singly diffracted field is given by

$$E_S = E_0(\rho_1 + s \sin \theta_0) f_R(\nu, \phi_{01}, \phi_1, a) + E_0(\rho_2 - s \sin \theta_0) f_R(\nu, \phi_{02}, \phi_2, a). \quad (3-37)$$

To determine the field due to the multiple interaction between the two wedges, a table similar to that of Karp and Keller is constructed [43]. By referring to this table and using Eq. (3-26), the total multiply diffracted field  $E_m$  is obtained by adding all types of fields in the table. Thus  $E_m$  can be written in the form

$$E_m = \left\{ E_0(2s) f_R(\nu, \phi_{02}, \pi, a) [ E_0(2s) E_0(\rho_2) \cdot f_R(\nu, \pi, \pi, a) f_R(\nu, \pi, \phi_2, a) + E_0(\rho_1) \cdot f_R(\nu, \pi, \phi_1, a) ] + E_0(2s) f_R(\nu, \phi_{01}, \pi, a) \cdot [ E_0(2s) E_0(\rho_1) f_R(\nu, \pi, \phi_1, a) f_R(\nu, \pi, \pi, a) + E_0(\rho_2) f_R(\nu, \pi, \phi_2, a) ] \right\} \cdot [ 1 - E_0^2(2s) f_R^2(\nu, \pi, \pi, a) ]^{-1}. \quad (3-38)$$

Hence, the total diffracted field  $E^d$  equals  $E_S + E_m$  which is valid in the range

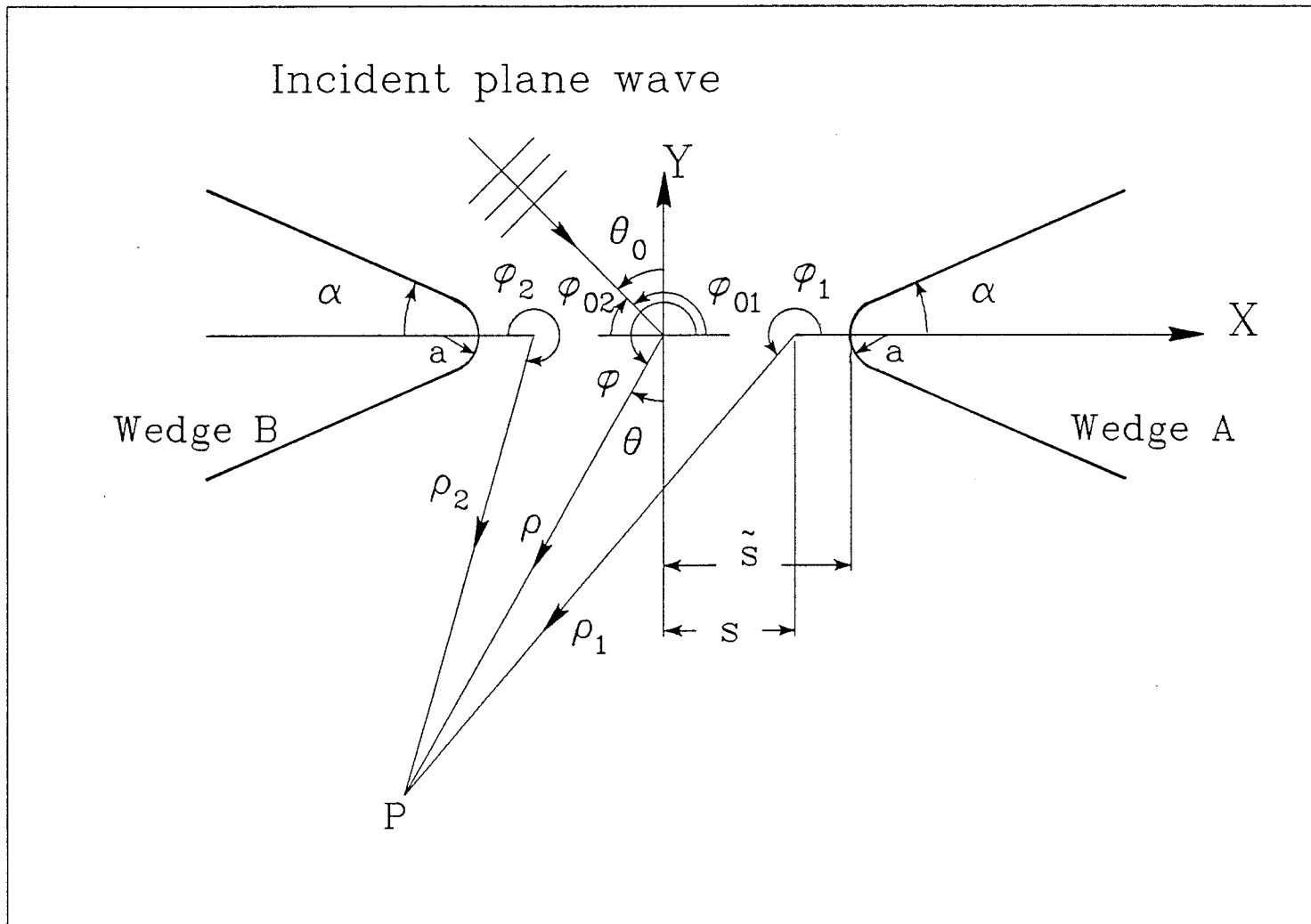


Fig. 3-4 : Double rounded-wedge geometry.

$$-\pi/2 + 2\gamma \leq \theta \leq \pi/2 - 2\gamma \text{ and } 0 \leq \gamma < \pi/4.$$

The total diffracted field is then expressed in a normalized coordinate system with a common origin centered between the two wedges. Employing the well known approximations for the far field and using the resulting relations between the angles and distances shown in Fig. 3-4 and given by Eqs. (2-47) to (2-49), the total diffracted field may be expressed as

$$E^d = E_0(\rho) F(\theta, s, \nu, a) \quad (3-39)$$

where the diffracted field pattern  $F$  of the double rounded wedge is given by

$$\begin{aligned} F(\theta, s, \nu, a) = & e^{jks(\sin\theta - \sin\theta_0)} f_R(\nu, \phi_{01}, \phi_1, a) \\ & + e^{-jks(\sin\theta - \sin\theta_0)} f_R(\nu, \phi_{02}, \phi_2, a) \\ & + E_0(2s) \left\{ e^{jks\sin\theta} f_R(\nu, \pi, \phi_1, a) \right. \\ & \cdot [f_R(\nu, \phi_{02}, \pi, a) + E_0(2s) f_R(\nu, \phi_{01}, \pi, a) \\ & \cdot f_R(\nu, \pi, \pi, a)] + e^{-jks\sin\theta} f_R(\nu, \pi, \phi_2, a) \\ & \cdot [f_R(\nu, \phi_{01}, \pi, a) + E_0(2s) f_R(\nu, \phi_{02}, \pi, a) \\ & \cdot f_R(\nu, \pi, \pi, a)] \left. \right\} [1 - E_0^2(2s) f_R^2(\nu, \pi, \pi, a)]^{-1}. \quad (3-40) \end{aligned}$$

The transmission coefficient  $\tilde{T}$  for a plane wave incident at any angle  $\theta_0$  is given by

$$\tilde{T} = \text{Re} [(1 - j) F(\theta, s, \nu, a) / 2k\bar{s}] \quad (3-41)$$

where  $\bar{s} = s + a + a / \sin\gamma$  and  $F$  is given by Eq. (3-40) in the limit as  $\theta$  approaches  $\theta_0$ . It is obvious that as  $a$  approaches zero,  $\tilde{T}$  approaches  $T$  which is the

transmission coefficient of a sharp double wedge of aperture  $2s$  given by Eq. (3-16).

#### 3.4 Scattering by a double wedge and a parallel cylinder

An asymptotic solution based on the field scattered by three objects due to an incident E-polarized plane wave has not received great attention in the literature. A possible approach is to use fictitious line sources, properly located according to the geometry of each scatterer, to account for the interaction fields between the scatterers. In this section we show that it is possible to apply an asymptotic technique for two or more different scatterers provided that all of them are infinite along one of the coordinate axes. Examples of such scatterers are infinite cylinders with arbitrary cross sections, half planes, wedges with sharp, rounded, or capped edges, or any combination of these bodies. In the present geometry, we consider a circular conducting or dielectric cylindrical scatterer located half way between the edges of a double sharp wedge or along the normal to the aperture plane of two sharp wedges at a distance  $d$  from the center. Both the cylindrical scatterer and the double wedge are assumed to be infinite in the  $z$  direction. It should be pointed out that any improvement in the diffraction or scattering behavior of a double wedge (or a slit) using a third body (as shown in Fig. 3-5) could be useful particularly for tandem or coupled apertures and aperture arrays. A similar loading of the full aperture of a slit by a circular dielectric cylinder was investigated by Hurd and Sachdeva [86] whose solution is restricted to narrow slit widths ( $ks \ll 2.4 / \sqrt{\epsilon_r}$ ) and yields a maximum error of 2.1 % in the transmission coefficient when  $\epsilon_r = 1$ .

In the following analysis the interaction fields between the cylindrical scatterer and the two wedges are clearly presented by simple relations using the known solutions for the scattered field by a wedge alone and a cylindrical scatterer alone due to plane wave incidence and line source excitation.

For a line source of unit amplitude at  $(\rho_0, \phi_0)$  and parallel to the  $z$  axis, the total field in the presence of the wedge is the incident field  $E_i^i$ , given by Eq. (2-4)



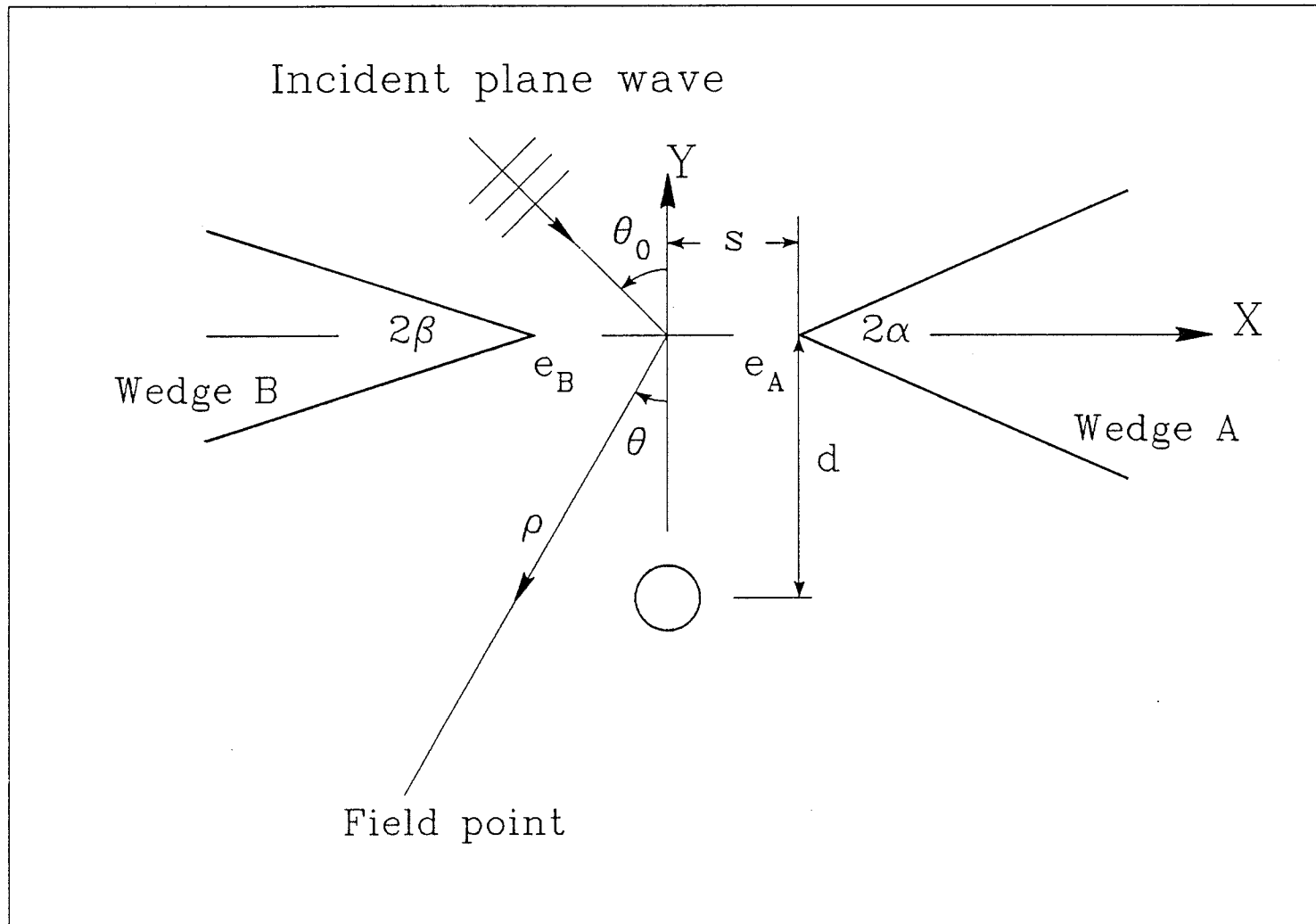


Fig. 3-5 : Double sharp-wedge and a cylindrical scatterer.

plus the scattered field  $E_i^{SW}$ . After some mathematical manipulations  $E_i^j$  can be written in the following form (see Appendix B)

$$E_i^j = \frac{-\eta k}{4} H_0(k\rho) e^{jk\rho_0 \cos(\phi - \phi_0)} \quad (3-42)$$

and by using the exact series solution of the total field due to a line source near a conducting sharp wedge [87],  $E_i^{SW}$  is found to be

$$E_i^{SW} = \frac{-\eta k}{4} H_0(k\rho) f^W(\phi, \rho_0, \phi_0, \nu) \quad (3-43)$$

where

$$f^W(\phi, \rho_0, \phi_0, \nu) = -e^{jk\rho_0 \cos(\phi - \phi_0)} + \frac{4}{\nu} \sum_{n=1}^{\infty} j^{\frac{n}{\nu}} J_{\frac{n}{\nu}}(k\rho_0) \sin \frac{n}{\nu}(\phi - \gamma) \sin \frac{n}{\nu}(\phi_0 - \gamma) \quad (3-44)$$

and where the asymptotic expression of the Hankel function is replaced by the Hankel function itself in the expression of  $E_i^{SW}$ .

For a plane wave of unit amplitude given by Eq. (2-1) the far diffracted field  $E_p^{dW}$  is the same as the far scattered field  $E_p^{SW}$  in the forward direction. Hence,  $E_p^{SW}$  may be obtained from Eqs. (3-1) and (3-3).

If the loading object is a circular cylinder defined by the surface  $\rho = a$  with axis along the  $z$  axis, the scattered fields due to line source and plane wave excitation of a circular cylinder are given by  $E_i^{SC}$  and  $E_p^{SC}$ , respectively [88,89], and may be rewritten in the following form

$$E_i^{SC} = \frac{-\eta k}{4} H_0(k\rho) f(\phi, \rho_0, \phi_0, a) \quad (3-45)$$

$$E_p^{SC} = \frac{-\eta k}{4} H_0(k\rho) g(\phi, \phi_0, a). \quad (3-46)$$

Here the superscript  $c$  refers to the cylinder,  $f$  and  $g$  are the scattered field patterns due to a line source field and an incident plane wave, respectively. For a conducting cylinder, the  $f$  and  $g$  functions in Eqs. (3-45) and (3-46) are denoted by  $f_c$  and  $g_c$  respectively, where

$$f_c(\phi, \rho_0, \phi_0, a) = - \sum_{n=0}^{\infty} \epsilon_n j^n \frac{J_n(ka)}{H_n(ka)} H_n(k\rho_0) \cos n(\phi - \phi_0) \quad (3-47)$$

and

$$g_c(\phi, \phi_0, a) = \frac{4}{\eta k} \sum_{n=0}^{\infty} \epsilon_n (-1)^n \frac{J_n(ka)}{H_n(ka)} \cos n(\phi - \phi_0) \quad (3-48)$$

whereas for a dielectric cylinder of relative permittivity  $\epsilon_r$ , the corresponding scattered field patterns  $f_d$  and  $g_d$  due to a line source field and a plane wave incident are given, respectively, by

$$f_d(\phi, \rho_0, \phi_0, a, \epsilon_r) = - \sum_{n=0}^{\infty} \epsilon_n j^n T_n H_n(k\rho_0) \cos n(\phi - \phi_0) \quad (3-49)$$

and

$$g_d(\phi, \phi_0, a, \epsilon_r) = \frac{4}{\eta k} \sum_{n=0}^{\infty} \epsilon_n (-1)^n T_n \cos n(\phi - \phi_0) \quad (3-50)$$

where

$$T_n = \frac{k J_n(k_1 a) J_n'(ka) - k_1 J_n(ka) J_n'(k_1 a)}{k J_n(k_1 a) H_n'(ka) - k_1 H_n(ka) J_n'(k_1 a)} \quad (3-51)$$

One may also use a circular cylindrical dielectric shell defined by the two surfaces  $\rho = \rho_a$  and  $\rho = \rho_b$  with its axis coinciding with the  $z$  axis and of inhomogeneous permittivity as a loading object. Due to the difficulty of finding a formal solution to the time harmonic electromagnetic fields in regions where the permittivity  $\epsilon$  is a

general function of position, one has to force the permittivity variations to fit in one of the special cases which has a formal solution. If  $\epsilon$  is proportional to  $\rho^{-2}$  and is a function of  $\phi$  in circular cylindrical coordinates, the  $z$  component of the electromagnetic fields can be represented by infinite series involving Mathieu functions as shown by Casey [90]. In Appendix C we formulate the solution of the problem of scattering by a plane wave incident on an infinitely long dielectric cylindrical shell having radial and azimuthal inhomogeneity profiles. The corresponding scattered field patterns due to a line source and an incident plane wave are then given, respectively by (see Appendix C),

$$f_s = \sum_{n=0}^{\infty} \epsilon_n c_n H_n(k\rho_0) \cos n(\phi - \phi_0) \quad (3-52)$$

and

$$g_s = \frac{-4}{\eta k} \sum_{n=0}^{\infty} \epsilon_n c_n j^n \cos n(\phi - \phi_0) \quad (3-53)$$

where the expansion coefficients  $c_n$  are determined by Eq. (C-19). From Eqs. (3-45) to (3-53) one notices that the far scattered field from a wedge or any of the above mentioned cylindrical scatterers due to either plane wave or line source excitation has the appearance of a cylindrical wave emanating from a fictitious inhomogeneous line source at the edge of the wedge or at the axis of the cylindrical scatterer.

In case of two conducting wedges separated by a distance  $2s$ , where  $2ks \gg 1$  and a circular cylinder (or a cylindrical shell) whose axis is parallel to the edges of the two wedges, and where all three bodies are illuminated by a plane wave of unit amplitude (see Fig. 3-5), the field at any point is considered to be composed of the incident field  $E_p^i$  plus a scattered field  $E^S$  from each of the two wedges and the cylindrical scatterer. The latter field consists of an unperturbed term due to the three scatterers plus an interaction field which will be evaluated using three fictitious

line sources located at the wedge edges ( $e_A$  and  $e_B$ ) and along the cylindrical scatterer axis. If the plane wave incidence angle is restricted such that the incident field does not illuminate the lower faces of the wedges, the scattered field  $E^S$  in the forward direction is given by

$$E^S = E^{S1} + E^{S2} + E^{S3} \quad (3-54)$$

where

$$E^{S1} = \frac{-\eta k}{4} H_0(k\rho_1) [ e^{-jks \sin \theta_0} g^W(\phi_1, \phi_{01}, \nu_1) + c_3 f^W(\phi_1, l_1, \phi_{31}, \nu_1) + c_2 f^W(\phi_1, 2s, \phi_{21}, \nu_1) ] \quad (3-55)$$

$$E^{S2} = \frac{-\eta k}{4} H_0(k\rho_2) [ e^{+jks \sin \theta_0} g^W(\phi_2, \phi_{02}, \nu_2) + c_3 f^W(\phi_2, l_2, \phi_{32}, \nu_2) + c_1 f^W(\phi_2, 2s, \phi_{12}, \nu_2) ] \quad (3-56)$$

$$E^{S3} = \frac{-\eta k}{4} H_0(k\rho_3) [ e^{-jkd \cos \theta_0} g(\phi_3, \phi_{03}, a) + c_1 f(\phi_3, l_1, \phi_{13}, a) + c_2 f(\phi_3, l_2, \phi_{23}, a) ] \quad (3-57)$$

$$\nu_1 = 2(\pi - \alpha) / \pi \quad (3-58)$$

$$\nu_2 = 2(\pi - \beta) / \pi . \quad (3-59)$$

In the above equations  $c_1$ ,  $c_2$ , and  $c_3$  are the unknown strengths of the line sources at  $e_A$ ,  $e_B$  and along the cylindrical scatterer axis, respectively.

For the determination of  $c_1$ ,  $c_2$  and  $c_3$  one may applying the principle of consistency of the scattered field components which are shown in Figs. 3-6 and 3-7. This leads to the following results

$$2c_1 - c_2 [ f^W(\phi_{31}, 2s, \phi_{21}, \nu_1) + f^W(\phi_{21}, 2s, \phi_{21}, \nu_1) ]$$

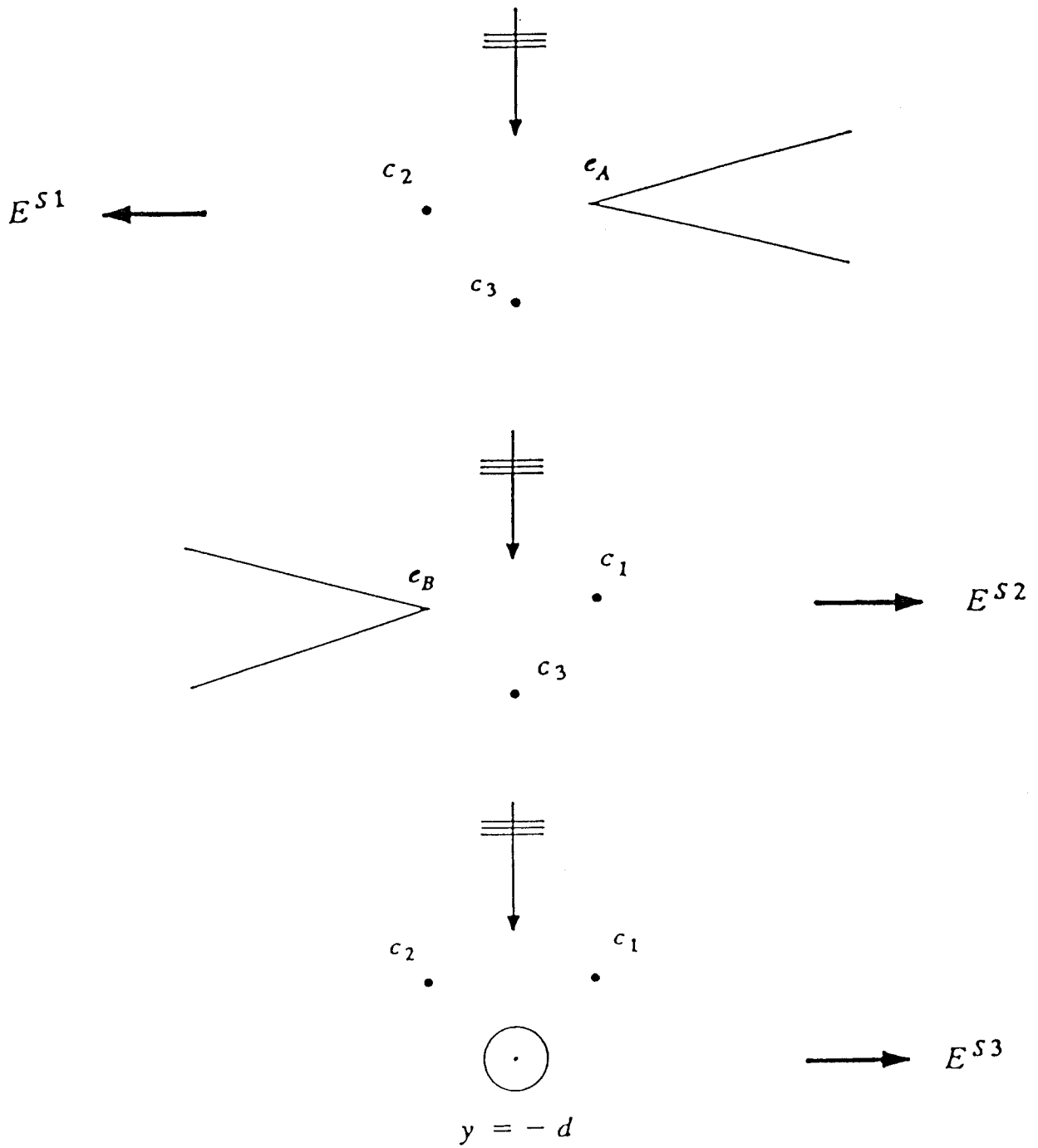


Fig. 3-6 : Scattered field components due to a plane wave incident on two sharp wedges and a parallel cylindrical scatterer.

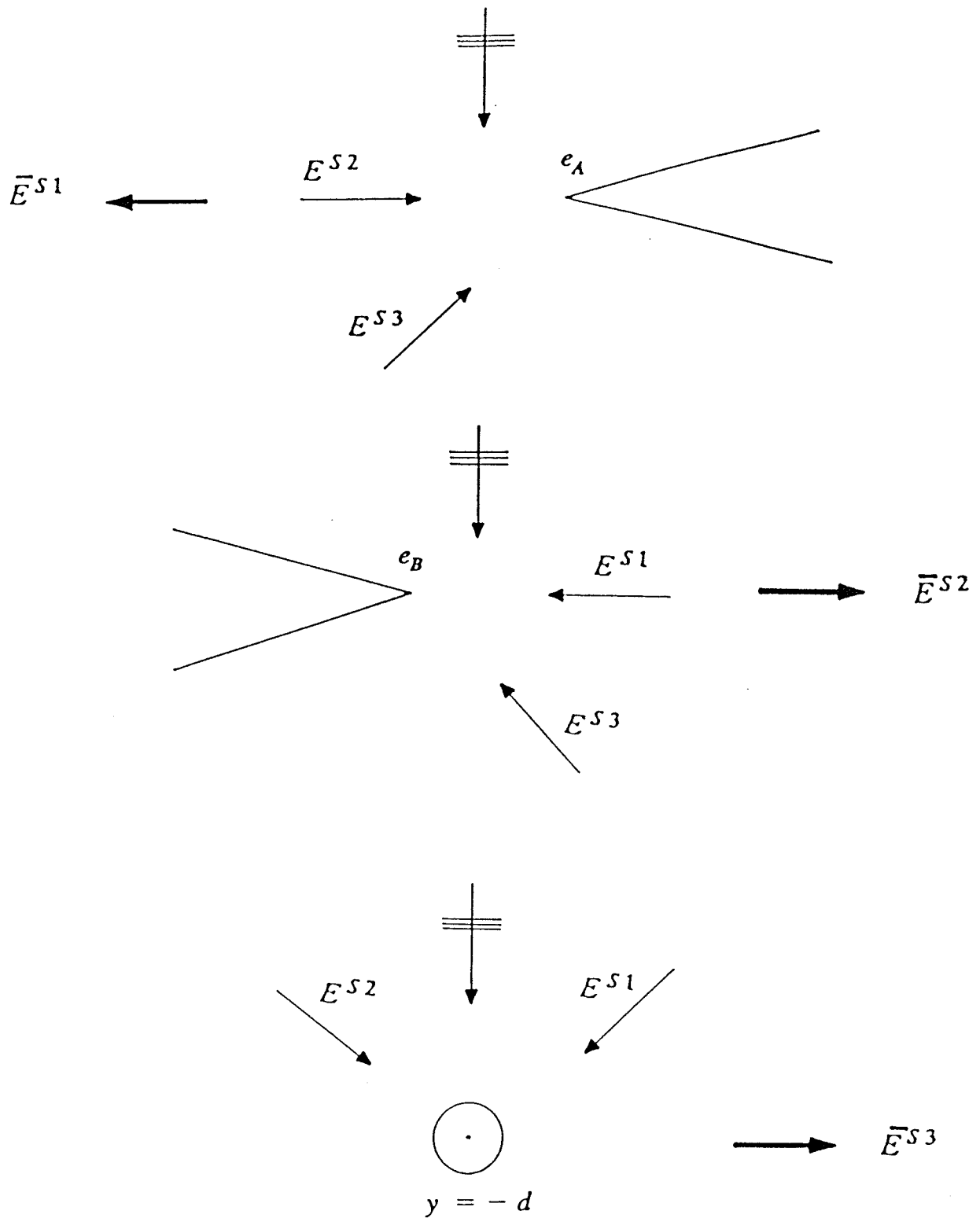


Fig. 3-7 : Alternative representation of the scattered field components due to a plane wave incident on two sharp wedges and a parallel cylindrical scatterer.

$$\begin{aligned}
 & - c_3 [ f^W ( \phi_{31}, l_1, \phi_{31}, \nu_1 ) + f^W ( \phi_{21}, l_1, \phi_{31}, \nu_1 ) ] \\
 & = e^{-jks \sin \theta_0} [ g^W ( \phi_{31}, \phi_{01}, \nu_1 ) + g^W ( \phi_{21}, \phi_{01}, \nu_1 ) ] \quad (3-60)
 \end{aligned}$$

$$\begin{aligned}
 & - c_1 [ f^W ( \phi_{32}, 2s, \phi_{12}, \nu_2 ) + f^W ( \phi_{12}, 2s, \phi_{12}, \nu_2 ) ] + 2c_2 \\
 & - c_3 [ f^W ( \phi_{32}, l_2, \phi_{32}, \nu_2 ) + f^W ( \phi_{12}, l_2, \phi_{32}, \nu_2 ) ] \\
 & = e^{+jks \sin \theta_0} [ g^W ( \phi_{32}, \phi_{02}, \nu_2 ) + g^W ( \phi_{12}, \phi_{02}, \nu_2 ) ] \quad (3-61)
 \end{aligned}$$

$$\begin{aligned}
 & - c_1 [ f ( \phi_{13}, l_1, \phi_{13}, a ) + f ( \phi_{23}, l_1, \phi_{13}, a ) ] \\
 & - c_2 [ f ( \phi_{13}, l_2, \phi_{23}, a ) + f ( \phi_{23}, l_2, \phi_{23}, a ) ] + 2c_3 \\
 & = e^{-jkd \cos \theta_0} [ g ( \phi_{13}, \phi_{03}, a ) + g ( \phi_{23}, \phi_{03}, a ) ] . \quad (3-62)
 \end{aligned}$$

Upon solving Eqs. (3-60), (3-61) and (3-62) for  $c_1$ ,  $c_2$  and  $c_3$ , the scattered field  $E^S$  is found and can be expressed in a normalized coordinate system, where the  $z$  axis coincides with the center of the aperture as shown in Fig. 3-5 and the well known far field conditions are used. In addition to Eqs. (2-47) to (2-49), we have  $\phi_{03} = \pi/2 + \theta_0$ ,  $\phi_3 = \phi_1$ ,  $\phi_{12} = \phi_{21} \approx \pi$ ,  $\phi_{13} = \psi \approx \tan^{-1}(d/s)$ ,  $\phi_{31} = \phi_{32} \approx \pi + \psi$ ,  $\phi_{23} \approx \pi - \psi$  and  $\rho_3 \approx \rho - d \cos \theta$ , where  $l_1$  and  $l_2$  are the distances between  $e_A$  and  $e_B$  and the cylindrical scatterer axis, respectively.  $E^S$  can then be written in the following form

$$E^S = \frac{e^{-jk\rho}}{\sqrt{\pi k \rho}} F ( \theta, s, d, \nu_1, \nu_2, a, \epsilon_r ) \quad (3-63)$$

where the scattered field pattern  $F$  of the present geometry is obtained from Eq. (3-



63) and the transmission coefficient  $\vec{T}$  for plane wave incidence is calculated using Eq. (3-16).

### 3.5 Numerical examples

Although the formulation is general, it seems reasonable to concentrate on the symmetric configuration where  $\theta_0 = 0^\circ$ ,  $\alpha = \beta = \gamma$ ,  $r_1 = r_2 = r$ ,  $\epsilon_{r1} = \epsilon_{r2} = \epsilon_r$  and  $s_1 = s_2 = s$ . Furthermore, when the field point approaches the wedge surface, the UTD is used to avoid the errors due to the non-uniform functions  $g^W$  and  $f^W$ . Fig. 3-8 shows the normalized  $E^d$  pattern for two wedges with  $\gamma = 15^\circ$  and  $ks = 5$ . The figure demonstrates the effects of  $E''$  on the far field diffraction pattern with and without the interaction term  $E''$ . The dependence of  $T$ ,  $c_1$  (or  $c_2$ ) and  $E''$  on  $ks$  is shown in Fig. 3-9 for  $\gamma = 15^\circ$ . It is apparent that  $T$  oscillates with varying  $ks$ , however the oscillations die down and  $T$  converges to unity as expected for large  $ks$ . The interaction term  $E''$  is damped in an oscillatory fashion with increasing  $ks$  and approaches zero when  $ks$  approaches infinity. The period of oscillation is equal to  $\pi$ . It is found that the location of maxima of  $E''$  remains the same while their peak values change for variations in  $\gamma$  [70,71]. Furthermore, one should point out that the oscillations in the current intensity ( $c_1$  or  $c_2$ ) due to  $E''$  is critically dependent on  $ks$ . The period of oscillations is again equal to  $\pi$ . The fact that the oscillations of  $E''$  and  $c_1$  (or  $c_2$ ) are similar confirms the dependence of  $E''$  on  $c_1$  (or  $c_2$ ).

Figure 3-10 shows the effect of the conducting cap radius on the normalized  $E^d$  pattern of a double capped wedge for  $ks = 8$  and  $\gamma = 5^\circ$ . It is found that the beamwidth increases with the cap radius. For example, as  $kr$  assumes the values 0.0, 0.3, 0.6 and 0.9 the beamwidth becomes  $17.03^\circ$ ,  $18.92^\circ$ ,  $21.5^\circ$  and  $22.59^\circ$ , respectively. However, for the case of a dielectric capped double wedge, Fig. 3-11 shows that the beamwidth decreases with  $\epsilon_r$  for  $ks = 7$ ,  $\gamma = 10^\circ$  and  $kr = 0.5$ . For the indicated values of  $\epsilon_r$ , namely 1, 5, 7 and 9, the corresponding values of the beamwidth are  $21.96^\circ$ ,  $19.11^\circ$ ,  $17.72^\circ$  and  $16.82^\circ$ , respectively. Similar reduction in

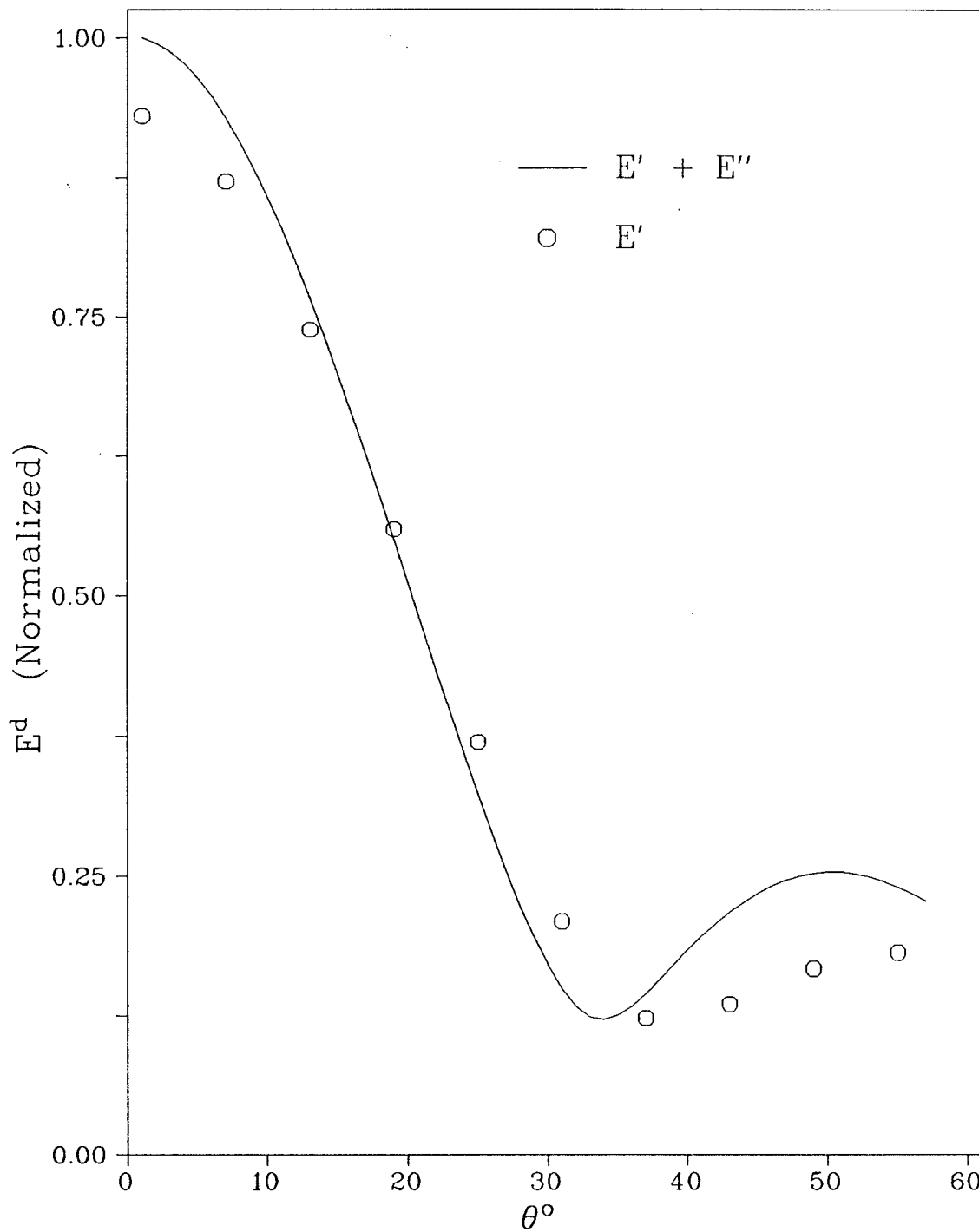


Fig. 3-8 : Normalized diffracted field vs.  $\theta$   
for  $\theta_0 = 0^\circ$ ,  $\gamma = 15^\circ$  and  $ks = 5$ .

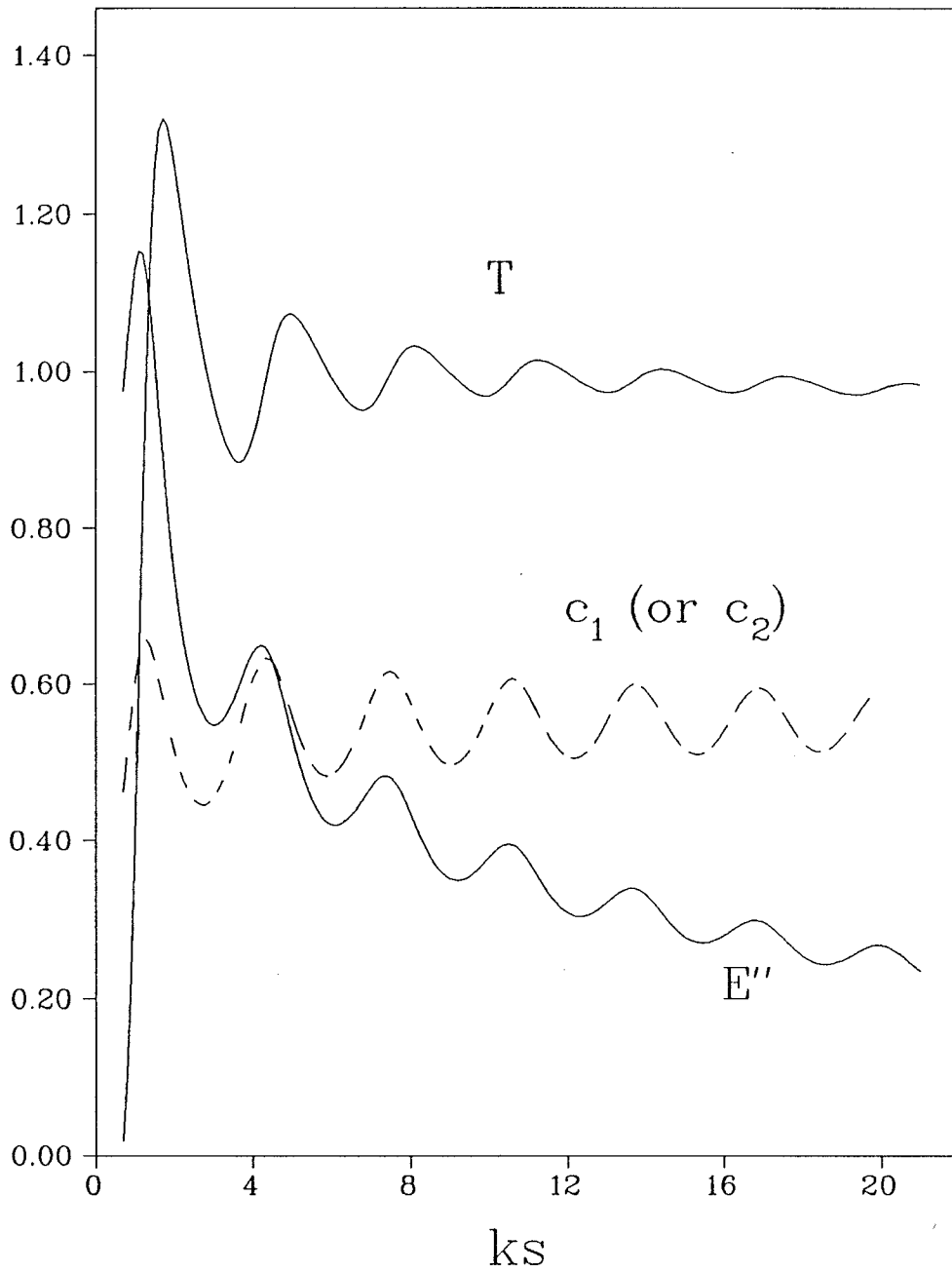


Fig. 3-9 : T,  $c_1$  (or  $c_2$ ) and  $E''$  vs.  $ks$   
for  $\theta_0 = 0^\circ$  and  $\gamma = 15^\circ$ .

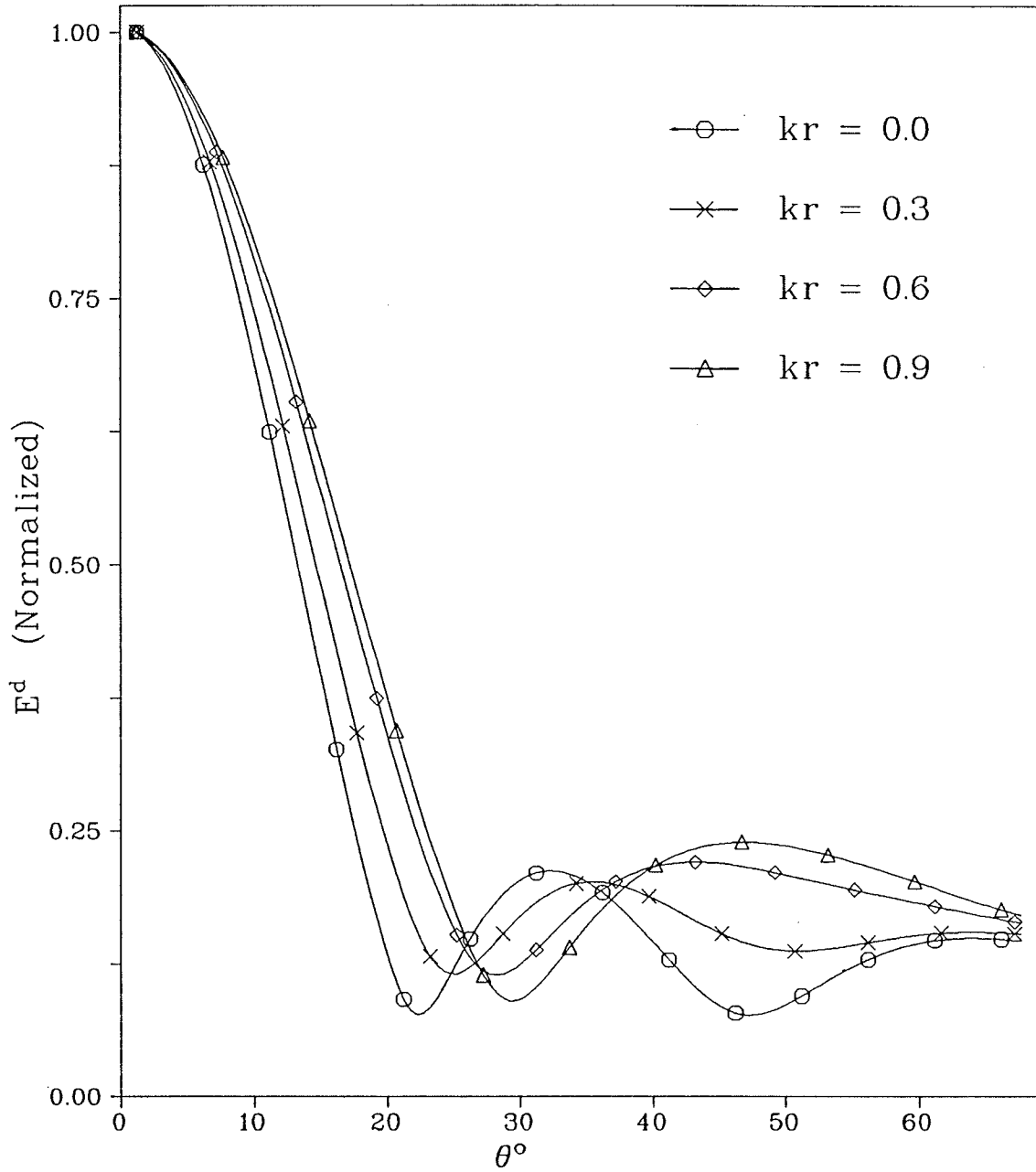


Fig. 3-10 : Normalized diffracted field vs.  $\theta$  of a double conducting capped-wedge for  $ks = 8$  and  $\gamma = 5^\circ$ .

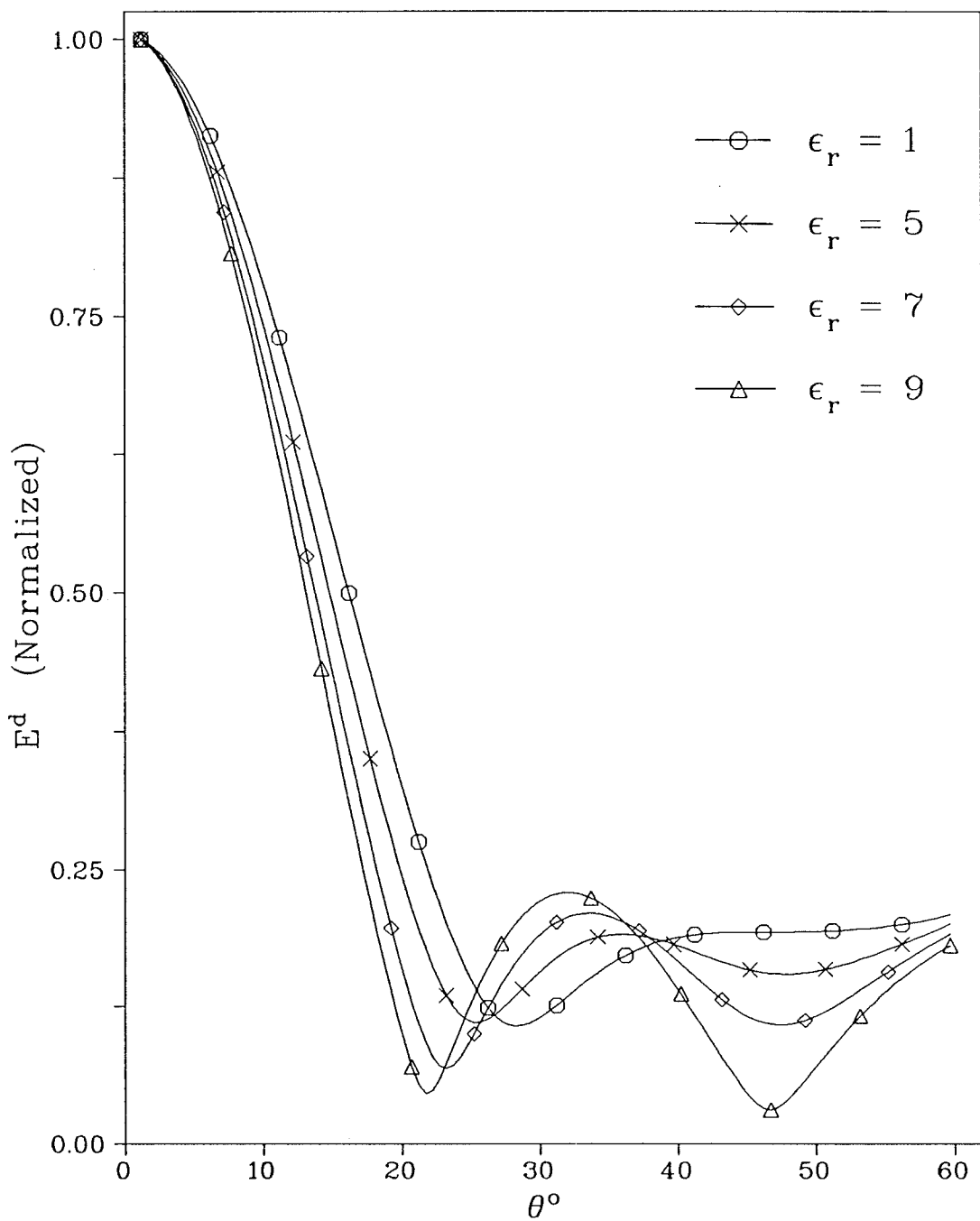


Fig. 3-11 : Normalized diffracted field vs.  $\theta$  of a double dielectric capped-wedge. for  $ks = 7$ ,  $\gamma = 10^\circ$  and  $Kr = 0.5$ .

the beamwidth is observed when the electric radius of the dielectric cap  $k_1r$  increases although this is not shown here.

The dependence of  $T$  on  $kr$  is shown in Fig. 3-12 for a conducting capped slit. It is clear that  $T$  decreases in general with  $kr$ . However, for large values of  $ks$  the effect of capping decreases and  $T$  approaches unity. For a dielectrically capped slit,  $T$  is found to be increasing with  $\epsilon_r$ , as shown in Fig. 3-13 for  $kr = 0.5$ . The agreement between the decrease in  $T$  with increasing  $kr$  (shown in Fig. 3-12) as well as the increasing beamwidth of the radiation pattern with  $kr$  (shown in Fig. 3-10) establishes the relation between  $T$  and the beamwidth. In other words the figures clearly show that  $T$  decreases with increasing beamwidth. Also, it is clear from Figs. 3-11 and 3-13 that  $T$  increases with decreasing beamwidth, as expected.

In Fig. 3-14, the effect of the interior wedge angle  $2\gamma$  on  $T$  is shown for  $kr = 0.5$  and  $\epsilon_r = 4$ . It is found that the peak to peak value of the oscillations of  $T$  increases with  $\gamma$  for fixed values of  $kr$  and  $\epsilon_r$ . A similar effect is also observed for a conducting capped double wedge. For large  $ks$  the oscillations die down and  $T$  converges to unity, as expected.

Figure 3-15 represents a comparison between the normalized  $E^d$  pattern of the two sharp wedges ( $E_2 = E_3 = 0$ ), two capped wedges ( $E_3 = 0, ka = 0.5$ ) and two rounded wedges ( $ka = 0.5$ ) when  $\theta_0 = 0^\circ$ ,  $ks = 10$  and  $\gamma = 15^\circ$ . As shown, there is a remarkable change in the pattern characteristics. As an example, the beamwidth, first sidelobe position and level shift from  $15.29^\circ, 27.15^\circ, -13.58$  dB for  $ka = 0$  to  $23.85^\circ, 37.61^\circ, -10.58$  dB for  $ka = 0.5$  ( $E_3 = 0$ ) and  $13.43^\circ, 23.05^\circ, -13.06$  dB, for  $ka = 0.5$ , respectively.

Figure 3-16 demonstrates the effects of rounding on the normalized  $E^d$  pattern for different values of  $ka$  with  $\theta_0 = 0^\circ$ ,  $ks = 10$  and  $\gamma = 10^\circ$ . Table 3-1 illustrates the pattern characteristics shown in Fig. 3-16, in which it is seen that the beamwidth decreases with  $ka$  as well as the first sidelobe position. It is also found that for

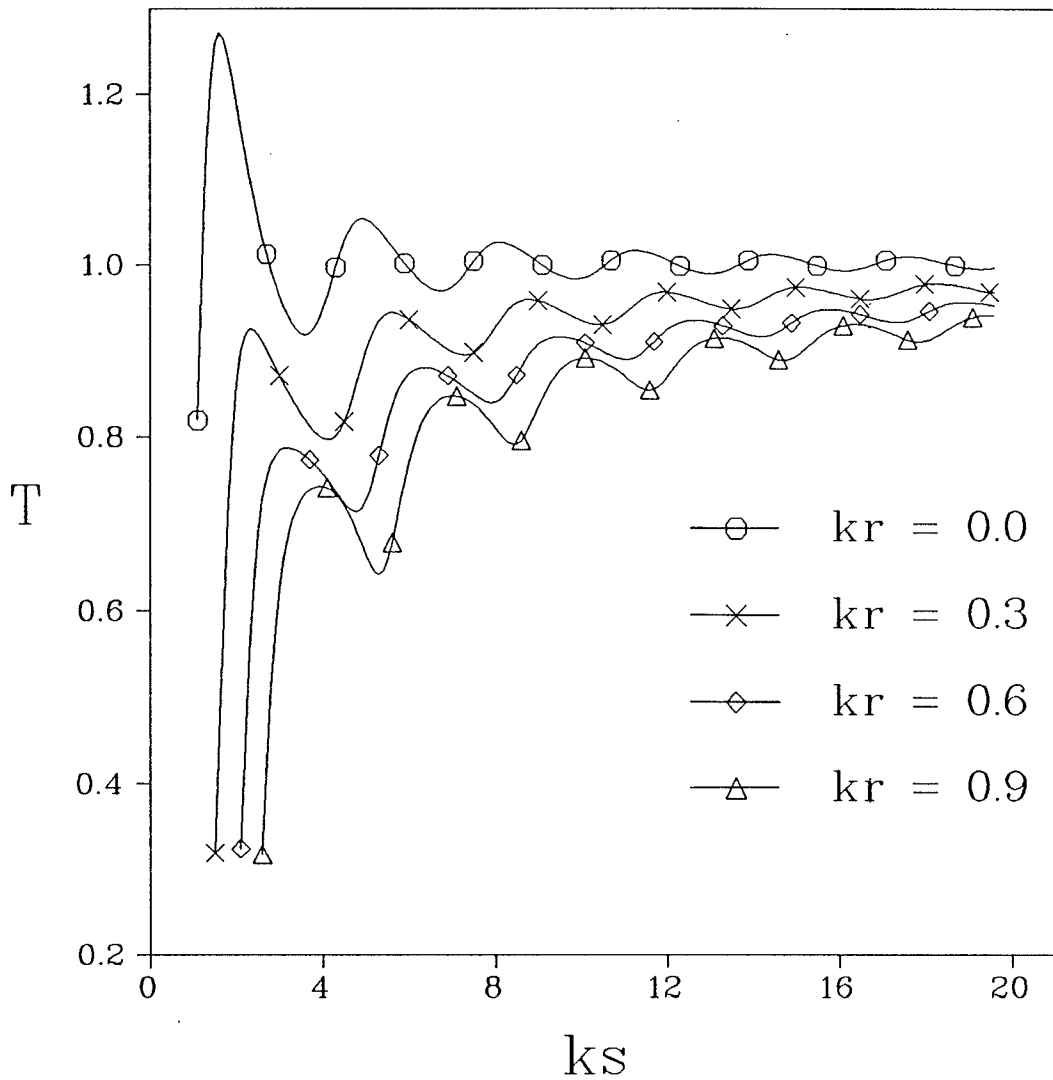


Fig. 3-12 :  $T$  vs.  $ks$  of a conducting capped-slit .

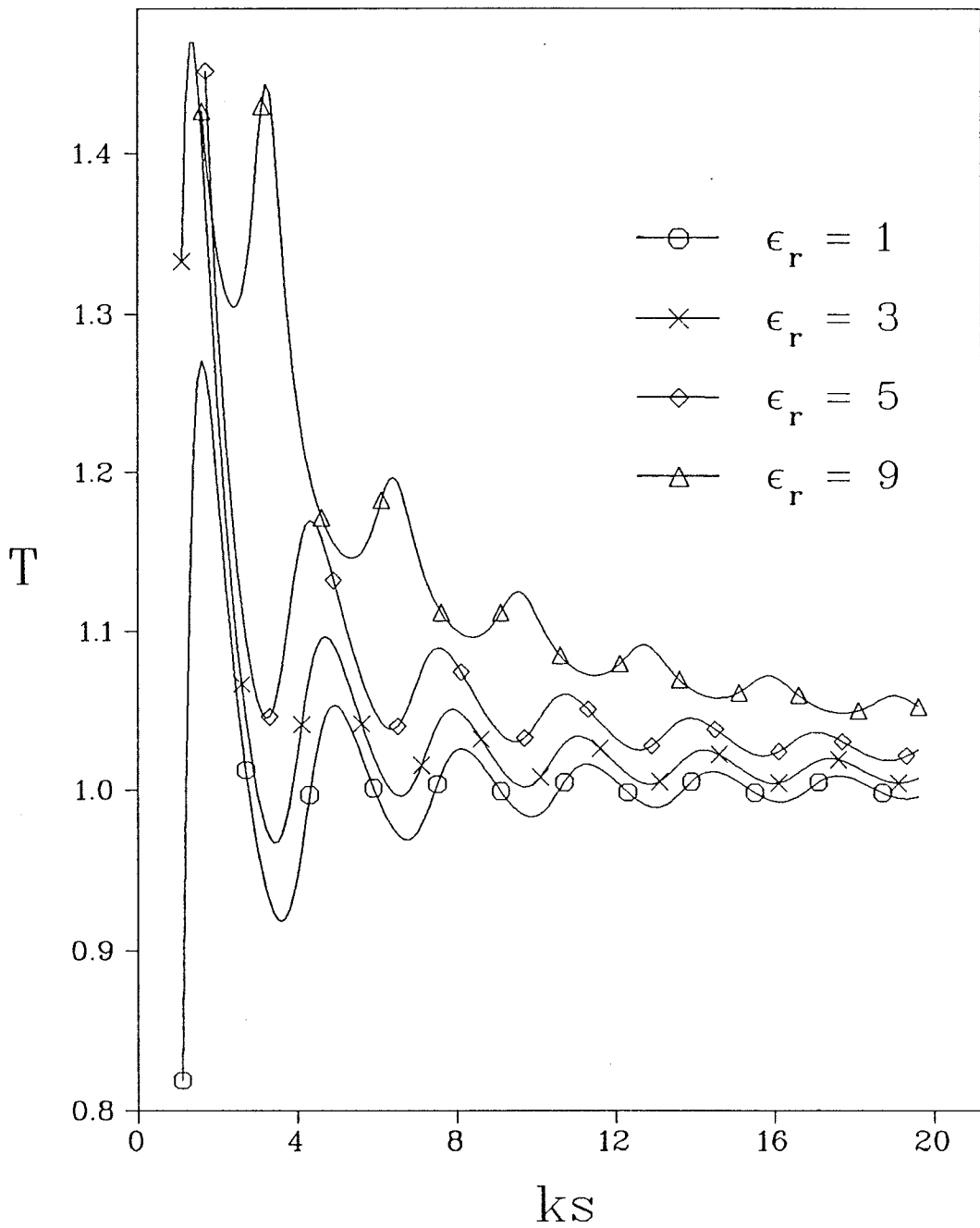


Fig. 3-13 :  $T$  vs.  $ks$  of a dielectric capped-slit for  $kr = 0.5$ .



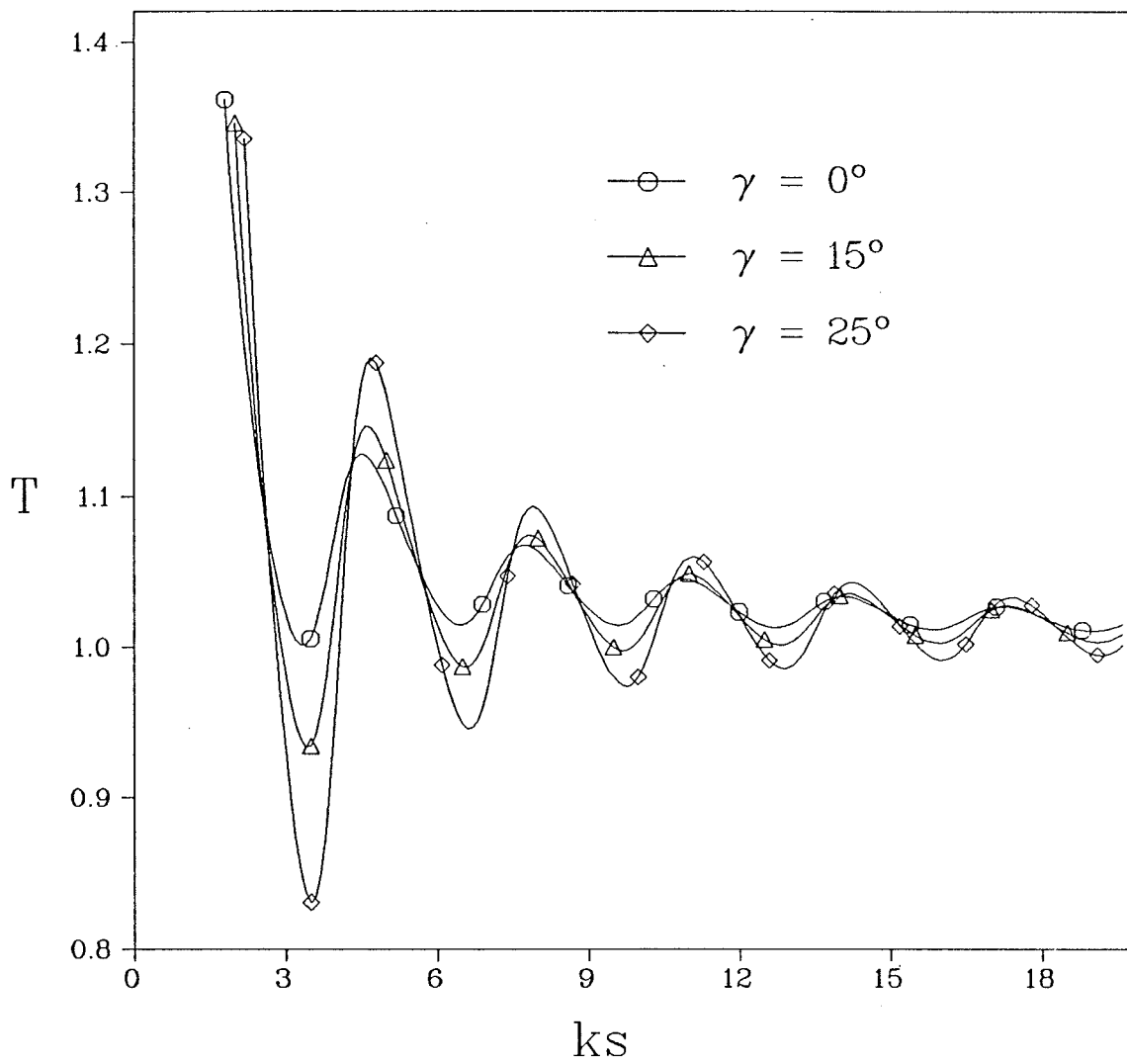


Fig. 3-14 :  $T$  vs.  $ks$  of a double dielectric capped-wedge for  $kr = 0.5$  and  $\epsilon_r = 4$ .

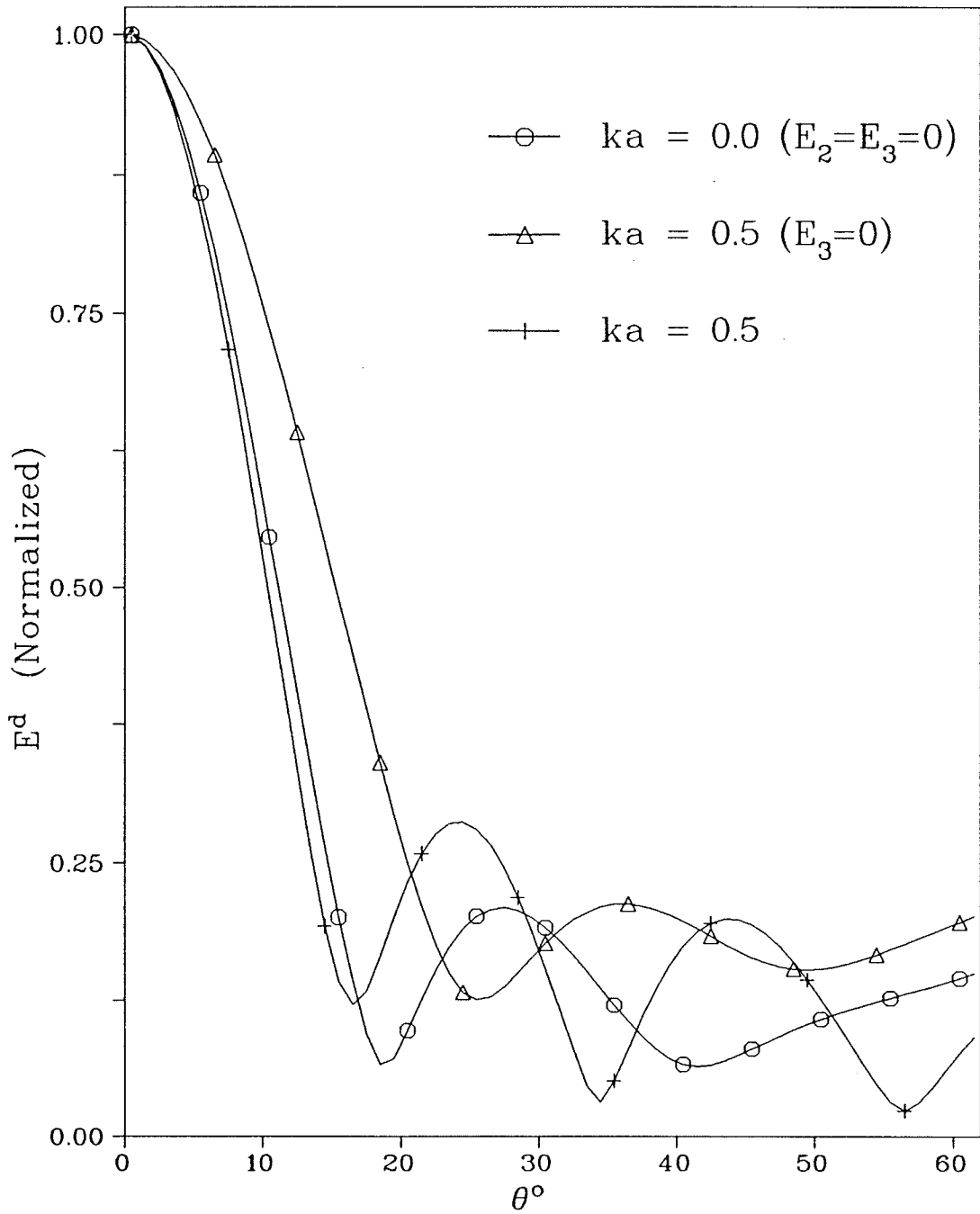


Fig. 3-15 : Normalized diffracted field vs. angle  $\theta$  of double rounded-wedge for  $\theta_0 = 0^\circ$ ,  $\gamma = 10^\circ$  and  $ks = 10$ .

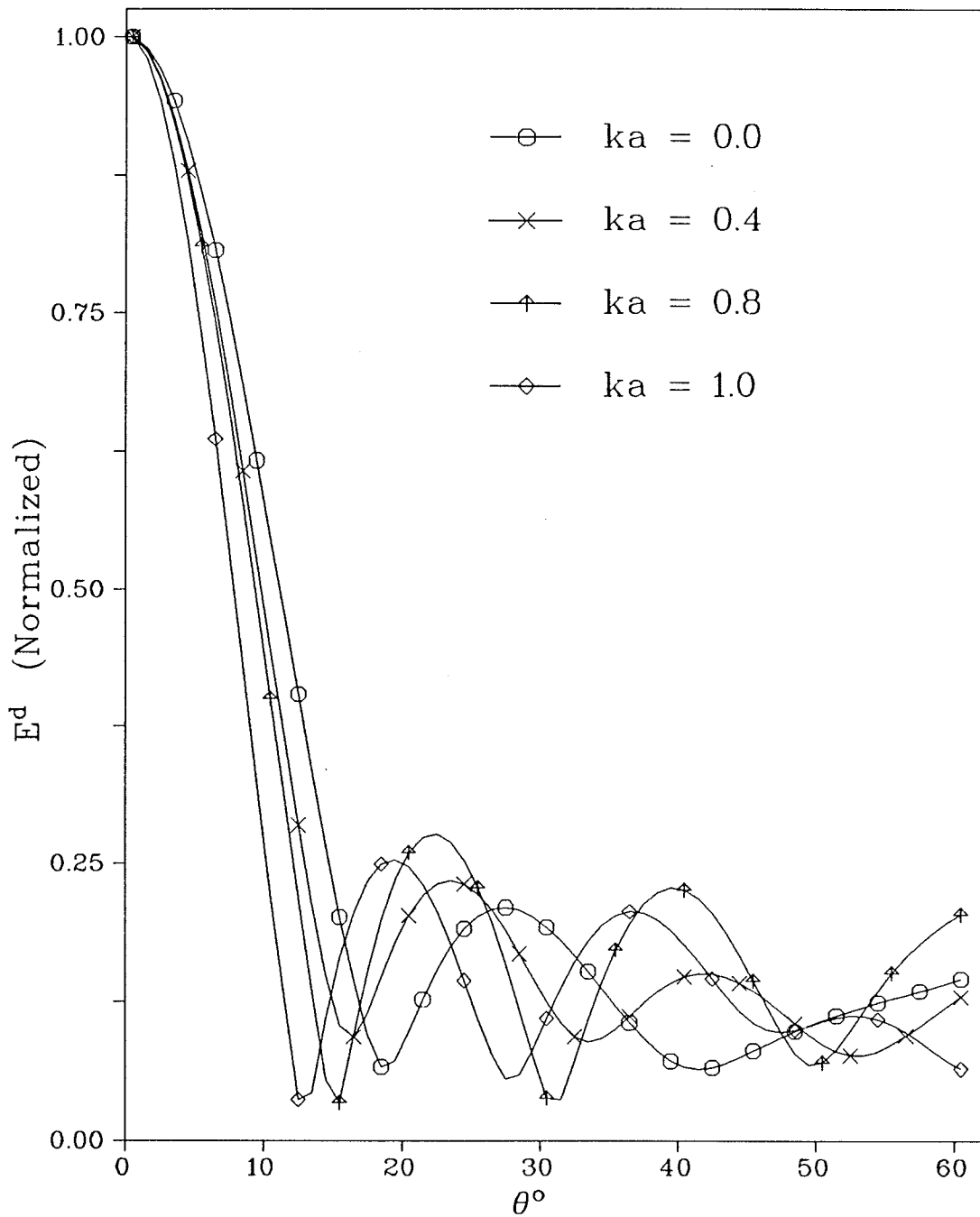


Fig. 3-16 : Normalized diffracted field vs. angle  $\theta$  of double rounded-wedge for  $\theta_0 \cong 0^\circ$ ,  $\gamma = 10^\circ$  and  $ks = 10$ .

$ka$	Beam- width	First sidelobe	
		Position	Level
0.0	15.23 <sup>0</sup>	26.89 <sup>0</sup>	-13.56 dB
0.4	13.32 <sup>0</sup>	22.99 <sup>0</sup>	-12.61 dB
0.8	12.80 <sup>0</sup>	21.80 <sup>0</sup>	-11.16 dB
1.0	10.45 <sup>0</sup>	18.87 <sup>0</sup>	-11.93 dB

Table 3-1 : Diffraction pattern characteristics of a double rounded wedge for  $\theta_0 = 0^\circ$ ,  $ks = 10$  and  $\gamma = 10^\circ$ .

increasing values of  $ka$ ,  $\bar{T}$  decreases and is usually less than  $T$  for all values of  $ks$  [91,92].

The error and region of validity of the asymptotic solution regarding the geometry of Fig. 3-5 are investigated by comparing with numerical results based on the exact solution of the unloaded slit given by Skavlem for normally incident plane wave [34]. Skavlem employed the method of separation of variables to the wave equation in elliptic coordinates and was able to calculate the transmission coefficient for slits of  $0 \leq ks \leq 10$  to five correct decimal points. As shown in table 3-2 the transmission coefficient is computed using the diffraction pattern function  $f^W$  based on Eq. (3-4), the new  $f^W$  based on Eq. (3-44) as well as the corresponding function based on the UTD. It is obvious that the new expression for  $f^W$  produces more accurate values than those based on Eq. (3-4) or the UTD, whereas the error in the  $T$  values does not exceed 0.25 % for  $ks \geq 2$ . Furthermore, for oblique incidence, our results agree with the curves provided by Millar for different values of  $\theta_0$  away from grazing incidence ( $\theta_0 = 90^\circ$ ) [39]. It should be pointed out that Millar's investigation of the diffraction of an E-polarized plane wave was based on the solution by successive substitutions of a pair of integral equations. The resulting expression for  $T$  was in the form of a series in inverse powers of  $ks$  and is in good agreement with the exact results for  $ks \geq 4$ . This comparison emphasizes the validity of the present solution for the unloaded slit for  $ks \geq 2$ .

In the presence of the cylinder, there are no published solutions for this configuration to compare with. However, if  $ks_{1,2} \gg ka$  or  $k_1a$ , the asymptotic far field expression for the field scattered by the cylinder is valid for calculating the near field around the cylinder [93]. Hence, when the cylinder is present the accuracy of the results is dependent on  $ks_1$ ,  $ks_2$ ,  $ka$  and  $\epsilon_r$ .

The transmission coefficient for a slit with a circular cylinder at or down below the center of the aperture plane is shown in Figs. 3-17 and 3-18, respectively, for a

<i>ks</i>	<i>T</i>			
	Exact	Asymptotic		
		Based on (3-44)	Based on UTD	Based on (3-4)
1.0	0.54540	0.55843	0.56833	0.60538
1.2	0.87693	0.91569	0.90869	0.99629
1.4	1.11719	1.15646	1.14831	1.21318
1.6	1.21669	1.23058	1.24153	1.26970
1.8	1.22129	1.23321	1.23631	1.24293
2.0	1.18426	1.18717	1.18997	1.18802
2.4	1.08650	1.08358	1.08225	1.07780
3.0	0.97202	0.96819	0.96605	0.96293
3.4	0.92824	0.92629	0.92519	0.92345
4.0	0.94244	0.94351	0.94392	0.94615
5.0	1.04992	1.04989	1.05078	1.05125
6.0	0.99559	0.99575	0.99420	0.99471
7.0	0.97174	0.97169	0.97177	0.97237
8.0	1.02332	1.02318	1.02331	1.02390
9.0	1.00199	1.00158	1.00120	1.00121
10.	0.98224	0.98222	0.98220	0.98228

Table 3-2 : Slit transmission coefficient for  $\phi_0 = 90^\circ$ .

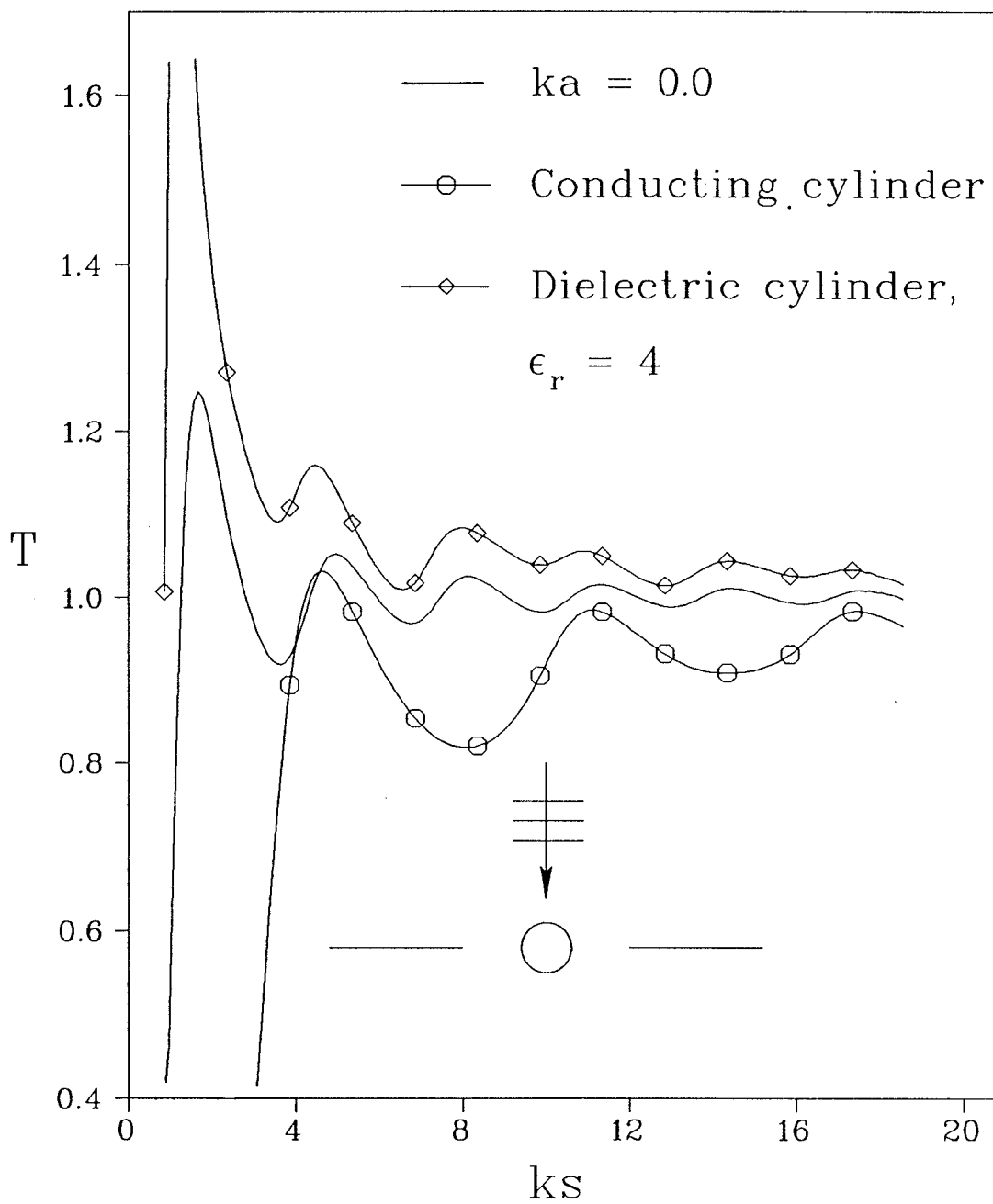


Fig. 3-17 :  $T$  vs.  $ks$  of a loaded slit for  $\theta_0 = 0^\circ$  and  $ka = 0.5$ .

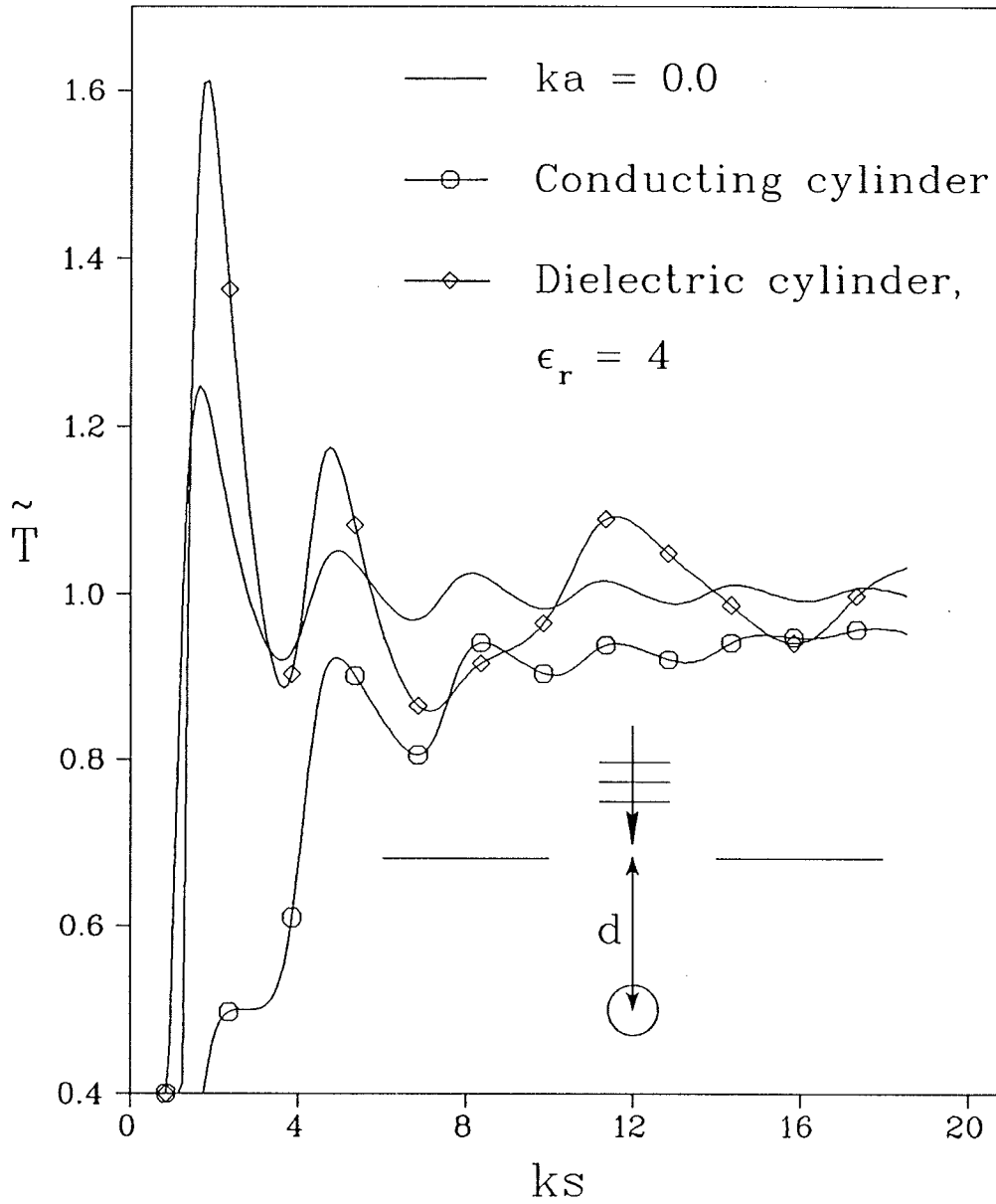


Fig. 3-18 :  $\tilde{T}$  vs.  $ks$  of a loaded slit for  $\theta_0 = 0^\circ$ ,  $ka = 0.5$  and  $kd = 5$ .



normally incident plane wave ( $\theta_0 = 0^\circ$ ) with  $ka = 0.5$  and  $\epsilon_r = 4$ . When the dielectric cylinder is at the center of the aperture plane (i.e.  $d = 0$ ),  $\bar{T}$  is always larger than  $T$ . However,  $\bar{T}$  decays in an oscillatory fashion with increasing  $ks$ , as expected, and tends to unity (i.e. geometrical optics value) as  $ks$  tends to infinity. However for a conducting cylinder,  $\bar{T}$  is in general less than  $T$ . If the loading cylinder is shifted down below the center of the aperture plane (Fig. 3-18), then  $\bar{T}$  oscillates around  $T$  for dielectric cylinder and oscillates with increasing amplitude tending to unity as  $ks$  tends to infinity for conducting cylinder.

The behavior of  $\bar{T}$  for an obliquely incident plane wave is shown in Figs. 3-19 and 3-20 for  $kd = 0$  and  $kd = 1.5$ , respectively. For  $\theta = 40^\circ$ ,  $\epsilon_r = 5, 9$  and  $ka = 0.3$ , Fig. 3-19 shows that  $\bar{T}$  exceeds unity at some values of  $ks$  and generally has large oscillations than that of the unloaded slit case ( $ka = 0$ ). Also it is observed that the peak value of  $\bar{T}$  lies in the lower range of  $ks$  ( $ks \leq 6$ ) and increases with  $\epsilon_r$ . For  $\theta_0 = 40^\circ$  and all other cylinder parameters kept constant (Fig. 3-20), one notices that the peak to peak value of oscillations decrease as  $kd$  exceeds zero. In Figs. 3-21 and 3-22,  $\bar{T}$  is shown for a conducting cylinder with different values of  $ka$ , namely 0.1, 0.2, 0.8,  $kd = 0$  (Fig. 3-21) and  $kd = 5$  (Fig. 3-22). The fact that loading with a conducting cylinder does not increase the transmission coefficient of a slit is possibly due to the effect of blocking of part of the incident field by the cylinder.

The effect of the interior wedge angle on  $\bar{T}$  of a double wedge in the presence of a conducting or dielectric cylinder is shown in Fig. 3-23 for  $\theta_0 = 0^\circ$ ,  $ka = 0.5$ ,  $\epsilon_r = 4$  and  $\gamma = 20^\circ$ . In comparing Figs. 3-17 and 3-23, it is found that the interior wedge angle changes the levels of maxima and minima of the oscillations of  $\bar{T}$ , whereas the peak positions remain the same.

The diffraction pattern of a slit loaded by an inhomogeneous dielectric shell located at the center of the aperture is shown in Fig. 3-24 for  $\phi_0 = 90^\circ$ ,  $\epsilon_a = 3$ ,  $k\rho_a = 0.2$ ,  $\eta = 2$ ,  $\delta = 1$  and different values of  $k\rho_b$ , namely 0.4, 0.6 and 1.0. It is

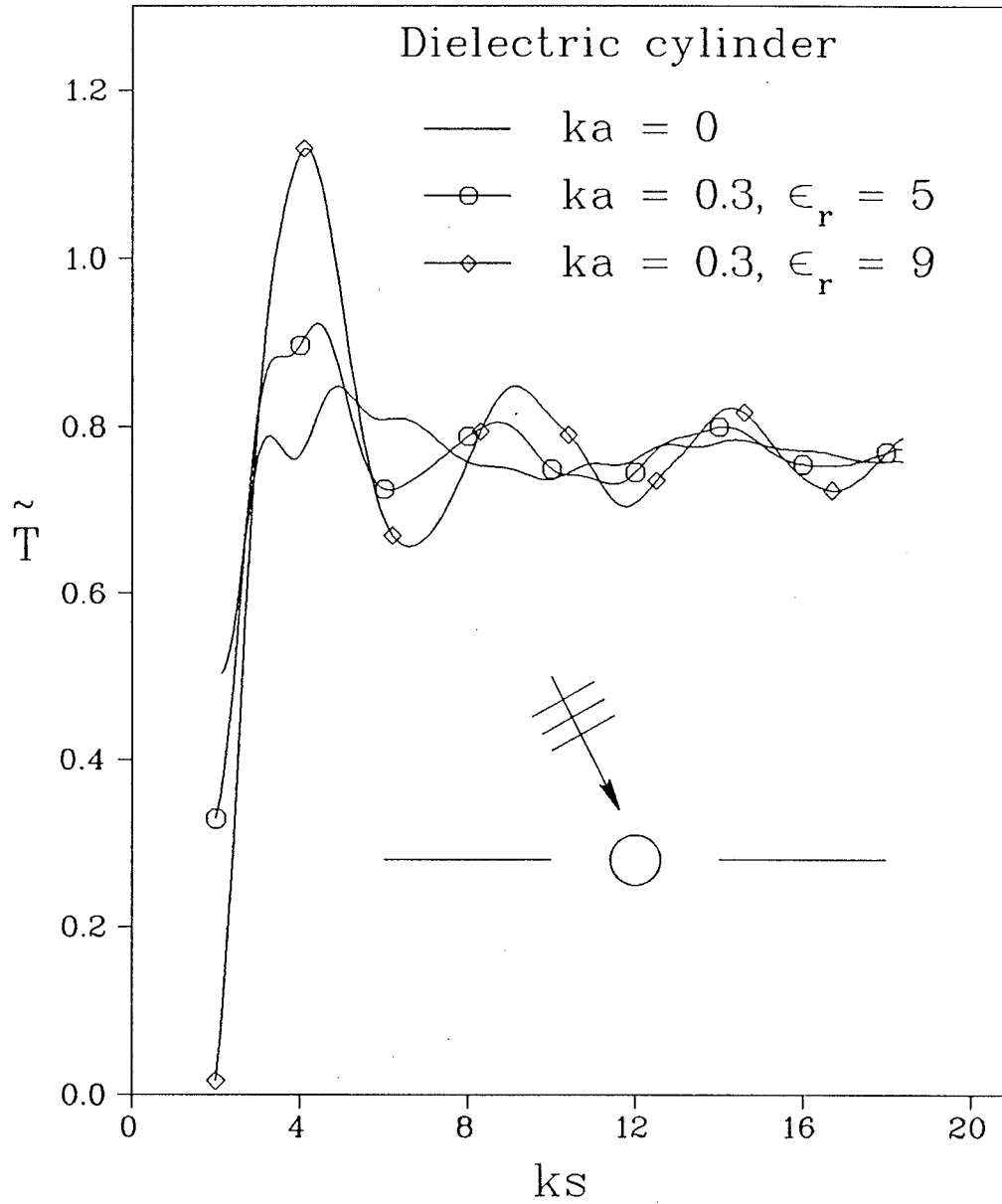


Fig. 3-19 : T vs. ks of a loaded slit  
for  $\theta_0 = 40^\circ$ .

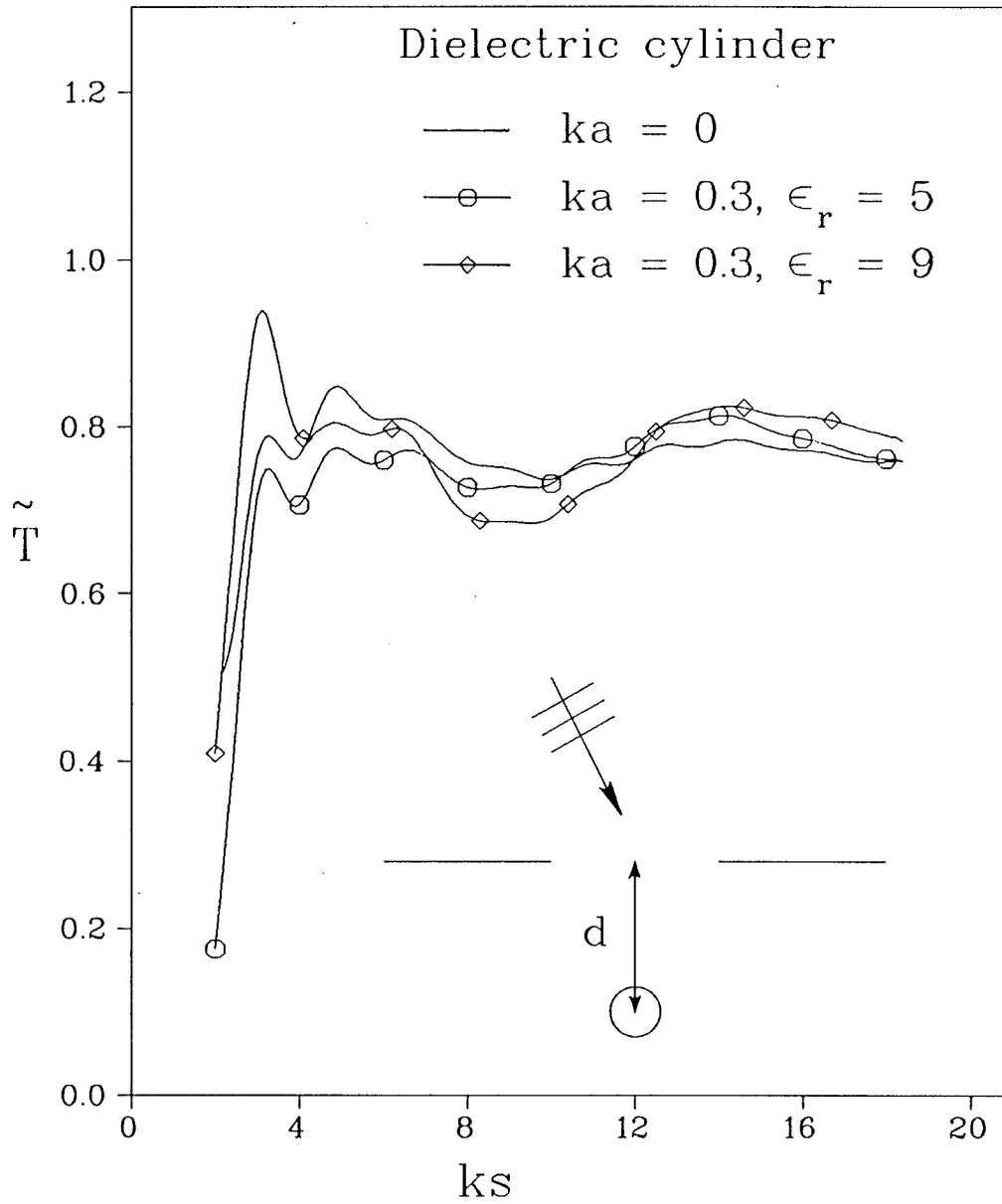


Fig. 3-20 :  $T$  vs.  $ks$  of a loaded slit  
for  $\theta_0 = 40^\circ$  and  $kd = 1.5$ .

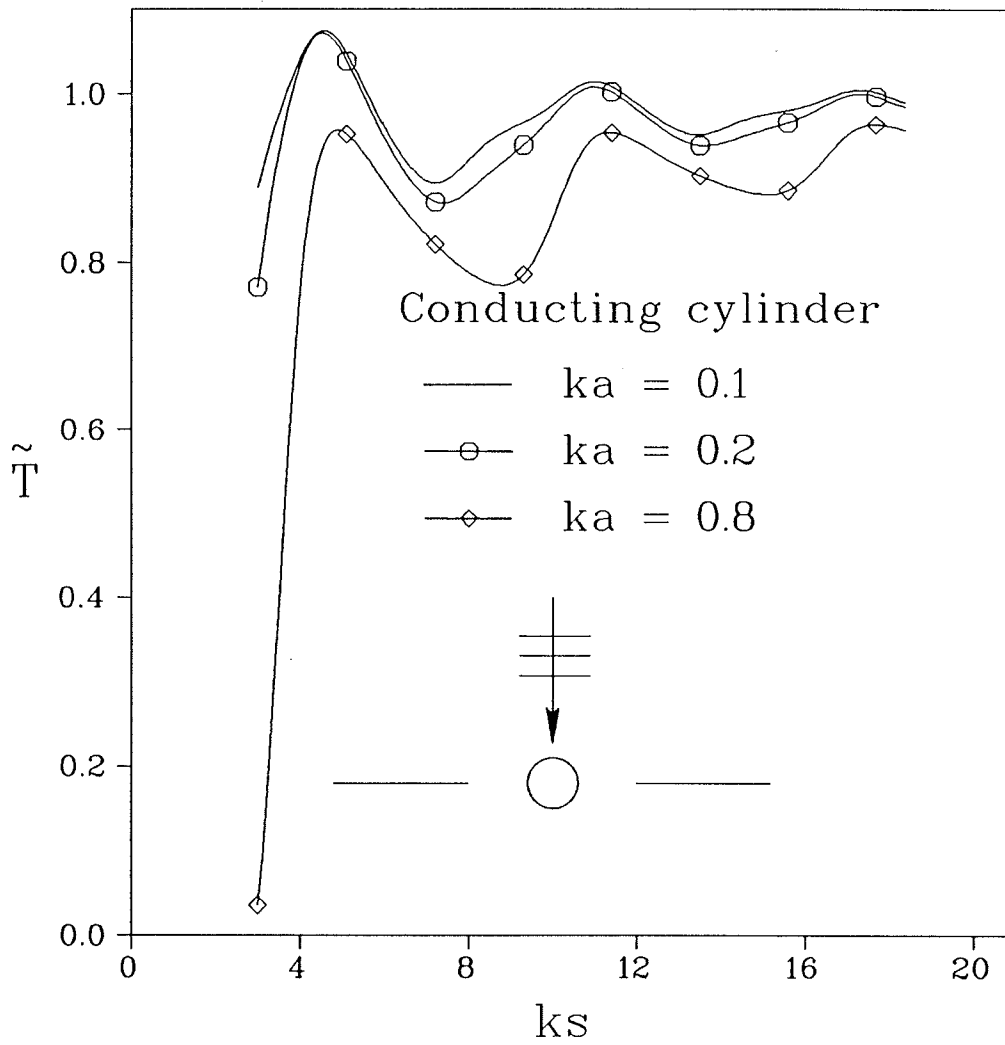


Fig. 3-21 :  $T$  vs.  $ks$  of a loaded slit for  $\theta_0 = 0^\circ$ .

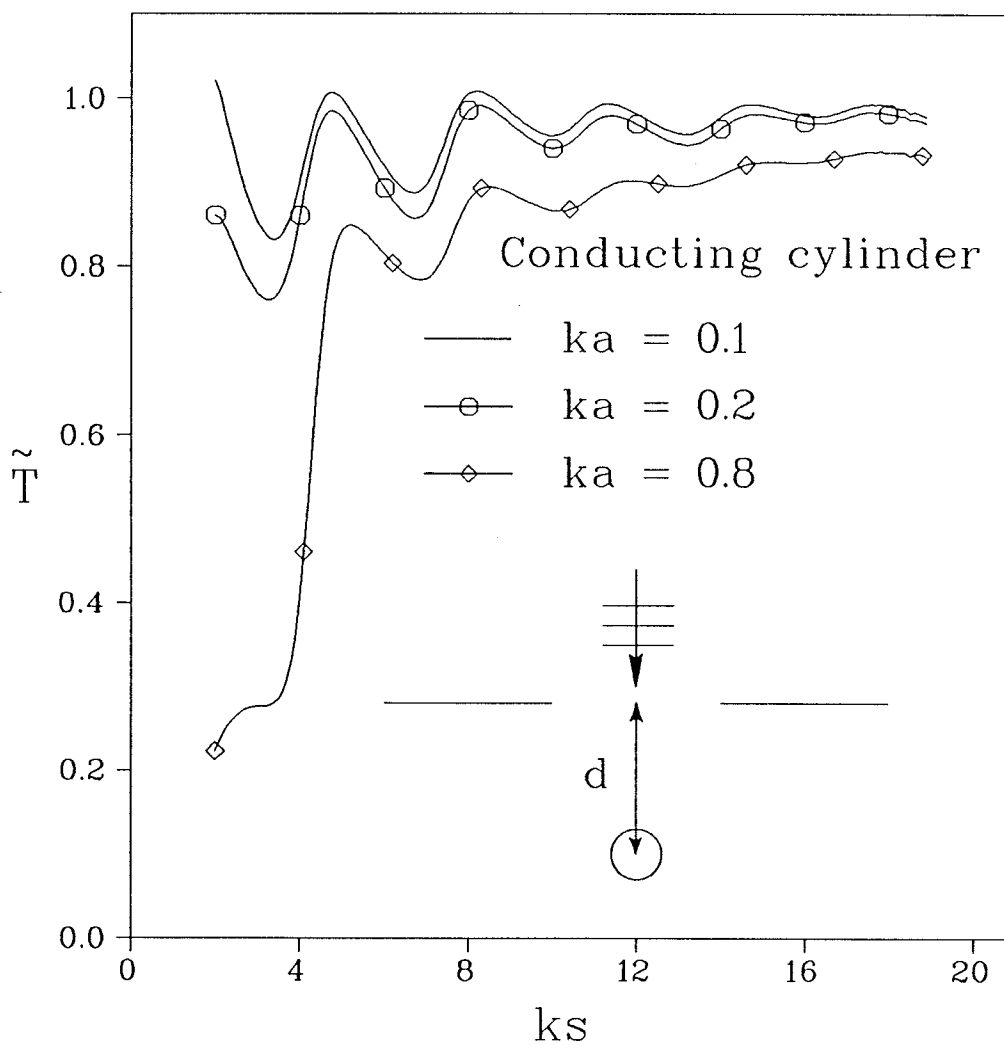


Fig. 3-22 :  $T$  vs.  $ks$  of a loaded slit for  $\theta_0 = 0^\circ$  and  $kd = 5$ .

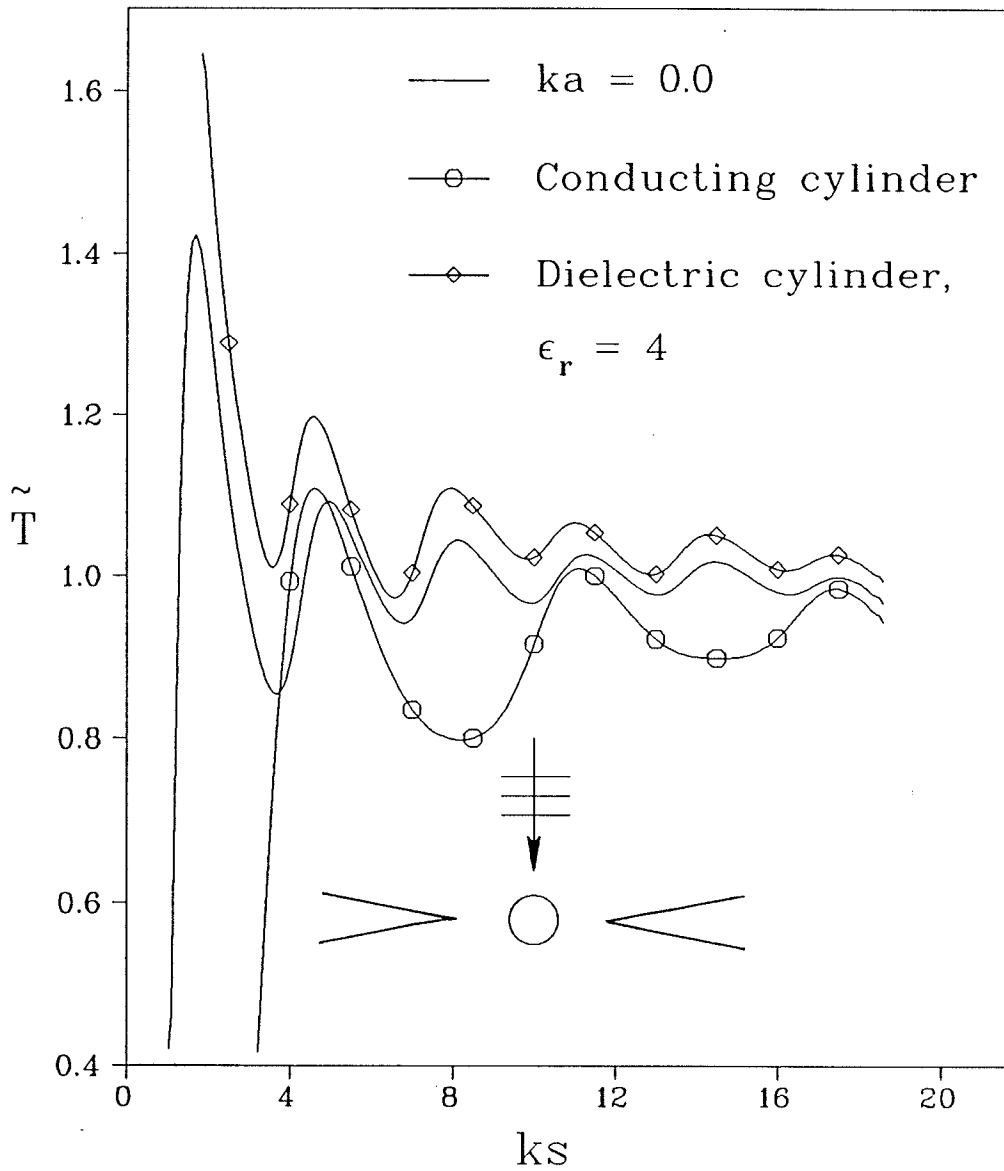


Fig. 3-23 :  $T$  vs.  $ks$  of a loaded double wedge for  $\theta_0 = 0^\circ$ ,  $ka = 0.5$  and  $\gamma = 20^\circ$ .

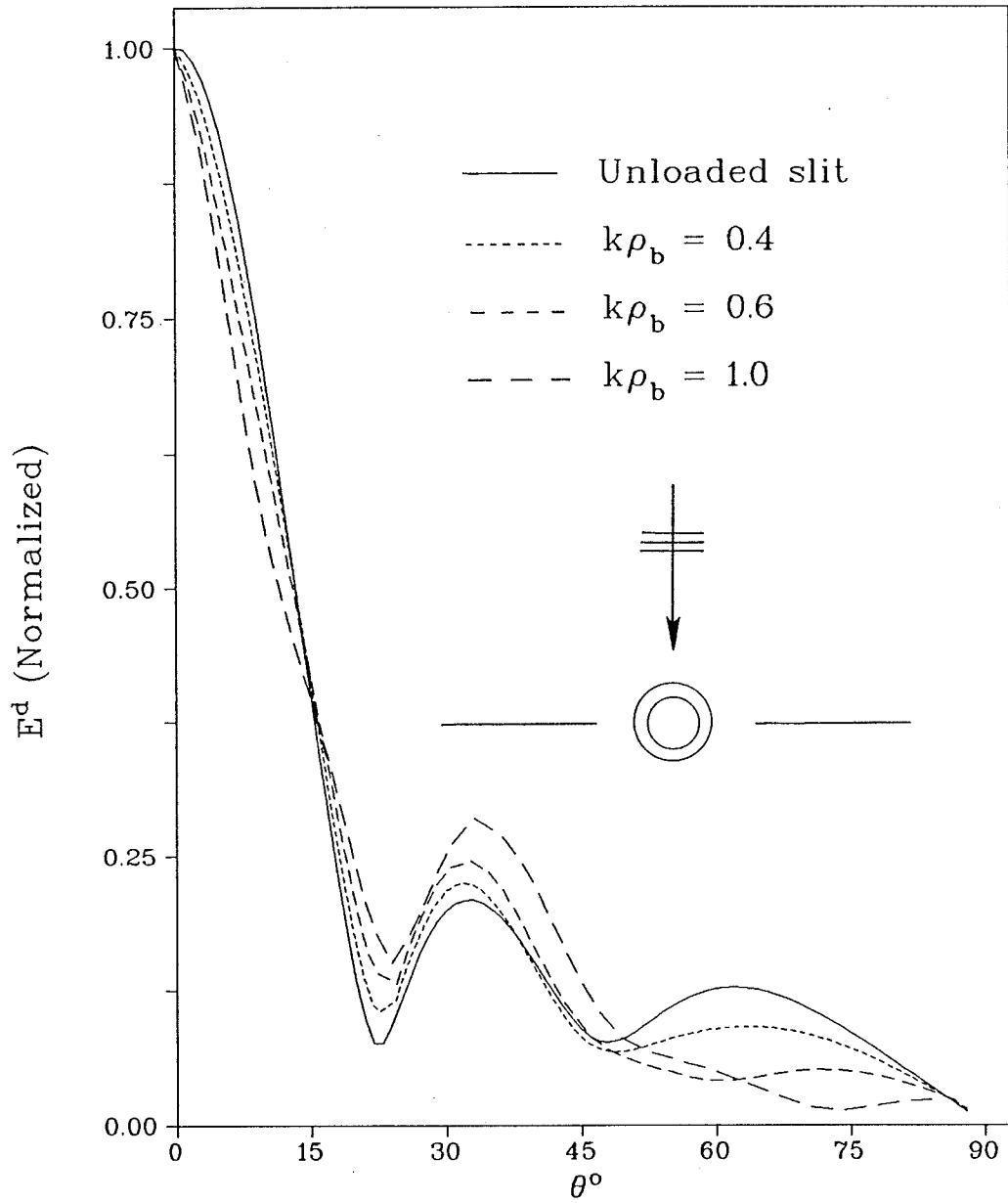


Fig. 3-24 : Diffracted field vs.  $\theta$  of a slit loaded by an inhomogeneous dielectric shell for  $k_s = 8$ ,  $\epsilon_a = 3$ ,  $k\rho_a = 0.2$ ,  $\eta = 2$  and  $\delta = 1$ .

clearly shown that the outer radius of the shell affects the beamwidth and level of the first sidelobe. One concludes that for the parameters shown, the increase in  $k\rho_b$  results in an increase in the sidelobe level and decrease in beamwidth.

To further investigate the diffraction pattern characteristics of a double wedge loaded by this type of inhomogeneous scatterer, we present tables 3-3 and 3-4. In tables 3-3 the variations in these characteristics are shown for different values of  $\delta$ , where  $\phi_0 = 90^\circ$ ,  $ks = 8$ ,  $\epsilon_a = 5$ ,  $k\rho_b = 1.0$ ,  $k\rho_a = 0.2$  and  $\eta = 2.5$ . The changes in these characteristics are shown in table 3-4 for different values of  $\eta$  with  $\delta = 1.0$  while  $\phi_0$ ,  $\epsilon_a$ ,  $k\rho_b$  and  $k\rho_a$  remain the same as in table 3-3. In addition to variations in beamwidth, sidelobe level and position due to the presence of a dielectric shell in the center of the aperture plane of a slit, it is found that  $T$  increases over the unloaded case for all cases studied.



$\delta$	Beam-width	Position of first null	First sidelobe		$T$
			Position	Level	
0.01	19.41°	22.66°	36.87°	-12.40 dB	1.05282
0.1	19.39°	22.73°	36.88°	-12.37 dB	1.053397
0.2	19.34°	22.97°	36.91°	-12.28 dB	1.055364
0.5	18.93°	24.85°	37.08°	-11.62 dB	1.071263
0.8	17.93°	27.09°	37.09°	-10.47 dB	1.104884
1.0	16.48°	23.79°	36.93°	-9.65 dB	1.130955
1.2	15.12°	27.12°	36.64°	-9.43 dB	1.147672
1.5	13.77°	26.25°	36.05°	-9.57 dB	1.147302
1.8	13.16°	25.43°	35.40°	-9.92 dB	1.131591
2.0	13.04°	25.07°	35.07°	-10.12 dB	1.122447

Table 3-3 : Diffraction pattern characteristics of a slit loaded by a cylindrical shell in the aperture plane for  $\phi_0 = 90^\circ$ ,  $ks = 8$ ,  $\epsilon_a = 5$ ,  $k\rho_b = 1.0$ ,  $k\rho_a = 0.2$  and  $\eta=2.5$ .

$\eta$	Beam-width	Position of first null	First sidelobe		$T$
			Position	Level	
2.0	13.43°	23.85°	33.85°	-10.89 dB	1.086759
2.2	13.19°	24.17°	34.18°	-10.66 dB	1.096530
2.5	13.03°	24.63°	34.61°	-10.39 dB	1.109869
2.7	13.01°	24.93°	34.93°	-10.20 dB	1.118564
3.0	13.14°	25.44°	35.40°	-9.91 dB	1.131864
3.2	13.37°	25.83°	35.73°	-9.72 dB	1.140707
3.5	14.07°	26.56°	36.25°	-9.46 dB	1.150876
3.7	14.97°	27.09°	36.61°	-9.40 dB	1.149546
4.0	17.39°	27.36°	37.06°	-10.12 dB	1.115615
4.2	18.87°	25.07°	37.09°	-11.54 dB	1.073484
4.5	19.76°	23.80°	35.32°	-13.53 dB	1.030141
4.7	19.45°	20.89°	32.99°	-13.67 dB	1.023326
5.0	18.35°	21.46°	32.05°	-12.97 dB	1.028158

Table 3-4 : Diffraction pattern characteristics of a slit loaded by a cylindrical shell in the aperture plane for  $\phi_0 = 90^\circ$ ,  $ks = 8$ ,  $\epsilon_a = 5$ ,  $k\rho_b = 1.0$ ,  $k\rho_a = 0.2$  and  $\delta=1.0$ .

## CHAPTER 4

### *SOLUTION BY MODIFIED METHOD OF MOMENTS*

We have introduced in Chapter 2 a new iterative technique for the scattering by two cylindrical bodies, where in each interaction a spectrum of cylindrical waves emanating from one body is used to excite the opposite scatterer. This technique does not suffer, in principle, from any limit on the separation between the scatterers and can handle small as well as large scatterers, provided that the scattering by a single body is manageable. As shown from the numerical results in Sec. 2.3, excellent agreement is obtained between the results due to the scattering by two cylinders using the CWS and the boundary value techniques. Furthermore, the diffraction by a double wedge is also presented and good agreement is observed with the exact solution for the special case of a slit as well as with two asymptotic solutions for the double wedge geometry of any wedge angle and wide separation. To further check the numerical results based on the CWS technique for the diffraction by a narrow double wedge geometry, we present in this chapter a numerical solution since experimental verification is practically impossible.

A useful numerical method for such problems is the MM [45,46] where the exact integral equation formulation is reduced to an approximate equivalent matrix form. The matrix system involves the unknown surface current distribution which is expressed in terms of suitable basis functions. The point matching technique is then used to solve the matrix system. The number of matching points depends on the length of the contour of the cross-section for conducting cylindrical scatterers. The MM, while being generally applicable to many scattering problems, is limited by the storage and computation time of available computers when the body dimensions are large relative to the wavelength. Regarding this limitation in dealing with two

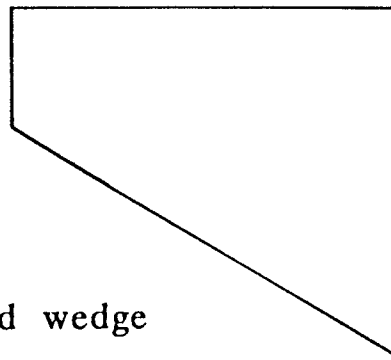
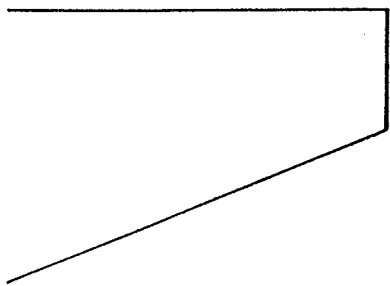
scatterers having large electrical dimensions, the MM in its classical form does not usually yield a convergent solution. However, one can apply the MM to infinite planar scatterers by first subtracting out the surface current density associated with the incident and reflected fields and then solve for the residual or the diffraction current [47,68]. It is also possible to apply the MM to electrically large scatterers if it is used to solve for the surface current that appears only due to the interaction between any two scatterers. In other words, the total surface current can be divided into two parts. The first part is the current that would appear on the surface if each scatterer is excited by the original source in isolation while the second part of the surface current is due to the interaction fields between the scatterers.

Another objective of this chapter is to confirm the validity of this new approach in order to numerically deal with large scatterers. In Sec. 4.1 the scattering by two large parallel conducting cylinders will be presented. The reduction in the execution time when applying this technique over other methods, namely the boundary value solution and the ordinary MM, is outlined for the case of the scattering by two large cylinders. Furthermore, the surface currents and the scattered field due to the interaction between the cylinders is investigated (in the backward and forward directions) as a function of the separation between the cylinders and the electrical radius of the cylinders.

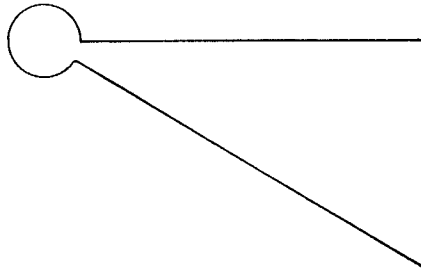
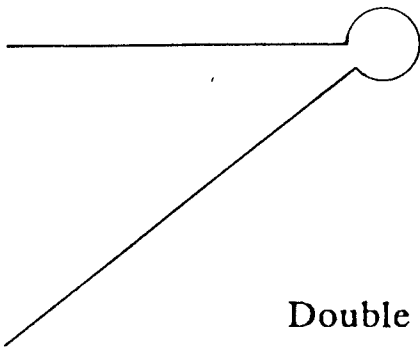
The diffraction by the aperture of a double semi-infinite wedge is also investigated in Sec. 4.2. The aperture is considered to be infinite along the  $z$  direction, whereas the edges of the two wedges may be loaded. The upper faces of the two wedges which are illuminated by the incident plane wave should be uniform in the region far from their edges to facilitate the evaluation of the total diffracted field [94,95]. The transmission coefficient of a plane wave incident on a slit geometry is computed and compared with the exact values to check the accuracy of the computation procedure. Then the diffraction characteristics of related geometries, namely, thick slit, double truncated wedge and double capped wedge (see Fig. 4-1) are



Thick slit



Double truncated wedge



Double capped wedge

Fig. 4.1 : Schematic diagram of different types of a double wedge geometry with non-sharp edges.

presented and compared with other available solutions.

#### 4.1 Scattering by two parallel conducting circular cylinders

If two parallel conducting circular cylinders are illuminated by an incident plane wave as shown in Fig. 2-3, the  $z$  directed electric linear current density  $J$  on the surface of either cylinder can be divided into two parts, i.e.

$$J = J' + J'' \quad (4-1)$$

where  $J'$  is the current on the surfaces of the scatterers when each is illuminated by the plane wave in isolation.  $J''$  is the additional surface current due to the multiple interaction between the scatterers.

Using Eqs. (2-1), (2-3) and (4-1), an integral equation over the only unknown  $J''$  can be obtained, i.e.

$$\begin{aligned} E_p^i - \frac{\eta k}{4} \int_{C_1} J'(\rho_1) H_0(k|\bar{p}-\bar{\rho}_1|) dC_1 \\ - \frac{\eta k}{4} \int_{C_2} J'(\rho_2) H_0(k|\bar{p}-\bar{\rho}_2|) dC_2 \\ = \frac{\eta k}{4} \int_{C_1+C_2} J''(\rho) H_0(k|\bar{p}-\bar{\rho}|) dC' \end{aligned} \quad (4-2)$$

where  $C_1$  and  $C_2$  are the contours of the cylinders 1 and 2, respectively.

It is obvious from the physical view point that the first integral on the right hand side of Eq. (4-2) cancels the incident plane wave when  $\bar{p}$  represents a point on contour  $C_1$ , whereas the incident plane wave is canceled by the second integral if  $\bar{p}$  represents a point on  $C_2$ . The remaining integral in each case ( $\bar{p}$  on  $C_1$  or  $\bar{p}$  on  $C_2$ ) represents the scattered field from one cylinder at a point on the surface of the other cylinder.

As a result of the above discussion, Eq. (4-2) reduces to a matrix form by applying the method of moments, i.e.

$$[l_{mn}] [\alpha_n] = [g_m] \quad (4-3)$$

where the unknown current  $J''$  is expressed as a linear combination of pulse functions with unknown coefficients  $\alpha_n$ , i.e.

$$J'' \approx \sum_{n=1}^N \alpha_n J_n \quad (4-4)$$

and where  $J_n = 1$  on  $\Delta C_n$  and 0 elsewhere while  $N$  is the total number of current pulses assumed. The point matching technique is then used to solve the matrix system. As a result, the elements of  $l_{mn}$  are then given by [46]

$$l_{mn} = \begin{cases} \frac{\eta k}{4} H_0(k \sqrt{(x_m - x_n)^2 + (y_m - y_n)^2}) \Delta C_n & , m \neq n \\ \frac{\eta k}{4} [ 1 - j \frac{2}{\pi} (\gamma - \ln (\frac{k \Delta C_n}{4 e})) ] \Delta C_n & , m = n \end{cases} \quad (4-5)$$

where Euler's constant  $\gamma$  is 0.577215665  $\dots$ ,  $e = 2.718281828 \dots$  and  $m, n = 1, 2, 3, \dots, N$ .

Since the elements of  $g_m$  represent the scattered field from cylinder 1 (or cylinder 2) at a point on the surface of cylinder 2 (or cylinder 1), the exact expression for the scattered field from a cylinder due to plane wave incidence is used. Thus, we can write

$$g_m = - \sum_{l=0}^{\infty} \epsilon_l e^{jl \frac{\pi}{2}} \frac{J_l(kb)}{H_l(kb)} H_l(k \rho_m) \cos l(\phi_m - \phi_0) \quad (4-6)$$

where  $\rho_m$  and  $\phi_m$  represent the mid point of any  $\Delta C_m$  on  $C_1$  in terms of the local coordinates of cylinder 2 (i.e.  $\rho_2$  and  $\phi_2$ ) and  $\epsilon_l$  is Neumann's number. For any  $\Delta C_m$  on  $C_2$ ,  $g_m$  is given by

$$g_m = - \sum_{l=0}^{\infty} \epsilon_l e^{jl \frac{\pi}{2}} \frac{J_l(ka)}{H_l(ka)} H_l(k \rho_m) \cos l(\phi_m - \phi_0) \quad (4-7)$$

where  $\rho_m$  and  $\phi_m$  are expressed in terms of the local coordinates of cylinder 1 (i.e.  $\rho_1$  and  $\phi_1$ ).

After solving for  $J''$  the scattered field  $E''$  due to the interaction between the cylinders is given by

$$E'' = \frac{-\eta k}{4} \int_{C_1+C_2} J''(\phi') H_0(k|\bar{\rho} - \bar{\rho}'|) dC' \quad (4-8)$$

while the non-interaction scattered field  $E'$  and the scattered field pattern are given by Eqs. (2-40) and (2-50), respectively.

#### 4.2 Diffraction by two wedges with blunt edges

When two wedges with sharp edges are excited by an incident plane wave (as shown in Fig. 2-1) the electric linear current density on the conducting surface can be divided as given by Eq. (4-1), where  $J'$  represents the current on the upper ( $J^U$ ) and lower ( $J^L$ ) surfaces of the wedge and is given exactly by Eq. (2-18) while  $J''$  is evaluated using the ordinary MM. However,  $J$  on the surface of two wedges with blunt edges, due to the incident wave and all the interactions between the wedges, can be divided into a physical optical current  $J^{PO}$  and a residual or diffraction current denoted by  $J^d$ . i.e.

$$J = J^{PO} + J^d \quad (4-9)$$

where

$$J^{PO} = 2\hat{n} \times \vec{H}^i \quad (4-10)$$

Here  $\vec{H}^i$  is the incident magnetic field vector and  $\hat{n}$  is a unit outer vector normal to the upper surface of either wedge. Since the incident field is a plane wave, Eq. (4-10) can be written in terms of the local coordinates of either wedge as

$$J^{PO}(x,0) = \frac{2}{\eta} \sin \phi_0 e^{jkx \cos \phi_0} \quad (4-11)$$



From Eqs. (2-2) and (2-3) we can obtain an integral equation whose only unknown quantity is  $J^d$  by using Eqs. (4-9) to (4-11), i.e.

$$E_p^i - \frac{\eta k}{4} \int_{-\infty}^{\infty} J^{PO}(x') H_0(k |\bar{\rho} - \bar{x}'|) dx' = \frac{\eta k}{4} \left\{ - \int_{-s_2}^{s_1} J^{PO}(x') H_0(k |\bar{\rho} - \bar{x}'|) dx' + \int_{C_1+C_2} J^d(\rho') H_0(k |\bar{\rho} - \bar{\rho}'|) dC' \right\}. \quad (4-12)$$

It is obvious that the unknown current  $J^d$  diminishes with increasing distance from the edge along the surface of either wedge. Thus,  $C_1+C_2$  in Eq. (4-12) is a finite contour on which  $J^d$  exists and is determined by the paths from point  $l_1$  to point  $l_2$  and from point  $l_3$  to point  $l_4$  as shown in Fig. 2-2.

Since the reflected wave  $E_p^r$  from a conducting infinite plane may be expressed as the radiation field from the surface current excited on the infinite plane by the incident wave, we obtain the following :

$$\frac{-\eta k}{4} \int_{-\infty}^{\infty} J^{PO}(x') H_0(k |\bar{\rho} - \bar{x}'|) dx' = \begin{cases} -E_p^i & \text{for } y < 0 \\ E_p^r & \text{for } y > 0 \end{cases}. \quad (4-13)$$

It is clear from Eq. (4-13) that the left hand side of Eq. (4-12) reduces to zero. Thus Eq. (4-12) may be rewritten in the following form :

$$\int_{-s_2}^{s_1} J^{PO}(x') H_0(k |\bar{\rho} - \bar{x}'|) dx' = \int_{C_1+C_2} J^d(\rho') H_0(k |\bar{\rho} - \bar{\rho}'|) dC' \quad (4-14)$$

Now, the MM can be applied to the above equation to solve for the unknown part of the surface currents  $J^d$ . For the special case of two sharp wedges, Eq. (4-14) reduces to

$$\int_{-s_2}^{s_1} J^{PO}(x') H_0(k|\bar{\rho}-\bar{x}'|) dx' - \int_{C_1+C_2} [J'(\rho') - J^{PO}(\rho')] H_0(k|\bar{\rho}-\bar{\rho}'|) dC'$$

$$= \int_{C_1+C_2} J''(\rho') H_0(k|\bar{\rho}-\bar{\rho}'|) dC' . \quad (4-15)$$

where  $J''$  is the only unknown part of the surface current due to the interaction between the two wedges.

Once the total current distribution on the surfaces of the two wedges is known, the near as well as far fields can be evaluated using well known relations. The scattered field at a far observation point can be evaluated using Eq. (2-3) while if the identities given by Eq. (4-13) are used, the diffracted field can be written as

$$E^d = \frac{-\eta k}{4} \left\{ \int_{C_1+C_2} J^d(\rho') H_0(k|\bar{\rho}-\bar{\rho}'|) dC' - \int_{-s_2}^{s_1} J^{PO}(x') H_0(k|\bar{\rho}-\bar{x}'|) dx' \right\} . \quad (4-16)$$

Substituting Eq. (4-11) in Eq. (4-16) and using the usual far field approximations, the diffracted field pattern  $F(\phi)$  can be normalized by the factor  $\frac{e^{-jk\rho}}{\sqrt{\pi k\rho}}$  and expressed as

$$F(\phi) = \frac{e^{-j\pi/4} \left[ e^{jks_1\psi} - e^{-jks_2\psi} \right]}{\sqrt{2}\psi}$$

$$- \frac{\eta k}{2\sqrt{2}} e^{j\pi/4} \int_{C_1+C_2} J^d(\rho') e^{jk\rho' \cos(\phi - \phi')} dC' \quad (4-17)$$

where

$$\psi = \cos \phi - \sin \theta_0 \quad (4-18)$$

$$\phi = \frac{3\pi}{2} + \theta . \quad (4-19)$$

An example of near field calculations is the aperture field  $E_z^i$  (where  $y = 0$  and  $-s_2 \leq x \leq s_1$ ), which can be evaluated by adding the incident field  $E_p^i$  to the scattered field  $E^S$ . The result is given by

$$E_z^i(x) = \frac{\eta k}{4} \left\{ \int_{-s_2}^{s_1} J^{PO}(x') H_0(k|\bar{x}-\bar{x}'|) dx' - \int_{C_1+C_2} J^d(\rho') H_0(k|\bar{x}-\bar{\rho}'|) dC' \right\}. \quad (4-20)$$

### 4.3 Numerical examples

A computer program based on the above analysis was written to calculate the surface current distribution and the scattered field pattern with and without incorporating the effect of the interactions between the two scatterers. To check the accuracy of the procedure, the total scattered field pattern from the two cylinders is compared with numerical results obtained from an available boundary value solution [59,60] for different cases. One of such cases is shown in Fig. 4-2, where  $ka = kb = 5$ ,  $ks_1 = ks_2 = 8$  and  $\phi_0 = 90^\circ$ . It is clear from the figure that the proposed solution is in complete agreement with the boundary value solution of the scattering by two cylinders.

In Fig. 4-3 the scattering pattern of two cylinders of larger radii, namely  $ka = kb = 7$ , and for  $ks_1 = ks_2 = 8$  and  $\phi_0 = 90^\circ$ , is presented. Again, it is to be noticed that the two indicated curves are in good agreement although the execution time of the program based on the boundary value solution was 1.5 times as long. It is also worth mentioning that the same scattered field pattern is obtained by using the ordinary method of moments with  $N = 72$  whereas in the present solution  $N$  was set equal to 36. The execution time by the ordinary method of moments was 2.2 times the execution time by the proposed technique.

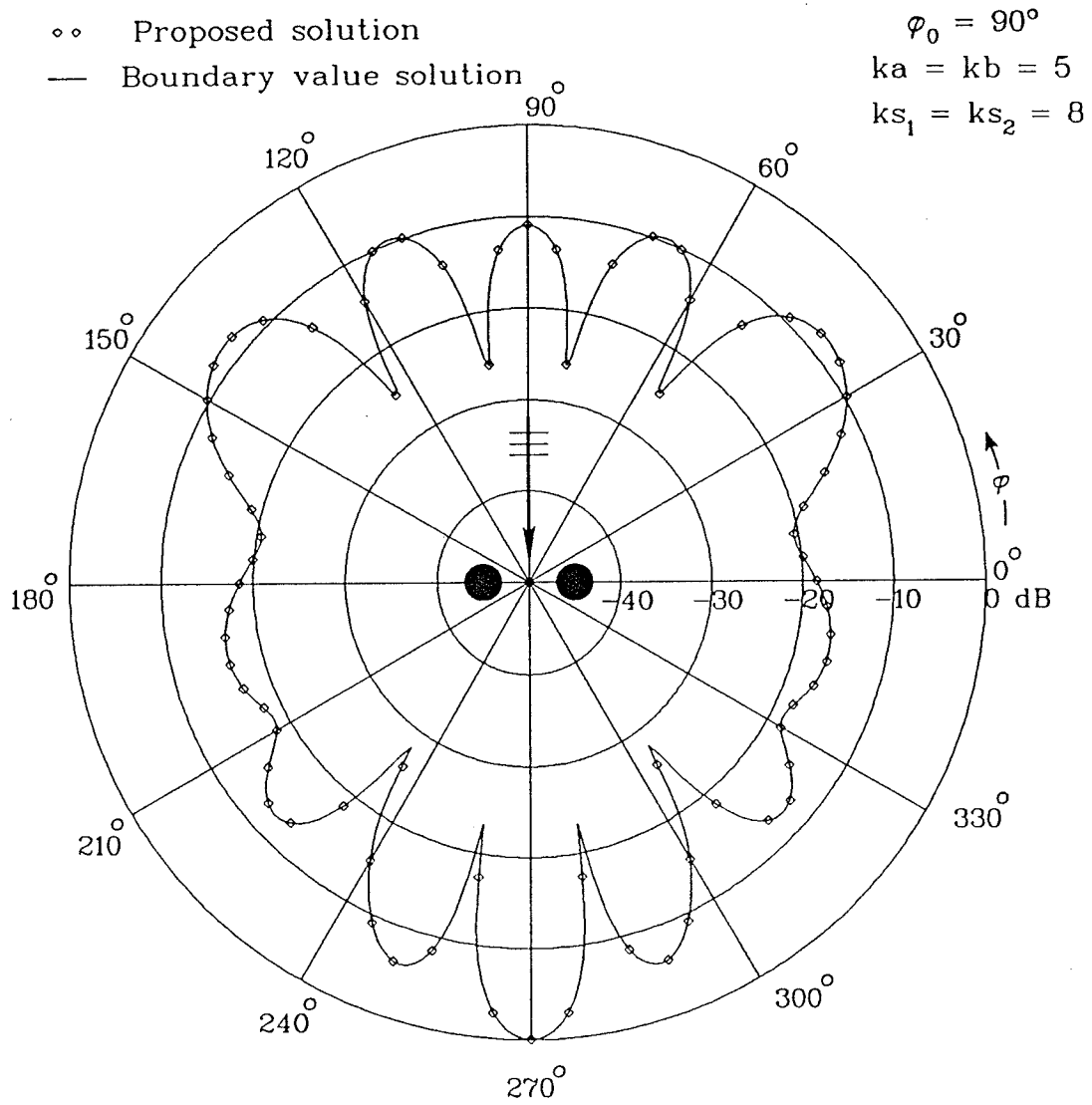


Fig. 4-2 : Scattered field pattern for two circular cylinders.

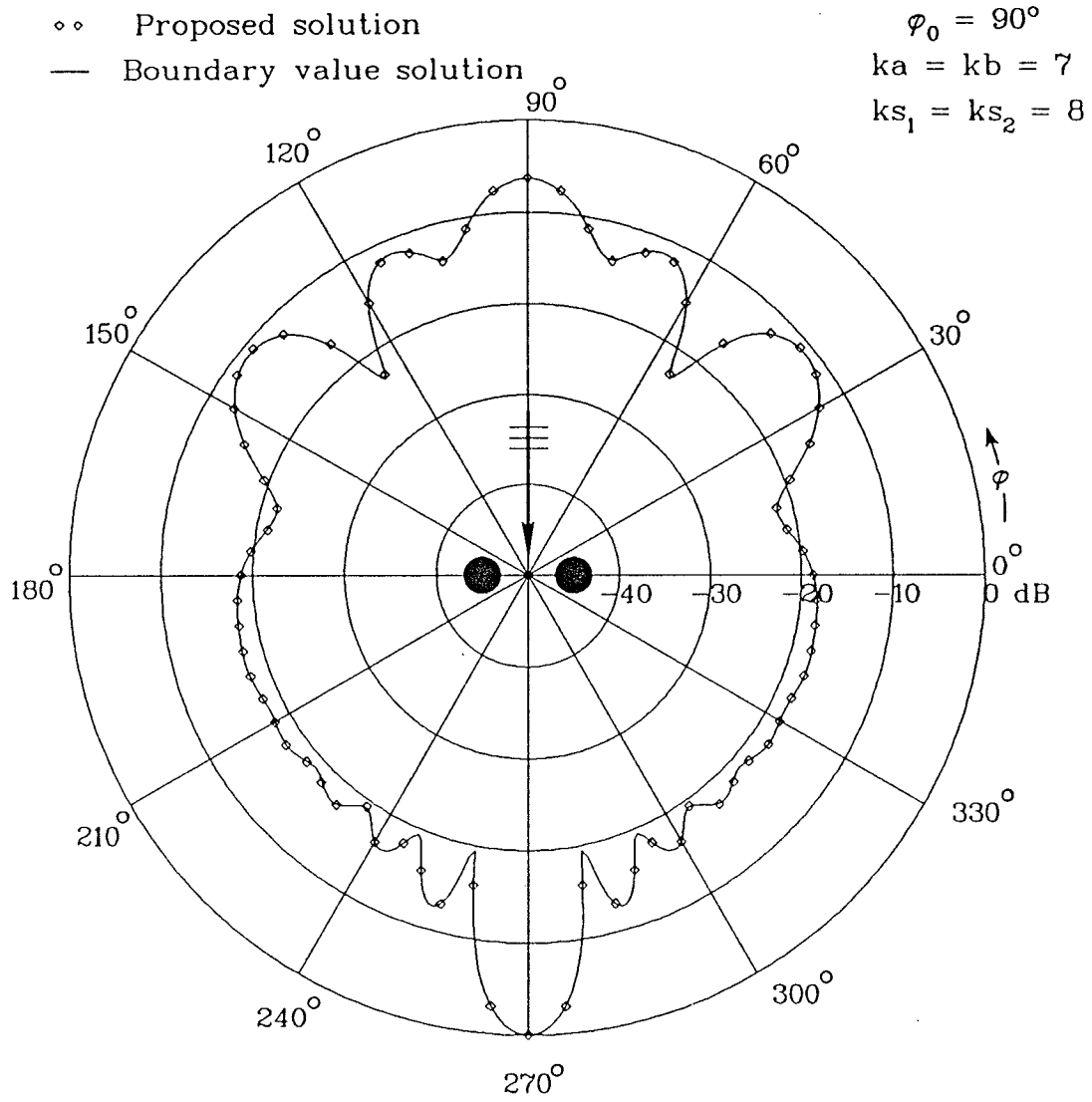


Fig. 4-3 : Scattered field pattern for two circular cylinders.

The amplitude of the surface current on cylinder 1 due to interactions between the two cylinders is shown in Fig. 4-4 for different values of  $ka$ . The cylinder shown in Fig. 4-4 (cylinder 1) is one of two identical cylinders in the double cylinder geometry presented in Fig. 2-3 with  $kb = ka$ ,  $ks_1 = ks_2 = 5$  and  $\phi_0 = 90^\circ$ . Regarding this geometry, there is a symmetry with respect to the  $y$  axis, whereas there is no symmetry around the  $x$  axis. Due to the asymmetry around the  $x$  axis, one notices that the peak value of  $J''$  is not at  $\psi = 180^\circ$ . However, it is found that  $J''$  decays in an exponential form and tends to a very small value when  $\psi$  approaches  $0^\circ$ . Moreover, it is found that the peak value does not monotonically increase with  $ka$ . To illustrate this behavior, we present Fig. 4-5 where the scattered field pattern due to the interaction between the cylinders is shown as a function of  $ka$  for the forward ( $\phi = 270^\circ$ ) and backward ( $\phi = 90^\circ$ ) directions. The figure indicates that for  $\phi_0 = 90^\circ$ ,  $ks_1 = ks_2 = 5$  there exists certain values of  $ka$  where the forward and backward interaction fields are maximum and this explains the variations in the levels of the peak value of  $J''$  in Fig. 4-4.

Since the interaction component of the scattered field is an important quantity in the multiple scattering analysis, we further investigate the effect of the electrical separation between the centers of the two cylinders on  $E''$  in Fig. 4-6 for  $ka = kb = 1$  and  $\phi_0 = 90^\circ$ . Here  $E''$  is found to be decaying in an oscillatory fashion with respect to  $ks$  and tends to zero when  $ks$  tends to infinity. It is also noticed that the peak value of  $E''$  in the forward direction is larger than the corresponding peak value in the backward direction. Furthermore, it is found that the oscillations are similar in both the forward and backward directions and the period of oscillations is very close to  $\pi$ .

Regarding the double wedge geometry, we will consider for the sake of simplicity in the numerical computations the symmetric case where  $ks_1 = ks_2 = ks$ ,  $\alpha = \beta = \gamma$  and  $\phi_0 = 90^\circ$  (or  $\theta_0 = 0^\circ$ ). Furthermore, the finite integrals in Eqs. (4-14), (4-15) and (4-16) are normalized to match the integration formulas of the

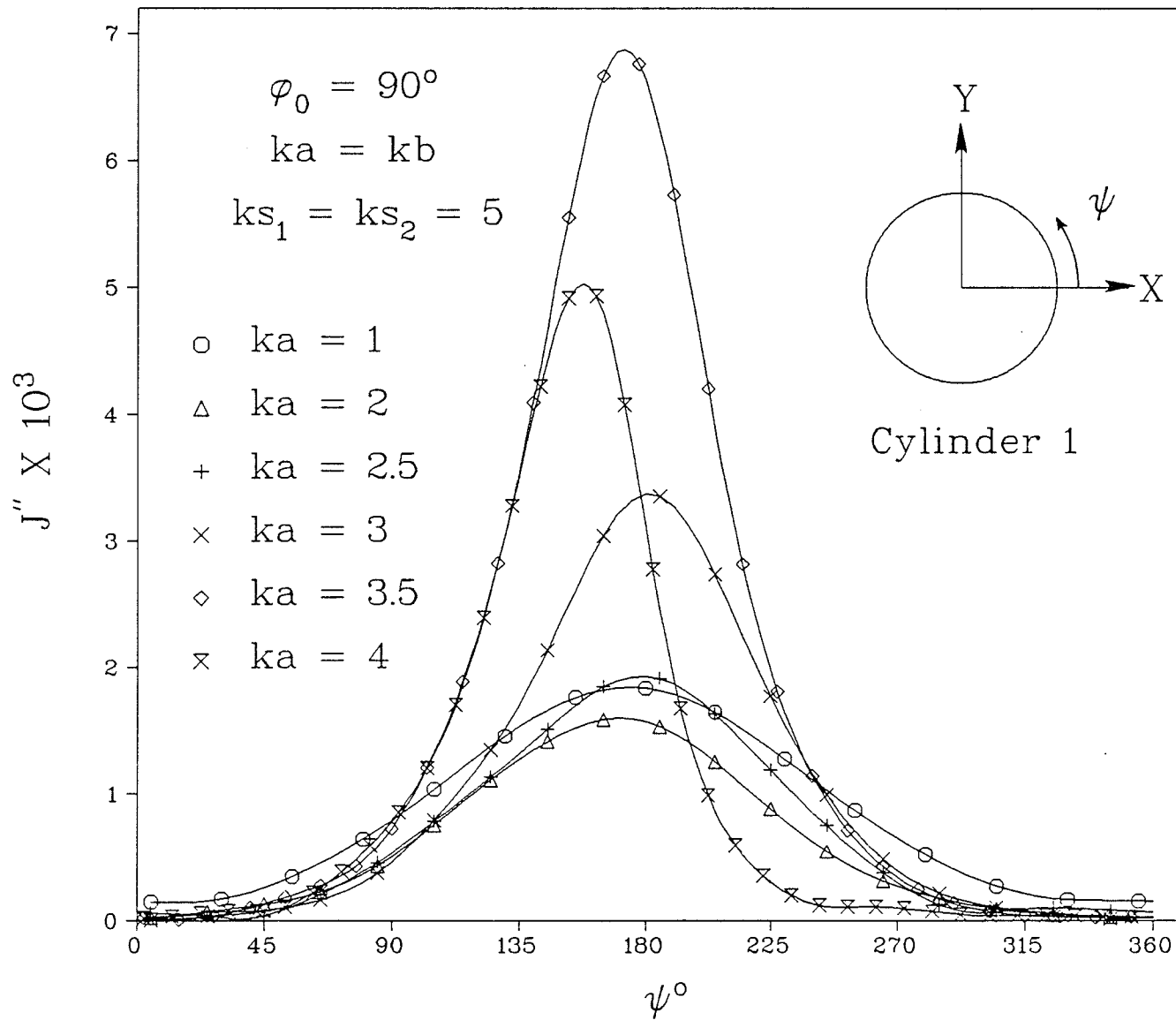


Fig. 4-4 : Amplitude of the interaction current vs.  $\psi$ .

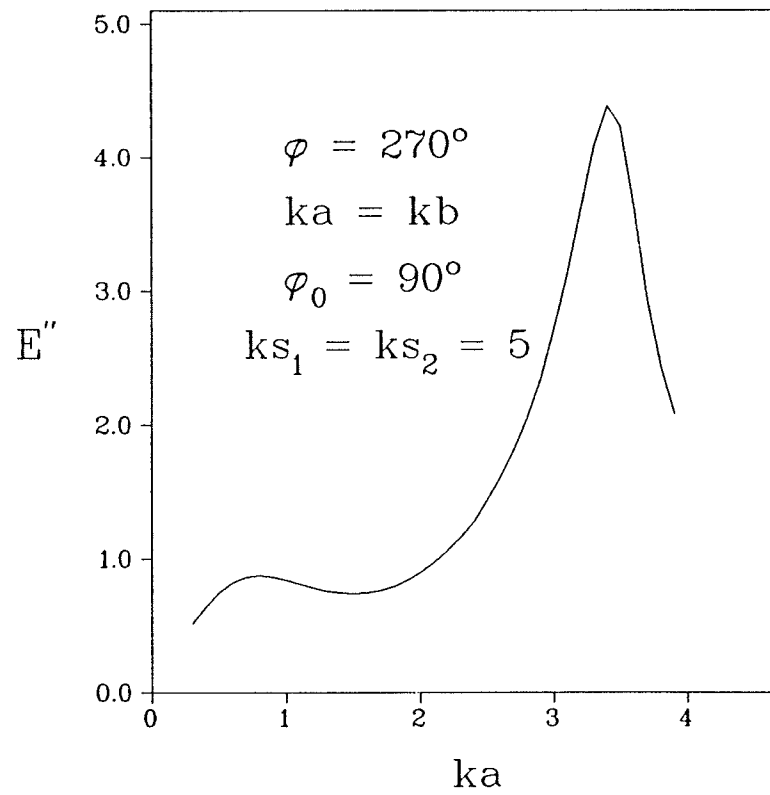
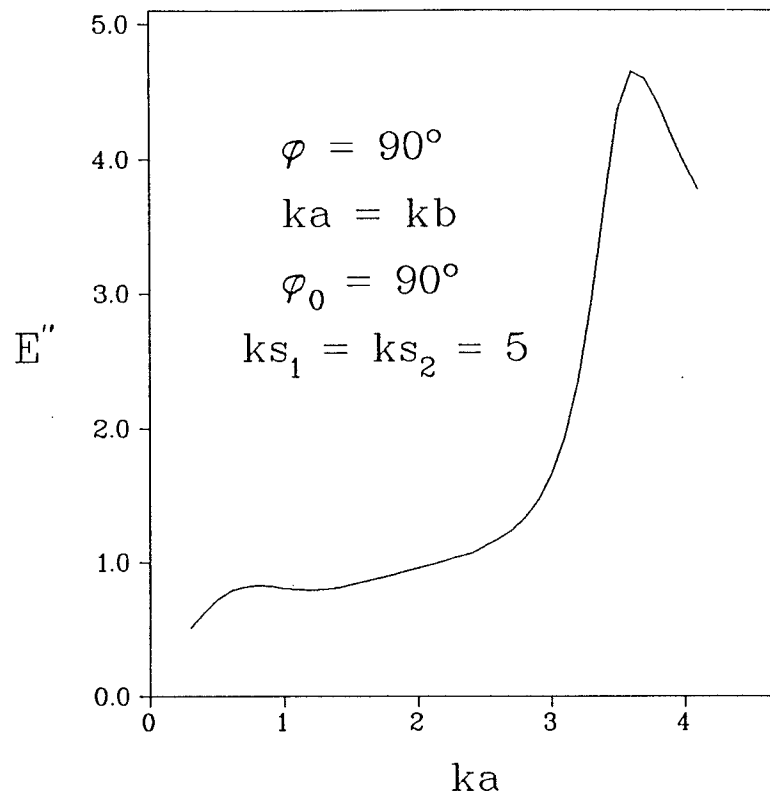


Fig. 4-5 : Amplitude of the interaction field vs.  $ka$ .



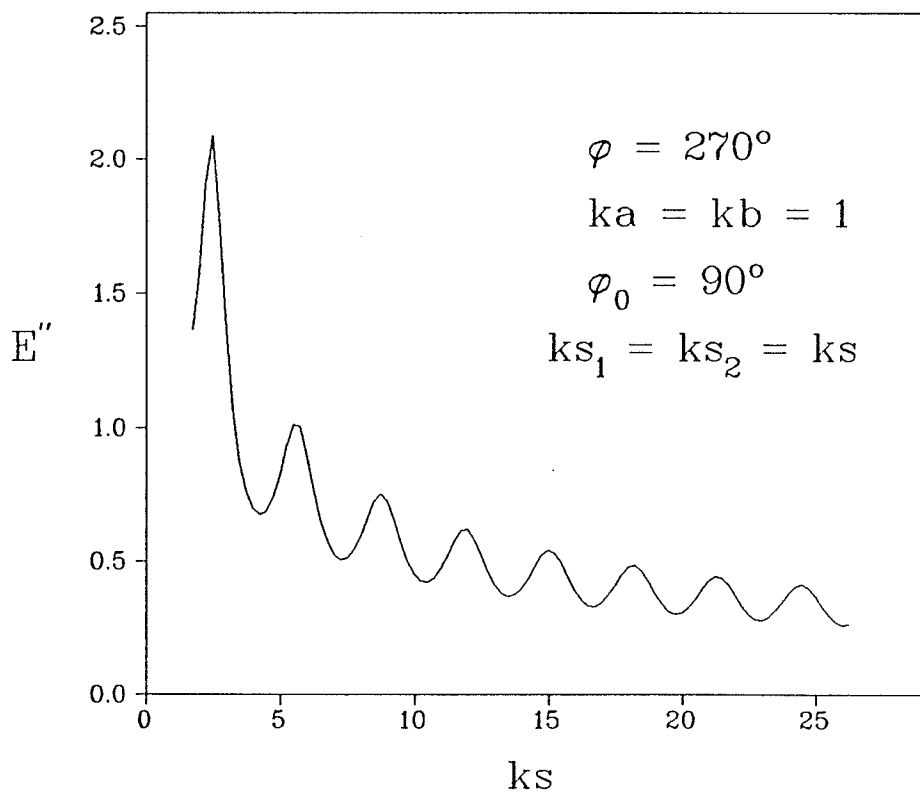
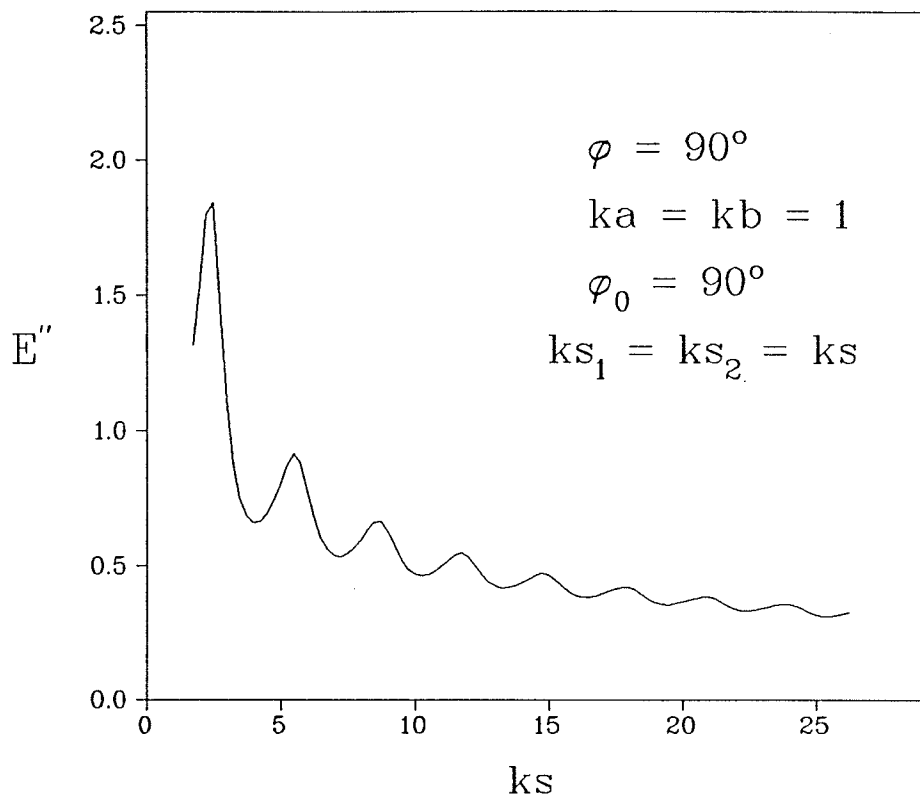


Fig. 4-6 : Amplitude of the interaction field vs. ks.

Gaussian type [96]. Therefore the value of any of these integrals is reduced to sum of a finite number of terms. Each term consists of the integrand (evaluated at one of the zeroes of the Legendre polynomials) times a weighting factor. A forty point integration is used in all our calculations. The thin slit case is considered first where the transmission coefficient  $T$  defined by Eq. (3-16) is calculated and compared with the exact values [34] in table 4-1. From this table one notices that for all values of  $ks \geq 1.0$  the absolute value of the percent error does not exceed 0.28%. It is worth mentioning that the number of sampling points on the contour  $C_1+C_2$  was 180 points. For higher accuracy, especially for small values of  $ks$  where severe interaction between the two edges takes place, one should increase this number of points. In Fig. 4-7 the transmission coefficient of a double wedge is shown as a function of wedge angle  $\gamma$  and for different values of  $ks$ , namely 1, 2 and 4. As shown in the figure, there is good agreement between the results based on the numerical and the CWS methods for all indicated edge to edge separations. This verifies the validity of the CWS technique [97,99] for diffraction by narrow double wedge geometries.

For better understanding of the behaviour of the diffracted field due to edge-edge interaction in the double wedge geometry, it is worth presenting some numerical values for the amplitude and phase of the aperture field. In Figs. 4-8 and 4-9, we show the amplitude ( $E_z^i$ ) and phase ( $\psi$ ) of the aperture field of the slit geometry for  $\phi_0 = 90^\circ$  and different values of  $ks$ . As shown, the amplitude of the aperture field oscillates around unity for large values of  $ks$ . Although the number of oscillations increases with  $ks$ , the peak to peak value of the oscillations decreases with  $ks$ , as expected. The phase of the aperture field is also found to be oscillating for large values of  $ks$  and the oscillations are around  $0^\circ$ , whereas for small values of  $ks$ ,  $\psi$  is almost constant through the whole aperture and  $E_z^i$  has a cosine shape where the peak value is proportional to  $ks$ .

In Fig. 4-10 the electrical current component  $J^d$  on the surface of a thick slit (of electrical thickness  $kd$ ) is shown and compared with the corresponding current

<i>ks</i>	<i>T</i>		Percent error
	Exact	Numerical	
0.2	0.00262	0.00156	-40.51
0.4	0.02392	0.02192	-8.35
0.6	0.09484	0.09213	-2.85
0.8	0.26059	0.25781	-1.07
1.0	0.54540	0.54388	-0.28
1.2	0.87693	0.87771	0.09
1.4	1.11719	1.11961	0.22
1.6	1.21669	1.21929	0.21
1.8	1.22129	1.22329	0.16
2.0	1.18426	1.18549	0.10
2.4	1.08650	1.08688	0.03
3.0	0.97202	0.97138	-0.07
3.4	0.92824	0.92746	-0.08
4.0	0.94244	0.94244	0.00
5.0	1.04992	1.05121	0.12
6.0	0.99559	0.99521	-0.04
7.0	0.97174	0.97170	0.00
8.0	1.02332	1.02403	0.07
9.0	1.00199	1.00175	-0.02
10.	0.98224	0.98211	-0.01

Table 4-1 : Slit transmission coefficient vs. *ks* for  $\phi_0 = 90^\circ$ .

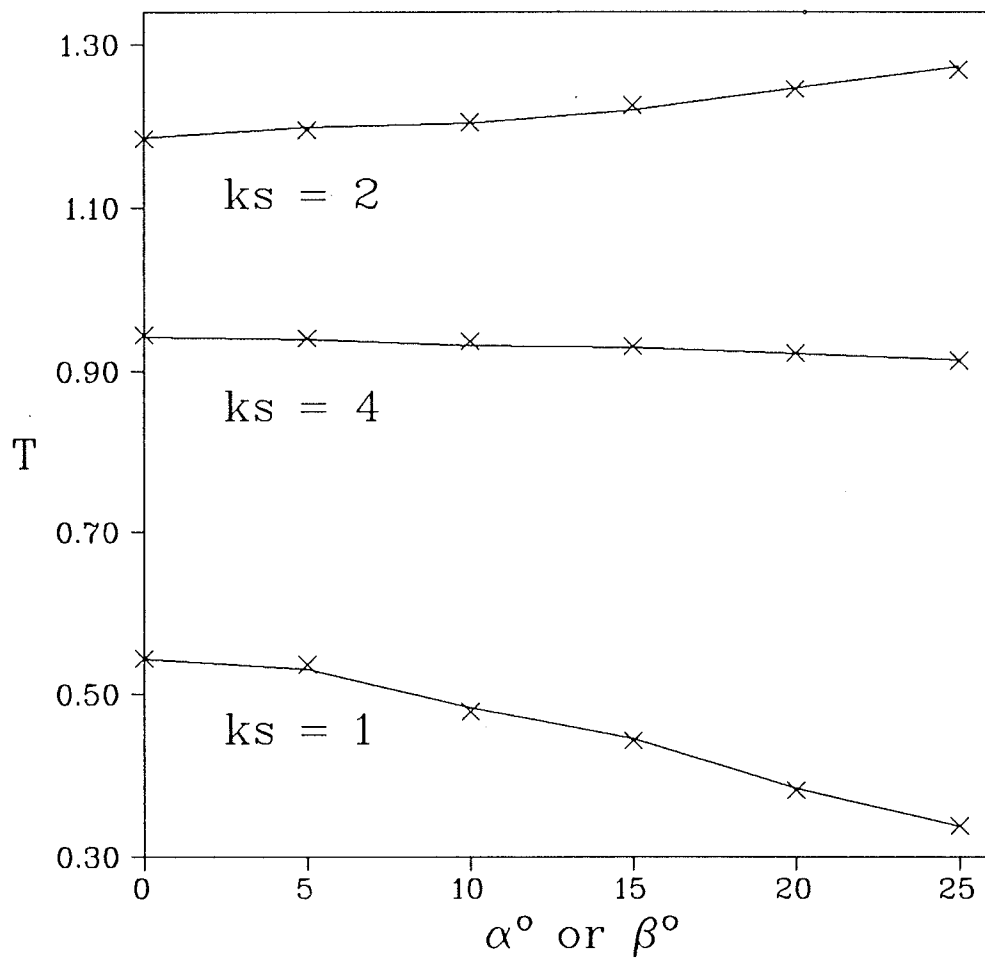


Fig. 4-7 : T vs. wedge angle  $\gamma$ .

— Numerical  
x x x C W S (N = 6)

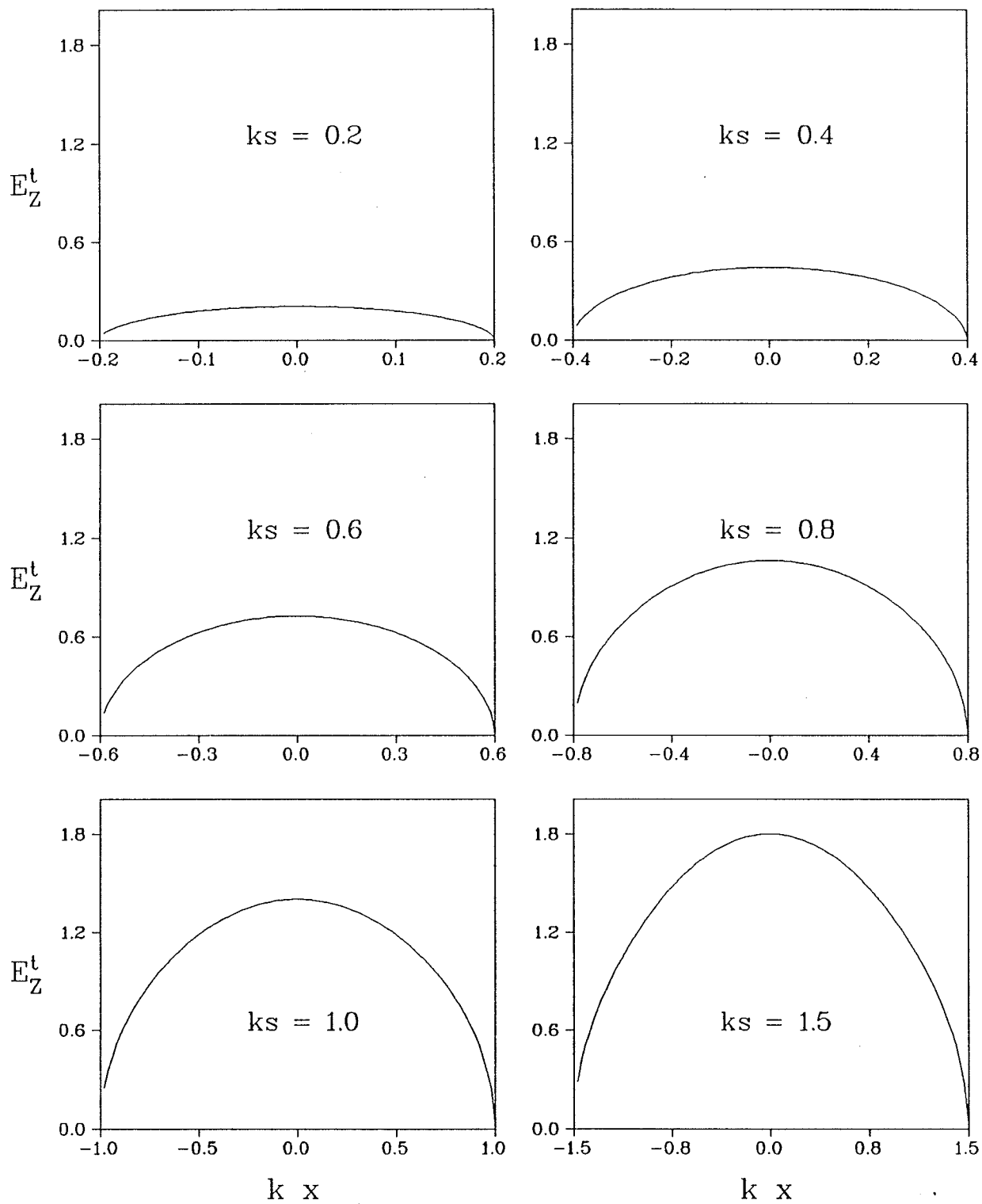


Fig. 4-8a : Amplitude of the slit aperture field for  $\varphi_0 = 90^\circ$

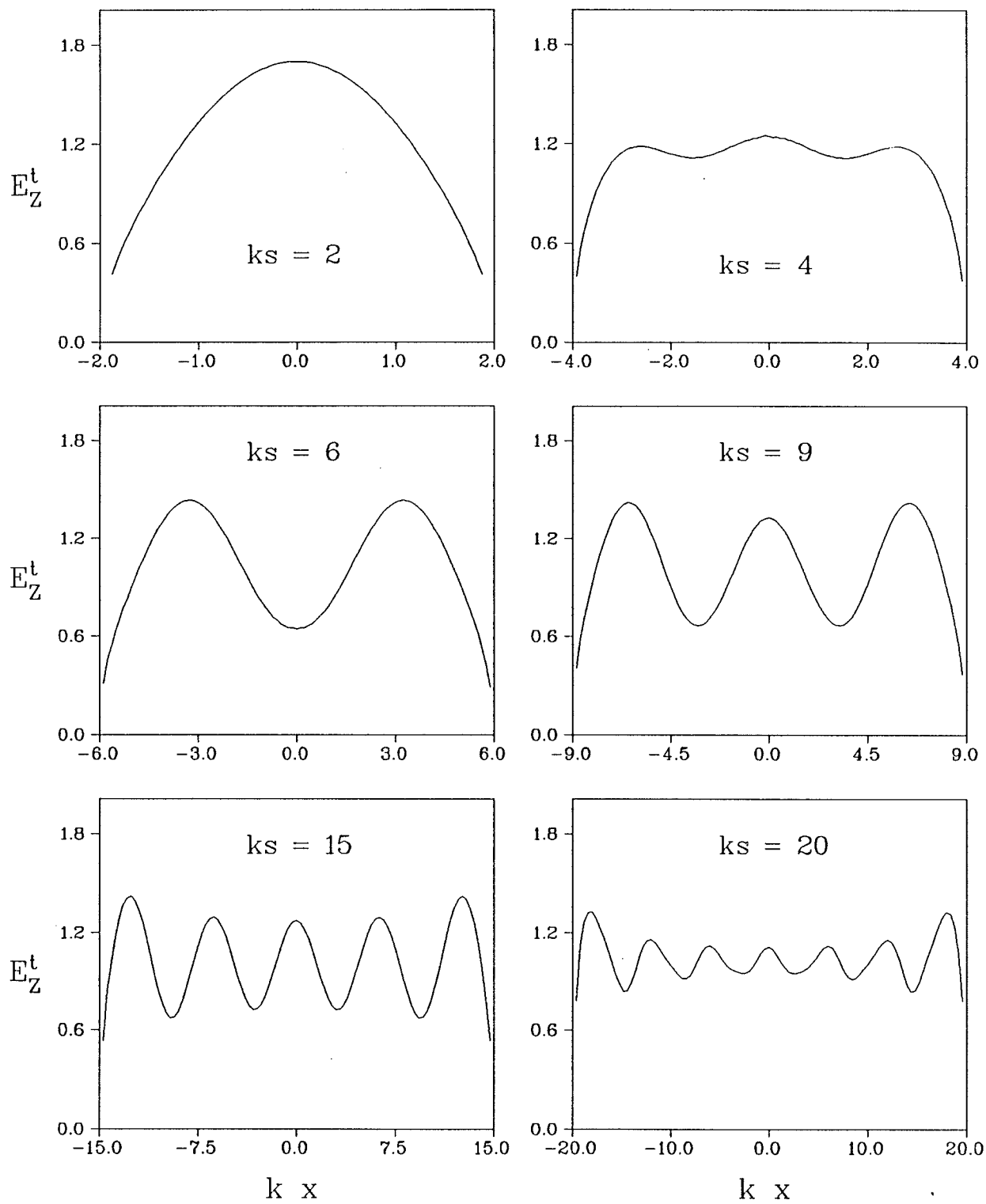


Fig. 4-8 b : Amplitude of the slit aperture field for  $\varphi_0 = 90^\circ$

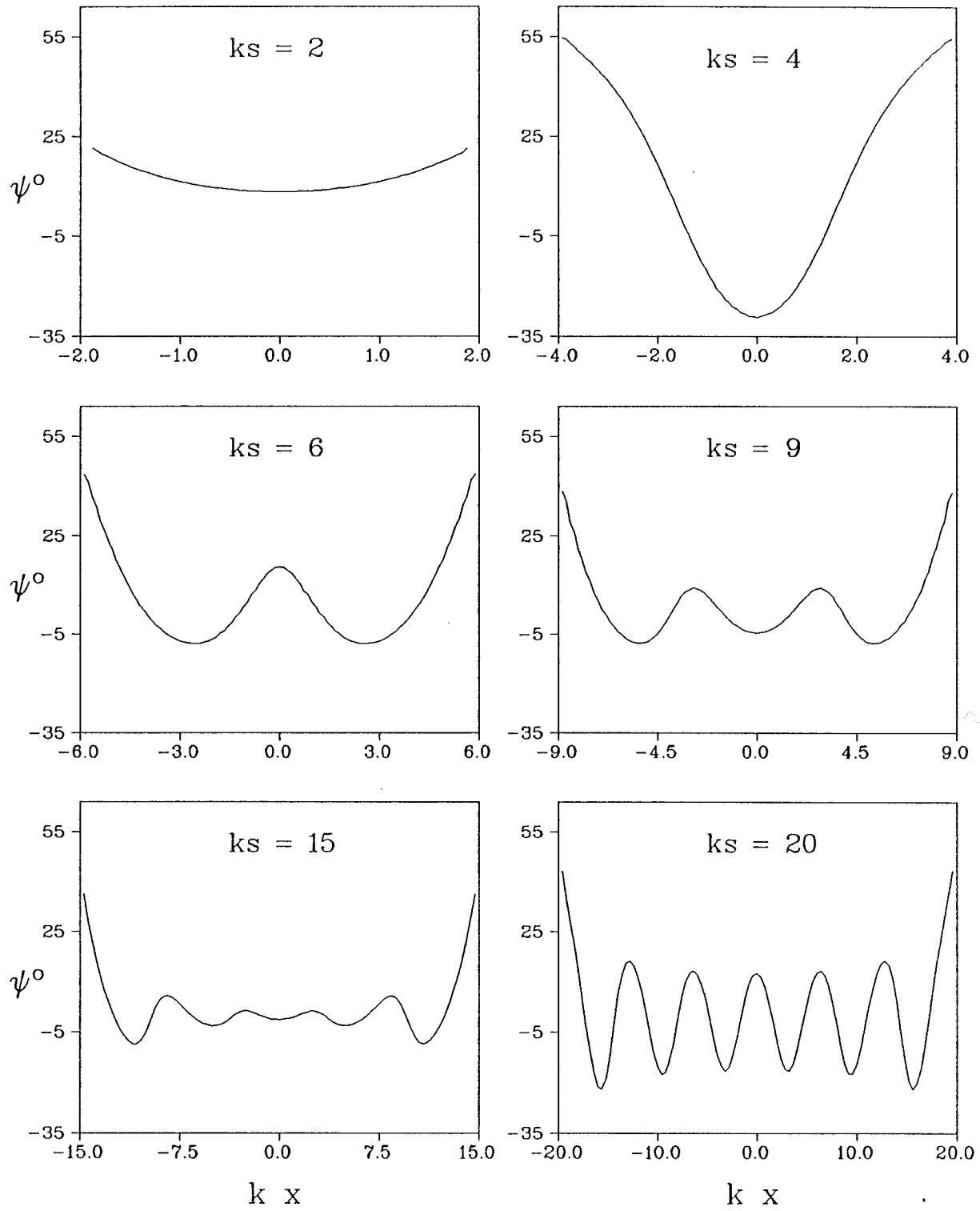


Fig. 4-9: Phase of the slit aperture field for  $\varphi_0 = 90^0$ .

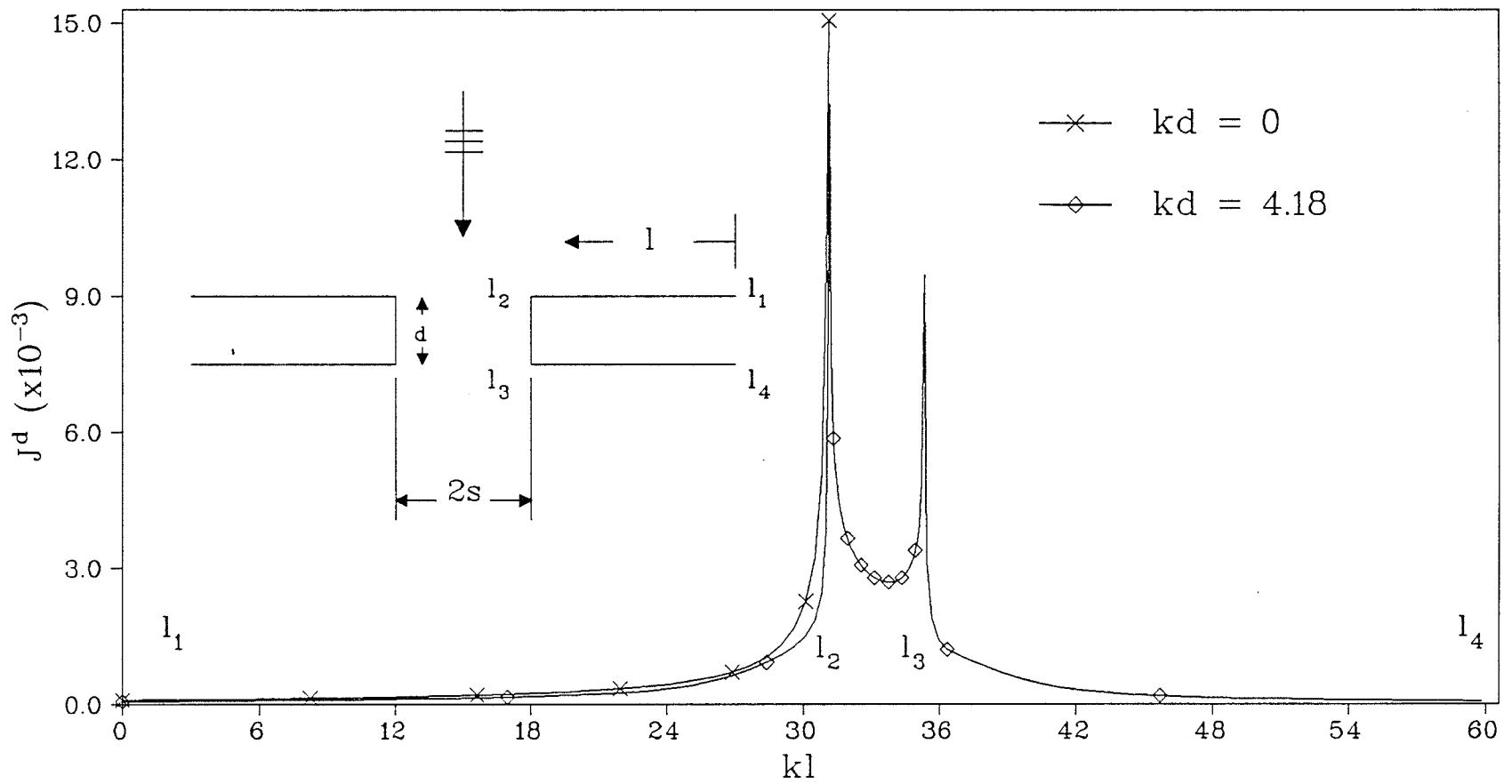


Fig. 4-10: Current density vs.  $kl$  for  $ks = 8.06$ .



on the surface of a thin slit. The resulting diffracted field patterns for the same geometries are presented in Fig. 4-11 where the results for the thick slit are compared the experimental results reported in [44] and good agreement is observed. To illustrate the effect of  $kd$  on the  $E^d$  pattern, consider the case where  $\phi_0 = 90^\circ$ ,  $ks = 8.06$ . For this case the beamwidth and the first sidelobe level of the  $E^d$  pattern vary from  $18.76^\circ$  and  $-13.4$  dB for  $kd = 0$  to  $22.37^\circ$  and  $-12.6$  dB for  $kd = 4.18$ , respectively. Figures 4-12 and 4-13 show the amplitude of  $J^d$  and the  $E^d$  pattern of a double truncated wedge, respectively, for  $\phi_0 = 90^\circ$ ,  $ks = 8.06$  and  $\gamma = 15^\circ$ , for two values of  $kd$ , namely  $kd = 0$  (which corresponds to a double sharp-wedge) and  $kd = 4.18$ . In comparing the two curves in Fig. 4-13, we find that the effect of  $kd$  on the  $E^d$  pattern of a double wedge is similar to the effect of  $kd$  on the  $E^d$  pattern of a thick slit. To further investigate the diffraction pattern characteristics of a double truncated wedge, we present tables 4-2, 4-3 and 4-4 where the independent parameters in these tables are  $kd$ ,  $\gamma$  and  $ks$ , respectively. Referring to table 4-2, it is found that small truncations do not have significant effect on the beamwidth, position of the first null and first sidelobe position and level for the case where  $\phi_0 = 90^\circ$ ,  $ks = 7$  and  $\gamma = 20^\circ$ . However, for large values of  $kd$  significant changes in the diffraction pattern characteristics are observed. It is clear that the effects of the interior wedge angle  $\gamma$  on the diffraction pattern of a truncated double wedge (as shown in table 4-3 for  $\phi = 90^\circ$ ,  $ks = 7$  and  $kd = 0.5$ ) become significant for large values of  $\gamma$ . With respect to table 4-4, where  $\phi_0 = 90^\circ$ ,  $\gamma = 10^\circ$  and  $kd = 0.5$ , it is obvious that the electrical separation between the two wedges is the parameter with most effect on the diffraction characteristics of the double wedge.

The diffraction by a double capped wedge is also investigated where the electrical radius of the cap is denoted by  $kr$ . It should be noticed that for this geometry, the limits of the first integration in Eqs. (4-14) and (4-15) and those of the last integration in Eq. (4-16), which are denoted by  $-s_1$  and  $s_2$ , should be changed to  $-(s_2+r)$  and  $(s_1+r)$ , respectively. Fig. 4-14 shows the  $E^d$  pattern of a capped slit

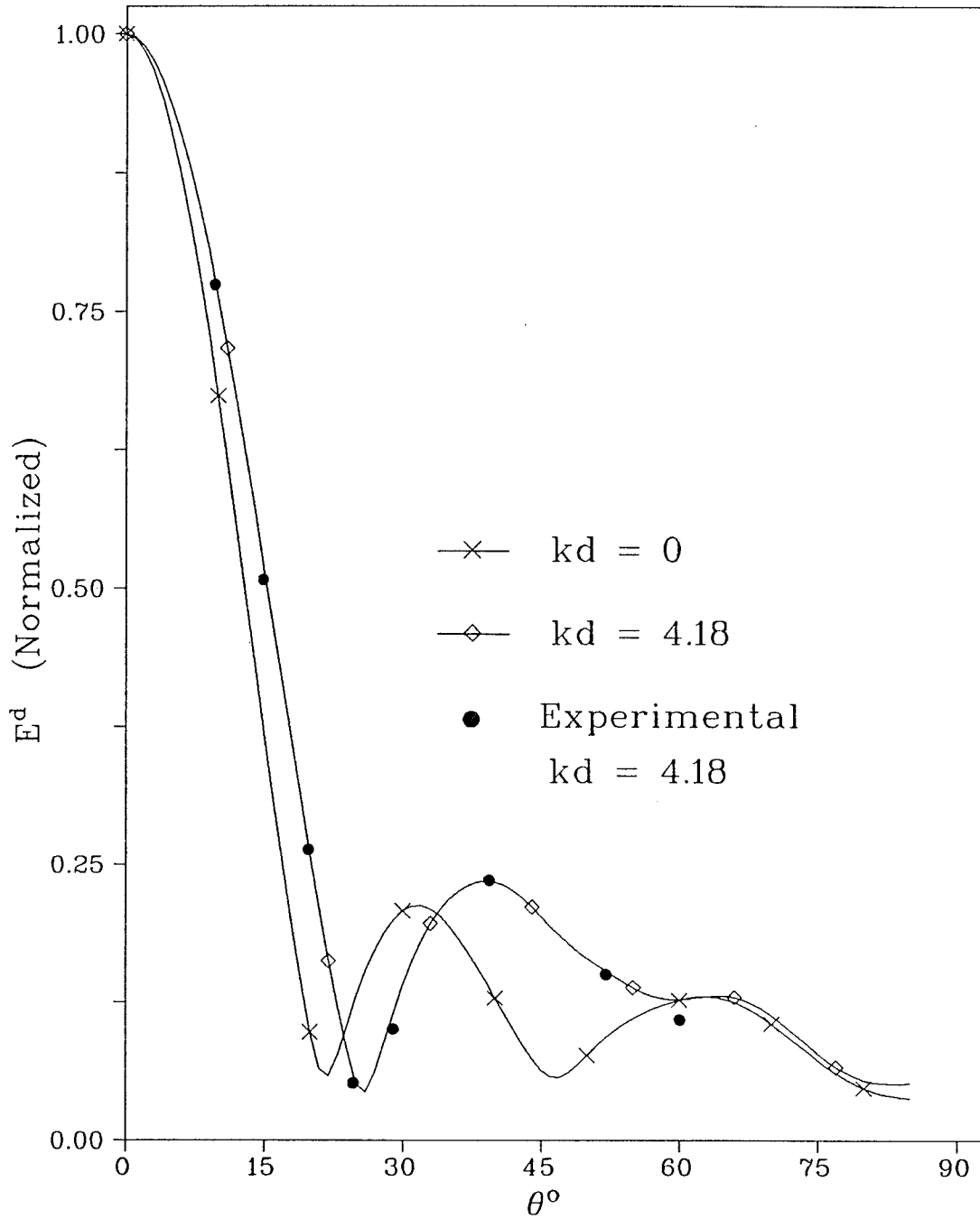


Fig. 4-11 : Normalized diffracted field vs. angle  $\theta$  of a thick slit for  $ks = 8.06$  .

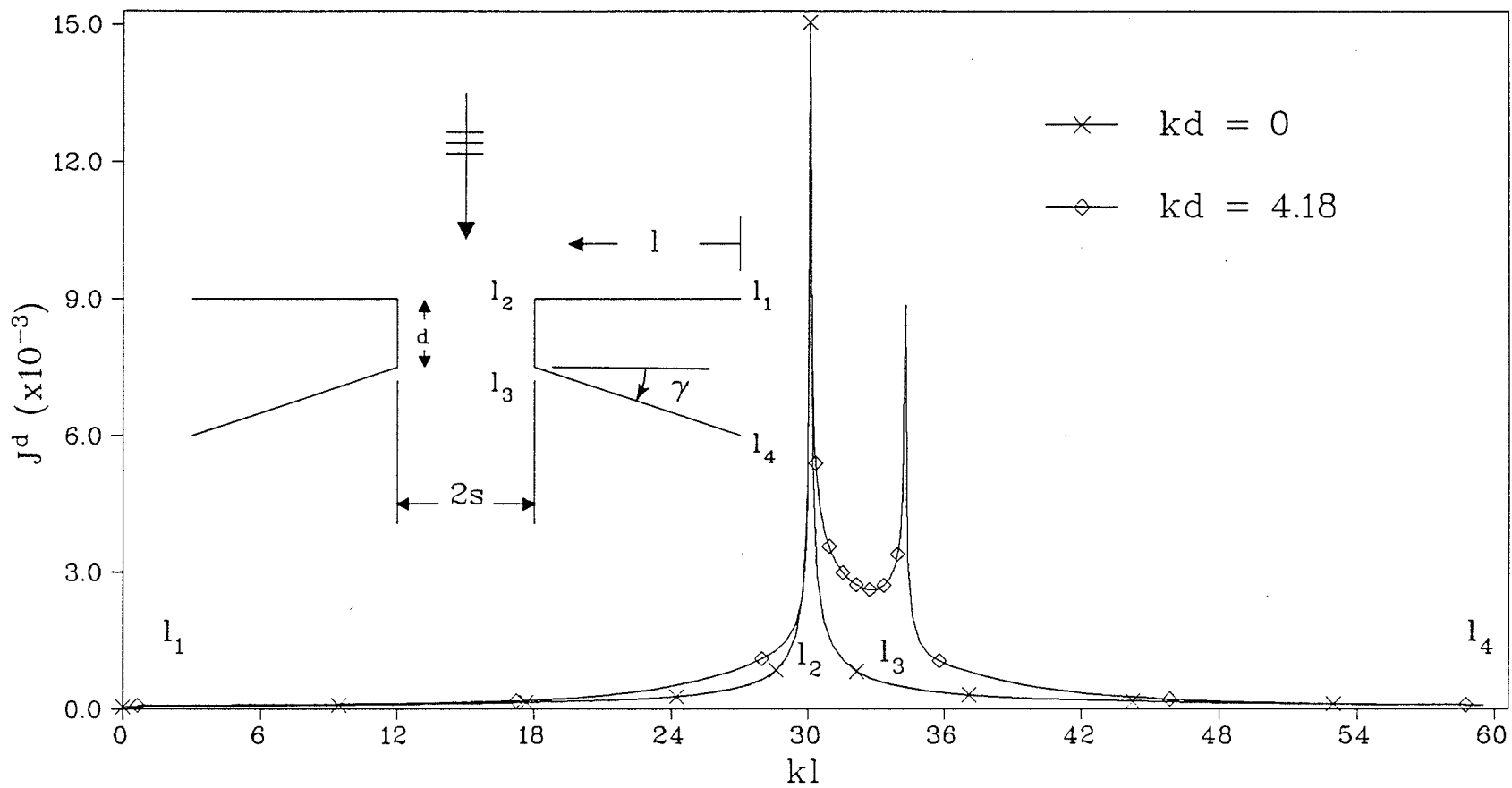


Fig. 4-12 : Current density vs.  $kl$  for  $k_s = 8.06$  and  $\gamma = 15^\circ$ .

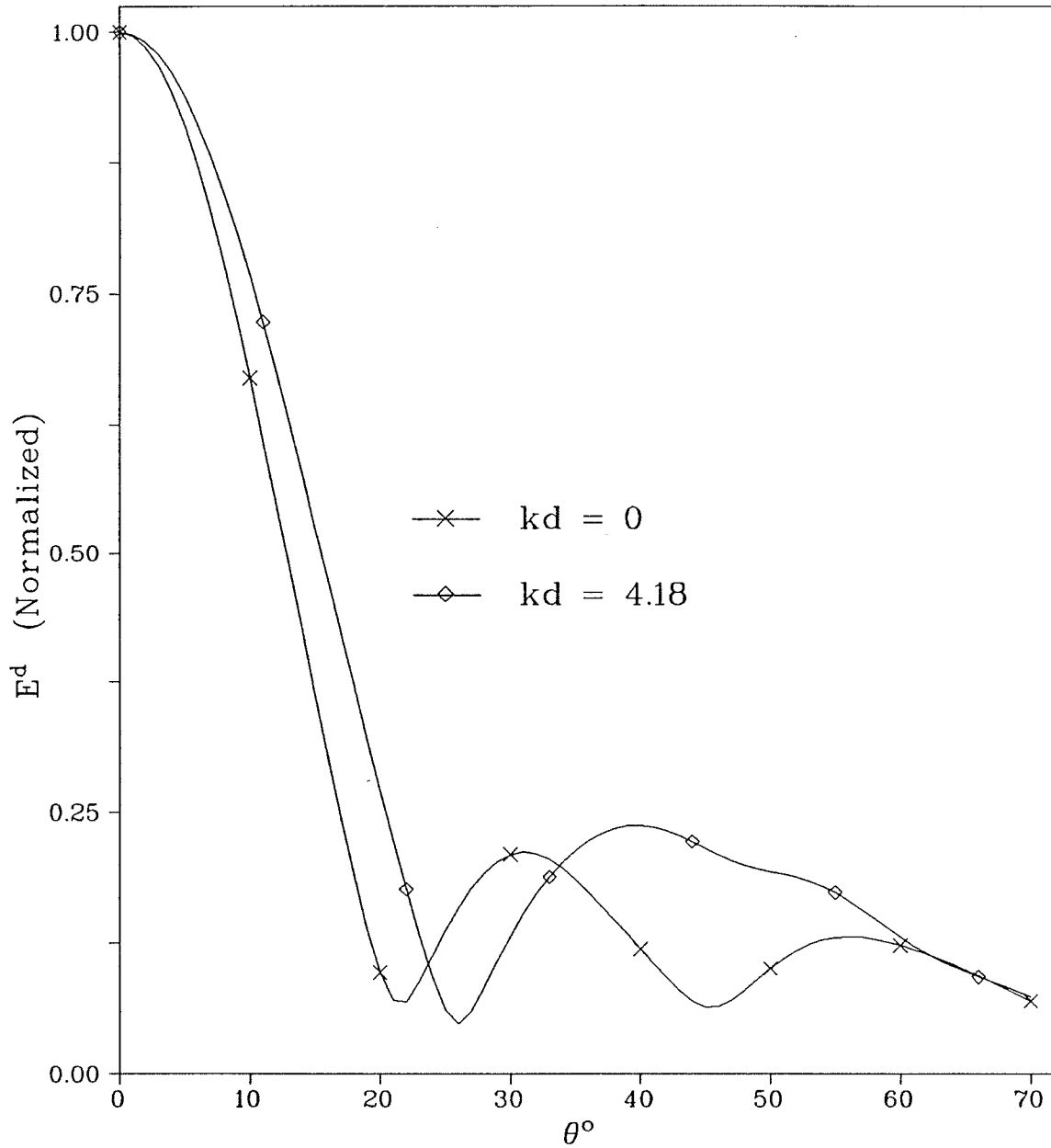


Fig. 4-13 : Normalized diffracted field vs. angle  $\theta$  of a double truncated-wedge for  $\gamma = 15^\circ$  and  $ks = 8.06$ .

$kd$	Beam-width	Position of first null	First sidelobe		$T$
			Position	Level	
0.0	23.09°	28.89°	45.58°	-13.36 dB	0.96382
0.1	23.49°	29.00°	45.75°	-13.04 dB	0.95114
0.2	23.87°	29.75°	45.74°	-12.81 dB	0.94004
0.3	24.15°	29.79°	45.87°	-12.61 dB	0.93235
0.4	24.45°	29.83°	45.83°	-12.44 dB	0.92453
0.5	24.67°	29.85°	45.86°	-12.31 dB	0.91921
0.6	24.87°	29.88°	45.89°	-12.89 dB	0.91451
0.7	25.08°	29.89°	45.84°	-12.12 dB	0.91009
0.8	25.21°	29.90°	45.78°	-12.06 dB	0.90751
0.9	25.40°	29.89°	45.68°	-12.00 dB	0.90437
1.0	25.52°	29.87°	45.59°	-11.97 dB	0.90253
1.5	25.71°	29.74°	45.04°	-11.95 dB	0.90095
2.0	25.58°	29.14°	44.34°	-12.13 dB	0.90527
2.5	25.29°	28.34°	43.38°	-12.35 dB	0.91075

Table 4-2 : Diffraction pattern characteristics of a double truncated wedge for  $\phi_0 = 90^\circ$ ,  $ks = 7$  and  $\gamma = 20^\circ$ .

$\gamma$	Beam-width	Position of first null	First sidelobe		$T$
			Position	Level	
$0^\circ$	$24.74^\circ$	$29.00^\circ$	$46.60^\circ$	-13.07 dB	0.92329
$5^\circ$	$24.85^\circ$	$29.69^\circ$	$46.97^\circ$	-12.89 dB	0.92114
$10^\circ$	$24.88^\circ$	$29.79^\circ$	$46.93^\circ$	-12.66 dB	0.91966
$15^\circ$	$24.77^\circ$	$29.87^\circ$	$46.56^\circ$	-12.46 dB	0.91956
$20^\circ$	$24.68^\circ$	$29.86^\circ$	$45.89^\circ$	-12.31 dB	0.91884
$25^\circ$	$25.05^\circ$	$29.72^\circ$	$44.84^\circ$	-12.15 dB	0.91266
$30^\circ$	$26.35^\circ$	$29.19^\circ$	$43.91^\circ$	-11.89 dB	0.89746
$35^\circ$	$28.07^\circ$	$28.78^\circ$	$43.35^\circ$	-11.71 dB	0.87918

Table 4-3 : Diffraction pattern characteristics of a double truncated wedge for  $\phi_0 = 90^\circ$ ,  $ks = 7$  and  $kd = 0.5$ .

$ks$	Beam-width	Position of first null	First sidelobe		$T$
			Position	Level	
2	68.84°	—	—	—	1.10639
3	59.87°	—	—	—	0.94977
4	49.29°	—	—	—	0.82909
5	30.79°	35.83°	48.20°	-12.09 dB	0.90854
6	27.17°	32.05°	48.16°	-12.70 dB	0.97944
7	24.88°	29.79°	46.93°	-12.66 dB	0.91966
8	19.95°	22.99°	32.71°	-13.79 dB	0.98217
9	17.84°	20.58°	30.26°	-13.13 dB	0.98932
10	16.75°	19.30°	28.37°	-13.24 dB	0.95151
12	13.68°	15.67°	22.55°	-13.43 dB	0.96169
15	10.91°	12.33°	17.99°	-13.36 dB	0.96389
20	8.31°	9.91°	13.63°	-13.12 dB	0.95519

Table 4-4 : Diffraction pattern characteristics of a double truncated wedge for  $\phi_0 = 90^\circ$ ,  $\gamma = 10^\circ$  and  $kd = 0.5$ .

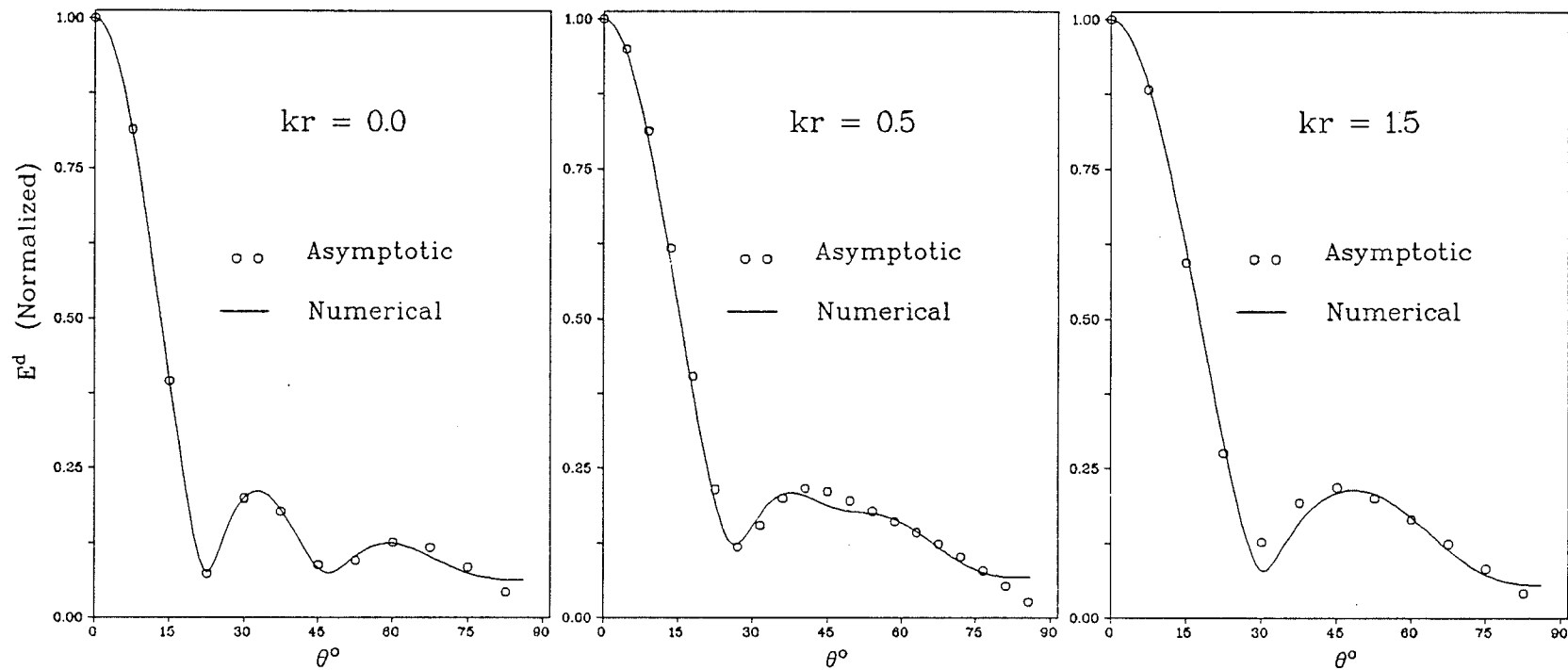


Fig. 4-14 : Normalized diffracted field vs. angle  $\theta$  of a conducting capped-slit for  $ks = 8$ .



for different values of  $kr$ , namely 0.0, 0.5 and 1.5 and where  $\phi_0 = 90^\circ$  and  $ks = 8$ . Moreover, the corresponding diffraction patterns computed using an asymptotic solution [72,73] are also shown in the figure. It is obvious that the deviations between the two curves increases with  $kr$ . This is due to the fact that the asymptotic solution is valid for small values of  $kr$ . Furthermore, one notices that the cap affects the diffraction pattern characteristics especially for large values of  $kr$ . In addition to the changes in the diffraction pattern due to the conducting cap, it is also clear from Fig. 4-15 that the amplitude of the aperture field of a double capped wedge is greatly affected by  $kr$ . It seems that for large values of  $kr$  the oscillations in the amplitude of the aperture field disappear, leading to a cosine shape distribution. To further investigate this geometry, tables 4-5, 4-6 and 4-7 are included. In table 4-5 where  $\phi_0 = 90^\circ$ ,  $ks = 7$  and  $\gamma = 20^\circ$ , the beamwidth, first null and first sidelobe level and position increase with  $kr$ . However,  $T$  is found to decrease with increasing values of  $ks$ . The effect of the internal wedge angle on the diffraction pattern characteristics for  $\phi_0 = 90^\circ$ ,  $kr = 0.5$  and  $ks = 7$  is illustrated in table 4-6. From the table it is clear that small changes are observed for the given parameters. This indicates again that the wedge angle does not produce significant effects on the diffraction pattern for wide separations between the two wedges regardless of the shape of the edge of either wedge. Finally, it is clearly shown in table 4-7 that the beamwidth and first sidelobe level of the  $E^d$  pattern decrease with  $ks$  when  $\phi_0 = 90^\circ$ ,  $\gamma = 10^\circ$  and  $kr = 0.5$ . However the  $T$  values oscillate around a value less than unity. This indicates that the transmission coefficient of a double conducting capped wedge is always less than the corresponding value of  $T$  of the uncapped case for all possible separations. In general the transmission coefficient is found to be more sensitive to any small variations in  $kd$ ,  $kr$ ,  $\gamma$  or  $ks$  than the remaining parameters that describe the diffraction pattern.

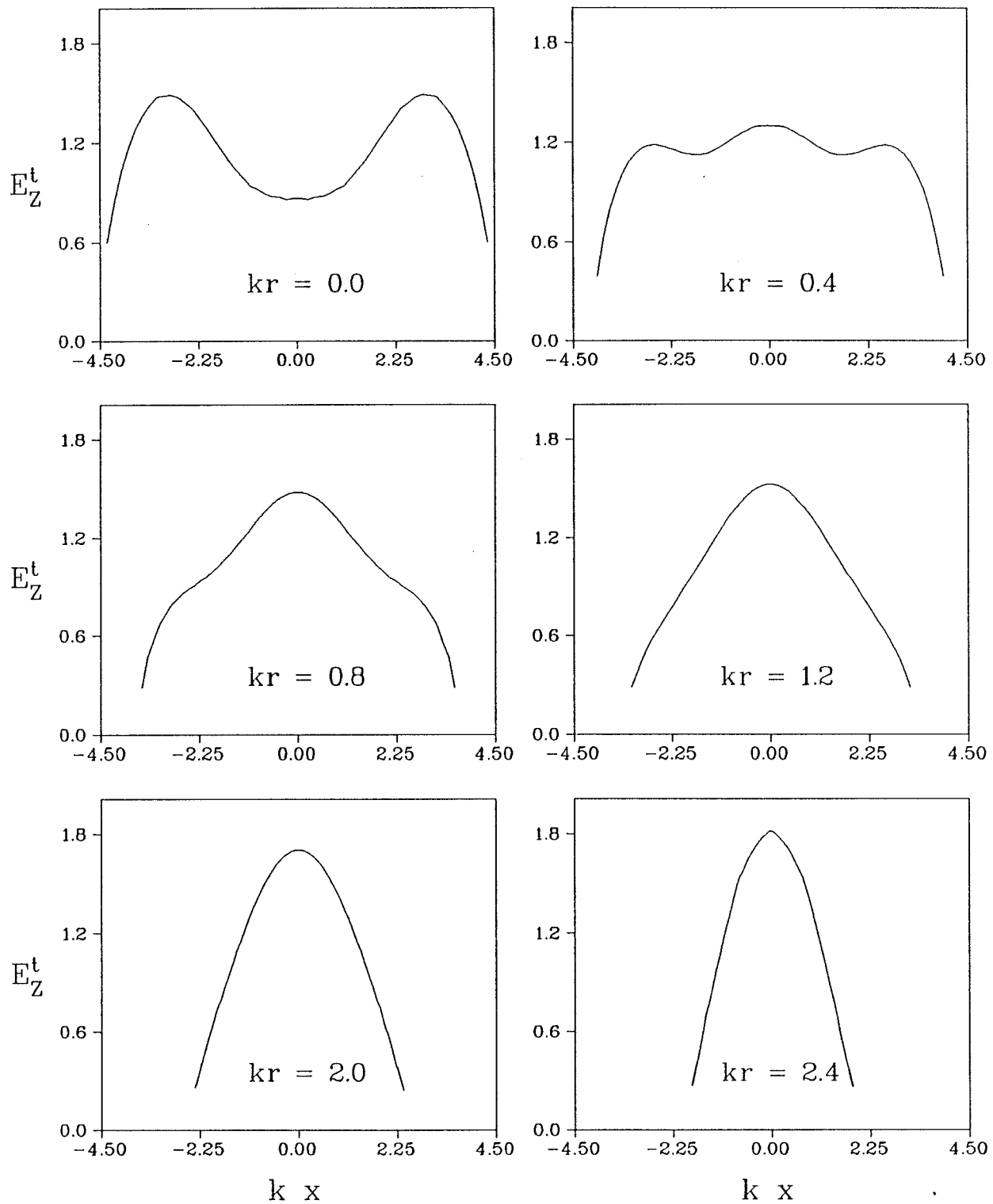


Fig. 4-15 : Amplitude of the aperture field of a double capped wedge for  $\varphi_0 = 90^\circ$ .

$kr$	Beam-width	Position of first null	First sidelobe		$T$
			Position	Level	
0.0	23.09°	28.89°	45.58°	-13.36 dB	0.96382
0.05	23.44°	28.99°	45.63°	-13.20 dB	0.95200
0.1	23.78°	29.47°	45.72°	-13.05 dB	0.94115
0.3	24.94°	30.11°	46.18°	-12.58 dB	0.90652
0.5	25.90°	30.83°	46.56°	-12.40 dB	0.88064
0.7	26.56°	31.25°	46.96°	-12.33 dB	0.86176
0.9	27.01°	31.83°	47.35°	-12.37 dB	0.84588
1.0	27.15°	31.97°	47.56°	-12.34 dB	0.83994
1.5	27.68°	33.84°	48.60°	-12.24 dB	0.79741
2.0	30.54°	38.76°	46.03°	-10.45 dB	0.67879

Table 4-5 : Diffraction pattern characteristics of a double capped wedge for  $\phi_0 = 90^\circ$ ,  $ks = 7$  and  $\gamma = 20^\circ$ .

$\gamma$	Beam-width	Position of first null	First sidelobe		$T$
			Position	Level	
$0^\circ$	$26.14^\circ$	$30.81^\circ$	$48.26^\circ$	-12.84 dB	0.87952
$5^\circ$	$26.18^\circ$	$30.86^\circ$	$48.16^\circ$	-12.73 dB	0.87886
$10^\circ$	$26.13^\circ$	$30.93^\circ$	$47.83^\circ$	-12.58 dB	0.87896
$15^\circ$	$25.97^\circ$	$30.95^\circ$	$47.30^\circ$	-12.47 dB	0.88036
$20^\circ$	$25.90^\circ$	$30.83^\circ$	$46.56^\circ$	-12.40 dB	0.88064
$25^\circ$	$26.38^\circ$	$30.53^\circ$	$45.65^\circ$	-12.34 dB	0.87542
$30^\circ$	$27.61^\circ$	$30.10^\circ$	$44.69^\circ$	-12.25 dB	0.86323
$35^\circ$	$28.93^\circ$	$29.50^\circ$	$44.08^\circ$	-12.24 dB	0.85074

Table 4-6 : Diffraction pattern characteristics of a double capped wedge for  $\phi_0 = 90^\circ$ ,  $ks = 7$  and  $kr = 0.5$ .

$ks$	Beam-width	Position of first null	First sidelobe		$T$
			Position	Level	
2	83.24°	—	—	—	0.64026
3	70.29°	—	—	—	0.86163
4	54.82°	—	—	—	0.76612
5	36.11°	39.64°	44.43°	-9.97 dB	0.84029
6	29.17°	33.17°	49.51°	-11.81 dB	0.92322
7	26.17°	30.98°	47.88°	-12.36 dB	0.87797
8	21.91°	25.81°	36.68°	-14.16 dB	0.89533
9	18.81°	21.49°	31.35°	-12.79 dB	0.94600
10	17.23°	19.96°	29.42°	-13.05 dB	0.92275
12	13.80°	15.67°	22.84°	-13.07 dB	0.95971
15	10.95°	12.17°	18.06°	-13.21 dB	0.96382
20	8.28°	9.91°	13.57°	-13.29 dB	0.95688

Table 4-7 : Diffraction pattern characteristics of a double capped wedge for  $\phi_0 = 90^\circ$ ,  $\gamma = 15^\circ$  and  $kr = 0.5$ .

## CHAPTER 5

### *DISCUSSION AND CONCLUSIONS*

In Chapter 2 the multiple scattering of an incident plane wave by two bodies is investigated. A novel technique based on the cylindrical wave spectrum is presented and applied to some practical configurations. The validity of this technique is verified by comparing the numerical results due to the scattering by two parallel conducting cylinders with those obtained using the boundary value solution and the method of moments. The technique is then used to solve for the diffraction by a double wedge which has no exact solution except for the special case of the slit geometry. Again good agreement between computed data for the transmission coefficient of a slit and the exact values is obtained. It appears that this theory along with the approximation used to facilitate the diffraction by semi-infinite scatterers, provides accurate results for slits of any half electrical width greater than or equal to unity.

One of the main advantages of the CWS technique is that it simplifies the handling of the scattering by multiple objects because the method deals with each body individually. Another advantage of the technique is that the memory size required to apply the CWS technique is linearly proportional to the total number of Huygens current sources, whereas in the MM the order of the impedance matrix is proportional to the square of the number of points at which the unknown surface currents are evaluated. Moreover, in the CWS technique no matrix inversion is required.

In principle, the CWS technique is applicable for the scattering by many objects without any restriction on their size or separation. However, it is found that large execution time is needed in order to achieve good accuracy for complicated geometries. The procedure used here is capable of yielding both near and far fields

in terms of known solutions for each body involved in isolation.

As far as the asymptotic solution is concerned, it is clear that the improvement in dealing with edge-to-edge interaction developed in Chapter 3 using fictitious inhomogeneous line sources located at the edges could lead to a wider domain of validity of the ray-optical method. Thus it could be applied to an increasing number of waveguide and free space scattering problems especially for scatterers which involve edges and corners. Moreover, it is found that when cylindrical dielectric edge caps are introduced significant changes in the diffraction characteristics of the double wedge problem is observed. Furthermore, the loading of the aperture plane by a cylindrical scatterer indicates considerable changes in the transmission coefficient. Loading the aperture by a dielectric cylinder of homogeneous or inhomogeneous permittivity profiles yields an increase in the transmission coefficient over the unloaded aperture, while a lower transmission coefficient is observed when a conducting cylinder is used. Rounding the edges of the wedges or using cylindrical conducting caps at the edges in the double wedge geometry produces a lower transmission coefficient whereas, the use of cylindrical dielectric caps of homogeneous permittivity yields a higher transmission coefficient relative to the unloaded case.

With regard to the numerical solution presented in Chapter 4, the diffracted field due to a plane wave incident on two wedges forming a slit type geometry is formulated using an integral equation for the surface current. The use of the ordinary method of moments to solve for the unknown surface currents will not yield a convergent solution due to the semi-infinite dimensions of the wedges and the fact that the total current does not vanish on the illuminated surface for this type of excitation. Therefore, the surface current is divided into two components, namely a known non-interaction term and an unknown term due to the infinite number of interactions between the wedges. The non-interaction term is considered to be the physical optics current for those geometries which have wedges with non-sharp edges, whereas the exact surface current for a single wedge is used for double

wedges with sharp edges. The interaction term is then evaluated using the ordinary method of moments since it decays with increasing distance from the edge along the surface of either wedge. It is found that this technique leads to an efficient solution and makes it possible to use the method of moments for the multiple scattering by bodies of semi-infinite or large dimensions without the need for a large size computer memory. Furthermore, by applying this technique the saving in execution time over the ordinary method of moments or even the exact boundary value solution increases with the electrical dimensions of the scatterers. Numerical results for the diffracted fields and transmission coefficients for a variety of related structures such as the thin slit, thick slit, double truncated wedge and double capped wedge are presented and compared with available solutions. It should be noted that this method is applicable to arbitrary number of cylinders or scatterers of different shapes.

It is found, in general, that the diffraction pattern of a double wedge is less sensitive to small truncation or capping than the transmission coefficient. Moreover, it is also noticed that the interior wedge angle has a significant effect on the diffraction pattern characteristics only for small wedge to wedge separation distances. Although an incident plane wave is assumed throughout the present analysis, the extension to more practical types of excitations (e.g. line source field) is simple and straightforward.

### 5.1 Suggestions for future research

Many promising problems arise from the present study and their investigations may lead to some useful results and applications. As an example, although we have used the CWS technique for the scattering by cylindrical objects, it is obviously of interest to extend this technique to handle three-dimensional scattering problems by using a spherical wave spectrum (SWS) due to induced point sources in each interaction between the scatterers. Another interesting study involves the extension of the CWS technique to deal with dielectric and dielectric coated cylindrical conductors



by using the polarization currents in the dielectric media and the electrical linear currents on the conducting surfaces. Furthermore, the CWS technique can be used to solve for the scattering by  $N$  infinite circular conducting cylinders forming one or two dimensional array which can be achieved easily, especially if the symmetry is considered in the analysis.

It should be noted that the efficiency of the modified MM solution could be substantially improved by introducing a GTD term in the basis functions to represent the diffraction current as shown by Burnside et. al. for diffraction by a single right angle conducting wedge [100].

With respect to loading the aperture plane of the double wedge, it is obvious that finding the optimal parameters that produce a higher transmission coefficient when using a lossy dielectric cylinder or a dielectric lens as a loading object is of great interest. Another possibility is to fill the aperture of a thick slit or a double truncated wedge by a lossy or inhomogeneous dielectric material in order to focus the main diffracted lobe in a certain direction.

Since the surface current distribution is the main parameter in determining the diffraction properties of the double wedge, it is useful to investigate the effect of loading one or both surfaces of the the two wedges by a lossy dielectric lining or by introducing corrugations to further control the surface current distribution. It is also possible to place the corrugations on the truncated edges of a double truncated wedge geometry.

So far, we have used only passive elements to modify the diffraction characteristics of the double wedge geometry. Another possibility, of course, is to use an active elements and one of these geometries, which requires further investigation, is the diffraction of the field of an array of sources by the double wedge geometry. It is worth mentioning that a similar excitation of a single finite wedge was investigated and significant changes in the radiation characteristics of the corner array are

reported elsewhere [101,102].

Finally, since the diffraction by an imperfectly conducting or a dielectric wedge is available [103-110], it is of great interest to investigate the extension of the techniques used in this thesis to solve for the diffraction by a double dielectric or imperfectly conducting wedge.

## APPENDIX A

### DERIVATION OF EQUATION (2-21)

The physical optics current of a plane wave incident on an infinite conducting plane is given by

$$J^{PO} = \frac{2}{\eta} \sin \phi_0 e^{jkx \cos \phi_0} \quad (\text{A-1})$$

the corresponding scattered field is

$$E_{PO}^S(\rho, \phi) = -\frac{k}{2} \sin \phi_0 \int_0^{\infty} e^{jkx \cos \phi_0} H_0(k|\bar{\rho} - \bar{x}|) dx \quad (\text{A-2})$$

however for normally incident plane wave ( $\phi_0 = 90^\circ$ ),  $E_{PO}^S$  reduces to

$$E_{PO}^S(\rho, \phi) = -\frac{k}{2} \int_0^{\infty} H_0(k|\bar{\rho} - \bar{x}|) dx. \quad (\text{A-3})$$

For a single sharp wedge illuminated by an incident plane wave,  $E_{PO}^S$  is zero in the region far from the wedge edge. However, near the edge  $E_{PO}^S$  for  $\phi_0 = 90^\circ$  can be given by Eq. (A-3) where  $\rho$ ,  $\phi$  are the local coordinates of the wedge. Since we are interested in the value of  $E_{PO}^S$  at the edge of the opposite wedge, i.e. at  $\rho = s_{12}$  and  $\phi = 180^\circ$ , Eq. (A-3) reduces to

$$E_{PO}^S(s_{12}, 180) = -\frac{k}{2} \int_0^{\infty} H_0(k(s_{12} + x)) dx. \quad (\text{A-4})$$

Letting  $s_{12} + x = t$ , we obtain

$$E_{PO}^S(s_{12}, 180) = -\frac{k}{2} \int_{s_{12}}^{\infty} H_0(kt) dt$$

$$\begin{aligned} &= -\frac{k}{2} \left[ \int_0^{\infty} H_0(kt) dt - \int_0^{s_{12}} H_0(kt) dt \right] \\ &= -\frac{1}{2} + \frac{k}{2} \int_0^{s_{12}} H_0(kt) dt. \end{aligned} \tag{A-5}$$

Thus if the effect of the  $E_{PO}^S$  is compensated by a line source located at the edge of the wedge, the amplitude  $C_0$  of this line source is given by

$$C_0 = \left[ \frac{2}{\eta k} - \frac{2}{\eta} \int_0^{s_{12}} H_0(kt) dt \right] / H_0(ks_{12}). \tag{A-6}$$

## APPENDIX B

### FAR SCATTERED FIELD PATTERN OF A LINE SOURCE EXCITING A SHARP WEDGE

The incident field from a line source of unit amplitude in free space at an observation point  $p$  ( $\rho, \phi$ ) in the cylindrical coordinate system is given by

$$E_i^i = \frac{-\eta k}{4} H_0(k \rho') \quad (\text{B-1})$$

where  $\rho'$  is the distance between the point  $p$  and the line source position ( $\rho_0, \phi_0$ ). For far observation points (i.e.  $k \rho \gg 1$ ) we have

$$\rho' = \rho - \rho_0 \cos(\phi - \phi_0) \quad (\text{B-2})$$

and upon using the large argument approximation for the Hankel function, the incident field expression reduces to

$$E_i^i = \frac{-\eta k}{4} \sqrt{\frac{2j}{\pi k \rho}} e^{-jk \rho} e^{+jk \rho_0 \cos(\phi - \phi_0)} \quad (\text{B-3})$$

The above expression can be easily written in the following form

$$E_i^i = \frac{-\eta k}{4} H_0(k \rho) e^{+jk \rho_0 \cos(\phi - \phi_0)} \quad (\text{B-4})$$

In the presence of a sharp wedge defined by two faces at  $\phi = 0^\circ$  and  $\phi = 2\pi - \gamma$  and its along the  $z$  axis, the total field  $E_i^i$  is given by

$$E_i^i = \frac{-\eta k}{v} \sum_{n=1}^{\infty} J_{\frac{n}{v}}(k \rho_0) H_{\frac{n}{v}}(k \rho) \sin\left(\frac{n}{v} \phi\right) \sin\left(\frac{n}{v} \phi_0\right) \quad , \rho > \rho_0 \quad (\text{B-5})$$

where

$$\nu = (2\pi - \gamma) / \pi. \quad (\text{B-6})$$

For far field observation points,  $E'$  becomes

$$E'_i = \frac{-\eta k}{\nu} \sqrt{\frac{2j}{\pi k \rho}} \sum_{n=1}^{\infty} J_{\frac{n}{\nu}}(k \rho_0) j^{\frac{n}{\nu}} \sin\left(\frac{n}{\nu} \phi\right) \sin\left(\frac{n}{\nu} \phi_0\right). \quad (\text{B-7})$$

Thus the far scattered field  $E_i^S$  is given by

$$\begin{aligned} E_i^S = & \frac{-\eta k}{\nu} H_0(k \rho) \sum_{n=1}^{\infty} J_{\frac{n}{\nu}}(k \rho_0) j^{\frac{n}{\nu}} \sin\left(\frac{n}{\nu} \phi\right) \sin\left(\frac{n}{\nu} \phi_0\right) \\ & + \frac{\eta k}{4} H_0(k \rho) e^{+jk \rho_0 \cos(\phi - \phi_0)} \end{aligned} \quad (\text{B-8})$$

where the large argument expression of the Hankel function is replaced by the Hankel function itself. As a result the far scattered field pattern  $f^W$  can be determined according to the following definition

$$E_i^S = \frac{-\eta k}{4} H_0(k \rho) f^W. \quad (\text{B-9})$$

It should be noted that the scattered field patterns  $f_c$  and  $f_d$  defined by Eqs. (3-47) and (3-49) are derived using the same procedure used in this Appendix to determine  $f^W$ .

## APPENDIX C

### SCATTERING BY A CYLINDRICAL DIELECTRIC SHELL WITH RADIAL AND AZIMUTHAL PERMITTIVITY PROFILES

For a dielectric shell with outer and inner radii  $\rho_a$  and  $\rho_b$ , respectively, and a permittivity variation of the form

$$\epsilon(\rho, \phi) = \epsilon_a \left(\frac{\rho_0}{\rho}\right)^2 (\eta - \delta \cos 2\phi) \quad (\text{C-1})$$

where  $\epsilon_a$ ,  $\rho_0$ ,  $\eta$  and  $\delta$  are constants, the dielectric medium is considered inhomogeneous in two coordinate variables, namely  $\rho$  and  $\phi$  in the circular cylindrical coordinates. The field in region I (see Fig. C-1) is then the super-position of the incident and scattered waves and is given by

$$E_z^I(\rho, \phi) = E_0 \left\{ \sum_{n=0}^{\infty} \epsilon_n j^n J_n(k\rho) \cos n\psi + \sum_{n=0}^{\infty} \epsilon_n c_n H_n(k\rho) \cos n\psi \right\} \quad (\text{C-2})$$

where  $\psi = \phi - \phi_0$ . The first summation in Eq. (C-2) represents the incident plane wave  $E_0 e^{j k \rho \cos \psi}$  expressed in circular cylindrical coordinates and  $J_n(k\rho)$  is the Bessel function of the first kind of argument  $k\rho$  and order  $n$ . The second summation represents the scattered wave where  $c_n$  are unknown coefficients to be determined while  $H_n(k\rho)$  is the Hankel function of the second kind of argument  $k\rho$  and order  $n$  and is used to denote an outward traveling wave. The  $\phi$  component of the magnetic field in region I is then given by

$$H_\phi^I(\rho, \phi) = \frac{E_0}{j \omega \mu_0} \left\{ \sum_{n=0}^{\infty} \epsilon_n j^n k J_n'(k\rho) \cos n\psi \right.$$

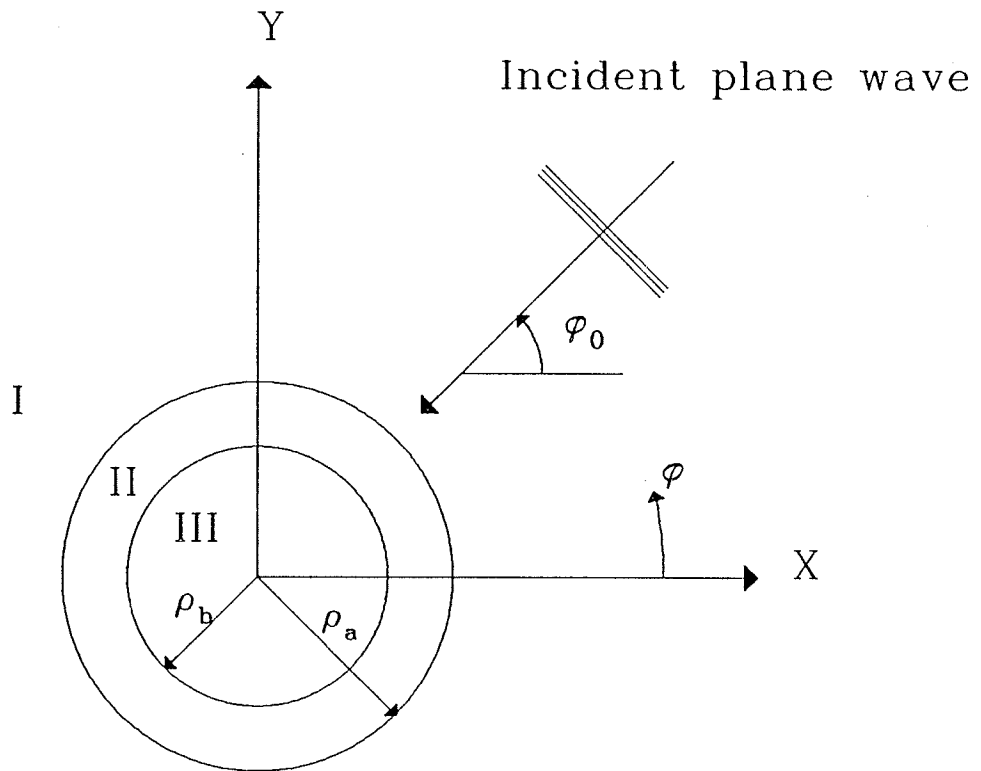


Fig C-1 : Plane wave incident on a cylindrical dielectric shell in circular cylindrical co-ordinates .



$$+ \left. \sum_{n=0}^{\infty} \epsilon_n c_n k H_n'(k\rho) \cos n\psi \right\} \quad (\text{C-3})$$

where the prime indicates differentiation with respect to the argument  $k\rho$ .

For region II, where  $\epsilon$  is given by Eq. (C-1),  $E(\rho, \phi)$  satisfies the following equation

$$\frac{1}{\rho} \frac{\partial}{\partial \rho} \left( \rho \frac{\partial E_z}{\partial \rho} \right) + \frac{1}{\rho^2} \frac{\partial^2 E_z}{\partial \phi^2} + \omega^2 \mu_0 \epsilon E_z = 0 \quad (\text{C-4})$$

by means of separation of variables based on the assumption that  $E_z(\rho, \phi) = \rho^{\pm \alpha} \Phi(\phi)$  [90], Eq. (C-4) reduces to

$$\frac{d^2 \Phi}{d\phi^2} + (a - 2q \cos 2\phi) \Phi = 0 \quad (\text{C-5})$$

where  $a = \alpha^2 + \omega^2 \mu_0 \epsilon_a \rho_0^2 \eta$ ,  $q = \frac{1}{2} \omega^2 \mu_0 \epsilon_a \rho_0^2 \delta$ , and  $\alpha$  is the separation constant. Equation (C-5) represents a Mathieu differential equation. Since the problem is symmetric with respect to the  $\psi = 0$  plane, only even solutions of  $\Phi(\phi)$  should be considered. In addition,  $E_z$  has a period of  $2\pi$  in  $\phi$ . Hence a superposition of all possible solutions satisfying these conditions is given by

$$E_z^{II}(\rho, \phi) = E_0 \sum_{n=0}^{\infty} \left\{ [d_{2n} \rho^{\alpha_{2n}} + b_{2n} \rho^{-\alpha_{2n}}] ce_{2n}(\psi, q) + [d_{2n+1} \rho^{\alpha_{2n+1}} + b_{2n+1} \rho^{-\alpha_{2n+1}}] ce_{2n+1}(\psi, q) \right\} \quad (\text{C-6})$$

where  $\alpha_m = \sqrt{a_m - \omega^2 \mu_0 \epsilon_a \rho_0^2 \eta}$  and  $a_m$  is the characteristic number of the Mathieu function  $ce_m(\psi, q)$ . The cosine elliptic functions  $ce_m(\psi, q)$  and  $ce_{2m+1}(\psi, q)$  have periods of  $\pi$  and  $2\pi$ , respectively [111]. The field  $H_\phi$  in region II is then given by

$$E_z^{II}(\rho, \phi) = \frac{E_0}{j \omega \mu_0} \sum_{n=0}^{\infty} \left\{ \left[ \alpha_{2n} (d_{2n} \rho^{\alpha_{2n}-1} - b_{2n} \rho^{-\alpha_{2n}-1}) ce_{2n}(\psi, q) \right] \right. \\ \left. + \left[ \alpha_{2n+1} (d_{2n+1} \rho^{\alpha_{2n+1}-1} - b_{2n+1} \rho^{-\alpha_{2n+1}-1}) ce_{2n+1}(\psi, q) \right] \right\} \quad (C-7)$$

since the field should be finite at  $\rho = 0$ , the field in the interior region can be expressed as an infinite series of Bessel functions of the first kind, i. e.

$$E_z^{III}(\rho, \phi) = E_0 \sum_{n=0}^{\infty} \epsilon_n g_n J_n(k\rho) \cos n\psi \quad (C-8)$$

and as a result

$$H_{\phi}^{III}(\rho, \phi) = \frac{E_0}{j \omega \mu_0} \sum_{n=0}^{\infty} \epsilon_n g_n k J_n'(k\rho) \cos n\psi. \quad (C-9)$$

The unknown expansion coefficients  $d_m, b_m, c_m$  and  $g_m$  are evaluated from the continuity of the tangential fields  $E_z$  and  $H_{\phi}$  at  $\rho_a$  and  $\rho_b$ . The condition that  $E_z^I$  and  $E_z^{II}$  are equal at  $\rho = \rho_a$  leads to

$$\sum_{n=0}^{\infty} \epsilon_n \left\{ j^n J_n(k\rho_a) + c_n H_n(k\rho_a) \right\} \cos n\psi \\ = \sum_{n=0}^{\infty} \left\{ \left[ d_{2n} \rho_a^{\alpha_{2n}} + b_{2n} \rho_a^{-\alpha_{2n}} \right] ce_{2n}(\psi, q) \right. \\ \left. + \left[ d_{2n+1} \rho_a^{\alpha_{2n+1}} + b_{2n+1} \rho_a^{-\alpha_{2n+1}} \right] ce_{2n+1}(\psi, q) \right\}. \quad (C-10)$$

The left hand side of Eq. (C-10) is then multiplied by  $ce_m(\psi, q)$  where the right hand side is multiplied by the expansion of  $ce_m(\psi, q)$ , i.e.

$$ce_{2m}(\psi, q) = \sum_{r=0}^{\infty} A_{2r}^{2m} \cos 2r\psi \quad (C-11)$$

in which the coefficients  $A_{2r}^{2m}$  can be computed [111] once  $q$  and the characteristic numbers  $a_m$  are known. Integrating both sides of the resulting equation from 0 to  $2\pi$  and using the orthogonal properties of the Mathieu and the trigonometric functions [112], we obtain

$$d_{2m} \rho_a^{\alpha_{2m}} + b_{2m} \rho_a^{-\alpha_{2m}} = \sum_{r=0}^{\infty} \epsilon_{2r} j^{2r} J_{2r}(k \rho_a) A_{2r}^{2m} + \sum_{r=0}^{\infty} \epsilon_{2r} c_{2r} H_{2r}(k \rho_a) A_{2r}^{2m}. \quad (C-12)$$

Again multiplying Eq. (C-10) by  $ce_{2m+1}(\psi, q)$  and using the expansion

$$ce_{2m+1}(\psi, q) = \sum_{r=0}^{\infty} A_{2r+1}^{2m+1} \cos(2r+1)\psi \quad (C-13)$$

and integrating from 0 to  $2\pi$ , we obtain

$$d_{2m+1} \rho_a^{\alpha_{2m+1}} + b_{2m+1} \rho_a^{-\alpha_{2m+1}} = \sum_{r=0}^{\infty} \epsilon_{2r+1} j^{2r+1} J_{2r+1}(k \rho_a) A_{2r+1}^{2m+1} + \sum_{r=0}^{\infty} \epsilon_{2r+1} c_{2r+1} H_{2r+1}(k \rho_a) A_{2r+1}^{2m+1} \quad (C-14)$$

where  $m = 0, 1, 2, 3, \dots$  and  $r = 0, 1, 2, \dots$ .

Equations (C-12) and (C-14) can be combined to form a matrix equation, i.e.

$$[U][D] + [W][B] = [S] + [Z][C] \quad (C-15)$$

where each element of the matrices  $[D]$ ,  $[B]$  and  $[C]$  is one of the unknown expansion coefficients  $d_p$ ,  $b_p$  and  $c_p$ , respectively. The matrices  $[U]$  and  $[W]$  are diagonals and each of their elements is given by  $\rho_a^{\alpha_i}$  and  $\rho_a^{-\alpha_i}$ , respectively. Each element of the column matrix  $[S]$  is denoted by  $s_l$  and is given by  $\sum_{i=0}^{\infty} \epsilon_i j^i J_i(k \rho_a) A_i^l$ .  $[Z]$  is a square matrix with elements  $z_{l,p}$  given by

$\epsilon_p H_p(k \rho_a) A_p^l$  while the integers  $p, l$  and  $i$  have the values  $0, 1, 2, \dots$ .

For  $H_\phi^I$  to be equal to  $H_\phi^{II}$  at  $\rho = \rho_a$  we should have

$$\begin{aligned} & \sum_{n=0}^{\infty} \epsilon_n j^n k J_n'(k \rho_a) \cos n\psi + \sum_{n=0}^{\infty} \epsilon_n c_n k H_n'(k \rho_a) \\ &= \sum_{n=0}^{\infty} \left\{ \alpha_{2n} \left[ d_{2n} \rho_a^{\alpha_{2n}-1} - b_{2n} \rho_a^{-\alpha_{2n}-1} \right] ce_{2n}(\psi, q) \right. \\ & \quad \left. + \alpha_{2n+1} \left[ d_{2n+1} \rho_a^{\alpha_{2n+1}-1} - b_{2n+1} \rho_a^{-\alpha_{2n+1}-1} \right] ce_{2n+1}(\psi, q) \right\}. \end{aligned} \quad (C-16)$$

Replacing the Mathieu functions in Eq. (C-16) by their expansions as given in Eqs. (C-11) and (C-13) and multiplying by  $\cos m\psi$  and integrating from  $0$  to  $2\pi$ , we obtain

$$\begin{aligned} & \epsilon_{2m} j^{2m} k J_{2m}'(k \rho_a) + \epsilon_{2m} c_{2m} k H_{2m}'(k \rho_a) \\ &= \sum_{n=0}^{\infty} \alpha_{2n} \left[ d_{2n} \rho_a^{\alpha_{2n}-1} - b_{2n} \rho_a^{-\alpha_{2n}-1} \right] A_{2m}^{2n} \end{aligned} \quad (C-17)$$

and

$$\begin{aligned} & \epsilon_{2m+1} j^{2m+1} k J_{2m+1}'(k \rho_a) + \epsilon_{2m+1} c_{2m+1} k H_{2m+1}'(k \rho_a) \\ &= \sum_{n=0}^{\infty} \alpha_{2n+1} \left[ d_{2n+1} \rho_a^{\alpha_{2n+1}-1} - b_{2n+1} \rho_a^{-\alpha_{2n+1}-1} \right] A_{2m+1}^{2n+1}. \end{aligned} \quad (C-18)$$

Equations (C-17) and (C-18) are combined and written in the following matrix form

$$[C] = [F] + [T][D] + [X][B] \quad (C-19)$$

where  $[F]$  is a column matrix in which each element,  $f_p$  is given by  $-j^p J_p'(k \rho_a) / H_p'(k \rho_a)$ , the elements of  $[T]$  and  $[X]$  are denoted by

$t_{p,l}, x_{p,l}$  and are given by  $\alpha_l \rho_a^{\alpha_l - 1} A_p^l / [\epsilon_p k H_p'(k \rho_a)]$ ,  
 $-\alpha_l \rho^{-\alpha_l - 1} A_p^l / [\epsilon_p k H_p'(k \rho_a)]$ , respectively.

Following the same procedure at  $\rho = \rho_b$  we obtain after some manipulations

$$([\bar{U}] - [Y][\bar{T}])[D] = ([Y][\bar{X}] - [\bar{W}])[B] \quad (C-20)$$

where  $[\bar{U}]$  and  $[\bar{W}]$  are diagonal matrices and each of their elements is given by  $\rho_b^{\alpha_l}$  and  $\rho_b^{-\alpha_l}$ , respectively.  $[Y]$ ,  $[\bar{T}]$  and  $[\bar{X}]$  are square matrices and their elements are denoted by  $y_{l,p}, \bar{t}_{p,l}, \bar{x}_{p,l}$  and given by  $\epsilon_p J_p(k \rho_b) A_b^l$ ,  $\alpha_l \rho_b^{\alpha_l - 1} A_b^l / [\epsilon_b k J_p'(k \rho_b)]$  and  $-\alpha_l \rho_b^{-\alpha_l - 1} A_b^l / [\epsilon_p k J_p'(k \rho_b)]$ , respectively. Furthermore, the coefficients  $g_p$  are given by

$$g_p = \frac{1}{\epsilon_p k J_p'(k \rho_b)} \sum_{n=0}^{\infty} \alpha_n \left[ d_n \rho_b^{\alpha_n - 1} - b_n \rho_b^{-\alpha_n - 1} \right] A_p^n. \quad (C-21)$$

Equations (C-15), (C-19) and (C-20) are solved for the unknown matrices  $[D]$ ,  $[B]$  and  $[C]$ . The results are

$$[D] = \left\{ [U] - [Z][T] - ([Z][X] - [W]) \left( [Y][\bar{X}] - [\bar{W}] \right)^{-1} \cdot ([\bar{U}] - [Y][\bar{T}]) \right\}^{-1} ([S] + [Z][F]) \quad (C-22)$$

$$[B] = \left( [Y][\bar{X}] - [\bar{W}] \right)^{-1} ([\bar{U}] - [Y][\bar{T}])[D]. \quad (C-23)$$

Once the vectors of the unknowns  $d_p$  and  $b_b$  are computed from Eqs. (C-22) and (C-23), respectively, we can obtain the unknowns  $g_p$  and  $c_p$  from Eqs. (C-21) and (C-19), respectively, which completes the solution.

Since all the matrices are infinite, they are suitably truncated during the computations in order to lead to a convergent solution.

The properties of the plane wave scattering by any cylindrical body of infinite length are described in terms of the echo width which is denoted by  $W(\phi)$  and defined by Harrington [89] as follows :

$$W(\phi) = \lim_{\rho \rightarrow \infty} 2\pi\rho \left| \frac{E^S(\rho, \phi)}{E^i} \right|^2 \quad (C-24)$$

where  $E^i$  and  $E^S$  are the incident and scattered fields, respectively. From Eqs. (C-2) and (C-24) the echo width of the dielectric cylindrical shell is given by

$$W(\phi) = \frac{4}{k |E^i|^2} \left| \sum_{n=0}^{\infty} \epsilon_n c_n j^n \cos n\psi \right|^2 \quad (C-25)$$

where the Hankel function is replaced by its asymptotic expression for large argument.

For the sake of comparison, an alternative way of calculating the fields as well as the echo width due to scattering by a cylindrical shell is also computed using the method of moments. It should be noted that the application of the method of moments for the scattering by dielectric bodies is fully explained in the literature [113-114]. This method is used here for solving the integral equation for the resulting scattered field by expanding the unknown in terms of pulse functions and using point matching procedure for testing, hence generating a well conditioned matrix whose elements are easily evaluated. Further, to account for the permittivity variations in both  $\rho$  and  $\phi$  directions, each shell is divided into a number of subshells in the  $\rho$  direction and each subshell is divided into another number of equal cells to allow for variations in the  $\phi$  direction. The number of subshells and the cells are suitably chosen to give accurate results such that the edge dimension of each cell should not exceed  $0.2\lambda/\sqrt{\epsilon_r}$  where  $\epsilon_r$  is the relative permittivity of the cell as proposed and verified by Richmond [113].

Figure C-2 shows the echo width of a cylindrical dielectric shell with  $\rho_a = 0.27 \lambda$ ,  $\rho_b = 0.25\lambda$  and excited by a plane wave incident at angle  $\phi_0 = 180^\circ$ . In this figure the solid curve represents the boundary value solution, whereas the squares represent the computed echo width based on the method of moments. During the computations by the moment method, the shell was subdivided into 3 subshells and each subshell was divided into 26 equal cells. Excellent agreement is observed from the two curves in Fig. C-2, however, it should be mentioned that the method of moments is not suitable for problems with this type of inhomogeneity relative to the solution obtained by the boundary value approach. This is clearly understandable when we note that the execution time for the case shown in Fig. C-2 was 15 times longer by the method of moments than by the boundary value method. The method of moment results showed excellent agreement with published data by Richmond [114] for a dielectric shell of constant permittivity. Remarkable changes in the echo width and the radiation pattern, corresponding to different values of  $\delta$ ,  $\eta$ ,  $\rho_a$  and  $\epsilon_a$ , are also investigated and the results are reported elsewhere [115,116].

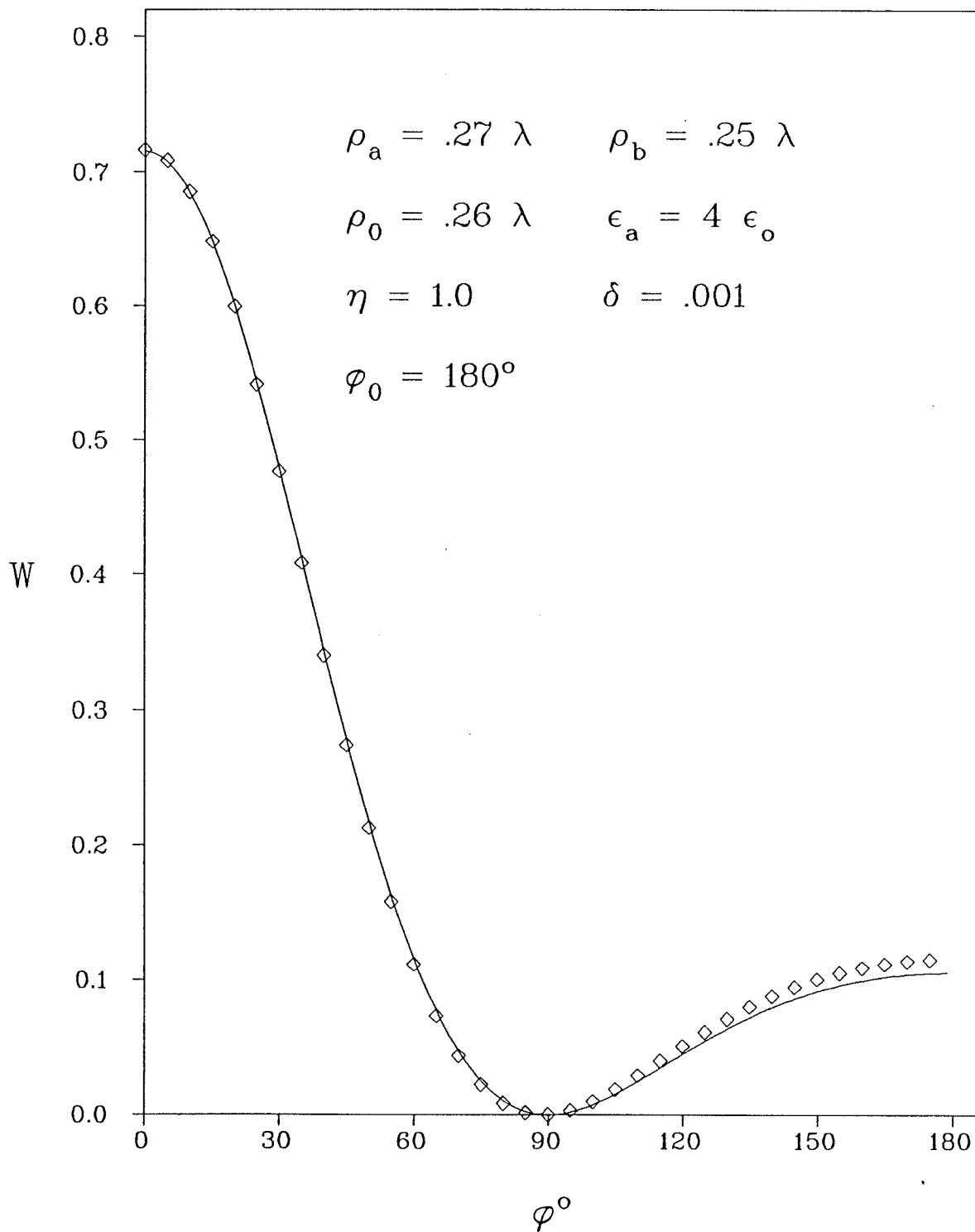


Fig C-2 : W vs.  $\varphi$  .



## REFERENCES

- [1] S. J. Maurer and L. B. Felsen, "Ray-optical techniques for guided waves", Proc. IEE, vol. 55, pp. 1718-1729, 1967.
- [2] H. M. Nussenzveig, "Solution of a diffraction problem, I and II", Phil. Trans. of the Royal Soc. of London, vol. 252(A), pp. 1-51, 1959.
- [3] C. M. Amaral and J. W. Vidal, "Evanescent-mode effects in the double-wedge problem", App. Sci. Res., vol. 11(B), pp. 1-25, 1963.
- [4] J. B. Keller, "The geometrical theory of diffraction", Proc. of Symposium on Microwave Optics, Eaton Electronics Research Laboratory, McGill University, Montreal, Canada, June 1953.
- [5] J. B. Keller, "Diffraction by an aperture", J. Appl. Phys., vol. 28, pp. 426-444, 1957.
- [6] J. B. Keller, "Diffraction by an aperture II", J. App. Phys., vol. 28, pp. 570-579, 1957.
- [7] J. B. Keller, "Geometrical theory of diffraction", J. of Opt. Soc. of Am., vol. 52, pp. 116-130, 1962.
- [8] J. B. Keller, "One hundred years of diffraction theory", IEEE Trans. Ant. and Prop., vol. AP-33, pp. 123-126, 1985.
- [9] R. B. Dybdal, R. C. Rudduck and L. L. Tsai, "Mutual coupling between  $TEM$  and  $TE_{01}$  parallel-plate waveguide apertures", IEEE Trans. Ant. and Prop., vol. AP-14, pp. 574-580, 1966.

- [10] R. C. Rudduck and L. L. Tsai, "Aperture reflection coefficient of *TEM* and *TE*<sub>10</sub> mode parallel-plate waveguides", IEEE Trans. Ant. and Prop., vol. AP-16, pp. 83-89, 1968.
- [11] D. C. Wu, R. G. Rudduck and E. L. Pelton, "Application of a surface integration technique to parallel-plate waveguide radiation pattern analysis", IEEE Trans. Ant. and Prop. vol. AP-17, pp. 280-285, 1969.
- [12] H. Henke, H. Fruchting and R. Winz, "Diffraction by a flanged parallel-plate waveguide and a slit in a thick screen", Radio Science, vol. 14, pp. 11-18, 1979.
- [13] M. A. Hamid, "Reflection coefficient of a horn-waveguide junction", IEEE Trans. Ant. and Prop., vol. Ap-15, pp. 564-565, 1967.
- [14] E. V. Jull, "Reflection from the aperture of a long E-plane sectoral horn", IEEE Trans. Ant. and Prop., vol. Ap-20, pp. 62-68, 1972.
- [15] M. F. Iskander and M. Hamid, "Scattering coefficients at a waveguide-horn junction", Proc. IEE, vol. 123, pp. 123-127, 1976.
- [16] V. A. Borovikov and V. A. Kaloshin, "Scattering matrix of the waveguide-horn junction", Radio Engineering and Electronic Physics, vol. 29, pp. 54-63, 1984.
- [17] R. E. Wilkerson, "Approximations to the double knife-edge attenuation coefficient", Radio Science, vol. 1 (New series), pp. 1439-1443, 1966.
- [18] L. E. Vogler, "An attenuation for multiple knife-edge diffraction", Radio Science, vol. 17, pp. 1541-1546, 1982.
- [19] J. H. Whittaker, "Near-field ray calculation for multiple knife-edge diffraction", Radio Science, vol. 19, pp. 975-986, 1984.
- [20] V. A. Borovikov and V. P. Narbut, "Radiation pattern of a slotted-waveguide antenna with wedges", Radio Engineering and Electronic Physics, vol. 25, pp. 44-52, 1980.

- [21] R. G. Kouyoumjian and P. H. Pathak, "A uniform geometrical theory of diffraction for an edge in a perfectly conducting surface", Proc. IEEE, vol. 62, pp. 1448-1461, 1974.
- [22] R. G. Kouyoumjian, "The geometrical theory of diffraction and its application", in "Numerical and Asymptotic Techniques in Electromagnetics", edited by R. Mittra, Springer, New York, pp. 165-215, 1975.
- [23] R. Tiberio and R.G. Kouyoumjian, "An analysis of diffraction at edges illuminated by transition region field", Radio Science, vol. 17, pp. 323-336, 1982.
- [24] R. Tiberio and R. G. Kouyoumjian, "Calculation of the high-frequency diffraction by two nearby edges illuminated at grazing incidence", IEEE Trans. Ant. and Prop., vol. Ap-32, pp. 1186-1196, 1984.
- [25] E. Luneburg and R. A. Hurd, "Diffraction by an infinite set of soft/hard parallel half planes", Radio Science, vol. 17, pp. 453-462, 1982.
- [26] E. Luneburg and R. A. Hurd, "Diffraction by an infinite set of hard and soft parallel half planes", Can. J. Phys. vol. 60, pp. 1-9, 1982.
- [27] D. S. Jones, "Double knife-edge diffraction and ray theory", Quart. J. Mech. Appl. Math., vol. 26, pp. 1-28, 1973.
- [28] S. W. Lee and J. Boersma, "Ray-optical analysis of fields on shadow boundaries of two parallel plates", J. Math. Phys., vol. 16, pp. 1746-1764, 1975.
- [29] J. Boersma, "Diffraction by two parallel half-planes", Quart. J. Mech. Appl. Math., vol. 28, pp. 405-426, 1975.
- [30] Y. Rahmat-Samii and R. Mittra, "On the investigation of diffracted fields at the shadow boundaries of staggered parallel plates - a spectral domain approach", Radio Science, vol. 12, pp. 659-670, 1977.

- [31] S. W. Lee, Y. Rahmat-Samii and R. C. Menendez, "GTD, ray field and comments on two papers", IEEE Trans. Ant. and Prop., vol AP-26, pp. 352-354, 1978.
- [32] V. A. Kaloshin, "Multiple diffraction on semiplanes", Radio Engineering and Electronic Physics, vol. 27, pp. 56-61, 1982.
- [33] P. M. Morse and H. Feshbach, Methods of Theoretical Physics, New York: McGraw-Hill, 1953.
- [34] S. Skavlem, "On the diffraction of scalar plane waves by a slit of infinite length", Arch. Math. Naturvidensk., vol. 51, pp. 61-80, 1952.
- [35] P. M. Morse and P. J. Rubenstein, "The diffraction of waves by ribbons and by slits", Physical Review, vol. 54, pp. 895-898, 1938.
- [36] C. J. Bouwkamp, "Diffraction theory", Rep. Prog. in Phys., vol. 17, pp. 35-100, 1954.
- [37] P. C. Clemmow, "Edge currents in diffraction theory", IRE Trans. Ant. and Prop., vol. AP-4, 82-287, 1956.
- [38] S. N. Karp and A. Russek, "Diffraction by a wide slit", J. Appl. Phys., vol. 27, pp. 886-894, 1956.
- [39] R. F. Millar, "Diffraction by a wide slit and complementary strip: I and II", Proc. Camb. Phil. Soc., vol. 54, pp. 479-511, 1958.
- [40] H. Levine, "Diffraction by an infinite slit", J. Appl. Phys., vol. 30, pp. 1673-1682, 1959.
- [41] P. C. Clemmow, "A method for the exact solution of a class of two dimensional diffraction problems", Proc. Roy. Soc., vol. 205(A), pp. 286-308, 1951.
- [42] P. C. Clemmow, The Plane Wave Spectrum Representation of Electromagnetic Field, New York: Pergamon, 1966.

- [43] S. N. Karp and J. B. Keller, "Multiple diffraction by an aperture in a hard screen", *Optica Acta*, vol. 8, pp. 61-72, 1961.
- [44] S. C. Kashyap and M. Hamid, "Diffraction characteristics of a slit in a thick conducting screen", *IEEE Trans. Ant. and Prop.*, vol AP-19, pp. 499-507, 1971.
- [45] M. G. Andreasen, "Scattering from parallel metallic cylinders with arbitrary cross-section", *IEEE Tran. Ant. and Prop.*, vol. AP-12, pp. 746-754, 1964.
- [46] R. F. Harrington, *Field Computation by Moment Methods*, New York: MacMillan, 1968.
- [47] N. Morita, "Diffraction of electromagnetic waves by a two-dimensional aperture with arbitrary cross-sectional shape", *Electronic and Communications in Japan*, vol. 54-B, pp. 58-61, 1971.
- [48] M. Hamid, A. Mohsen and W. M. Boerner, "Diffraction by a slit in a thick conducting screen", *J. of Appl. Phys.*, vol. 40, pp. 3882-3883, 1969.
- [49] S. C. Kashyap, M. Hamid and N. J. Mostowy, "Diffraction pattern of a slit in a thick conducting screen", *J. of Appl. Phys.*, vol. 42, pp.894-895, 1971.
- [50] B. R. Teague and N. R. Zitron, "Diffraction by an aperture between two wedges", *Appl. Sci. Res.*, vol. 26, pp. 127-137, 1972.
- [51] N. Zitron and S. N. Karp, "Higher order approximation in multiple scattering I : Two dimensional scalar case", *J. Math. Phys.*, vol. 2, pp. 394-402, 1961.
- [52] M. Hamid and A. Al-Solaiman, "New types of dielectric-loaded horn antennas", *Int'l. J. of Elec.*, vol. 55, pp. 729-750, 1983.
- [53] R. V. Row, "Theoretical and experimental study of electromagnetic scattering by two identical conducting cylinders", *J. Appl. Phys.*, vol. 26, pp. 666-675, 1955.
- [54] V. Twersky, "Scattering of waves by two objects", in "Electromagnetic Waves", University of Wisconsin Press, Madison, Wisc. ,pp. 361-389, 1962.

- [55] R. F. Millar, "The scattering of plane wave by a row of small cylinders", *Can. J. of Phys.*, vol. 38, pp. 272-289, 1960.
- [56] B. A. Howarth and T. J. Pavlasek, "Multiple induction: a novel formulation of multiple scattering of scalar waves", *J. Appl. Phys.*, vol. 44, pp. 1162-1167, 1973.
- [57] B. A. Howarth, "Multiple scattering resonances between parallel conducting cylinders", *Can. J. Phys.*, vol. 51, pp. 2415-2427, 1973.
- [58] K. Hongo, "Multiple scattering by two conducting circular cylinders", *IEEE Trans. Ant. and Prop.*, vol. AP-26, pp. 748-751, 1978.
- [59] J. W. Young and J. C. Bertrand, "Multiple scattering by two cylinders" *J. Acoust. Soc. of Am.*, vol. 58, pp. 1190-1195, 1975.
- [60] H. Ragheb and M. Hamid, " Scattering by N parallel conducting circular cylinders", *Int'l. J. of Electronics*, vol. 59, pp. 407-421, 1985.
- [61] C. R. Mullin, R. Sandburg and C. O. Velline, "A numerical technique for the determination of scattering cross sections of infinite cylinders of arbitrary geometrical cross section", *IEEE Trans. Ant. and Prop.*, vol. AP-13, pp. 141-149, 1965.
- [62] A. Z. Elsherbeni and M. Hamid, "An improved moment method for the scattering by large conducting cylinders", *Proc. IEEE/AP-S Symposium*, Philadelphia, Pennsylvania, U.S.A., pp. 285-288, June 1986.
- [63] A. Z. Elsherbeni and M. Hamid, "Scattering by parallel conducting circular cylinders", *IEEE Trans. Ant. and Prop.*, vol. AP-35, March 1978.
- [64] R. F. Harrington, "Time-Harmonic Electromagnetic Fields", New York: McGraw Hill, Ch. 5, 1961.
- [65] J. D. Hunter, "Surface current density on perfectly conducting polygonal cylinders", *Can. J. of Phys.*, vol. 50, pp. 139-150, 1972.

- [66] M. F. Iskander and M. Hamid, "Scattering by a regular polygonal conducting cylinder", AEU, vol. 30, pp. 403-408, 1976.
- [67] M. Kaye, P. K. Musthy and G. A. Thiele, "An iterative method for solving scattering problems", IEEE Trans. Ant. and Prop., vol. AP-33, pp. 1272-1279, 1985.
- [68] N. Morita, "Diffraction by arbitrary cross-sectional semi-infinite conductor", IEEE Trans. Ant. and Prop., vol. AP-19, pp. 358-364, 1971.
- [69] N. Morita, "Comments on diffraction by arbitrary cross-sectional semi-infinite conductor", IEEE Trans. Ant. and Prop., vol. AP-20, pp. 517-519, 1972.
- [70] A. Z. Elsherbeni and M. Hamid, "Asymptotic diffraction by a double wedge", Proc. IEEE/AP-S Symposium, Boston, Mass., U.S.A., pp. 227-230, June 1984.
- [71] A. Z. Elsherbeni and M. Hamid, "Diffraction by a wide double wedge", IEEE Trans. Ant. and Prop., vol. AP-32, pp. 1262-1265, 1984.
- [72] A. Z. Elsherbeni and M. Hamid, "Diffraction by a double capped-wedge", Proc. North American Radio Science Meeting (URSI), Vancouver, Canada, p. 230, June 1985.
- [73] A. Z. Elsherbeni and M. Hamid, "Diffraction by a wide double wedge with capped edges", IEEE Trans. Ant. and Prop., vol. AP-34, pp. 947-951, 1986.
- [74] W. Stutzman and G. Thiele, Antenna Theory and Design, New York: John Wiley, Ch. 9, 1981.
- [75] A. W. Adey, "Field of a dielectric-loaded infinite corner reflector", Can. J. Phys., vol. 36, pp. 438-445, 1958.
- [76] S. J. Towaij, M. Hamid and A. Mohsen, "Diffraction by an infinite corner reflector transversely loaded by concentric dielectric slabs", Int. J. of Electronics, vol. 33, pp. 241-253, 1972.

- [77] M. Hamid, "Diffraction coefficient of a conducting wedge loaded with a cylindrical dielectric slab at the apex", IEEE Trans. Ant. and Prop., vol. AP-21, pp. 398-399, 1973.
- [78] M. Hamid S. J. Towaij, "Diffraction by a half-plane with a cylindrical dielectric cap", IEEE Trans. Ant. and Prop., vol. AP-20, pp. 663-665, 1972.
- [79] S. N. Karp, "Diffraction by a tipped wedge with application to blunt edges", Div. EM Res., Inst. Math. Sci., New York Univ., New York, Rep. No. EM52, 1953.
- [80] J. B. Keller, "How dark is the shadow of a rounded-ended screen?", J. Appl. Phys., vol. 30, pp. 1452-1454, 1959.
- [81] R. G. Kouyoumjian and W. D. Burnside, "The diffraction by a cylinder-tipped half-plane", IEEE Trans. Ant. and Prop., vol. AP-18, pp. 424-426, 1970.
- [82] J. B. Keller and D. G. Magiros, "Diffraction by a semi-infinite screen with a rounded end", Comm. pure and Appl. Math., vol. 14, pp. 457-471, 1961.
- [83] Y. T. Chu, V. E. Anderson, H. H. Hubbell and T. L. Ferrell, "Asymptotic solution for the diffraction of an electromagnetic plane wave by a cylinder-tipped half-plane", J. Opt. Soc. of Am., vol. 73, pp. 768-775, 1983.
- [84] W. Hallidy, "On uniform asymptotic Green's functions for the perfectly conducting cylinder tipped wedge", IEEE Trans. Ant. and Prop., vol. AP-33, pp. 1020-1025, 1985.
- [85] R. A. Ross and M. Hamid, "Scattering by a wedge with rounded edge", IEEE Trans. Ant. and Prop., vol. AP-19, pp. 507-516, 1971.
- [86] R. A. Hurd and B. K. Sachdeva, "Scattering by a dielectric-loaded slit in a conducting plane", Radio Science, vol. 10, pp. 565-572, 1975.



- [87] G. L. James, "Geometrical Theory of Diffraction for Electromagnetic Waves", London: Peter Peregrinus Ltd., pp. 60-65, 1980.
- [88] A. Z. Elsherbeni and M. Hamid, "Diffraction by a double wedge in the presence of a circular cylinder", Proc. of the National Radio Science Meeting, University of Colorado, Boulder, Colorado, U.S.A., p. 129, January 1986.
- [89] A. Z. Elsherbeni and M. Hamid, "Scattering by a double wedge and a parallel cylinder", Int'l. J. of Electronics, vol. 60, pp. 367-380, 1986.
- [90] K. Casey, "Two-dimensional electromagnetic fields in azimuthally inhomogeneous media", IEEE Trans. Ant. and Prop., vol. AP-19, pp. 571-572, 1971.
- [91] A. Z. Elsherbeni and M. Hamid, "Diffraction by the aperture between two rounded wedges", Proc. second Jordan International Electrical and Electronic Engineering Conf. (JIEEEEC'85), Jordan, pp. 549-553, April 1985.
- [92] A. Z. Elsherbeni and M. Hamid, "Diffraction by a wide double wedge with rounded edges", IEEE Trans. Ant. and Prop., vol. AP-33, pp. 1012-1015, 1985.
- [93] K. Hongo, M. Kumazawa and H. Hori, "Scattering of electromagnetic plane waves by a circular cylinder", IEEE Trans. Ant. and Prop., vol. AP-25, pp. 898-900, 1977.
- [94] A. Z. Elsherbeni and M. Hamid, "Scattering and transmission properties for a class of two-dimensional double bodies", Proc. Antenna Technology and Applied Electromagnetic Symposium, University of Manitoba, Winnipeg, Manitoba, Canada, August 1986.
- [95] A. Z. Elsherbeni and M. Hamid, "Diffraction and transmission properties of a class of double wedges", Canadian J. of Physics, vol. 65, January 1987.
- [96] M. Abramowitz and A. Stegun, "Handbook of Mathematical Functions with Formulas, Graphs and Mathematical Tables", National Bureau of Standards, Applied Mathematics Series 55, Sec. 25, 1964.

- [97] A. Z. Elsherbeni and M. Hamid, "Integral solution for the diffraction by a double cylindrical wedge", Proc. Antenna Technology and Applied Electromagnetic Symposium, University of Manitoba, Winnipeg, Manitoba, Canada, August 1986.
- [98] A. Z. Elsherbeni and M. Hamid, "Rigorous solution of the double wedge diffraction problem", Proc. URSI International Symposium on Electromagnetic Theory, Budapest, Hungary, pp. 128-130, August 1986.
- [99] A. Z. Elsherbeni and M. Hamid, "A novel cylindrical wave spectrum for analysis of scattering by multiple bodies", IEE proceedings, Part H, vol. 134, February 1987.
- [100] W. D. Burnside, C. L. Yu and R. J. Marhefka, "A technique to combine the geometrical theory of diffraction and the moment method", IEEE Trans. Ant. and Prop., vol. Ap-23, pp. 551-558, 1975.
- [101] H. Ragheb, A. Z. Elsherbeni and M. Hamid, "On the optimum design of the corner array", Proc. Conf. On Precision Electromagnetic Measurement, Delft, The Netherlands, pp. 162-163, August 1984.
- [102] H. A. Ragheb, A. Z. Elsherbeni and M. Hamid, "Radiation characteristics of the corner array", Int'l. J. of Electronics, vol. 60, pp. 229-238, 1986.
- [103] T. B. A. Senior, "Diffraction by an imperfectly conducting wedge", Communication on Pure and Applied Mathematics, vol. 12, pp. 337-372, 1959.
- [104] M. Hamid, "Diffraction coefficient of a conducting wedge loaded with a dielectric slab on the illuminated surface", IEEE Trans. Ant. and Prop., vol. AP-21, pp. 728-729, 1973.
- [105] T. B. A. Senior, "Diffraction tensors for imperfectly conducting edges", Radio Science, vol. 10, pp. 911-919, 1975.

- [106] G. L. James, "Uniform diffraction coefficients for an impedance wedge", *Electronics Letters*, vol. 13, pp. 403-404, 1977.
- [107] Te-kao Wu and L. L. Tsai, "Scattering by a dielectric wedge : A numerical solution", *IEEE Trans. Ant. and Prop.*, vol. AP-25, pp. 570-571, 1977.
- [108] J. B. Andersen and V. V. Solodukhov, "Field behavior near a dielectric wedge", *IEEE Trans. Ant. and Prp.*, vol. AP-26, pp. 598-602, 1978.
- [109] C. S. Joo, J. W. Ra and S. Y. Shin, " Scattering by right angle dielectric wedge", *IEEE Trans. Ant. and Prop.*, vol. AP-32, pp. 61-69, 1984.
- [110] R. Tiberio, G. Pelosi and G. Manara, "A uniform GTD formulation for the diffraction by a wedge with impedance face", *IEEE Trans. Ant. and Prop.*, vol. Ap-33, pp. 867-873, 1985.
- [111] N. McLachlan, *Theory and Applications of Mathieu Functions*, New York: Dover Publications, 1964.
- [112] I. Gradshteyn and I. Ryzhik, *Table of Integrals, Series and Products*, London: Academic Press, 1965.
- [113] J. H. Richmond, "Scattering by a dielectric cylinder of arbitrary cross-section shape ", *IEEE Trans. Ant. and Prop.*, vol. AP-13, pp. 334-341, 1965.
- [114] J. H. Richmond, "TE-wave scattering by a dielectric cylinder of arbitrary cross-section shape", *IEEE Trans. Ant. and Prop.*, vol. AP-14, pp. 460-464, 1966.
- [115] A. Z. Elsherbeni and M. Hamid, "Scattering by a cylindrical dielectric shell with radial and azimuthal permittivity profiles", *Proc. International Symposium on Microwave Technology in Industrial Development*, Campinas, SP, Brazil, pp. 77-80, July 1985.
- [116] A. Z. Elsherbeni and M. Hamid, "Scattering by a cylindrical dielectric shell with inhomogeneous permittivity profiles", *Int'l. J. of Electronics*, vol. 58, pp. 559-562, 1985.